THE IMPACT OF ICE CONDITIONS ON LOCAL SCOUR AROUND BRIDGE PIERS

by

Faye Hirshfield

B.Sc., University of Northern British Columbia, 2008
M.Sc., University of Northern British Columbia, 2010

THESIS SUBMITTED IN PARTIAL FULFILLMENT OF THE REQUIREMENTS FOR
THE DEGREE OF
DOCTOR OF PHILOSOPHY
IN
NATURAL RESOURCES AND ENVIRONMENTAL STUDIES

THE UNIVERSITY OF NORTHERN BRITISH COLUMBIA

April 2015

ABSTRACT

Ice cover imposes an additional boundary layer on a river channel and can influence sediment transport around bridge structures. The main objective of this study was to gain a better understanding of how ice cover is related to local scour around bridge piers. A set of flume experiments were completed investigating local scour around bridge piers under open channel, smooth ice and rough ice cover conditions. Three different non-uniform sediments were used with D_{50}'s of 0.47, 0.50 and 0.58 mm. The location of the average maximum velocity under rough ice cover ranged from 0.36-0.43H and for smooth cover was 0.41H, with depth (H) measured from the channel bed to water surface. Turbulent intensity was greater under ice cover than open channel conditions. Local pier scour under rough and smooth ice cover was on average 37 and 20 percent greater than open channel scour depth respectively. The maximum scour depth always occurred at the pier face. Greater pier scour under ice cover is related to larger streamwise and downward flow velocities at the pier face under rough ice cover. The scour hole velocity for rough and smooth ice cover was 33 and 15 percent greater than open channel scour hole velocity respectively. Under all channel covers an armour layer formed in the scour hole. For all experiments, as the armour layer size increased, the maximum local scour depth decreased.

A critical assessment of current bridge research and construction was also conducted in order to address how this study contributes to modern day bridge design. It was found that this study addresses current knowledge gaps in bridge manual used in North America. Specifically, study results concerning scour hole depth under ice cover and scour hole flow fields under ice cover are important contributions to the field of bridge hydraulics.

Table of Contents

LIST OF TABLES

LIST OF FIGURES

GLOSSARY

Letters

b	pier width (cm)
B	channel width (cm)
C_u	coefficient of uniformity
d_{max}	maximum scour depth
D	diameter of sediment particle (m)
D_{10}	10th percentile particle diameter (mm)
D_{16}	16th percentile particle diameter (mm)
D_{50}	50th percentile particle diameter (mm)
D_{50a}	median sediment size of the armour layer (mm)
D_{60}	60th percentile particle diameter (mm)
D_{84}	84th percentile particle diameter (mm)
D_{90}	90th percentile particle diameter (mm)
D_g	geometric mean
F, F_r	Froude number
F_{rc}	critical Froude number
F_o	densimetric Froude number
F_L	buoyant force
F_w	downward force
F_D	drag force
F_R	resistant force
g	gravitational acceleration (m/s^2)
H, h	approach flow depth (cm)
n_b	Manning's roughness coefficient for channel bed
n_i	Manning's roughness coefficient for ice
Q	volumetric discharge (m^3/s)
p_s	sediment density (kg/m^3)
p	fluid density (kg/m^3)

R_e	Reynolds number
R_{e*}	shear Reynolds number
R_h	hydraulic radius
RMS_x	streamwise turbulent intensity
RMS_y	lateral turbulent intensity
RMS_z	vertical turbulent intensity
T^*_c, T^*	dimensionless shear stress, critical Shields value
T_{bc}	critical bed shear stress
TKE	turbulent kinetic energy
U_*, u_*	shear velocity (m/s)
u_{*c}	critical shear velocity (m/s)
u	streamwise turbulent intensity
U	average approach velocity (m/s)
U_c	critical velocity (m/s)
U_x	steamwise velocity (m/s)
U_y	lateral velocity (m/s)
U_z	vertical velocity (m/s)
V	volume
V_x	velocity in horizontal direction (m/s)
v	vertical turbulent intensity
x	horizontal longitudinal direction
y	horizontal transverse direction
z	vertical direction, vertical distance from bed

Symbols

σ_g	geometric standard deviation
ν	kinetic viscosity of fluid
χ	Einstein multiplication factor
σ	surface tension

ACKNOWLEDGEMENT

1.0 INTRODUCTION

1.1 Background

Scour is defined as the removal of material by running water (Chang, 1992). River bed materials around stream banks, bridge piers and bridge abutments can be eroded and carried away downstream. Scour that occurs around bridge piers can threaten the structural integrity and cause bridge failure. Even though considerable research has been conducted around bridge design and construction, bridges still fail due to scour during times of flooding, extreme debris build-up and winter ice events (Melville and Coleman, 2000). Between 1966 and 2005 there were 1502 bridge collapses in the United States (Briaud et al., 2007). According to the New York State Department Bridge Failure Database river bed scour was responsible for 878 of the failures (Briaud et al., 2007). For instance, in April 1987, the Schoharie Creek Bridge in New York collapsed during spring freshet. Spring flows were higher than normal and produced an estimated 50 year flood. Ten people perished in the accident. The United States National Transportation safety board ruled the bridge collapsed due to sediment scour around the bridge pier (Hains and Zabilansky, 2007).

Countries that lead the way in bridge research are New Zealand through the University of Auckland in conjunction with Transit New Zealand and the United States (US) through the Federal Highway Administration (FHWA) in conjunction with University Transportation Centres. Studies are typically conducted in hydraulic laboratory flumes under open channel conditions and considerable research has focused on sediment scour processes around bridge structures (Alabi, 2006; Guo, 2012; Khwairakpam et al., 2012; Melville, 2008; Oliveto et al., 2002; Raikar and Dey, 2009). The specific topic of pier scour has been widely studied over the past three decades and summarized in reviews (Beltaos, 2000; Deng and Cai, 2010). A

number of master's and doctoral theses have been produced examining pier, abutment and spur dyke scour (Aliba, 2006; Hoque, 2009; Miranda, 2004; Zhang, 2005; Yang, 2005).

Very few studies, however, have looked at how winter ice cover conditions influence sediment transport around bridge structures. A bridge over the White River in Vermont experienced a number of ice jam breakups over several years; in the winter of 1990 the White River Bridge failed. Examination into the failure revealed that the bridge foundation gradually became deteriorated due to riverbed scour around the piers (Zabilansky, 1996). The difficulty in studying pier scour under ice cover lies in the dangerous field conditions surrounding river ice and maintenance of instrumentation around bridge structures. This research focuses on measuring sediment transport processes under ice covered conditions around bridge piers.

1.2 Statement of the problem and research objectives

Since ice cover imposes an additional boundary layer on a channel, causing the maximum flow velocity to migrate closer to the channel bed (Sui et al., 2010; Wang et al., 2008) local pier scour processes should be different under ice cover than scour under open channel conditions. Investigating pier scour development under ice conditions is important in engineering and design of bridges to ensure public safety.

The main objective of this thesis is to gain a better understanding of how ice cover is related to local scour around bridge piers. The following are the research objectives of this thesis:

(1) Conduct experimental flume investigation for local pier scour. Examine (a) scour depth and volume, (b) scour hole particle size distribution and (c) scour hole velocity flow field under open channel, smooth ice and rough ice cover conditions.

(2) Investigate relationships between the following variables:

    a. ice cover roughness versus flow velocity distribution

    b. channel cover versus turbulent intensity and Reynolds stress

    c. scour depth versus particle size (D_{50}) and pier width

    d. scour depth and scour profile versus channel cover

    e. scour area and volume versus channel cover

    f. scour depth and scour hole velocity profiles according to channel cover

    g. channel cover and armour layer size

In fulfilling objective number 2, the following parameters will be used for dimensional analysis:

    a. pier width

    b. scour depth

    c. approach velocity

    d. water depth

    e. viscosity

    f. particle size (D_{50})

    g. channel roughness and ice cover roughness

(3) Conduct a critical analysis of research practices as they relate to bridge design. Specifically, empirical equations, scaling practices and computational fluid dynamics pertaining to bridge scour studies and assess how components of this research work fit into current bridge research.

1.3 Significance of research

In the field of hydraulic engineering it is standard to conduct flume experiments to investigate relationships between fluid flow and hydraulic structures. To date, three studies have investigated the influence of ice cover on local pier scour. Batuca and Dargahi (1986) compared local scour around a pier under open water and floating cover conditions. Through visual observations they found that the general size of the scour hole was greater under ice covered conditions. Olsson (2000) compared pier scour depths under open, smooth and rough ice cover and found that the rough ice cover resulted in a greater scour depth than the smooth cover. Uniform sand was used. Olsson found that ice cover may increase the local scour depth by 25-35 percent under live bed conditions. Hains (2004) studied the impacts of a fixed cover on local pier scour. A fixed ice cover is not free to change position in accordance to river flow or water level. A fixed ice cover can occur when ice attaches itself to the pier or channel sides. The author examined pier scour under both floating and fixed covers along with open channel conditions. Scour depths were similar under fixed and floating ice cover conditions.

As elements of this thesis are similar to the above three studies, it is important to highlight how this research is original and differs from that found in the current literature.

(1) Numerous studies exist that investigate flow turbulence and scour depth around bridge piers under open channels. It is the open channel literature in which pier scour equations have been developed. This thesis examines pier scour under smooth and rough ice cover. While it is noted that the three previous studies have investigated pier scour under ice, there is still not a strong body of academic literature addressing

this topic. This thesis will expand on the three previous studies as explained in the following points.

(2) The majority of existing open channel scour experiments along with the ice cover experiments by Hains (2004), Olsson (2000), Batuca and Dargahi (1986) use uniform sediment. The current research uses non-uniform sediment which allows for examination of armour layer development within the scour hole. Using non-uniform sediment is also more aligned to representing natural river systems.

(3) Scour hole velocity profiles under smooth and rough ice cover are measured in this thesis. To the author's knowledge there are no studies that measure scour hole flow fields under ice cover.

As there is not a strong body of literature addressing pier scour under ice cover, it is anticipated that findings from this study will be written up for potential publications in relevant engineering journals. A summary of publication plans can be found in the conclusion, Chapter 7.

2.0 LITERATURE REVIEW

2.1 Types of scour

Chang (1992) defined scour as the removal of material by running water. Similarly, Breusers et al. (1977) stated that scour is a natural process resulting from water flow in rivers. A bridge can constrict river flow by introducing additional structures such as abutments and piers. A constricted channel may have increased flow velocities and therefore and increased capacity for sediment transport. Riverbed scour can be broadly classified as general scour, local scour and contraction scour. Aliba (2006) provides the following definitions for scour.

General scour: can occur regardless of whether a river obstruction is present; involves the overall lowering of the channel bed along the longitudinal profile. General scour occurs when the river hydrology undergoes a change which leads to degradation of the channel bed. Human induced general scour can be caused by dam construction and streambed mining. General scour can also occur over short time periods as a result of flooding or seasonal freshet events.

Local scour: scour that is directly related to the presence of a river obstruction and involves the removal of sediment from the base of bridge structures such as piers and abutments. When water flow encounters a bridge pier or abutment, the flow is directed downward towards the river bed and along the sides of the obstruction (Diab et al., 2010). The down flow causes sediment transport away from the base of the bridge structure. Local scour will be further discussed in Section 2.2.

Contraction scour: occurs when the river channel is constricted either by natural (landslide) or human means (a bridge). When the flow area is reduced, the average flow velocity and bed shear stress increase which then increase the erosive forces acting upon the channel bed (Ozalp, 2013). Increased erosion will move bed material from the contracted section until equilibrium is reached. Bridges that cause a narrowing of the channel can be expected to have higher flow velocities and larger scour depths (Zevenbergen et al., 2012). In circumstances where the estimated depths from contraction scour are too large, the bridge crossing length must be increased in order to reduce scour.

Live-bed scour: occurs when a stream is carrying a substantial sediment load and sediment is transported into the scour depression all the while local flow fields are also removing sediment from the scour hole. Live-bed scour commonly occurs in natural river systems and also in re-circulating flumes. Flow through flumes typically do not have upstream sediment being deposited in the scour hole so live-bed scour does not occur.

Clear water scour: occurs when there is no sediment transport into the scour hole but rather only sediment transport out of the scour hole. This occurs when there is no upstream supply of sediment. This rarely occurs in active river channels.

2.2 Sediment transport around bridge piers

  The flow pattern around a bridge pier is typically divided into 4 components: (1) the down-flow at the pier face (2) the horseshoe vortex (3) the bow wave and (4) the wake vortices. The following is a description of each component.

(1) Down-flow: the flow velocity decreases as it approaches a bridge pier and is reduced to zero upon meeting the pier face, forming a stagnation point. When the flow hits the pier face the overall channel depth also increases. The increase in flow depth depends on the approach velocity and the pier shape (Yanmaz, 2002). As flow velocity decreases from the water surface towards the riverbed, the resulting pressure gradient at the pier also decreases from the water surface towards the riverbed. As flow velocity decreases towards the channel bed so does the pressure. This pressure gradient creates down-flow at the pier face.

(2) Horseshoe vortex: the downward flow also interacts with the incoming river flow and results in a vortex system as shown in Figure 1. The vortex flow then moves along the side of the pier downstream. Due to the shape of the vortex, flow around a pier is often referred to in the literature as the 'horseshoe vortex' (Zhao et al., 2010). The horseshoe vortex is typically formed after a scour hole is generated (Ozalp, 2013). The intensity of the horseshoe vortex depends on the pier geometry and degree of turbulent flow (Yanmaz, 2002).

(3) Bow wave: the bow wave occurs at the upstream side of the pier at the water surface. The bow wave originates from the increase in water depth as the approach flow hits the pier face and a stagnation point is created. Richardson and Davis (2001) found that for low flow depths the bow wave causes the horseshow vortex to become weaker and leads a reduction in scour depth.

(4) Wake vortex: as flow passes the sides of a pier, flow separation occurs and wake vortices form (Figure 1). These wake vortices also contribute to erosion of sediment around the base

of the pier. Wake vortices are transferred downstream by the approach flow and work to transport sediment that is already entrained by the down-flow and horseshoe vortex (Melville and Coleman, 2000). The strength of the horseshoe vortex is much larger than the wake vortices hence the maximum scour depth typically occurs upstream of the pier face.
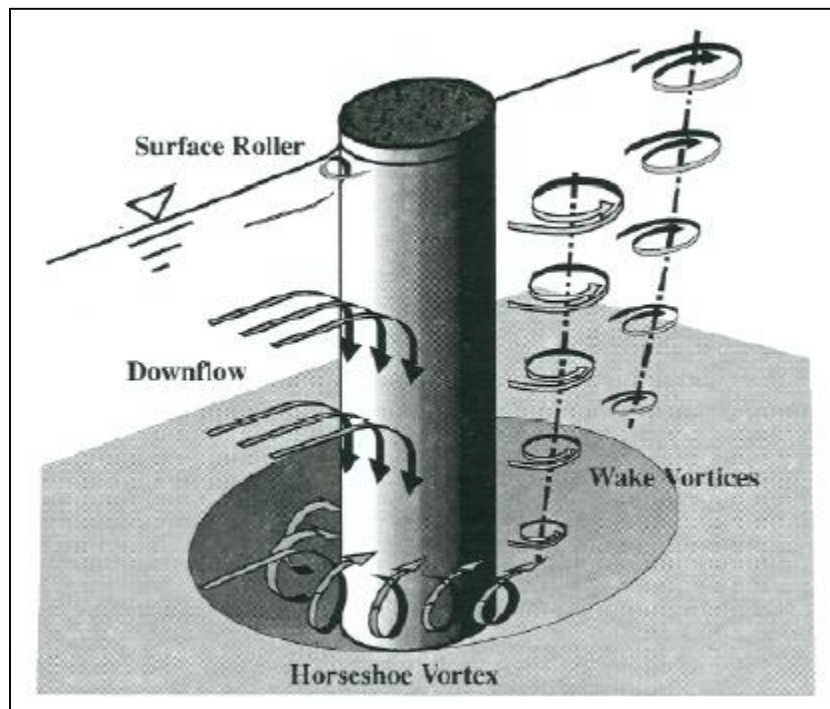
Figure 1. Flow pattern around circular pier (taken from Melville & Coleman, 2000).

The main mechanism that causes scour at bridge piers is the down-flow and subsequent horseshoe vortices that form at the base of the scour hole (Muzzammile et al., 2004). The down-flow reaches the channel bed and transports sediment away from the pier base creating a scour hole. The strength of the down-flow reaches a maximum just below the natural bed level (Alabi, 2006). Once the down-flow reaches the channel bed it interacts with the oncoming flow and a complex vortex system develops. As indicated in Figure 1, flow past the sides of the cylinder separates and wake vortices are formed. Both the horseshoe and wake

vortices erode sediment from the pier base. The strength of the wake vortices however is reduced with distance downstream and sediment deposition is common downstream of the pier (Richardson and Davies, 1995).

Numerous studies have examined the factors which affect the magnitude of local pier scour (Lagasse et al., 2001; Melville and Coleman, 2000; Raudkivi and Ettema, 1983; Richardson and Davies, 1995). The following parameters have been recognized as affecting local scour depth and can be grouped by the following headings according to Breusers et al. (1997):

- Bed sediment parameters: cohesiveness of sediment, grains size distribution, particle mass density, particle shape, bed roughness and angle of repose.
- Pier parameters: orientation (angle of attack), size, shape, spacing and number of piers.
- Flow parameters: flow velocity, flow depth, shear velocity and velocity distribution.
- Fluid parameters: kinematic viscosity, mass density and acceleration due to gravity.

The following is a brief summary of the effects of the above parameters on pier scour as outlined by Melville and Coleman (2000).

Local scour depth under clear water conditions will increase with velocity until a maximum threshold velocity is reached. The maximum scour depth occurs when $u_*/u_{*c} = 1$. (where u_* is the shear velocity and u_{*c} is the critical shear velocity). Flow depth is usually referred to as flow shallowness and is examined by relating flow depth (H) to the pier width (b). At ratios of b/H < 0.7, local scour is dependent only on pier width, and at ratios of 0.7< b/H<5 scour depth is dependent on both pier width and flow depth. Pier diameter and scour depth are related as the greater the pier diameter the stronger the vortex system. The larger the

pier width, the stronger the flow vortices and the larger the scour hole volume and scour depth. Pier shape is only important if complete axial flow can be guaranteed. In other words, even a small angle of attack will eliminate the effectiveness of a streamlined pier shape. A study by Mostafa (1994) compared all pier shapes and concluded that a circular shape minimizes scour depth to the greatest extent. Sediment coarseness also affects local scour depth. Sediment coarseness as defined by Melville and Coleman (2000) is the ratio of pier width to mean grain size of bed material, b/D_{50}. Local scour depth is affected by sediment coarseness at ratios of $b/D_{50} < 50$. Sediment nonuniformity also effects local scour depth. For non-uniform sediments, close to the threshold velocity, armouring of the scour hole will occur. This will reduce the local scour depth in comparison to uniform sediments.

2.3 Incipient motion of sediment particles

Incipient motion of sediment occurs when flow intensity in a channel is barely sufficient to entrain bed particles. The hydrodynamic forces of a fluid acting on the particles are responsible for their motion (Kanellopoulos, 1998). Since sediment is transported along a riverbed in a complex manner, it can be challenging to define the flow conditions in which sediment will move. For this reason studies focus on the flow conditions surrounding the initial motion or incipient motion of sediment. As indicated in Figure 2, there are four primary forces acting upon a sediment particle: F_L represents the lift or buoyancy force, F_W indicates the force downward from the submerged weight, F_D is the drag force and F_R is the resistance force.
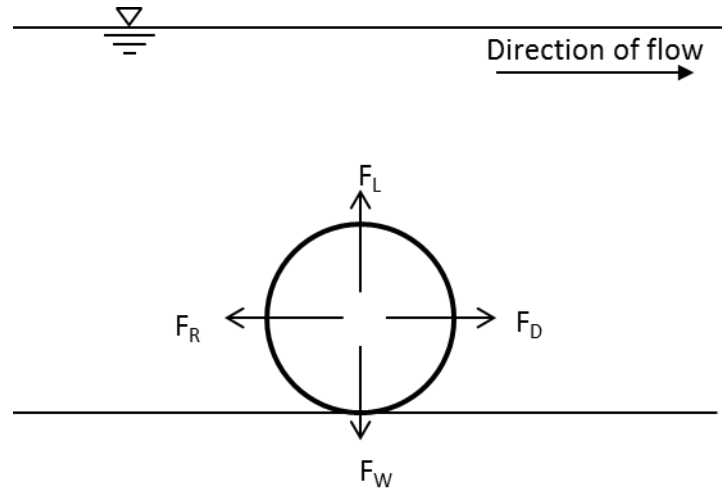
Figure 2. Overview of forces acting on a sediment particle.

In order for incipient motion to occur one of the following conditions must be satisfied:

$$F_D = F_R \qquad\qquad\qquad 2.1$$

$$F_L = F_W \qquad\qquad\qquad 2.2$$

A number of variables affect the lift, weight, drag and resistance forces acting on a sediment grain. Shields, in 1936 was the first to develop a relationship between hydraulic variables and sediment characteristics in order to satisfy the conditions for incipient motion. Through dimensional analysis, Shields examined conditions in which bed particles are stable but on the verge of being moved. Shields determined that the critical conditions in which sediment is about to become entrained can be found by relating the critical Shields value (τ_c^*) and the shear Reynolds number (Re_*). The critical Shields value, also called the dimensionless shear stress, is given by the following relation:

$$\tau_c^* = \frac{\tau_{bc}}{(\rho_s - \rho)gD} \qquad\qquad\qquad 2.3$$

where $\tau_{bc} = \rho U_{*c}^2$ = critical bed shear stress for initiation of motion, U_{*c} is the critical shear velocity, $(\rho_s - \rho)$ is the density of sediment and water respectively, g is gravity and D is the diameter of the sediment particle.

The Reynolds number, R_e, is a dimensionless quantity that represents the ratio of inertial forces to viscous forces. The Reynolds number is typically used to characterize whether a flow is laminar or turbulent. Laminar flows occur at low Reynolds numbers where viscous forces are dominant, while turbulent flows are characterized by high Reynolds numbers where inertial forces are dominant. The Reynolds number can also be adapted to study the incipient motion of sediment through the particle Reynolds number. The particle Reynolds number is given as follows:

$$R_e = \left(\frac{U D_{50}}{v}\right) \qquad 2.4$$

where U is the flow velocity, D_{50} is the median particle diameter and v is the kinetic viscosity of fluid. When studying incipient motion the shear Reynolds number R^* is referred to as it uses the shear velocity and is written as:

$$R_* = \left(\frac{U_* D_{50}}{v}\right) \qquad 2.5$$

where U_* is the shear velocity. The graphical relationship between the dimensionless shear stress (τ_c^*) and the shear Reynolds number (R_*) is referred to as the Shields diagram which represents values in which incipient motion of sediment occur. The relationship is dimensionless so that the driving forces of particle motion can be compared to the resisting forces (particle size, particle density).

The incipient motion of sediment depends not only on hydraulic variables but also on the characteristics of the bed material itself. Incipient motion of non-uniform sediment is more complicated than uniform sediment since sediment in motion is influenced by the grain shape, interactions between grains and orientation in the channel bed. The Froude number represents the ratio of fluid inertial forces to fluid gravitational forces and is used to determine the resistance of an object flowing through water. The greater the Froude number, the greater the resistance exerted on water flow by the river bed material. The Froude number is given by,

$$F_r = \left(\frac{U}{\sqrt{gh}} \right) \qquad \qquad 2.6$$

where h is the flow depth. In order to use the Froude number to examine transport of bed material, the dimensionless form of the Froude number is used. The densimetric Froude number is the ratio of inertial forces to the submerged weight of the sand grain. The densimetric Froude number is written as:

$$F_o = \frac{U}{\sqrt{\frac{gD_{50}(\rho_s - \rho)}{\rho}}} \qquad \qquad 2.7$$

where D_{50} is the median grain size of the bed material.

While incipient motion of uniform sediment has been studied in the literature (Andrey and Gareth, 2000; Beheshti and Ataie, 2008; Buffington and Montgomery, 1997; Kanellopoulos, 1998; Vollmer and Kleinhans, 2007), studies that examine incipient motion of non-uniform sediment are limited. Xu et al. (2008) established a formula for incipient velocity of non-uniform bed material based upon the drag and uplift forces and verified the formula with field data. They found that the incipient velocity required for coarse non-uniform particles was less than the incipient velocity for uniform sediment. In addition, the authors

calculated that the incipient velocity for fine particles for non-uniform sediment was greater than that for uniform sediment.

2.4 Incipient motion of sediment under ice conditions

River ice cover imposes an extra boundary on flow, altering the flow velocity and water level in comparison to open channel flow (Shen and Wang, 1995). For ice cover conditions, the portion of upper flow is mainly influenced by the ice cover resistance while the lower flow is mainly influenced by the channel bed resistance (Sui et al., 2010). The maximum flow is located between the channel bed and ice cover depending on the relative magnitudes of the ice and bed resistance coefficients (Crance and Frothingham, 2008; Ettema et al., 2000; Lau and Krishnappan, 1985; Smith and Ettema, 1997). Generally, the maximum flow velocity is closer to the surface with the smallest resistance coefficient. In the case of narrow river channels or near river banks, the maximum flow velocity will not occur at the surface but rather slightly below the surface due to the resistance forces of the side banks (Wang et al., 2008).

Since ice cover imposes an added boundary on flow conditions, the incipient motion of sediment under ice cover is different from that for open channel flow. Wang et al. (2008) conducted a number of flume experiments examining the relationship between incipient motion of bed material and ice cover conditions. Since near-bed velocity is higher under ice covered conditions, a higher shear stress is exerted on the river bed (Wang et al., 2008). The threshold velocity for the incipient motion of sediment under ice cover decreases as the ice cover resistance increases. This is due to the increased kinetic energy exerted on the bed material as the near-bed velocity increases. The flow velocity required for initial movement of bed material under ice cover also increases with water depth (Wang et al., 2008). This

relationship is only valid if the resistance coefficients of the ice cover and channel bed remain constant.

Generally, the larger the roughness coefficient for ice cover, the greater the near bed flow velocity. In this situation, the larger the roughness coefficient for ice cover, the smaller the densimetric Froude number for incipient motion of river bed material (Wang et al., 2008). Since the near bed velocity is relatively high, larger sediment particles can be moved. However, if the roughness coefficient of the river bed is high, the near bed velocity will decrease; this in turn will increase the densimetric Froude number required for incipient motion of bed material.

As depicted in Figure 3, winter ice cover and ice jams can significantly alter the river bed. Based upon field observations of ice jam formation and frazil ice transport, Sui et al. (2000) proposed that frazil ice formation and riverbed deformation reinforce each other. The authors found:

(a) As an ice jam grows, the riverbed will be scoured. Once an ice jam begins to decrease and diminish, the riverbed material will undergo deposition. During the entire life of an ice jam, patterns of scour and deposition will be repeated.

(b) During ice cover, the decrease in river cross section causes river flow to take a path of least energy consumption. As a result, the riverbed will become deformed.
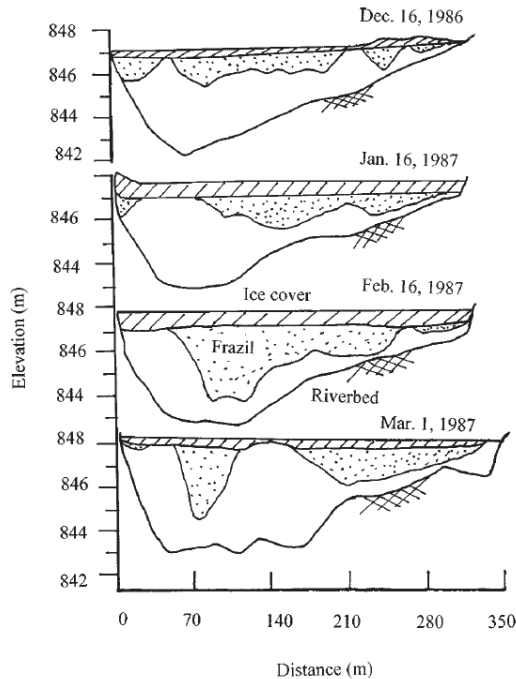
Figure 3. Changes incurred at a cross section of Hequ reach of
the Yellow River during an ice jam period (from Sui et al., 2000).

2.5 Summary and conclusions

With the exception of three studies: Hains (2004), Olsson (2000) and Batuca and Dargahi (1986), the majority of literature to date has focused on pier scour under open channel conditions. Since ice cover imposes an added boundary on flow conditions, the flow pattern and resulting incipient motion of sediment under ice cover is different from that for open channel flow. Generally, the larger the roughness coefficient for ice cover, the greater the near bed flow velocity and the greater the sediment transport around a bridge pier. This study attempts to gain a better understanding of how ice cover is related to local scour around bridge piers by conducting flume experiments as described in the following sections.

3.0 EXPERIMENTAL SETUP: FLUME CONSTRUCTION

3.1 Background

There is no hydraulic laboratory at UNBC and securing use of a hydraulic flume at another institution was not possible. As a result a flume was built at UNBC's Quesnel River Research Centre (QRRC).

Prior to commencing construction a survey was conducted of the flume literature to investigate present flume configurations and set-ups in hydraulic laboratories around the world. To the author's knowledge there are very few articles in the literature that review theoretical and experimental considerations for flume design (Ettema and Muste, 2004; Nowell and Jumars, 1987). The most extensive review by Nowell and Jumars (1987), concludes that no single flume design is applicable for all studies. Small flumes will have a smaller range in flow depths and discharge while larger flumes will have greater work and construction costs along with larger ranges in hydraulic parameters. Upon further investigation of the literature, it was found that the majority of hydraulic flumes are located indoors, have an average length of 20-30 m (or less) and an average width of 0.6 m. It is by these standards in which the flume constructed for this research was classified as a large scale flume. The following is details of the construction process.

3.2 Flume construction

The research centre has a number of outdoor fish rearing channels that are currently set up as flow-through systems. During my first field season in 2011, a fish rearing channel was converted into a hydraulic flume. The water source for the flume is a well situated uphill of the flume allowing for a gravity operated system. The well water runs through an aeration

tower prior to flowing downhill into the flume channel. The aeration tower's purpose is to oxygenate the water for fish rearing. Since the flume water originates from groundwater the water temperature in the flume ranged from 8.6-10.4 degrees Celsius. This is an important aspect of the flume as it resides outdoors and was operated during the summer, fall and early winter months.

The flume channel (original salmon spawning channel) is 80 m long, 2 m wide, 1.3 m deep and is located outside. Since the flume is outside exposed to the elements, a roof 40 m in length was constructed to cover the channel downstream from the weir (Figure 4a). The roof frame was constructed out of lumber and covered with greenhouse grade poly. Viewing windows were built by removing two 4 m sections of concrete wall and replaced with 6 mm thick Lexan Margard polycarbonate (Figure 4b). The viewing windows were framed with fir and cedar so the frame would expand and contract with the variable water pressure exerted on it (Figure 4c). The flume floor and viewing windows were sealed with industrial marine silicone and allowed to cure for 2 weeks. Two enclosed viewing buildings (Figure 4d) were also constructed so that the flume experiments could be viewed while being protected from outside weather elements. The viewing buildings were partially sunken into the ground to allow for viewing of the flume floor. The building foundations were constructed out of wood and lined with gravel to allow for drainage. Heaters were placed in the viewing buildings to maintain adequate temperatures for running pumps, computers and flow meters. Power was supplied to the flume via extension cords from nearby power outlets. In order to obtain an adequate range in flow velocity, three channel valves were diverted into the flume. A weir was constructed in the middle of the channel at 40 m to create a head tank (Figure 4f). A debris screen was installed prior to the weir in the head tank to control outside leaf debris from

entering the flow. Downstream from the weir a flow diffuser was installed in order to decrease the flow turbulence prior to the first sandbox (Figure 4e). The channel bed downstream of the weir was raised by 0.30 m, in order to create two sand boxes. This was done by constructing a plywood framed floor that was sanded and sealed with two sand box openings. The flume floor in front of each viewing window was a sandbox area measuring 5 m in length and 2 m in width. An adjustable tailgate was also installed at the end of the flume channel so the water depth could be altered. A schematic diagram of the flume with given dimensions is presented in Figure 5 and Figure 6.

Figure 4. (a) Construction of flume roof, (b) Viewing window and frame, (c) Concrete wall removal and frame for viewing window, (d) Enclosed viewing platform, (e) Flow diffuser, and (f) Flume head tank.

21
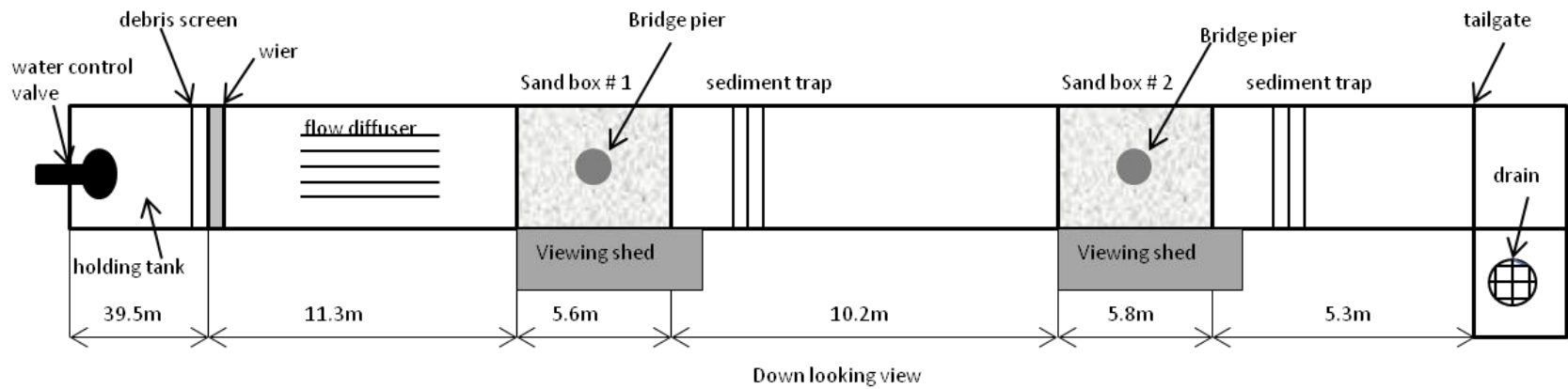
Figure 5. Schematic overhead view of flume with exact construction dimensions
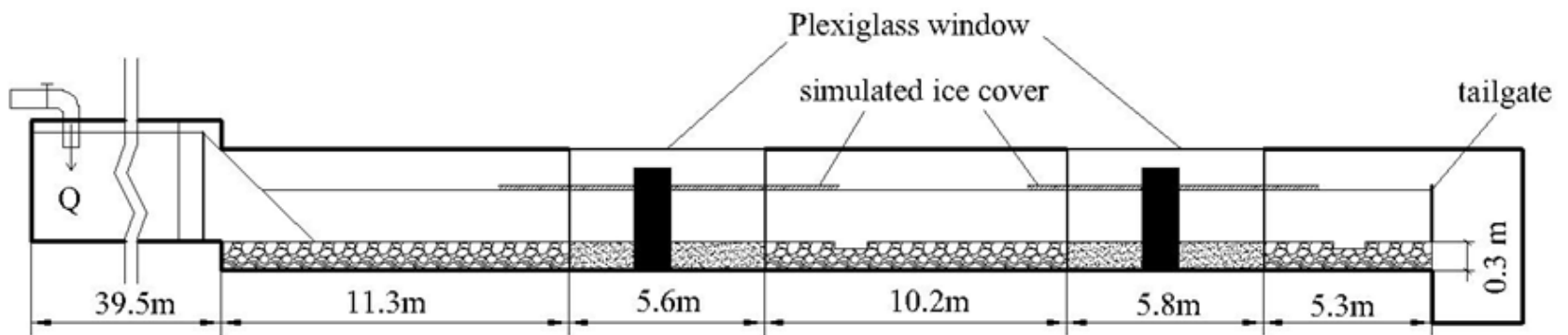
Figure 6. Side view of flume with exact dimensions.

3.3 Experimental runs

The main objective of this thesis is to investigate variables that affect pier scour depth, namely: channel cover, sediment grain size (D_{50}), pier width, flow velocity and flow depth. After a search of the flume literature, to my knowledge there is no criteria that researchers follow that indicate minimum number of flume runs, experimental run time or recommendations on selecting sediment grain size and flow velocity. Having never conducted flume experiments prior to this thesis, extensive consideration was given to deciding the experimental design criteria of the flume experiments.

In general, the procedures followed are that of the scientific method to manipulate independent variables (channel cover, grain size, pier size) while observing the dependant variable for change (scour depth). However many external factors influenced how the flume experiments were set up, all of which are summarized in the following sections.

Flume calibration:

Determining the range in flow velocity and water depth for flume experiments was dependant on finding a balance between the water supply system and the flume tailgate configuration. Since the flume is operated by a gravity fed system the discharge is controlled by opening and closing supply valves. The supply valves could only be opened in quarter increments due to the original set up for spawning channels. It was determined that a maximum of 1.25 valves could be opened to supply water to the head tank; any further supply of water would cause the head tank to overflow. Given that a supply of 1.25 valves did not provide sufficient approach velocity for all experiments, an additional valve was supplied to the flume, downstream of the weir, as shown in Figure 7. With a 2.25 valve configuration the

flow velocity was sufficient to operate the flume with up to a 20 cm tailgate setting. After completing water valve and tailgate testing, the upstream and downstream sandboxes were measured for approach velocity and flow depth under various valve and tailgate settings. Table 1 indicates the minimum and maximum hydraulic conditions under the present flume infrastructure. Considering the channel conditions in Table 1 along with using two pier sizes, it was decided that experiments would be completed in the upper and lower sandboxes in order to capture different flow depths and velocities. As a result of the flume tests it was concluded that six experimental runs could be completed for each channel cover incorporating both pier sizes. This resulted in 18 experimental runs per sediment type as outlined in Table 2.
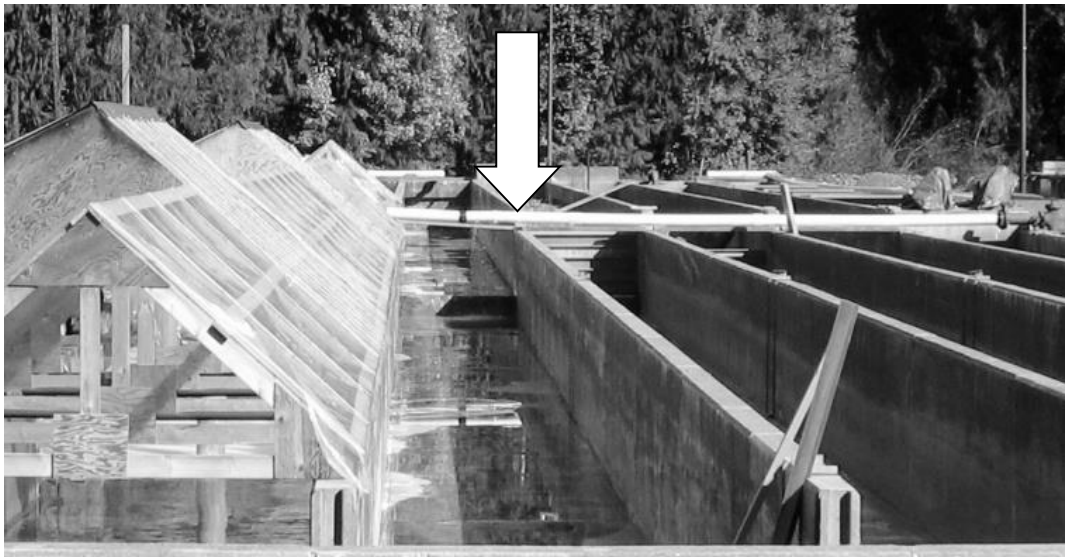
Figure 7. View of flume showing second valve configuration with white pipe entering flume roof just downstream of weir, white arrow indicates white pipe.

Table 1. Measured velocity and stage resulting from various valve and tailgate configurations. Configuration one and four were chosen for experimental conditions. Note: testing was also undertaken using three tailgates (0.30 m) and velocity was not sufficient for incipient motion to occur. In addition under the two tailgate configuration the small pier was always placed in the upstream sandbox since under such channel conditions in the downstream window no scour/incipient motion occurred.

Config-uration	# valves	# tailgates	Upstream sandbox		Downstream sandbox	
			stage (cm)	velocity (cm/s)	stage (cm)	velocity (cm/s)
1	1.25	1	10	23	13	20
2	1.25	2	21	12 * velocity too small for incipient motion	26	11 *velocity too small for incipient motion
3	2.25	1	10	36 *velocity too large leading to live bed scour	13	33 *velocity too large leading to live bed scour
4	2.25	2	21	25 *small pier only	26	23 *large pier only

Table 2. Example of experimental flume schedule for one sediment type.

Run #	D_{50} (mm)	Cover	Position in flume	# valves	# tailgates	Pier width (cm)
1	0.58	open channel	upstream	1.25	1	11
2	0.58	open channel	upstream	2.25	2	11
3	0.58	open channel	downstream	1.25	1	11
4	0.58	open channel	upstream	1.25	1	22
5	0.58	open channel	downstream	2.25	2	22
6	0.58	open channel	downstream	1.25	1	22
7	0.58	smooth ice	upstream	1.25	1	11
8	0.58	smooth ice	upstream	2.25	2	11
9	0.58	smooth ice	downstream	1.25	1	11
10	0.58	smooth ice	upstream	1.25	1	22
11	0.58	smooth ice	downstream	2.25	2	22
12	0.58	smooth ice	downstream	1.25	1	22
13	0.58	rough ice	upstream	1.25	1	11
14	0.58	rough ice	upstream	2.25	2	11
15	0.58	rough ice	downstream	1.25	1	11
16	0.58	rough ice	upstream	1.25	1	22
17	0.58	rough ice	downstream	2.25	2	22
18	0.58	rough ice	downstream	1.25	1	22

3.4 Experimental simulation time

An important factor that was considered in the experimental design was the time required for equilibrium scour depth to be reached. Upon review of pier scour studies in the literature, it was found that the subject of equilibrium scour is either (a) not addressed or spoken of in the paper at all, (b) defined by visual observation, (c) defined by a ratio of change over time or (d) determined that equilibrium scour could not be reached under the experimental conditions. One of the first studies to define equilibrium scour was Ettema's PhD thesis on bridge pier scour (1980): the time to equilibrium scour was defined as the time at which no more than 1 mm of incremental scour occurred within a timeframe of 4 hours. Most often equilibrium scour is defined through visual observation and a ratio of change over time (an overview of pier scour studies is provided in Table 3 along with equilibrium scour definitions). Given that every flume is different in dimension, discharge and sediment type it makes sense that equilibrium scour is a difficult topic to define. That being said since the influence of ice cover on pier scour is the main topic of this thesis, it is important that equilibrium scour be addressed.

During the testing/calibration phase of flume experiments (described under section 3.3 above) piers were placed in the sandbox and the scour hole was visually monitored at hourly increments. The scour hole test runs were monitored at the highest velocity configurations along with the highest depth configurations to ensure the maximum scour conditions would be obtained. The flume was typically started at 8 am and monitored hourly for changes in scour depth. After a period of 4 hours no change in scour depth was observed. After a period of 6 hours an armour layer had developed in the scour hole. The flume was run for 24 hours and still no change in scour depth was observed. At such time the experimental test results were

discussed with Dr. Sui (UNBC), and it was decided that flume experiments should last at least 20 hours to ensure the equilibrium scour had been reached. After discussion with the research centre staff it was decided that logistically the flume could run continuously throughout the night allowing for one simulation per 24 hour period. Providing photographic evidence of equilibrium scour tests proved difficult due to water ripples (Figure 8). Also, when looking through the viewing window at the scour hole, photographs at any angle were unable to capture inside the scour hole Figure 9.

Table 3. Summary of literature standards regarding the definition of equilibrium scour depth. Channel width is indicated by B.

Study	Flume width (m)	Flume length (m)	Number of runs	Length of runs (hrs)	Parameter of measure	Time for equilibrium scour depth addressed
Acharya (2011)	0.6	12.2	7	24	Spur dyke scour	Yes, decided 24hrs upon visual observation
Babaeyan-Koopaei and Valentine (1999)	2.5	22	12	7-8	Pier scour	No significant change after 3-4 hours so experiments stopped after 7-8 hours
Zhao et al. (2010)	4	45	28	2.35-4.5	Pier scour	Equilibrium scour reached when mean bed level change rate at front of cylinder was less than 0.03B per hour
Raikar and Dey (2005)	0.6	12	40	18-36	Pier scour	Visual observation
Sheppard et al. (2004)	6.1	38.4	14	41-616	Pier scour	Experiments stopped when change in scour depth did not exceed 0.05B during 24 hour period (proposed by Melville and Chiew, 1999).

Figure 8. Aug 26, 2012, 2:32pm flume testing. Water ripples did not allow for down facing photographs of the scour hole.
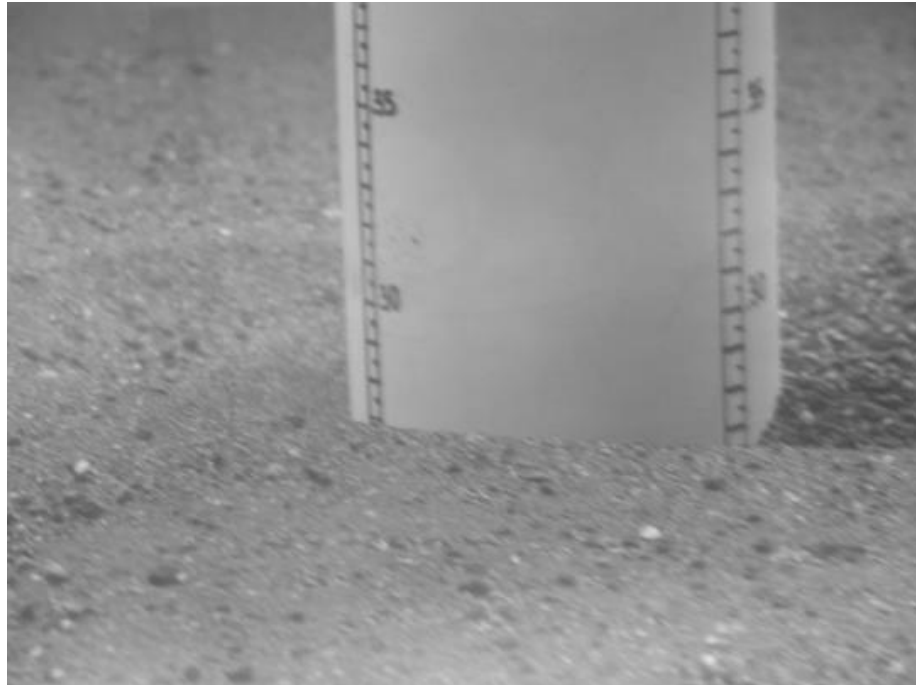
Figure 9. August 27, 2012, 3:35 pm, side angle photograph taken during flume testing, photograph inside scour hole was not practical due to flume design.

3.5 Flume sediment

Since the flume is a large scale flume, each sandbox required a minimum of 3 m^3 of sediment to sufficiently fill the recessed area. During transport in and out of the flume sediment was lost therefore it was standard to order 4 m^3 for each sandbox equalling a total of 8 m^3 of sand for each set of experimental runs. Given that 8 m^3 of sand is the size of an entire dump truck load (Figure 10), it was unrealistic and beyond the budget of this thesis to use manufactured engineering sand. Additionally, the objective of this thesis was to investigate scour depth under non-uniform sediment. Therefore landscape sand was used for flume experiments. All known sediment quarries within a 500 km radius of the research station were contacted. Sand samples were collected from the quarries, oven dried, sieved and median particle size (D_{50}) was calculated. The mason, concrete and bedding mix sand types were selected, with D_{50} = 0.47 mm, 0.58 mm, 0.50 mm, respectively (Table 4 and Figure 12). This selection was based upon the fact that the mason, concrete and bedding sand were the three most common sands mined from the surrounding quarries. In one instance, an alternative variety of bedding sand was sampled; however with a D_{50} of 0.18 mm it was too small for the flume experiments as live bed scour would occur. Given that three sand types were selected with 18 flume experiments per sand type, it was decided that a total of 54 flume runs were required for sufficient comparison between channel covers and sediment types. Between experiment sets, sand was manually moved in and out of both sandboxes (Figure 11).

Figure 10. Landscape sand sample that was used in flume.

Figure 11. Sand being shoveled from sandbox # 1.

Table 4. Particle size distribution of sands used during flume experiments.

	Mason sand (mm)	Concrete sand (mm)	Bedding sand mix (mm)
D_{10}	0.19	0.21	0.22
D_{16}	0.23	0.23	0.24
D_{20}	0.25	0.31	0.27
D_{30}	0.32	0.39	0.33
D_{40}	0.39	0.48	0.41
D_{50}	**0.47**	**0.58**	**0.50**
D_{60}	0.54	0.70	0.57
D_{70}	0.60	1.00	0.73
D_{80}	0.70	1.58	1.20
D_{84}	0.77	1.90	1.57
D_{90}	0.97	2.60	2.18
D_{99}	4.00	4.00	4.00
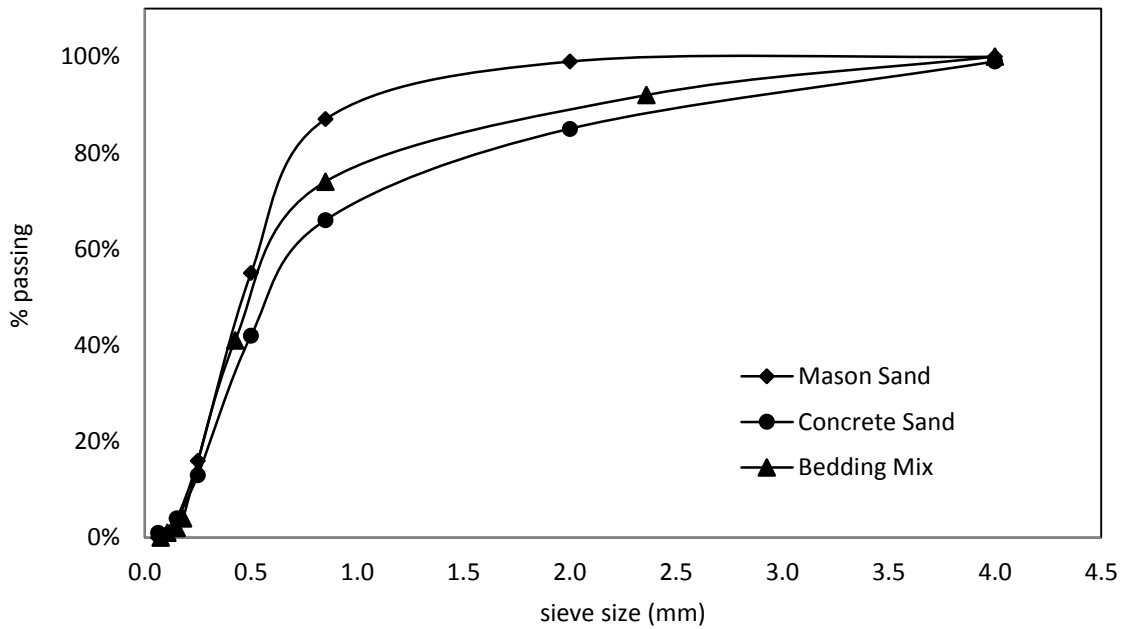
Figure 12. Particle size distribution of sediments used for flume experiments.

Variability of the three materials:

The Unified Soil Classification System along with sediment engineering textbooks typically regard soil as uniform when the coefficient of uniformity, equation 3.1, is less than 4 (Assaad et al., 2004). Additionally, if studies are investigating sand for more industrial application then it seems that a higher value of uniformity is also accepted. For example, Olufayo et al. (2010) use a uniformity of less than 5 to classify sand as uniform in laboratory experiments studying sand water storage systems for weir height classifications.

In the flume literature the geometric standard deviation, equation 3.2, is primarily used when classifying sediments as uniform or non-uniform. As described by Hoffmans and Verhejj (1997) sediment gradation is typically characterized using the geometric standard deviation (σ_g); for natural river sand the σ_g is approximately 1.8 and for uniform sand the σ_g is approximately 1.3. The standard deviation, coefficient of uniformity and geometric mean were calculated for the three sands used in this thesis (Table 5). Table 6 is a summary of standard deviation values found in the flume literature along with how the authors classified the sediment in each flume experiment. Based upon the values and conclusions of Table 6, the geometric standard deviation value of 1.83, 2.87, and 2.56 were used to classify the three sediments used in this thesis as non-uniform.

$$\text{Coefficient of uniformity (Allen Hazen, 1911)} \quad C_u = \frac{D_{60}}{D_{10}} \qquad\qquad 3.1$$

$$\text{Geometric standard deviation} \quad \sigma_g = \sqrt{D_{84}/D_{16}} \qquad\qquad 3.2$$

$$\text{Geometric mean } D_g = \sqrt{D_{84}D_{16}} \qquad\qquad 3.3$$

Table 5. Summary of geometric mean (D_g), standard deviation ($\boldsymbol{\sigma_g}$) and uniformity coefficient ($\boldsymbol{C_u}$) for the three sands used in flume experiments.

	Mason sand $D_{50} = 0.47$ mm	Concrete sand $D_{50} = 0.58$ mm	Bedding sand mix, $D_{50} = 0.50$ mm
D_g	0.42	0.66	0.61
σ_g	1.83	2.87	2.56
C_u	2.84	3.33	2.59

Table 6. Summary of literature values pertaining to geometric standard deviation of sediments used in flume experiments.

Author	D_{50} (mm)	σ_g	Classification of sediment as stated by authors
Muste et al. (2000)	0.25	1.4	Uniform sand
Raikar and Dey (2005)	4.10-14.25	>1.4	Non-uniform gravel
Oliveto and Hager (2002)	3.1	2.15	Relatively non-uniform
	1.2	1.80	Medium sediment non-uniformity
Ataie-Ashtiani and Aslani-Kordkandi (2013)	0.71	1.2	Uniform sand
Sheppard et al. (2004)	0.22-2.90	1.2-1.5	Near uniform sediment
Alabi (2006)	0.53	1.23	Uniform sand
Barbhuiya and Dey (2003)	0.52	1.21	Uniform sand
Link et al. (2008)	0.26	1.37	Uniform sand

Measure of sediment shape:

There are three main ways to express sediment shape: (1) roundness- a measure of the sharpness of the corners of the sediment grain, (2) sphericity – a measure of the degree of similarity between the grain and a perfect sphere, and (3) form – the overall appearance of the particle. A common measure of shape is the Corey Shape factor (*SF*) given by:

$$SF = \frac{c}{\sqrt{ab}}$$

3.4

Where '*a*' is the longest sediment axis, '*b*' is the median sediment axis and '*c*' is the shortest sediment axis. A spherical particle will have a shape factor of 1.0 while natural sands have a shape factor of 0.7 (Garcia, 2008). The shape factor is important as it relates to the fall velocity and transport of a particle. The majority of sediment transport equations were developed by studying uniform bed materials.

In the flume literature the incipient motion of sediment is often studied through the dimensionless shear stress, shear Reynolds number and shear velocity. These parameters all require a measure of the sediment diameter. Since a single grain size diameter cannot be calculated for the three sediment examples used in this research (as they are non-uniform) it is standard practice to use the D_{50} to represent the particle size D. The use of D_{50} in place of the particle size D for non-uniform sediments was originally studied and proven by Yang (2003) and can be found in the literature regarding flume experiments using non-uniform sand (Bong, 2012; Wang et al., 2008). It is proposed that the sediment D_{50} be used in all equations requiring a measure of sediment diameter.

3.6 Flume scaling and pier selection

Prior to commencing construction, a survey of the flume literature was conducted to investigate present flume configurations and set-ups in hydraulic laboratories around the world. The lengths, widths, shape and pump capacities of flumes all vary as it depends on the purpose for which the flume is being used. However, over the years there have been some standard scaling guidelines published in the flume literature that were used in designing/developing the present study. Table 7 is a summary table of the standard scaling guidelines presented in the literature along with dimensions of the current study flume. The

flume constructed for this thesis falls within the current scaling guidelines taken from the literature with the exception of flow depth to pier width. Further information which addresses this scaling issue can be found in the critical analysis section of this thesis, Section 6.1.1.

Bridge piers were constructed out of PVC plumbing pipe and were spherical in shape. Pier widths were determined by calculating the 5 and 10 percent of the flume width, resulting in pier widths of 11 cm and 22 cm. The ratio of channels width to pier diameter should be greater than 6.5 in order to avoid effects from the channel sidewall (Ataie-Ashtiani and Aslani-Kordkandi, 2013). Piers were placed in the centre of the sandbox and attached to the flume floor (Figure 13).
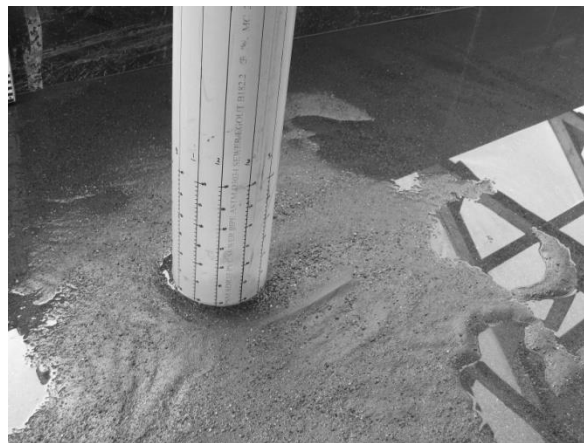
Figure 13. 22 cm PVC pier installed in sandbox.

Table 7. Summary of flume scaling guidelines and comparison to scaling ratios calculated from current study flume dimensions. Present flume ratios are on the left side of table with literature guidelines on right side of table.

Present flume dimensions	Width: 200cm Pier#1: 11cm Pier#2: 22cm D_{50}: 0.47 mm, 0.50 mm , 0.58 mm smallest flow depth: 10cm largest flow depth 26cm			
ratio Channel width : pier width	200cm:11cm Ratio: 18:1		Scaling guidelines from literature	
			Ataie-Ashtiani and Aslani-Kordkandi, 2013: The ratio of the channel width to pier width should be greater than 6.5 so to ensure that the flume wall has no effect on scouring.	
	200cm:22cm Ratio: 9:1		Alabi, 2006: For live bed scour the flume width should be at minimum 10 times the pier width for scour depths not to be reduced due to bed features being modified as they propagate through constriction. Shen and Schneider, 1969: the width of an experimental flume should be at least 8 times the pier size for clear-water scour conditions so that sidewall effects are minimized.	
ratio Flow depth : pier width	10cm:11cm Ratio: 1:1.1	10cm:22cm Ratio: 1:2.2	Scaling guidelines from literature	
	26cm:22cm Ratio: 1:1.2	26cm:11cm Ratio: 1:2.4	Ataie-Ashtiani and Aslani-Kordkandi, 2013: The ratio of the flow depth to pier width should be greater than 4 so the scour depth is independent of the flow depth.	
ratio pier width : D_{50}				Scaling guidelines from literature
	11cm: 0.47 Ratio: 1:23	11cm: 0.50 Ratio: 1:22	11cm: 0.58 Ratio: 1:19	Ataie-Ashtiani and Aslani-Kordkandi, 2013: The ratio of the pier diameter to the D_{50} needs to be greater than 50 so the size of sediment particles has no influence on scour depth.
	22cm: 0.47 Ratio: 1:47	22cm: 0.50 Ratio: 1:44	22cm: 0.58 Ratio: 1:38	Melville and Coleman, 2000: defined sediment coarseness as the ratio of pier width (b) to the mean grain size (D_{50}), b/D_{50}, the local scour is affected by sediment size as long as the ratio b/D_{50}<50. If b/D_{50}>50 the local scour is not influenced by the sediment coarseness. For b/D_{50} < 8, the individual grains are so large relative to the pier that scour is mainly due to entrainment at the flanks of the pier (Melville and Coleman, 2000).

			Ettema, 1980: found that grain size does not affect the scour depth if the pier width to grain size ratio exceeds the value of 50.
ratio Flume width : water depth	200cm:10 cm Ratio: 20:1	200cm:26 cm Ratio: 7.7:1	Scaling guidelines from literature
			Nowell and Jumars, 1987: a minimum value for the width to depth ratio is 5 in order to reduce boundary wall effects and effects of secondary circulation. "It is wise to try and get a ratio of 10:1, but designing and operating flumes is full of compromises between conflicting dimensionless groups and pragmatic limitations such as pump capacity" (p.100)

3.7 Channel cover

Flume simulations were conducted under open channel, smooth ice and rough ice conditions. Ice cover was created using standard 1.2 m x 2.4 m (4 x 8 foot) Styrofoam panels purchased at a local hardware store. Styrofoam density was 0.024 g/cm^3. The Styrofoam was placed inside the flume so that it floated on top of the water during simulation (Figure 14A). Rough ice cover was simulated by attaching small Styrofoam cubes to the underside of Styrofoam panels using toothpicks (Figure 14B). Styrofoam cubes were 2.5 cm x 2.5 cm x 2.5 cm in dimension and spaced 3 cm apart.
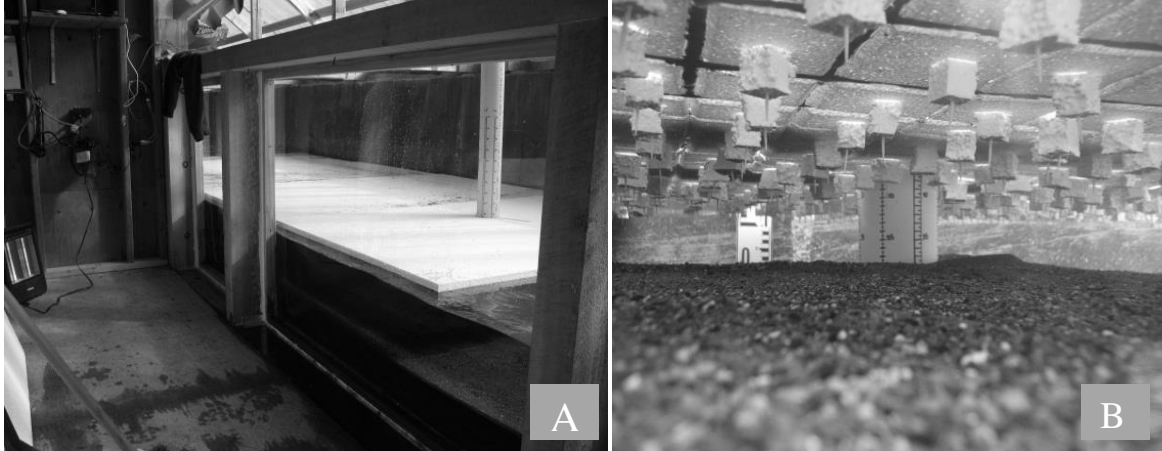
Figure 14. A: Styrofoam floating around the pier inside flume. B: Styrofoam cubes attached to create a rough ice cover.

3.8 Measuring flow velocity

Approach velocity and flow temperature were measured using a 2D flow meter by Sontek Incorporated, San Diego, USA (Figure 15, Figure 16). The Sontek IQ is rectangular in shape and is designed to mount on the channel bottom. The impact to flow is minimal as the Sontek IQ is sleek in shape. For this research, a constant approach velocity is required to ensure that the flume hydraulics were constant over a 24 hour period. A staff gauge was also installed in each sand box to manually verify water depth. The scour hole flow field was measured using a 10-Mhz acoustic Doppler velocimeter (ADV) by Sontek (Figure 17). The sampling volume of the 10-Mhz ADV is 10 cm from the sensor head. The ADV operates on the principal of a Doppler shift, measuring the phase change when the acoustic signal reflects off particles in the flow. The scour hole flow field was measured at 1 cm increments for the depth of the scour hole in front of the bridge pier for each experimental run (Figure 18 and 19). For ice covered experiments, removable flaps were cut in the Styrofoam to allow placement of the ADV for flow field measurements (Figure 18).
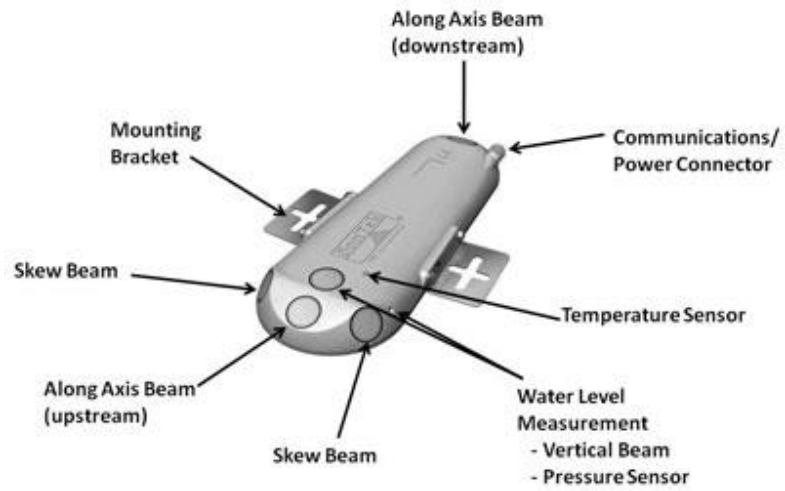
Figure 15. Diagram of 2D flow meter Sontek IQ (Sontek, 2014).

Figure 16. Sontek IQ mounted to flume floor.
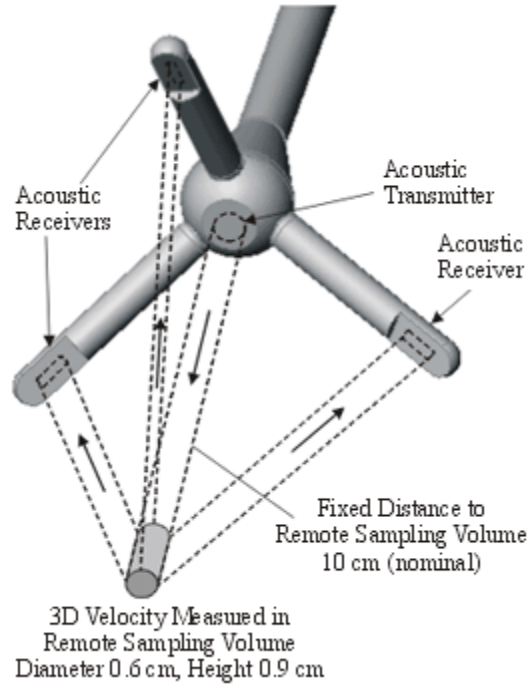
Figure 17. Sontek 10 MHz 3-dimensional ADV (Sontek, 2014).

Figure 18. Use of Sontek 10-Mhz ADV to measure scour hole velocity under ice cover.
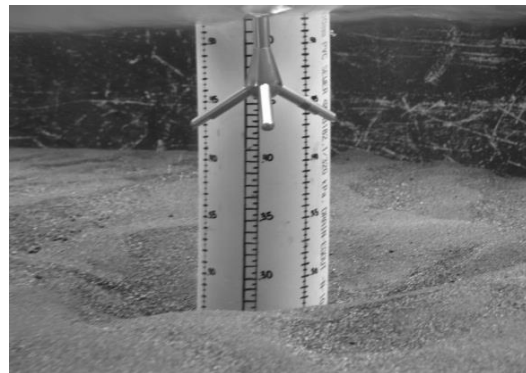
Figure 19. Sensor head of Sontek ADV measuring velocity inside scour hole.   .

40

3.9 Scour hole measurements

Upon completion of each experiment the flume was drained and the scour hole was contoured using manual calipers. Contour measurements were taken at 0.5-1 cm increments at preset numbered measuring points along each bridge pier (Figure 20). Three-dimensional contour data were recorded and entered into Surfer plotting software (Golden Software Incorporated, Golden, USA) and scour plots were generated.
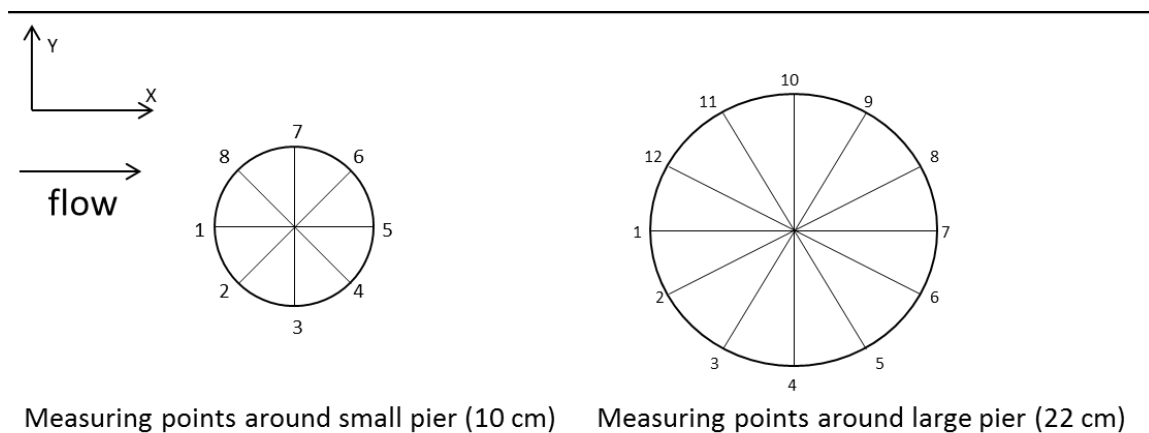
Figure 20. Numbered measuring points drawn on the outside of the small bridge pier (10 cm width) and large bridge pier (22 cm width) for scour hole contour points of reference.

3.10 Armour layer sampling

After each experimental run was completed, the flume was drained, the scour hole was contoured and samples of the armour layer were taken. The following section describes the methodology followed in sampling the armour layer. Armour layer thickness typically extends from the bed surface to the bottom of the largest (D_{max}) surface particle or the most commonly occurring particle size (D_{dom}). Here D_{dom} is approximated to equal D_{90} (Bunte and Abt, 2001). When sampling the armour layer, care should be taken to ensure the entire depth of the armour layer is considered otherwise finer particles are not sampled leading to a distribution that is

41

incorrectly large in diameter. The sampling methodology followed for collecting armour samples was taken from Bunte and Abt (2001). To my knowledge, the authors provide the most extensive review to date of armour layer sampling protocols. The following is a brief excerpt from their report (p.189):

Armour thickness is approximated by:

a) the c-axis of the D_{max} particle of the surface (Ettema, 1984);

b) the b-axis of the D_{max} particle size (Diplas and Fripp, 1992);

c) two times the b-axis of the D_{90} surface particle size (Simons and Sentürk 1992, p.654);

d) the embedded depth of the reach-average D_{dom} particle size;

e) the embedded depth of the local D_{max} particle size.

The five prediction criteria listed above result in different armour-layer depths when applied to the same deposit.

This is demonstrated in Figure 21. Since measuring the embedded depth of the armour layer was difficult due to the small scale of the sediments, the protocol followed under points (d) and (e) above was not applied. As the sediment was non-uniform the a, b and c-axis measurements were not used. Instead, two times the D_{90} of each sediment was used as a baseline for determining armour depth. The D_{90} values were 2.18 mm, 2.60 mm and 0.97 mm. The task of sampling the armour layer to the exact depth of two times the D_{90} values was virtually impossible. Therefore, the armour samples were taken from the top 5 mm of each scour hole (small tick lines on the pier represent 5 mm intervals), using the ruler drawn on the pier for a visual guide for sampling depth (Figure 22).
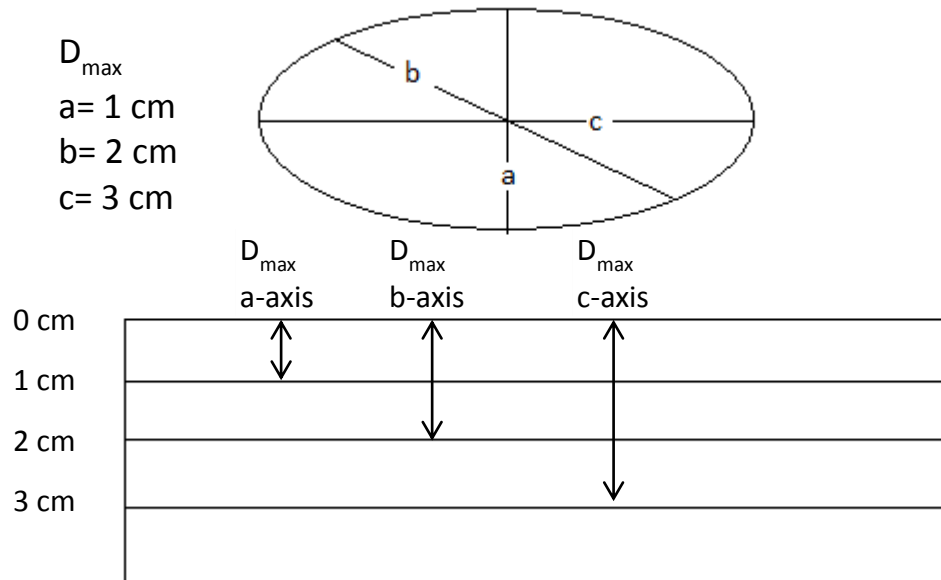
Figure 21. Differences in armour-layer thickness determined for the same deposit using various prediction criteria.
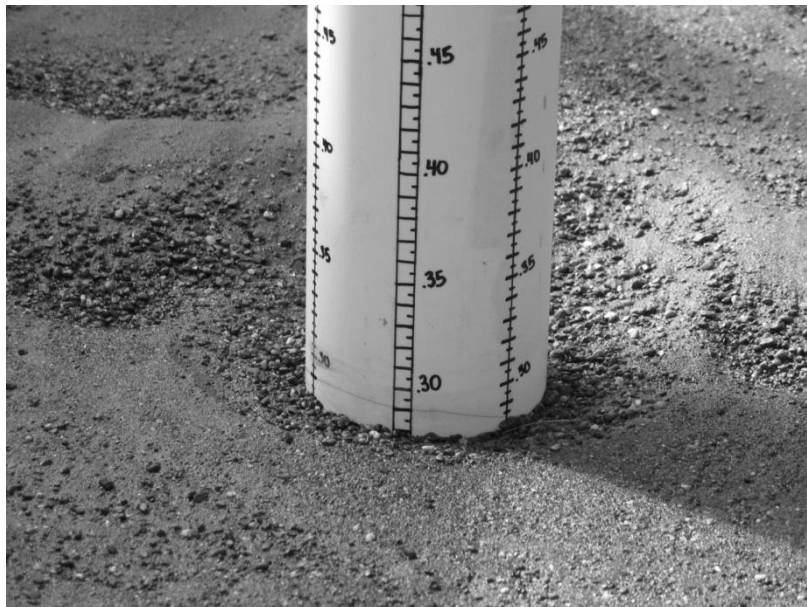
Figure 22. Example of armor layer in scour hole after experimental run # 1, September 22, 2012.

3.11 Flume operation procedures

Flume experiments were conducted for (1) open-flow conditions, (2) smooth ice conditions and (3) rough ice cover. The flume was operated by the following steps:

- position bridge pier in flume, level bed surface, set tail gate, place Styrofoam for ice covered runs, fill with water, start Sontek IQ. Note: for each simulation the flume was filled with water slowly so to prevent initial scour from occurring. This process would take approximately 20 minutes.

- maintain uniform water flow for duration of simulation time (20 hours).

- after 20 hours measure scour hole velocity profile in front of pier using Sontek ADV. Note: during all velocity measurements no person was standing in the flume, but rather a wooden platform was suspended above the water so measurements could be taken while not impacting the water flow.

- stop water, drain flume, download Sontek IQ data, take photographs, manually contour the scour hole with calipers and collect sediment samples from armour layer.

3.12 Flume data and error analysis

The data set generated from the 54 flume experiments is large and a number of software programs were used for data analysis. The following is a brief summary of the software and quality assurance procedures taken.

Sontek ADV: scour hole velocity and approach velocity were analyzed using the WinADV software supplied by Sontek. Velocity data were filtered for correlation, signal to noise ratio

and data spikes. Average values for each sampling time were calculated. Velocity data were filtered for correlations values above 70 (SonTek, 1997). Low correlation values indicate the output data was dominated by noise and no coherent velocity signals was used in velocity calculations (Khorsandi et al. 2012). The values of the correlation coefficient is a direct indication of the random errors produced by Doppler noise for the velocity data (Khorsandi et al. 2012). Once ADV data is filtered for correlation, signal to noise ratios and data spikes, it is assumed that velocity measurements are accurate within 0.25 cm/s (SonTek, 2014).

Sontek IQ: approach velocity for each sandbox was calculated using the IQ software statistics module. According to manufacturer specifications, (SonTek, 2014), the SonTek IQ velocity is accurate to within +/- 0.5 cm/s and water depth measurement are accurate to within +/- 0.0003 meters. The measured IQ water level was compared against the recorded staff gauge level for additional quality assurance. The measured IQ water temperature was compared against the ADV measured water temperature and was accurate to within 0.2 degrees Celsius.

Scour contours: since scour contours were manually measured with calipers and a measuring tape, profile measurements were accurate to within 0.01 cm. Contours were manually plotted on graph paper for determination of x, y, z data points. Standard 1 cm x 1 cm graph paper was used therefore transcription of plotted data points was subject to error within 0.01 cm. The Surfer12 plotting software by Golden was used to plot scour contours and calculate scour hole volume and area.

3.13 Summary and conclusions

This study required building a hydraulic flume. Prior to commencing flume construction, a survey was conducted of the flume literature to investigate present flume configurations and set-ups in hydraulic laboratories around the world. It was discovered, similar to conclusions by Nowell and Jumars (1987), that no single flume design was best suited for this study. Design criteria such as pier width, simulation time, equilibrium scour and number of simulations were decided based upon a survey of the literature; other design criteria such as flow velocity and flow depth were governed by the constraints of the flume infrastructure. Overall, flume construction and design allowed for a total of 54 experimental runs that operated within the scaling guidelines presented in the flume literature. The next sections describe results found during the investigation of the impact of ice cover on pier scour.

4.0 RESULTS AND DISCUSSION: VELOCITY AND TURBULENT FLOW FIELDS UNDER OPEN AND ICE COVERED CHANNEL

Given that this research required building a flume, this chapter firstly presents the experimental conditions of the flume. The flow fields, velocity profiles and Reynolds stresses are investigated under open, smooth and rough channel cover.

4.1 Experimental conditions

The following is the experimental conditions under which the flume was operated. As indicated in Table 8, each pier size (11 cm and 22 cm) were tested under two depth ranges, namely one tailgate configuration (9.5-13 cm depth) and two tailgate configurations (21-26 cm depth). Velocity varied slightly (up to 2 cm/s) for each replicate experiment as velocity was controlled by opening and closing gravity fed supply valves. Scour depth was investigated under three channel conditions; open, smooth ice and rough ice cover. Scour depth was also investigated under three sediment sizes; $D_{50} = 0.58$ mm, 0.50 mm, 0.47 mm. A total of 16 flume experiments were completed for each sediment size, examining scour depth under various channel conditions for each grain size.

Table 8. Summary of experimental conditions

Run #	D_{50} (mm)	Cover	Approach velocity (cm/s)	Water level (cm)	Position in flume	Pier width (cm)
1	0.58	open channel	23.2	9.5	upstream	11
2	0.58	open channel	23.7	21	upstream	11
3	0.58	open channel	24.0	13	downstream	11
4	0.58	open channel	23.2	9.7	upstream	22
5	0.58	open channel	21.7	24.4	downstream	22
6	0.58	open channel	21.1	13.3	downstream	22
7	0.58	smooth ice	23.3	9	upstream	11
8	0.58	smooth ice	20.0	21.6	upstream	11
9	0.58	smooth ice	22.6	13.1	downstream	11
10	0.58	smooth ice	23.3	9	upstream	22
11	0.58	smooth ice	22.6	25.6	downstream	22
12	0.58	smooth ice	21.8	13	downstream	22
13	0.58	rough ice	25.0	9.8	upstream	11
14	0.58	rough ice	26.0	20.5	upstream	11
15	0.58	rough ice	18.3	13.5	downstream	11
16	0.58	rough ice	23.5	10	upstream	22
17	0.58	rough ice	25.4	25.5	downstream	22
18	0.58	rough ice	18.2	13.4	downstream	22
19	0.47	open channel	23.5	9.8	upstream	11
20	0.47	open channel	27.1	21.4	upstream	11
21	0.47	open channel	19.4	13	downstream	11
22	0.47	open channel	23.5	9.8	upstream	22
23	0.47	open channel	22.8	24.3	downstream	22
24	0.47	open channel	22.6	13.4	downstream	22
25	0.47	smooth ice	23.3	9.7	upstream	11
26	0.47	smooth ice	23.3	21.5	upstream	11
27	0.47	smooth ice	20.1	9.8	downstream	11
28	0.47	smooth ice	23.3	21.4	upstream	22
29	0.47	smooth ice	24.6	13	downstream	22
30	0.47	smooth ice	22.9	12.9	downstream	22
31	0.47	rough ice	25.1	9.6	upstream	11
32	0.47	rough ice	28.1	25.8	upstream	11
33	0.47	rough ice	21.6	13	downstream	11
34	0.47	rough ice	25.1	12.8	upstream	22
35	0.47	rough ice	24.0	22.0	downstream	22
36	0.47	rough ice	21.6	13.0	downstream	22

37	0.50	open channel	23.2	11.2	upstream	11
38	0.50	open channel	24.1	23.1	upstream	11
39	0.50	open channel	20.5	13.4	downstream	11
40	0.50	open channel	23.2	10	upstream	22
41	0.50	open channel	22.7	21.1	downstream	22
42	0.50	open channel	20.2	13.2	downstream	22
43	0.50	smooth ice	22.0	9.9	upstream	11
44	0.50	smooth ice	23.3	24.6	upstream	11
45	0.50	smooth ice	22.6	13.1	downstream	11
46	0.50	smooth ice	22.0	9.8	upstream	22
47	0.50	smooth ice	22.5	21.6	downstream	22
48	0.50	smooth ice	21.2	13.1	downstream	22
49	0.50	rough ice	22.9	9.8	upstream	11
50	0.50	rough ice	26.0	25.9	upstream	11
51	0.50	rough ice	22.2	13.2	downstream	11
52	0.50	rough ice	22.9	13.0	upstream	22
53	0.50	rough ice	26.3	22.0	downstream	22
54	0.50	rough ice	22.5	13.0	downstream	22

4.2 Flume velocity profiles

The average velocity profiles corresponding to the various experimental conditions (open water, smooth cover and rough cover conditions) are presented in Figure 23. The velocity profiles were measured with the 10 MHz ADV under the two tailgate configuration (21-26 cm flow depth). In Figure 23, the depth of flow on the ordinate axis has been non-dimensionalized (vertical distance from bed/approach flow depth) to allow for comparisons between experiments with slightly different flow depths. The approach flow depth is measured as the vertical distance from the channel bed to the water surface and represented by the letter H (for the remainder of this thesis, H is used to denote the total flow depth or a fractional distance from the stream bed to the ice cover). As the ADV measuring volume is located 10

cm from the probe head, the velocity profile for each channel condition does not extend entirely to the water surface (Figure 23).

The velocity profiles under open channel conditions are logarithmic with flow velocity highest closer to the water surface and lowest near the channel bed (Figure 23). A logarithmic velocity profile is standard for open channel flow. The drag forces exerted on water near the river bed generally account for the decrease in flow velocity for open channel flow. Of note, however, since the ADV operates on the principal of a Doppler shift, it may be inferred that the near bed velocity most likely represents a mixture of both sediment and water velocity. Even though clear water scour was achieved, it is impossible to achieve water velocity only measurements within 1 cm of the bed. This was also noted by Muste et al. (2000).

River ice cover imposes an extra boundary on flow, altering the flow velocity and water level in comparison to open channel flow (Shen and Wang, 1995). For this study, the maximum velocity for both smooth and rough covered conditions is located approximately half way between the channel bed and ice cover (Figure 23). Under all D_{50}s the rough ice cover produced a larger maximum velocity in comparison to smooth ice cover (Table 9). The maximum velocity under rough ice cover is 17-20 percent larger than that under smooth ice conditions (Table 9). Zabilansky et al. (2006) also conducted flume experiments comparing smooth and rough ice cover and found that the maximum velocity for rough ice cover was 20 percent greater than that for smooth ice cover.

The velocity profile under ice conditions depends on the relative roughness of the ice. Under ice cover conditions, the portion of upper flow is mainly influenced by the ice cover resistance while the lower flow is mainly influenced by the channel bed resistance (Sui et al., 2010). The maximum flow is located between the channel bed and ice cover depending on the

relative magnitudes of the ice and bed resistance coefficients. Generally, the maximum flow velocity is closer to the surface with the smallest resistance coefficient. As found by Robert and Tran (2012), Sui et al. (2010) and Wang et al. (2008) it is expected that as the ice resistance increases (from smooth ice to rough ice cover), the maximum flow velocity will move closer to the channel bed. This was also noted by Muste et al. (2000), who measured maximum velocity under smooth cover at approximately 0.8H, while maximum velocity under rough cover was approximately 0.6H. Crance and Frothingham (2008) also found that under rough ice cover the maximum velocity was 2/10[ths] lower than under smooth ice cover.

For this study, the roughness coefficient for rough and smooth ice cover is 0.021 and 0.013 respectively, which are greater than the roughness coefficient for the respective channel bed D_{50}s (Table 10). The location of the maximum velocity for all D_{50}s and ice covers varies from 0.36-0.43H (Table 9). Contrary to previous findings, the maximum velocity for smooth ice cover under D_{50}=0.58 mm is 0.41H which is lower than the maximum velocity for rough ice cover at 0.43H (Table 9). However, under D_{50}=0.50 mm the average maximum velocity under rough ice cover is 0.36H and for smooth ice cover is 0.41H (Table 9). Turbulence and coarse ADV volume measurements may account for the smooth ice cover maximum velocity to occur closer to the channel bed than the rough ice cover maximum velocity (for D_{50}=0.58 mm only).

It is important to note that in a natural river system, the velocity profiles under ice cover would be under constant flux. This is supported by evidence from Crance and Frothingham (2008). The authors found that river flow erodes the ice underside and generally maintains a similar texture/roughness across a stream section. Areas of low discharge had rough ice while areas of high discharge had smoother ice cover. The authors also found that while a cross

section would have a consistent roughness, the texture could change from rough to smooth to

back to rough again on a weekly basis. This is an important consideration when modeling or

estimating velocity under ice cover.

Table 9. Maximum velocity and z/H values represented in Figure 23.

		Maximum velocity (cm/s)	Stage of maximum velocity (z/H)
Open channel		27.1	0.47
Smooth ice cover	$D_{50} = 0.47$ mm	ADV error	ADV error
	$D_{50} = 0.50$ mm	23.3	0.41
	$D_{50} = 0.58$ mm	23.3	0.41
Rough ice cover	$D_{50} = 0.47$ mm	28.0	0.41
	$D_{50} = 0.50$ mm	28.6	0.36
	$D_{50} = 0.58$ mm	29.2	0.43

Table 10. Roughness coefficients for channel material and ice cover. Associated equations used in calculating the roughness coefficient can be found in Chapter 5, Section 5.12.

Channel cover/bed material	Roughness coefficient
Channel $D_{50} = 0.58$ mm	0.0113
Channel $D_{50} = 0.50$ mm	0.0110
Channel $D_{50} = 0.47$ mm	0.0109
Rough ice cover	0.021
Smooth ice cover	0.013
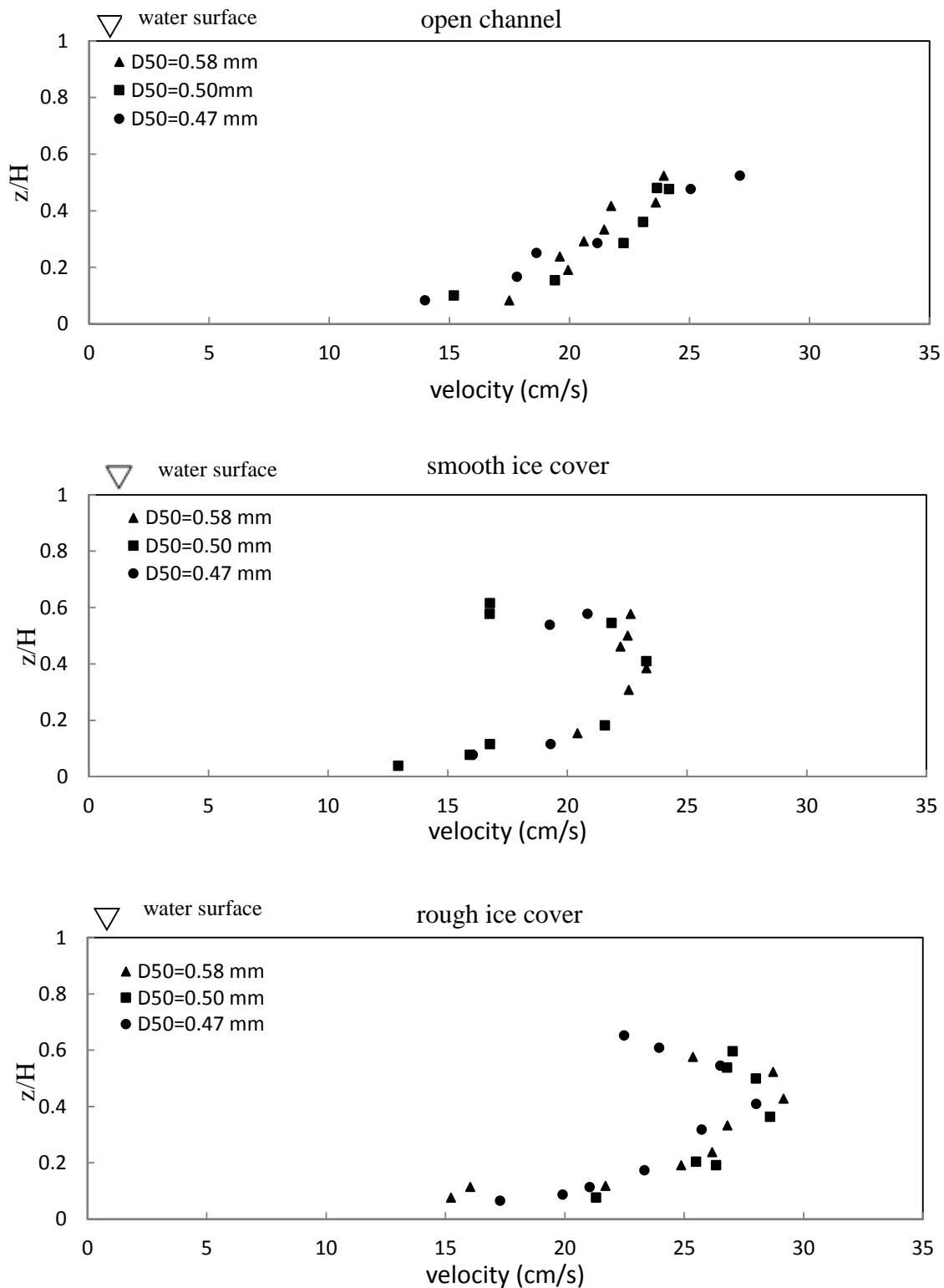
Figure 23. Velocity profiles for D_{50} = 0.58 mm, 0.50 mm, 0.47 mm under open channel, smooth cover and rough cover channel conditions. Velocity profiles were measured with the 10 MHz ADV and presented under the two tailgate configuration (21-26 cm flow depth). ADV measurements are accurate to +/- 0.25 cm/s.

4.3 Flume turbulent intensity

Since an ice cover imposes an added boundary on flow conditions the flow velocity distribution and turbulent intensity is different under an ice covered channel than that of open conditions. As discussed in the previous section, the near bed flow velocity under ice covered conditions is higher than that of open channel conditions. As the near bed velocity increases, the kinetic energy exerted on the bed also increases which can have implications for sediment transport hence why it is being discussed here. The turbulent kinetic energy indicates the energy that is extracted from turbulent eddies and is expressed as (Clifford and French, 1993):

$$\text{TKE} = 0.5(\text{RMS}_x^2 + \text{RMS}_y^2 + \text{RMS}_z^2) \qquad\qquad 4.1$$

The turbulent kinetic energy can be decomposed by examining the turbulent intensities for the streamwise turbulent intensity (RMS_x), the lateral turbulent intensity (RMS_y) and vertical turbulent intensity (RMS_z) components. The turbulence intensity values were determined from the standard deviation of instantaneous velocity fluctuations (RMS or root mean square). The RMS values were calculated based upon the velocity profiles measured in the approach flow section of the flume.

Figure 24 and Figure 25 show the turbulent intensities (RMS) for the streamwise (x) and vertical (z) flow components. The lateral turbulent component (y) was not presented as fluctuations for all measurements did not exhibit any meaningful patterns; this is similar to other studies reporting turbulent intensities (Faruque, 2009; Muste et al., 2000; Robert and Tran, 2012). The turbulent intensities were normalized by the shear velocity in order to make a dimensionless comparison.

As indicated in Figure 24, the streamwise turbulent intensity is a maximum just above the channel bed for rough ice cover and open channel conditions. Muste et al. (2000) suggests that this is due to the increased turbulence of sediment movement near the bed. The turbulent intensity reduces towards the surface for both open and rough cover conditions. Of note, Robert and Tran (2012) reported the streamwise and vertical turbulent intensities for rough cover as maximizing just above the channel bed but also at the water surface. In this study however, measurements were taken to a point 10 cm below the water surface due to the measuring volume of the ADV. In Robert and Tran (2012) they used a micro-ADV which had measuring capabilities of 5 cm below the sensors.
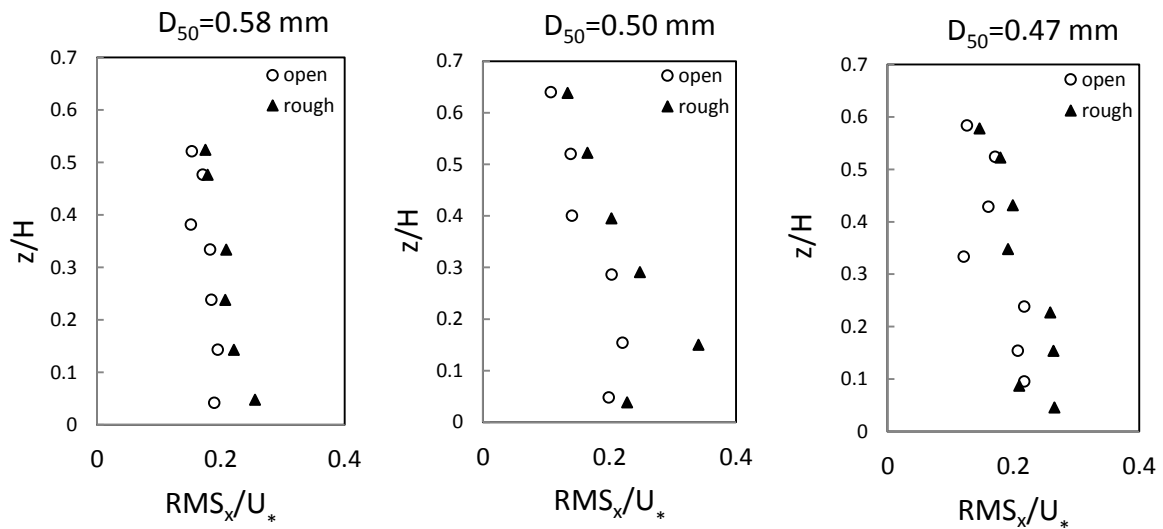
Figure 24. Spatially-averaged profiles of turbulent intensity for the streamwise (x) velocity component, normalized by the shear velocity (U_*), for open water and rough ice cover conditions.
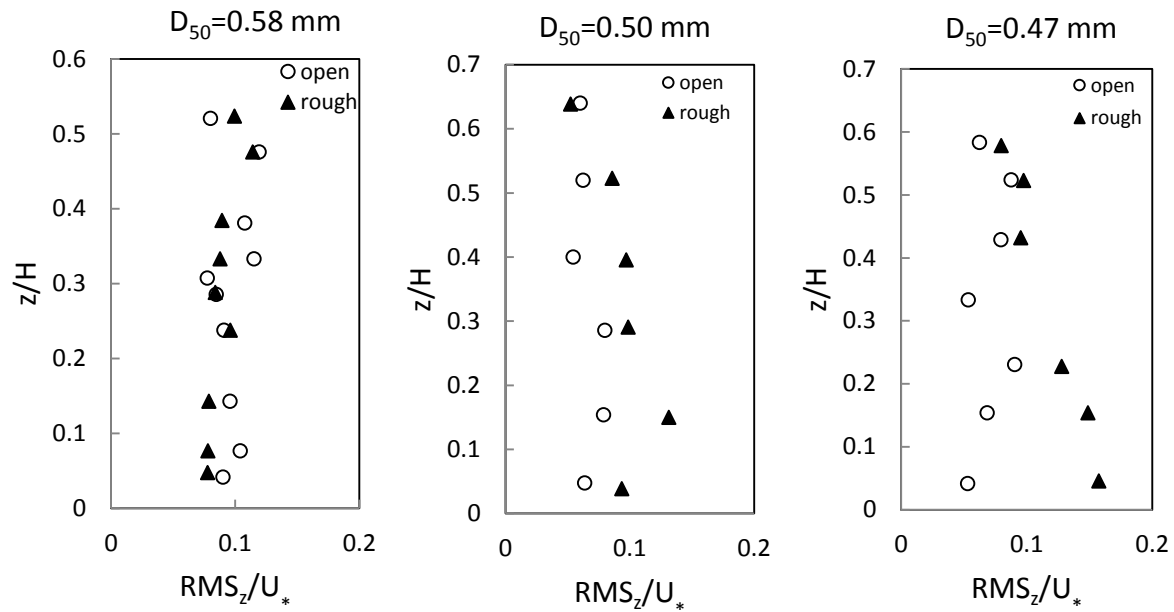
Figure 25. Spatially-averaged profiles of turbulent intensity for the vertical (z) velocity component, normalized by the shear velocity (U_*), for open water and rough ice cover.

The streamwise turbulent intensities for the rough flow were greater than those for open channel conditions (Figure 24). Faruque (2009) also found that streamwise turbulent intensities for rough ice cover were greater than those for open channel conditions. The vertical turbulent intensities are approximately one half than the streamwise turbulent intensities (Figure 24 and Figure 25). This indicates the flow is anisotrophic (directionally dependant as opposed to isotrophic- which would indicate identical measures of flow in all directions). This indicates that the turbulence is mainly associated with fluctuations in the streamwise velocity (Muste et al., 2000). There is no significant observed effect between open channel and smooth cover on both the streamwise and vertical turbulent intensity for the entire flow profile (Figure 26). For this reason, data points for each D_{50} were plotted on one graph rather than separated out.

The turbulent intensities are of interest when considering sediment transport as the strength of the turbulence will affect sediment suspension (Muste et al., 2000). A greater turbulence and therefore more kinetic energy under rough ice cover infer that there is a greater capacity for sediment transport to occur.

Flow reversal occurs in the wake region downstream of the pier which can also contribute to the decrease in sediment ridge size. Also, the turbulent kinetic energy behind the pier is isotropic and stronger than the turbulence upstream of the cylinder (Graf and Istiarto, 2003).
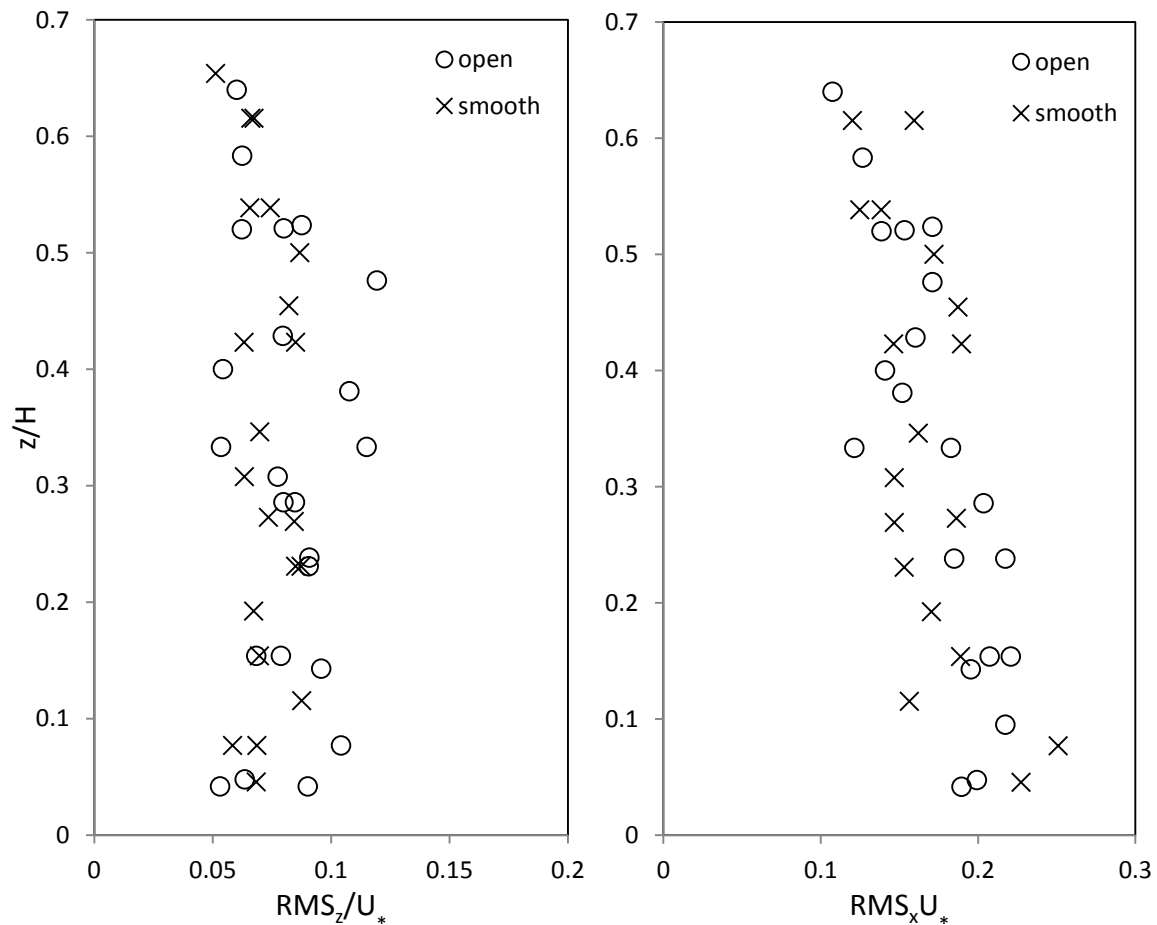
Figure 26. Spatially-averaged profiles of turbulent intensity for the vertical (z) and streamwise (x) velocity component, normalized by the shear velocity (U_*), for open water and smooth ice cover conditions.

4.4 Reynolds stresses

The Reynolds stress is defined as

$$-\overline{u_x u_z} = -\frac{1}{n}\sum_{l=1}^{n}(\tilde{u}_x - U_x)(\tilde{u}_z - U_z) \qquad 4.2$$

where u_x and u_z are the streamwise and vertical turbulent fluctuations, U_x and U_z are the time averaged streamwise and vertical velocities over n measurements and $\tilde{u}_x$ and $\tilde{u}_z$ are the instantaneous streamwise and vertical velocity components. As the Reynolds number is a measure of the balance in inertial to viscous forces, the Reynolds shear stress corresponds to a balance of mean linear momentum (Speziale, 1990) and is important in examining turbulent flows and sediment transport.

In general, there were only slight differences in the Reynolds stress values for open, smooth and rough covered flows (Figure 27 and Figure 28). Figure 27 indicates that in the upper portion of flow the Reynolds shear stress is smaller under rough cover in comparison to open channel conditions; however, of note the ADV sampling volume was 10 cm from the probe. Values of Reynolds shear stress obtain a maximum value closer to the channel bed in comparison to open channel conditions (Figure 27). Values of Reynolds shear stress gradually become smaller towards the surface for rough ice cover. The values of Reynolds shear stress do not show any significant differences in pattern between open channel and smooth cover conditions (Figure 28). For all sediment sizes, Reynolds stresses are greater in the near bed region under rough ice cover conditions.

Faruque (2009) found that surface roughness increases the contribution of turbulent events which produces a greater change in Reynolds shear stress distributions which can

potentially influence sediment transport. The shear stress distribution changes the most under rough cover for D_{50}=0.47 mm (Figure 27).

   With such small scale change in Reynolds shear stress and a sampling volume 10 cm away from the ADV probe, there is no clear trend as to whether smooth and rough ice cover significantly altered the Reynolds shear stress distribution over the flow profile.
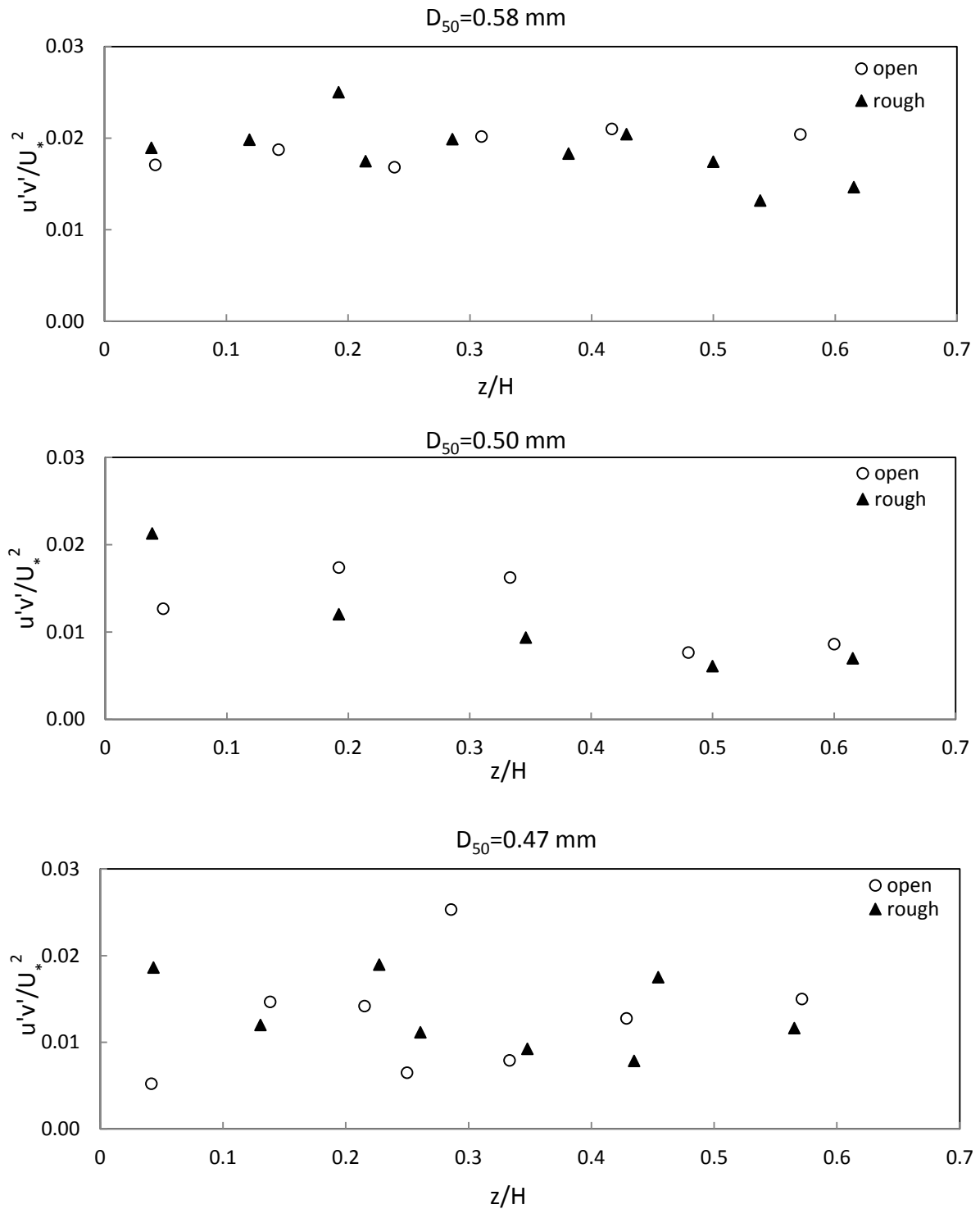
Figure 27. Reynolds shear stress, normalized by the shear velocity, for open and rough cover channel conditions.
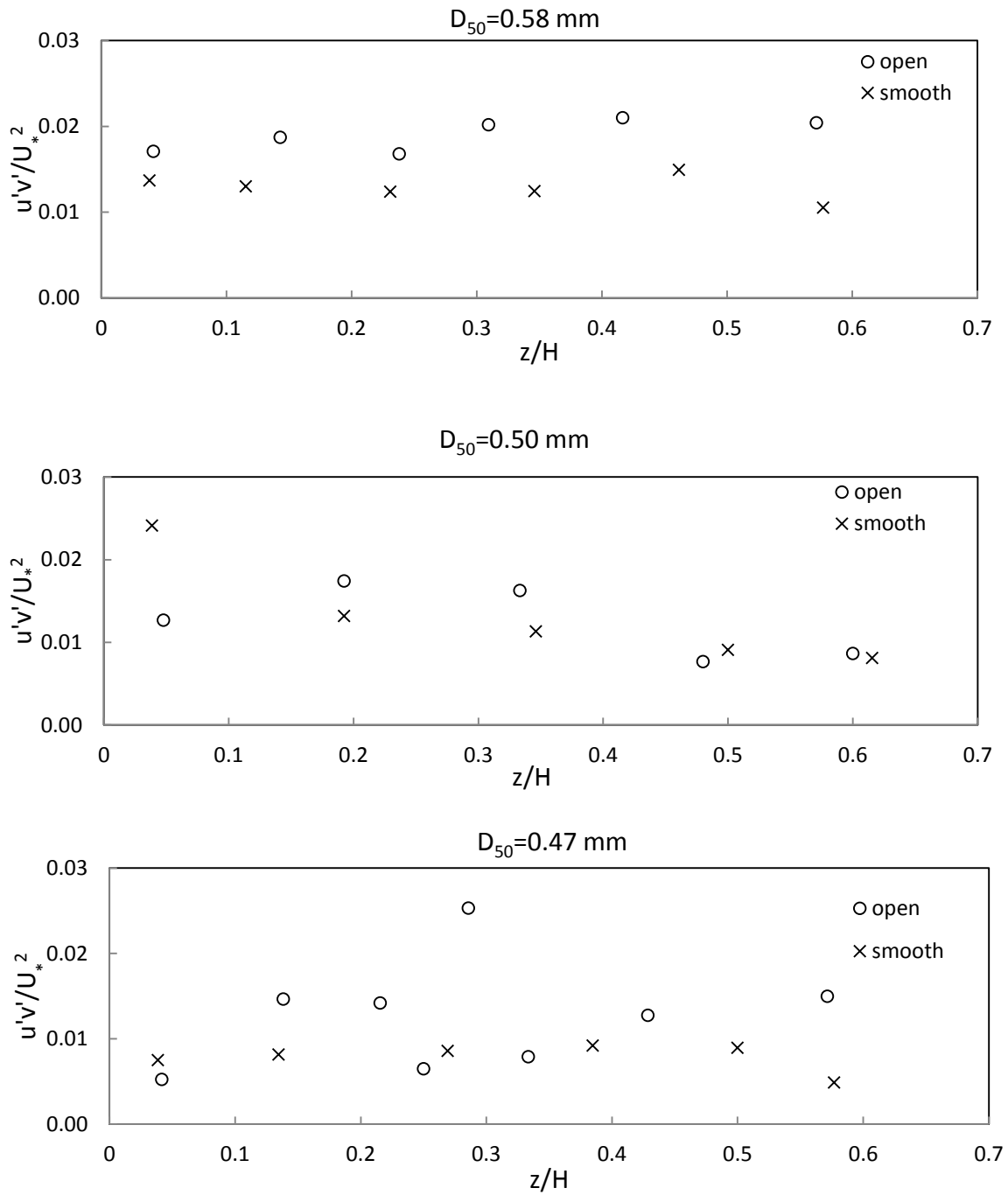
Figure 28. Reynolds shear stress, normalized by the shear velocity, for open and smooth cover channel conditions.

4.5 Summary and conclusions

The purpose of this chapter was to examine the experimental hydraulic conditions under open, smooth and ice covered conditions. In doing so the velocity profiles, turbulent intensities and Reynolds shear stresses were examined. All data for this chapter were derived from ADV measurements for two tailgate runs (21-26 cm depths) at $D_{50} = 0.47$ mm, 0.50 mm and 0.58 mm under open, smooth and rough channel conditions. The main limiting factor in some measurements was the fact that the ADV flow volume was 10 cm from the probe end, which did not allow for flow measurements immediately adjacent to the ice covers. While previous studies by Crance and Frothingham (2008) and Sui et al. (2010) have measured flow profiles under ice cover, this study builds upon work by Muste et al. (2000) and Robert and Tran (2012) by decomposing flow profiles and examining turbulent intensities which have important implications for sediment transport. As one of the main objectives of this thesis is to examine pier scour under ice cover, the causal mechanisms for sediment transport are important. The main findings from this chapter are summarized as follows:

(1) The average maximum velocities under rough ice cover were 0.36-0.43H and for smooth ice cover were 0.41H. The range in rough cover velocity compared to smooth cover is most likely due to the greater turbulent intensity measured under rough ice cover conditions. Smooth and rough ice cover causes the maximum velocity to migrate towards the channel bed. A higher velocity close to the channel bed indicates a greater capacity for sediment transport. There was not a consistent difference between the height of the maximum velocities between smooth and rough ice cover.

(2) The streamwise turbulent intensities for the rough flow were greater than those for open channel conditions and the vertical turbulent intensities were approximately one half than the streamwise turbulent intensities.   The strength of the turbulence will affect sediment suspension; a greater turbulence and therefore a greater kinetic energy under rough ice cover infer that there is a greater capacity for sediment transport under rough ice cover.

(3) There were only slight differences in the Reynolds stress values for open, smooth and rough covered flows. For all sediment sizes, Reynolds stresses were slightly greater in the near bed region under rough ice cover conditions. With such small scale change in Reynolds shear stress there is no clear trend as to whether smooth and rough ice cover significantly altered the Reynolds shear stress distribution over the flow profile.

5.0 RESULTS AND DISCUSSION:

SCOUR CHARACTERISTICS UNDER ICE COVER

The purpose of this chapter is to examine various hydraulic parameters as they relate to pier scour. Experimental flume results are presented relating pier scour depth to pier size, median size of bed material and channel cover. The scour area and scour hole morphology are also examined along with velocity profiles within the scour hole. Since non-uniform sediment was used, the armour layer within the scour hole is also investigated. Dimensional analysis is presented for hydraulic parameters as they relate to scour depth and the validity of multiple regression analysis is investigated. Also, since the flume was subject to scaling, information is provided as to how scaling effects were addressed in applicable sections.

5.1 Scour depth versus sediment grain size

Open channel:

Scour depth is compared under various grain sizes under the same flow and depth for open channel conditions. Results indicate that the largest scour depth occurs under smallest D_{50} while the smallest scour depth occurs under the largest D_{50} for all cover conditions (Figure 29). On average scour depths for open channel conditions are 50 percent larger for $D_{50}=0.47$ mm and 13.64 percent larger for $D_{50}=0.50$ mm compared to the largest sediment grain size $D_{50}=0.58$ mm. Of exception is the results measured for $D_{50}=0.58$ mm for runs 1 and 6 (Figure 29); the measured scour depth is larger than the scour depth for $D_{50}=0.50$ mm for the same runs. These two results do not align with the overall pattern of smaller scour depths with increasing D_{50} size. It is difficult to determine why in this case there was a deeper scour hole

64

for D_{50}=0.58 mm than for D_{50}=0.50 mm. The average armour layer size for these runs is very similar, varying by only 0.1 mm and velocity, varying by only 0.9 cm/s (Appendix A and C). A possible explanation for a smaller scour depth under D_{50}=0.50 mm may be due to the extent of the embedded depth of the armour layer grains for that specific run. Since non-uniform sediment was used, during each experimental set up, the bed was leveled around the pier; in doing so larger grains may have been raked around the pier which may have become embedded in the scour hole. Also, perhaps fluctuations in near bed turbulent intensity were slightly greater for D_{50}=0.58 mm leading to greater sediment transport around the bridge pier.
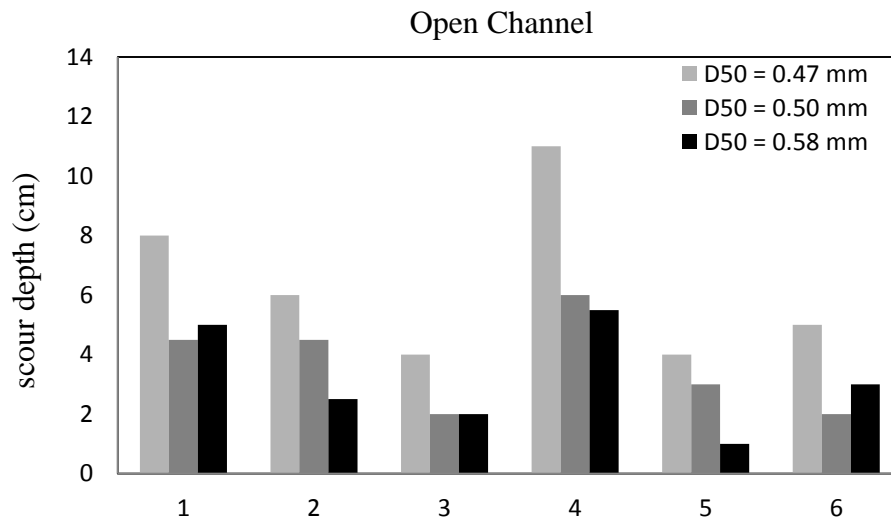
Figure 29. Maximum scour depth under open channel conditions for D_{50}=0.47 mm, D_{50}=0.50 mm, D_{50}=0.58 mm. Numbers 1-6 indicate experimental run number. For associated data values refer to Appendix B. Scour depth measurements subject to +/-0.02 cm error.

Smooth Cover:

Scour depth is compared under various grain sizes for the same flow and depth under smooth channel conditions. For all experimental runs, the smallest grain size resulted in the largest scour depth under smooth ice cover (Figure 30). The average scour hole depth for D_{50}=0.47 mm is 6.33 cm, D_{50}=0.50 mm is 3.66 cm and D_{50}=0.58 mm is 3.16 cm. On average,

maximum scour depth for $D_{50}=0.47$ mm is 56 percent greater than maximum scour depth for $D_{50}=0.58$ mm. The maximum scour depth for $D_{50}=0.50$ mm is 22.77 percent greater than that for $D_{50}=0.58$ mm.

Smooth Cover
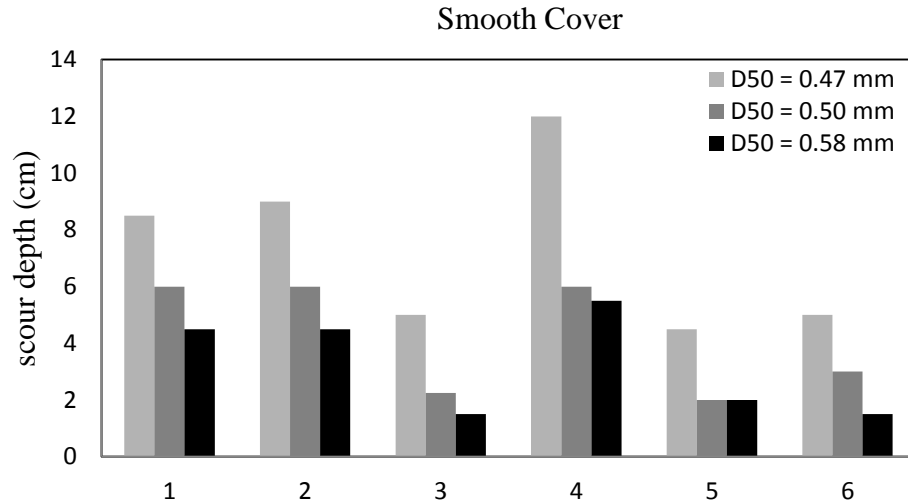
Figure 30. Maximum scour depth under smooth ice channel conditions for $D_{50}=0.47$ mm, $D_{50}=0.50$ mm, $D_{50}=0.58$ mm. Numbers 1-6 indicate experimental run number. For associated data values refer to Appendix B. Scour depth measurements subject to +/-0.02 cm error.

Rough Cover:

Scour depth is compared under various grain sizes under the same flow and depth for rough ice cover channel conditions. Just as with open and smooth channel conditions, results indicate that largest scour depth occurs under smallest D_{50} while the smallest scour depth occurs under the largest D_{50} for rough cover conditions (Figure 31). A reduction in grain size from 0.58 mm to 0.47 mm produces a 58 percent increase in maximum scour depth (under the same flow conditions). On average scour depths for rough ice cover channel conditions are 33 percent larger for $D_{50}=0.50$ mm compared to the largest sediment grain size $D_{50}=058$ mm.

66
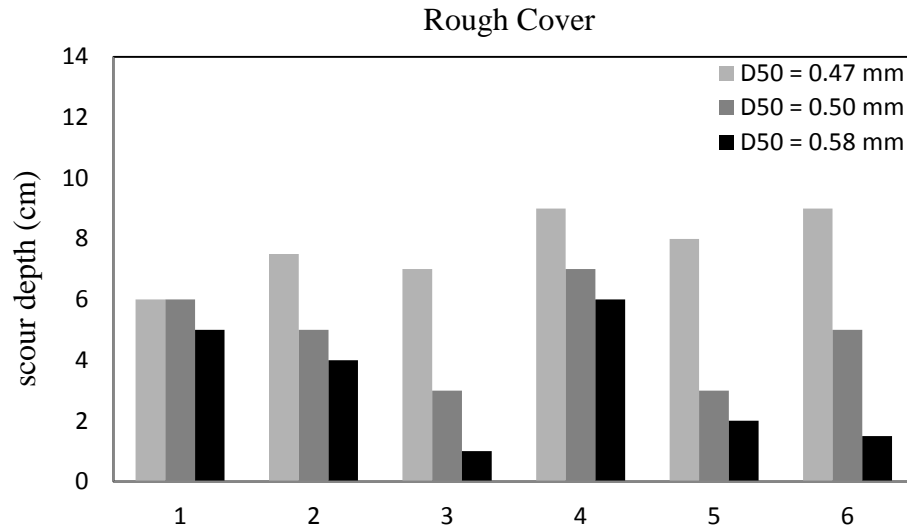
Rough Cover

Figure 31. Maximum scour depth under rough cover channel conditions for D_{50}=0.47 mm, D_{50}=0.50 mm, D_{50}=0.58 mm. Numbers 1-6 indicate experimental run number. For associated data values refer to Appendix B. Scour depth measurements subject to +/-0.02 cm error.

Summary of scour depth versus grain size:

When comparing scour depth to grain size the scaling of the experimental flume must be considered. Melville and Coleman (2000) stated that if the ratio of pier width to flow depth (b/h) is between 0.7-5.0 then local pier scour is dependent on both flow depth and pier width while if b/h is less than 0.7 than local pier scour depth is dependent only on pier width. For this thesis, the ratios of pier width to flow depth range from 0.42 to 2.2. In order to work around these scaling issues, maximum scour depth was compared between covers and sediment size while keeping pier width and flow depth constant for each corresponding run. In keeping all hydraulic parameters constant, the smallest sediment size D_{50}=0.47 mm yielded the largest pier scour depth under all channel covers. The largest scour depth occurs under smallest D_{50} while the smallest scour depth occurs under the largest D_{50}. It is interesting to note that even though the bed sediment sizes only differ by up to 11 mm the maximum scour

depths vary by up to 58 percent. For example, under rough cover the maximum scour depth is 38 percent larger for D_{50}=0.47 mm in comparison to D_{50}=0.50 mm, even though the difference in sediment size is only 3 mm.

It should also be noted that the choice of sediment size in laboratory models, and in this thesis, distorts the value of pier width to sediment size (b/D_{50}) in comparison to the prototype (real world bridge). In reality, bridge piers are much wider than their model counterparts, yet bed material typically remains within the same diameter ranges as used in flumes. As examined by Lee and Sturm (2009) this scaling issue leads to larger scour depths in the laboratory than in the field. Further discussion on scaling issues regarding the flume experiments undertaken in this thesis can be found in Chapter 6, Section 6.1.1.

5.2 Scour depth versus pier size

When analyzing local scour around bridge piers the scaling ratio between flow depth and pier width must be considered. As outlined by Melville and Coleman (2000), b/h < 0.7 indicates that scour depth is directly proportional to pier width. Given 0.7<b/h<5, scour depth is proportional to both pier width and flow depth. Therefore when comparing scour depth and to pier size, a subset of the experimental runs were selected: namely those runs where b/h > 0.7. For each comparison flow depth and sediment size were the same.

For the majority of experiments under the same hydraulic conditions a larger maximum scour hole was produced for the 22 cm pier (Figure 32, Figure 33, and Figure 34). For run 6 under open channel conditions the maximum scour depth for the 11 and 22 cm piers was the same. This also occurred for runs 2, 4 and 5 under smooth ice cover (Figure 33). On average, the maximum scour depth for the 22 cm pier was 25 percent larger than the 11 cm pier under

open channel conditions. The maximum scour depth for the 22 cm pier was 12 and 29 percent larger than the 11 cm pier for smooth and rough channel conditions respectively.

Since scouring is caused in part by the horseshoe vortex and the dimensions of the vortex system are a function of pier diameter, it is concluded that local pier scour is related to pier size (Breusers et al., 1977). Shen et al. (1969) also found that the vortex is proportional to the pier Reynolds number, which is a function of pier diameter. With a larger horseshoe vortex, the sediment transport capacity is greater hence the larger maximum scour depth under all conditions for the larger 22 cm pier.
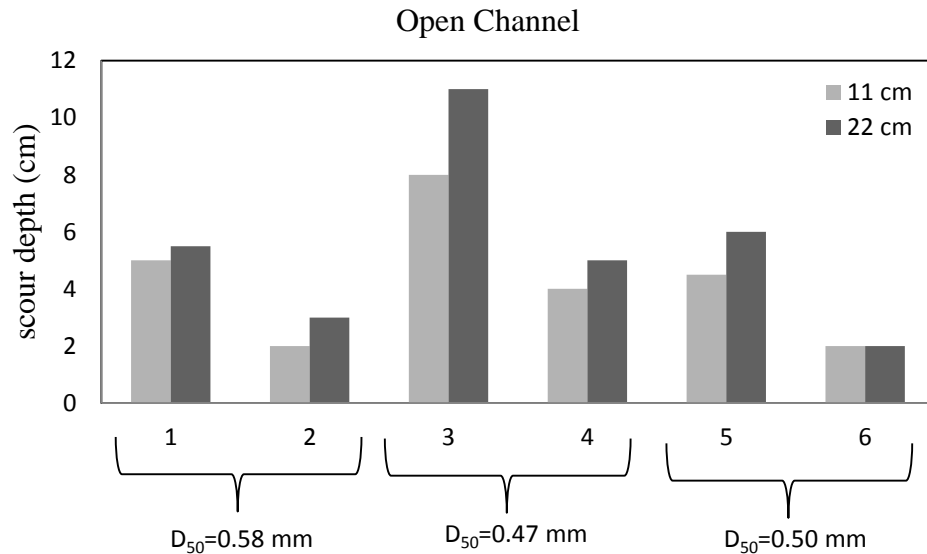
Figure 32. Maximum scour depth under open channel conditions for 11cm and 22 cm width pier. Numbers 1-6 indicate experimental run number. Scour depth measurements subject to +/-0.02 cm error.

Smooth Cover
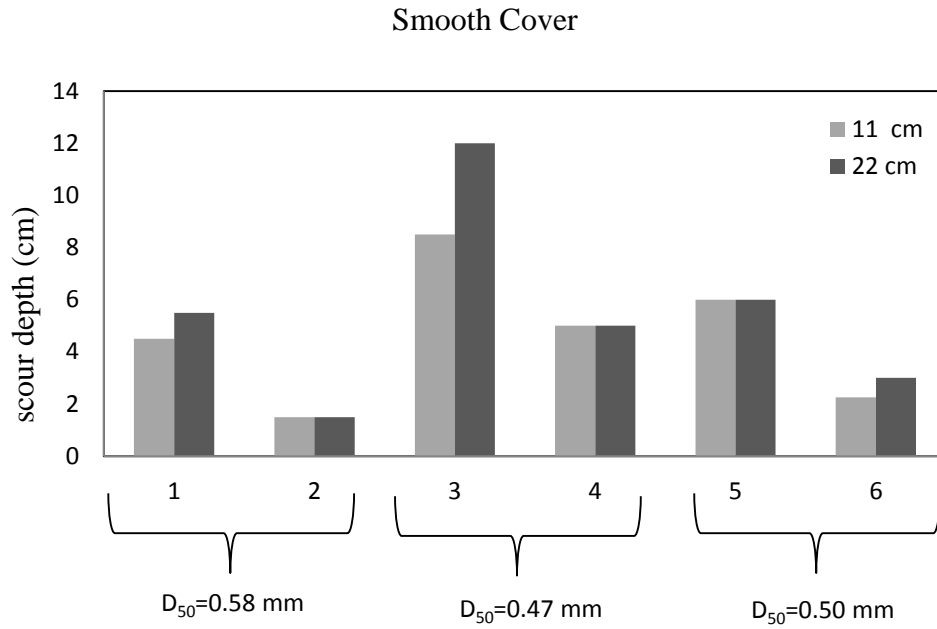
Figure 33. Maximum scour depth under smooth channel conditions for 11cm and 22 cm width pier. Numbers 1-6 indicate experimental run number. Scour depth measurements subject to +/-0.02 cm error.
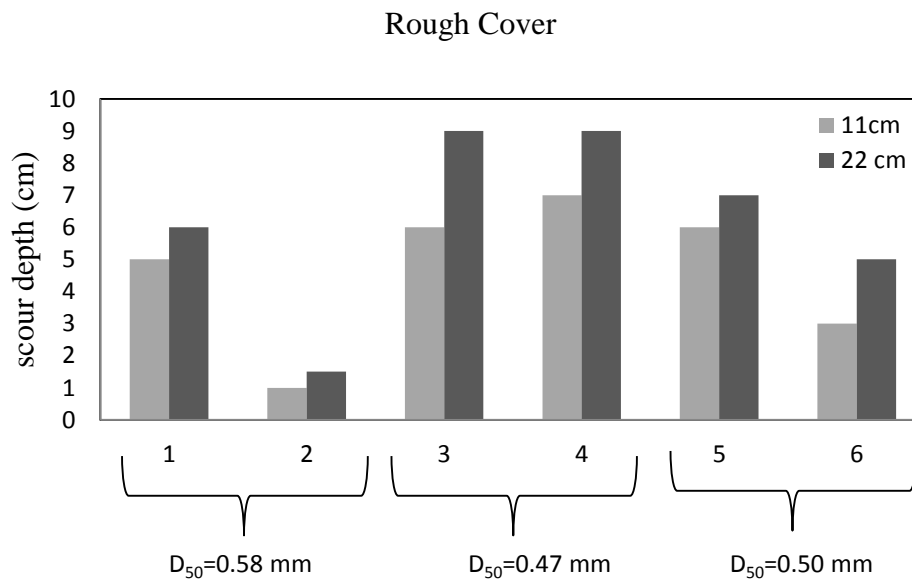
Rough Cover

Figure 34. Maximum scour depth under rough channel conditions for 11cm and 22 cm width pier. Numbers 1-6 indicate experimental run number. Scour depth measurements subject to +/-0.02 cm error.

5.3 Scour depth versus channel cover

As previously discussed, under the scaling conditions of the flume, scour depth automatically depends on both flow depth and pier width. Experimental runs with a pier width to flow depth (b/h) ratio of less than 0.7 were not considered for comparison in this section as scour depth at a 0.7 ratio is only dependant on pier width and not flow depth (Melville and Coleman, 2000). In addition, for some experiments the flow velocity was slightly greater than 2 cm/s between experimental runs which will increase variability in sediment transport. This was a result of the limitations in the gravity fed water system and differences in the flow velocity between the downstream and upstream sandboxes.

Under all sediment sizes rough ice cover scour depth is greater than open channel conditions for nine out of 15 experimental groupings (60 percent). Rough cover scour depth is equal to open channel scour depth for 2/15 experiments, and rough cover scour depth is less than open channel scour depth for 4/15 experiments (Figure 35, Figure 36 and Figure 37). On average, for all sediment sizes, rough ice cover scour depth is 37 percent greater than open channel scour depth (Table 11, Table 12, Table 13). Of note, the smaller the D_{50}, the greater the difference between ice cover scour depth and open channel scour depth. Under D_{50}s of 0.47, 0.50 and 0.58 mm the scour depth under rough ice cover was 46, 33 and 29 percent greater than open channel scour depth respectively (Table 11, Table 12, Table 13). Smooth ice cover produced a greater scour depth than open channel conditions for eight out of 15 experiment groupings (53 percent). On average, for all sediment sizes, smooth ice cover scour depth is 20 percent greater than open channel scour depth (Table 11, Table 12, Table 13). Smooth ice cover scour depth is equal to and less than open channel scour depth for 3/15 and 4/15 experiments respectively. The findings presented here, indicating that ice cover does not

always produce a greater pier scour depth, are different than the two previous studies in the literature.

Batuca and Dargahi (1986) and Olsson (2000) found that scour depth under smooth and rough cover is greater than scour depth under open channel conditions for all experimental runs. Batuca and Dargahi (1986) compared local scour around a pier under open water and floating ice cover conditions. A total of 34 experiments were performed under ice conditions using plywood and aluminum for channel cover. Sediment with a median diameter of D_{50}=0.41 mm and σ_g=1.88 (non-uniform sand) was used. Through visual observation they found that the general size of the scour hole was greater under ice covered conditions. Olsson (2000) compared pier scour depths under open, smooth and rough ice cover and found that the rough ice cover resulted in a greater scour depth than the smooth cover. Uniform sand with D_{50}=0.42 mm was used along with Styrofoam sheets to simulate ice cover. Experiments were run for 4 hours. Olsson (2000) found that ice cover may increase the local scour depth by 25-35 percent compared to open channel conditions.

The differences found in this study compared to Olsson's (2000) findings are most likely due to the sediment types used. This study used non-uniform sand and Olsson (2000) used uniform sediment. The mechanisms involved in non-uniform sediment transport are complex as grain shape, grain distribution and interactions between grains all influence incipient motion of sediment inside the scour hole (Xu et al., 2008). Wu et al. (2000) examined non-uniform sediment transport in alluvial rivers and developed a correction factor for the hiding and exposure factors associated with non-uniform sediment. The hiding and exposure factors of non-uniform sediment are stochastically related to the size and gradation of bed materials. Given that between each experiment the sediment in the flume was raked and

72

leveled, the arrangement of particles would be different for each experimental run. The down flow and associated vortices at the bridge pier would therefore transport sediment depending on the hiding and exposure factor of individual sediment grains (since after leveling the flume sediment would be arranged in a different way for each experiment). The micro environment around each bridge pier would be different in terms of turbulence since the fluid interactions with grains are different. This is reinforced by evidence of the large variability in the average armour layer size within each scour hole (Table 11, Table 12, Table 13). Also, the flume was 2 m wide with 11.3 m of flow between the head tank and first sandbox. Even though a flow diffuser was installed, each experimental run would have slightly different approach velocities, turbulence, and water temperature. (Water temperature fluctuated from 8.6-10.4 degrees Celsius between each run since the flume was outside. This would change parameters such as the water viscosity). Given that the arrangement of sediment, flow velocity, turbulence and water temperature were different for each experimental run the sediment transport potential around the bridge pier would also different for each experiment. The variation in scour depth with channel cover for this study may be a result of the variation in sediment and associated transport mechanisms as discussed above.

Of note however, Batuca and Dargahi (1986), found that ice cover produced a greater general size of scour hole compared to open channel conditions all the while using non-uniform sand. The authors did not physically measure the maximum scour depth but rather visually inspected the scour hole in drawing their conclusion. The sediment used in Batuca and Dargahi (1986) closely aligns with the D_{50}=0.47 mm sand used in this study. For the D_{50}=0.47 mm sediment, this study found that rough ice cover produced a greater scour depth for three out of five experimental groupings (Figure 37). The scour volume and area for each

scour hole was also measured and correlated with maximum scour depth (as discussed in the next section, Figure 41). As indicated in Figure 41, using the scour volume and area (or visually estimating the general size of the scour hole) is not always a good indication of maximum scour depth. In order to compare results between this study and Batuca and Dargahi (1986) actual measurements of maximums scour depth are required. Also, using plywood and aluminum for channel cover would create a different pressure at the water surface compared to using Styrofoam. It is assumed that plywood and aluminum would be much more rigid surfaces than Styrofoam and have less buoyancy.

As previously mentioned, this study resulted in rough ice cover producing greater pier scour depths for 9/15 experimental groupings. These results partially align with findings from Batuca and Dargahi (1986) and Olsson (2000). Rough ice cover produces greater down flow then open channel conditions (as discussed in detail in section 5.8, Figure 56 and Figure 57), and therefore under rough ice cover there is a greater capacity for sediment transport around the bridge piers. While 40 percent of the data for this study did not align with previous research, it is important to consider the characteristics of non-uniform sediment and that even in an experimental flume environment hydraulic parameters are not constant. Heterogeneous environments are more representative of natural rivers: highly variable with non-uniform sediment. While it has been previously found that ice cover produces greater down flow leading to greater pier scour, this study indicates that while ice cover does produce greater down flow, sediment uniformity is also important in considering pier scour.
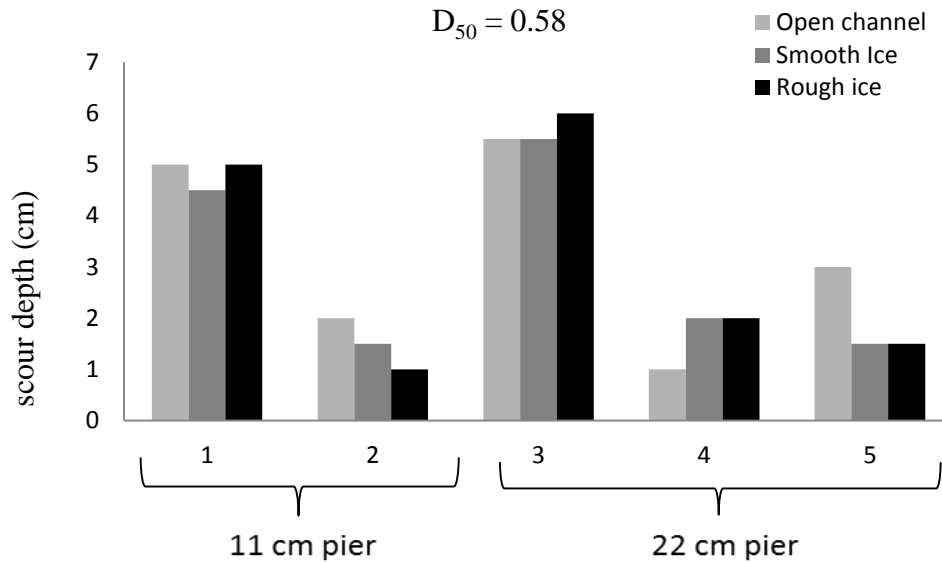
Figure 35. Maximum scour depth under open, smooth and rough channel condition for D_{50}=0.58 mm. Numbers 1-6 indicate experimental run number. Scour depth measurements subject to +/-0.02 cm error.

Table 11. Scour depth values associated with Figure 35.

Experimental run # $D_{50} = 0.58$ mm	open		smooth		rough	
	Scour depth (cm)	D_{50} armour layer (mm)	Scour depth (cm)	D_{50} armour layer (mm)	Scour depth (cm)	D_{50} armour layer (mm)
1	5	0.60	4.5	1.25	5	1.25
2	2	1.05	1.5	0.85	1	1.42
3	5.5	0.62	5.5	1.81	6	1.60
4	1	0.65	2	0.83	2	0.85
5	3	0.78	1.5	0.94	1.5	1.57
	average	0.74	average	1.14	average	1.34
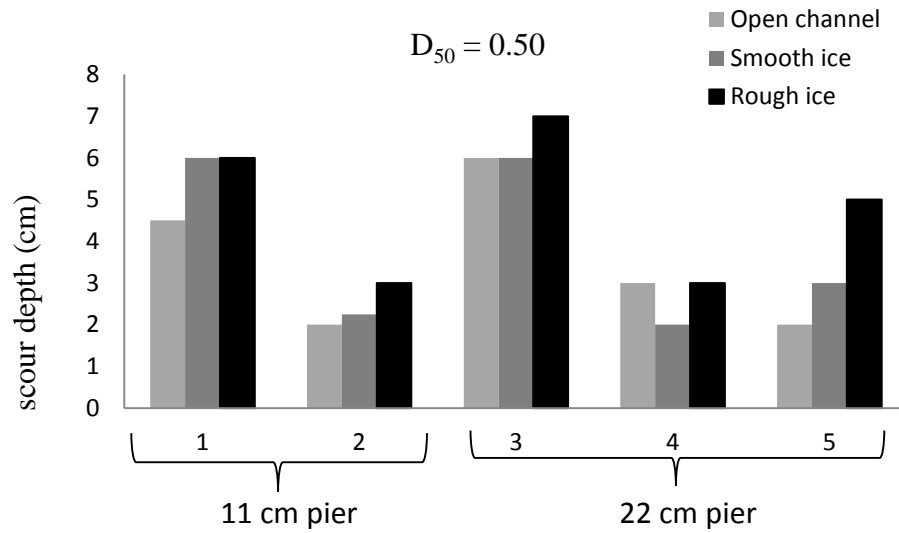
Figure 36. Maximum scour depth under open, smooth and rough channel condition for D_{50}=0.50 mm. Numbers 1-6 indicate experimental run number. Scour depth measurements subject to +/-0.02 cm error.

Table 12. Scour depth values associated with Figure 36.

Experimental run # D_{50} = 0.50 mm	open		smooth		rough	
	Scour depth (cm)	D_{50} armour layer (mm)	Scour depth (cm)	D_{50} armour layer (mm)	Scour depth (cm)	D_{50} armour layer (mm)
1	4.5	0.60	6	1.40	6	0.75
2	2	0.80	2.25	0.59	3	0.73
3	6	1.43	6	0.68	7	0.60
4	3	0.60	2	0.79	3	0.59
5	2	0.68	3	0.65	5	0.73
	average	0.82	average	0.82	average	0.68
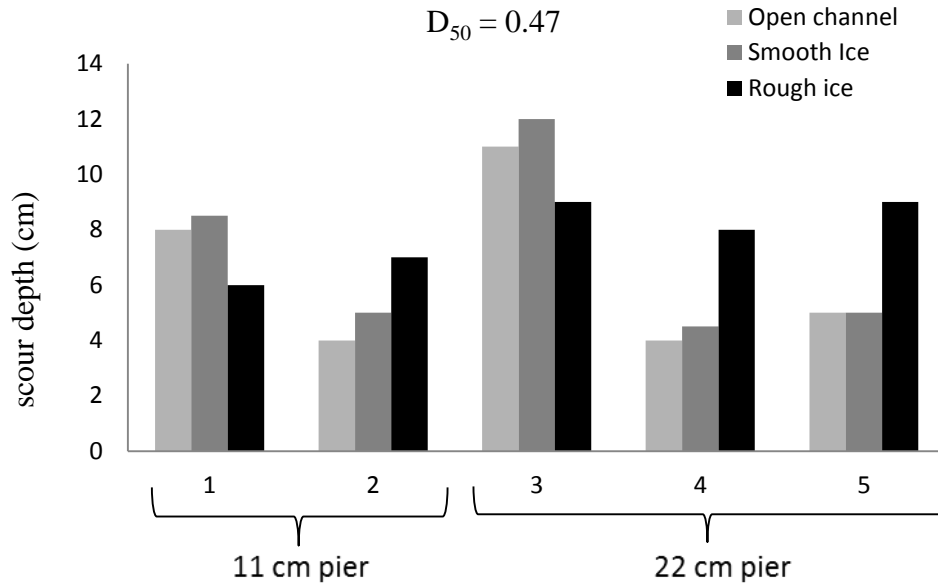
Figure 37. Maximum scour depth under open, smooth and rough channel condition for D_{50}=0.47mm. Numbers 1-6 indicate experimental run number. Scour depth measurements subject to +/-0.02 cm error.

Table 13. Scour depth values associated with Figure 37.

Experimental run # D_{50} = 0.47 mm	open		smooth		rough	
	Scour depth (cm)	D_{50} armour layer (mm)	Scour depth (cm)	D_{50} armour layer (mm)	Scour depth (cm)	D_{50} armour layer (mm)
1	8	0.48	8.5	0.40	6	0.55
2	4	0.50	5	0.49	7	0.45
3	11	0.59	12	0.55	9	0.57
4	4	0.43	4.5	0.30	8	0.49
5	5	0.45	5	0.53	9	0.48
	average	0.49	average	0.45	average	0.51

5.4 Scour area and volume

Much of the current literature focuses on the value and location of maximum scour depth around piers, however for purposes of bridge construction it is also important to consider the scour volume and scour area. Riprap and flow dispersal devices are common pier scour countermeasures (Beg and Beg, 2013) and it is essential to understand potential pier scour area and volume in countermeasure design.

Scour hole contours were manually measured and input into Surfer12 plotting software. The Surfer12 software was then used to calculate scour hole volume and area for each experimental run. The scour area (A) versus scour volume (V) was plotted in Figure 38, Figure 39 and Figure 40. Based upon these figures the following three relationships were developed:

For open channel:

$$V_{11 \text{ cm pier}} = 3.93A - 1787.5 \qquad\qquad 5.1$$

$$V_{22 \text{ cm pier}} = 3.81A - 2731 \qquad\qquad 5.2$$

For smooth cover:

$$V_{11 \text{ cm pier}} = 3.95A - 1367.4 \qquad\qquad 5.3$$

$$V_{22 \text{ cm pier}} = 4.88A - 5054.4 \qquad\qquad 5.4$$

For rough cover:

$$V_{11 \text{ cm pier}} = 2.63A - 733.36 \qquad\qquad 5.5$$

$$V_{22 \text{ cm pier}} = 3.84A - 2835.6 \qquad\qquad 5.6$$

It should be noted that the above equations are only practical for piers under the flume's scaling ratios. In all scenarios, there is a linear relationship between scour volume and area. Only two previous studies have looked at scour volume and area around bridge structures (Khwairakpam et al., 2012; Wu et al., 2014). Wu et al. (2014) found that there was a linear relationship between scour depth and volume around bridge abutments under ice cover. Khwairakpam et al. (2012) found an increasing relationship between flow depth, densimetric Froude number and scour hole geometry. The main conclusion drawn from this study is that the linear relationship between scour area and volume remains valid even under ice cover conditions. Also, scour area and volume increase with pier size.

Maximum scour depth was also plotted against scour volume and area (Figure 41). As indicated by the R values, there is not a strong correlation between maximum scour depth, scour area and scour volume. This study found that while the maximum scour depth typically occurs at the front of the pier, the remainder of the scour hole can be shallow and contain areas of sediment deposition. This is discussed more in the next section outlining scour patterns. It is important to understand scour depth is not a good indicator of scour area or volume when considering riprap for a scour countermeasure.

Also of note, using scour area as a measure of scour depth brings into question findings by Batuca and Dargahi (1986): the authors found that ice cover produced a greater general size of scour hole compared to open channel conditions all the while using non-uniform sand. As found in this study, a larger scour area may not always correlate to a larger maximum scour depth.
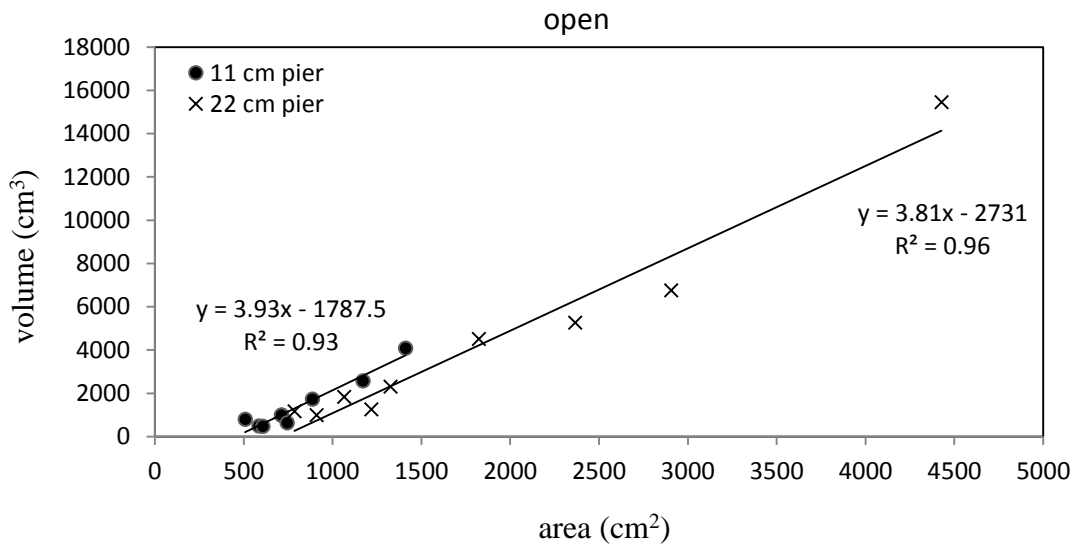
Figure 38. Variation of scour volume and area around bridge pier under open channel condition.
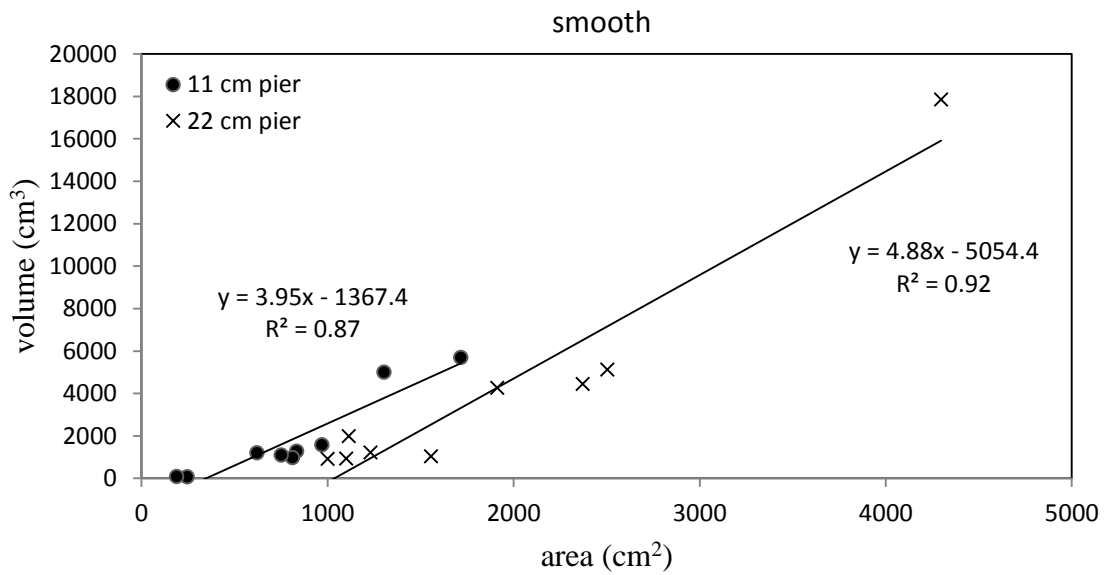
Figure 39. Variation of scour volume and area around bridge pier under smooth ice cover condition.
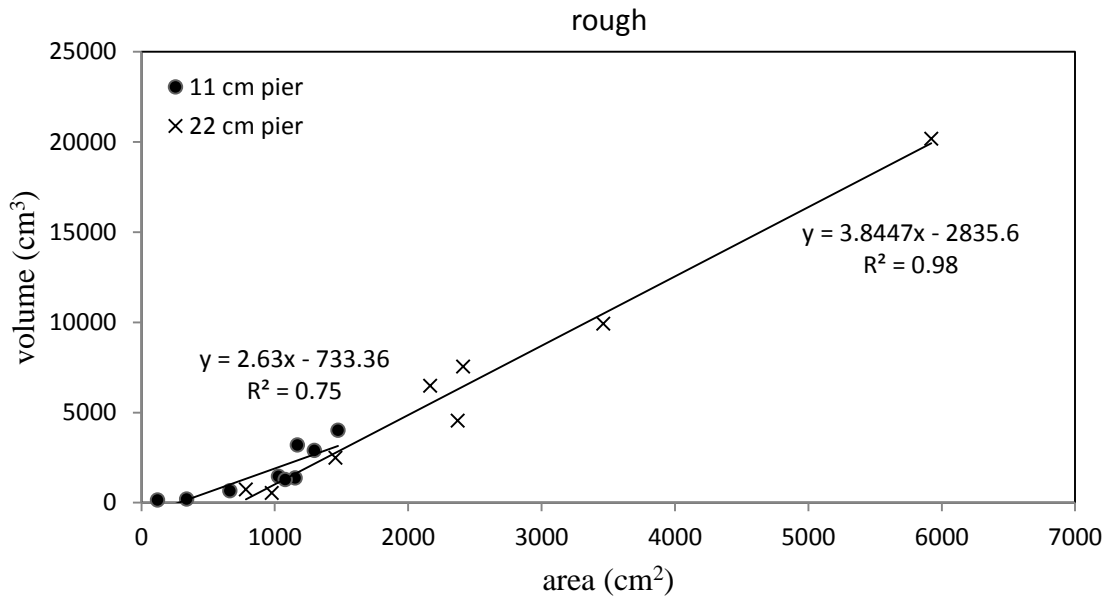
Figure 40. Variation of scour volume and area around bridge pier under rough channel condition.
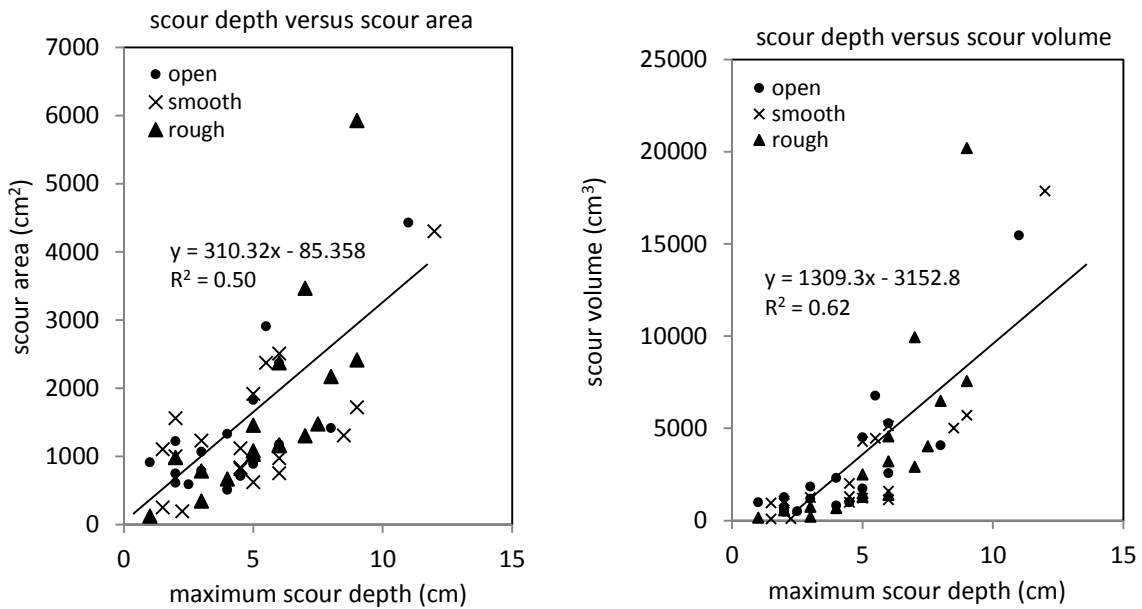
Figure 41. Maximum scour depth as related to the scour area and scour volume.

5.5 Scour patterns under open, smooth and rough ice cover

Scour hole contours were manually measured and input into Surfer12 plotting software. Surfer12 was used to generate 2-D and 3-D scour patterns in order to gain a better understanding of sediment transport patterns around bridge piers under ice cover. The 2-dimension contour plots, Figure 42, Figure 44 and Figure 46 show the scour depth characteristics for 11 and 22 cm piers. Negative or dark shaded contour values indicate erosion while lighter or positive values indicate deposition. Figure 43, Figure 45 and Figure 47 illustrate 3-dimension scour patterns produced by both pier diameters (b = 11 cm and 22 cm) under open, smooth and rough cover channel conditions.

Across all three D_{50}s, scour patterns were similar between pier sizes and channel cover; therefore a subset of plots were chosen to display typical scour and deposition patterns. All plots, Figure 42 to Figure 47, present scour patterns for D_{50}=0.47 mm, b = 11 and 22 cm, h = 0.21-0.26 m (two tailgate configuration) and U = 0.21-0.28 m/s. Photographs and scour plots were produced for each experimental run; however for the sake of avoiding repetition, scour plots presented here are a representative subset of the entire 54 run data set.

The following is a summary of scour characteristics based upon Figure 42 to Figure 47. Regardless of cover conditions, the location of maximum scour depth is always at the pier face. This phenomenon indicates that maximum scour depth is not overly influenced by contraction scour (otherwise maximum scour would occur along the pier sides). The scour depth decreases towards the downstream side of the pier and behind the pier is typically an area of deposition. Under all cover conditions, at lower velocities, (U< 0.22 m/s) scour is relatively limited downstream of the pier. Under higher velocities the scour hole extends around the entire pier circumference. Under all channel covers deposition downstream was

greater for the 22 cm pier and a distinct deposition ridge was formed downstream of the pier. The deposition ridge was most pronounced under open channel conditions and least defined under rough cover conditions. The decreased size of the sediment ridge for ice covered flows is most likely caused by greater turbulent intensity under ice cover, which would lead to increased sediment entrainment downstream of the pier.

open, 11 cm pier, h = 0.21 m, U = 27 m/s

open, 22 cm pier, h = 0.24 m, U = 0.23 m/s
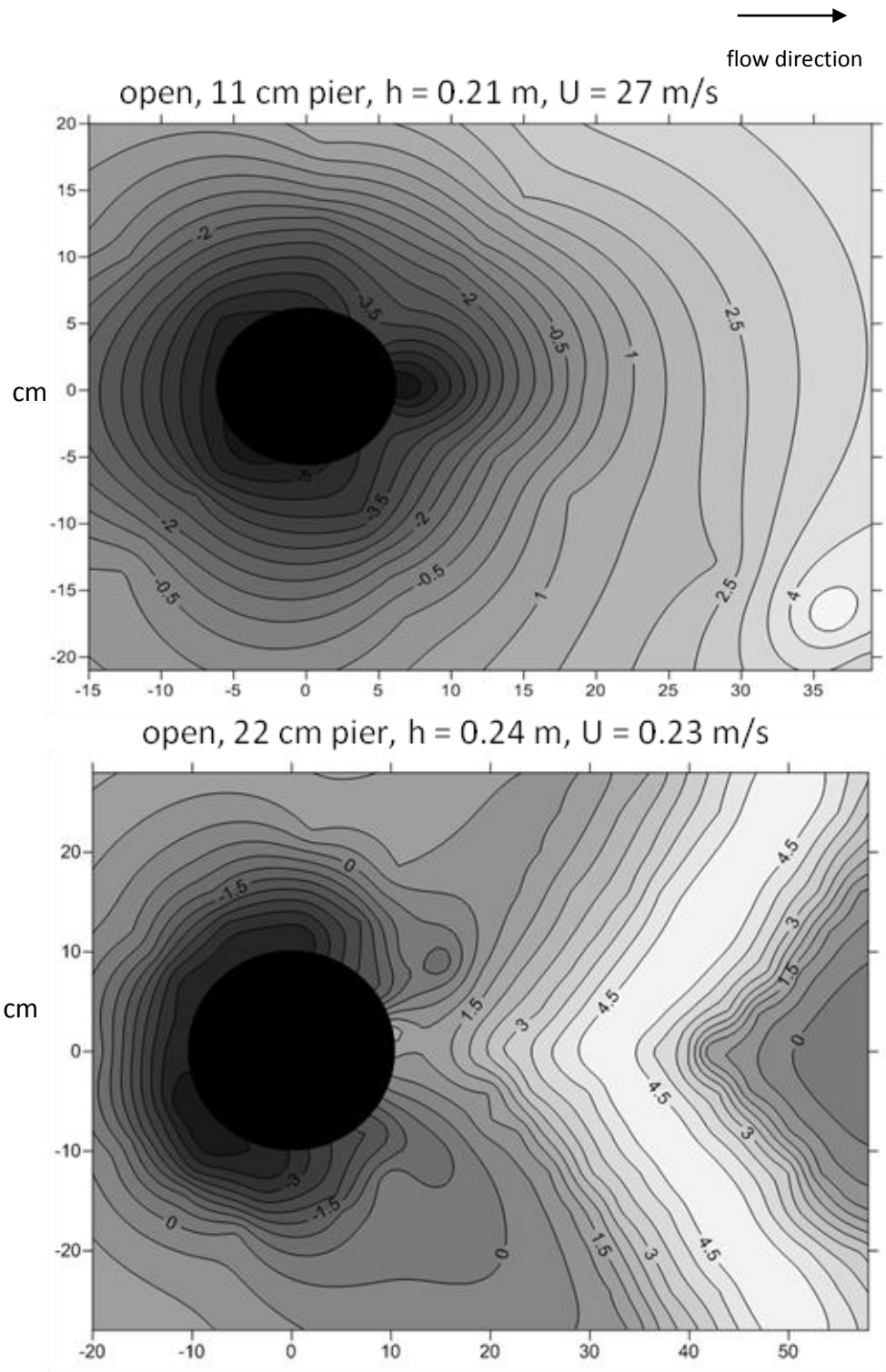
c

Figure 42. Scour pattern for 11 cm and 22 cm pier in units of centimeters, $D_{50} = 0.47$ mm, under open channel conditions.

open, 11 cm pier, h = 0.21 m, U = 27 m/s

flow direction

cm

cm

open, 22 cm pier, h = 0.24 m, U = 0.23 m/s

cm

cm
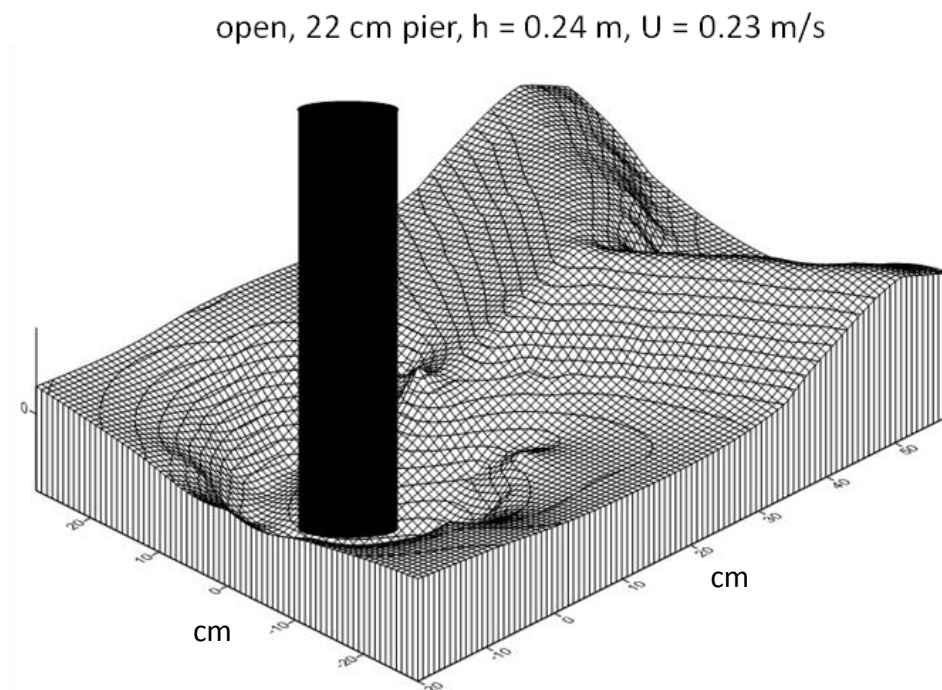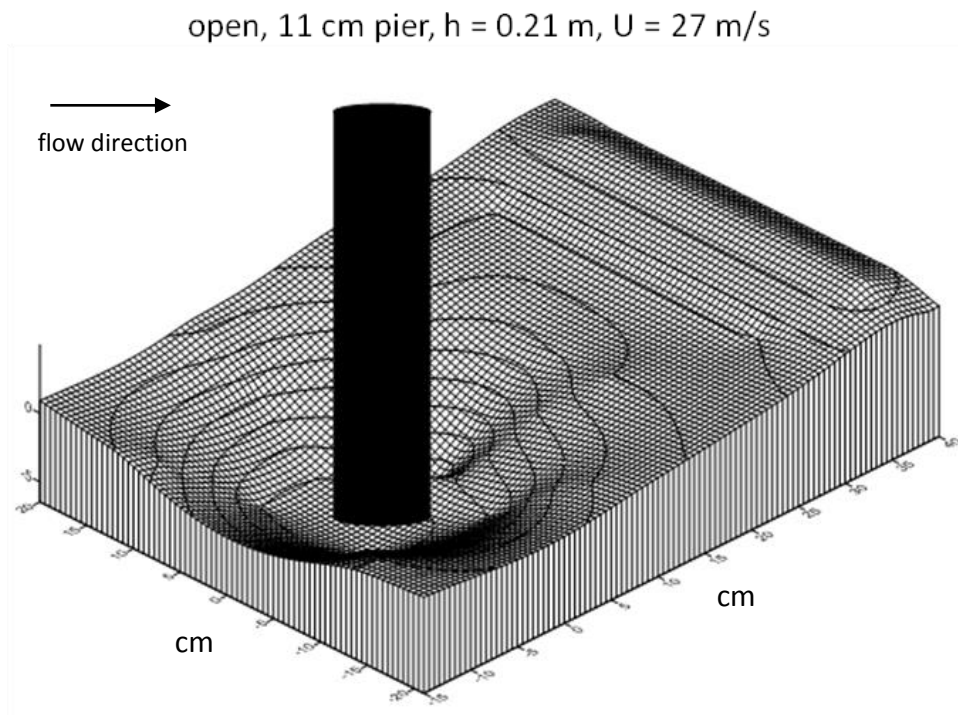
Figure 43. Scour patterns for 11 cm and 22 cm pier, $D_{50} = 0.47$ mm, under open channel condition.

flow direction

smooth, 11 cm pier, h = 0.22m, U = 0.23 m/s

smooth, 22 cm pier, h = 0.26 m, U = 0.25 m/s
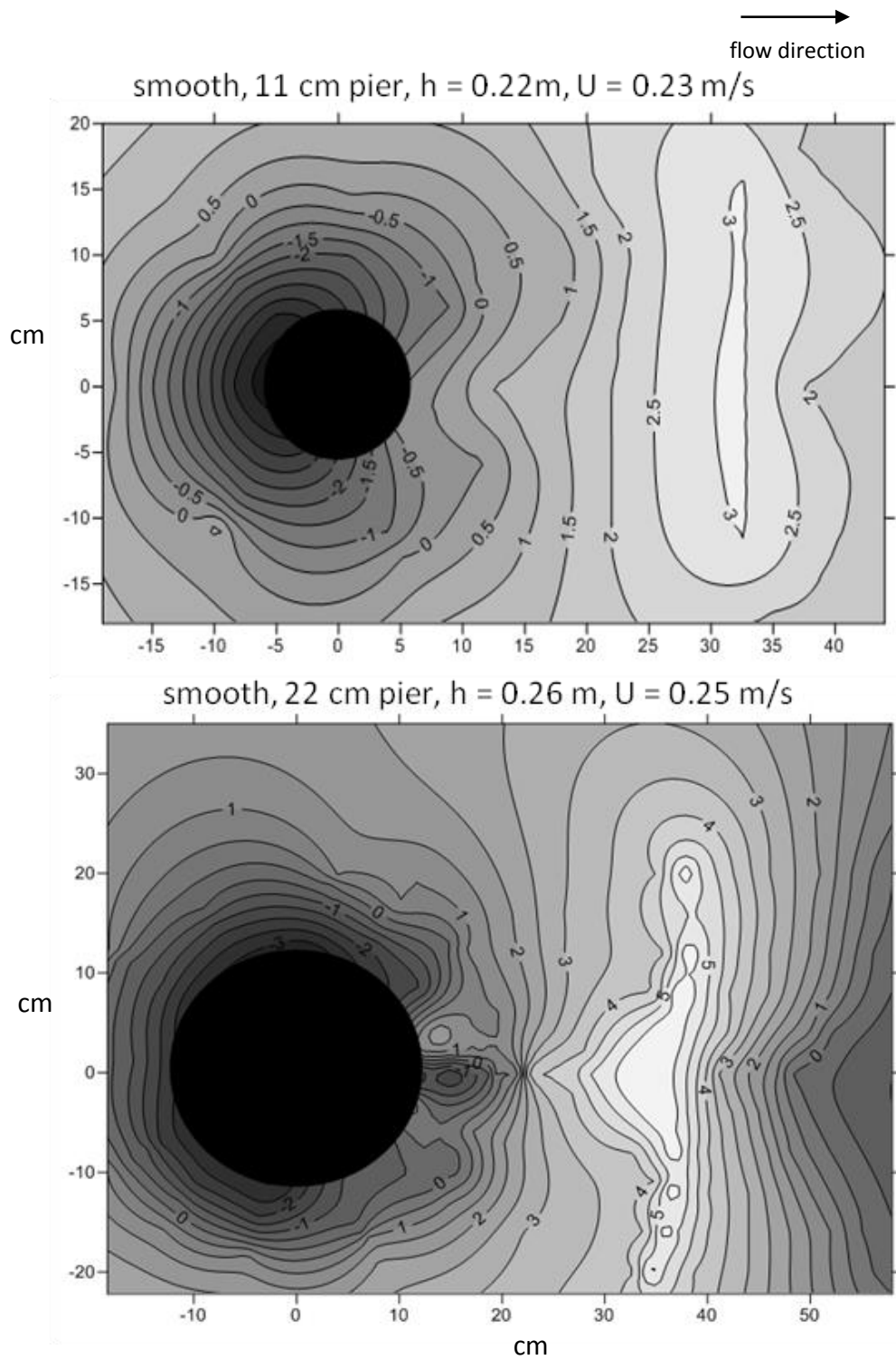
Figure 44. Scour pattern for 11cm and 22 cm pier, D_{50} = 0.47 mm, under smooth channel cover.

smooth, 11 cm pier, h = 0.22m, U = 0.23 m/s

flow direction

cm

cm

smooth, 22 cm pier, h = 0.26 m, U = 0.25 m/s

cm

cm
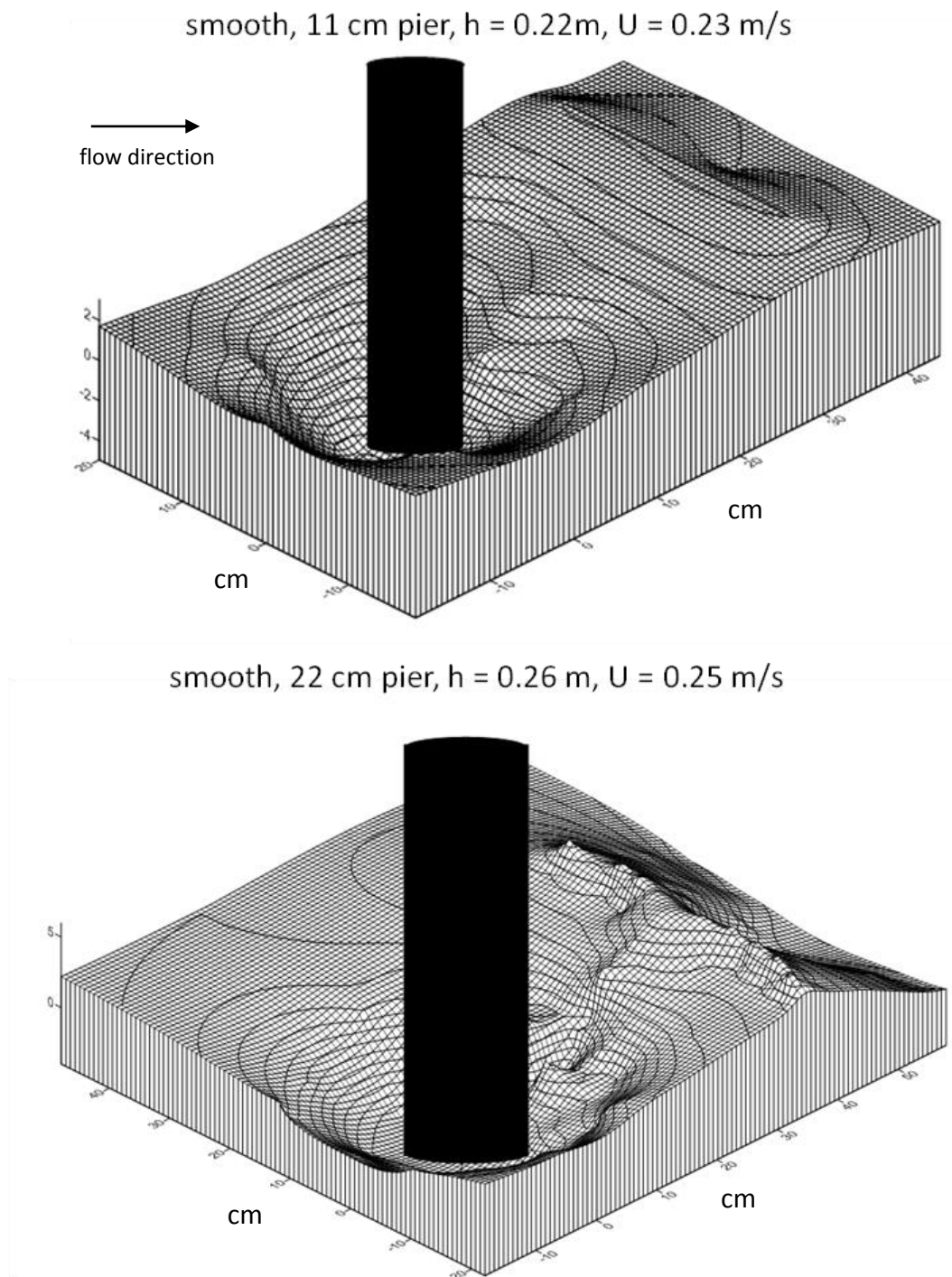
Figure 45. Scour pattern for 11 cm and 22 cm pier, $D_{50} = 0.47$ mm, under smooth ice cover channel condition.
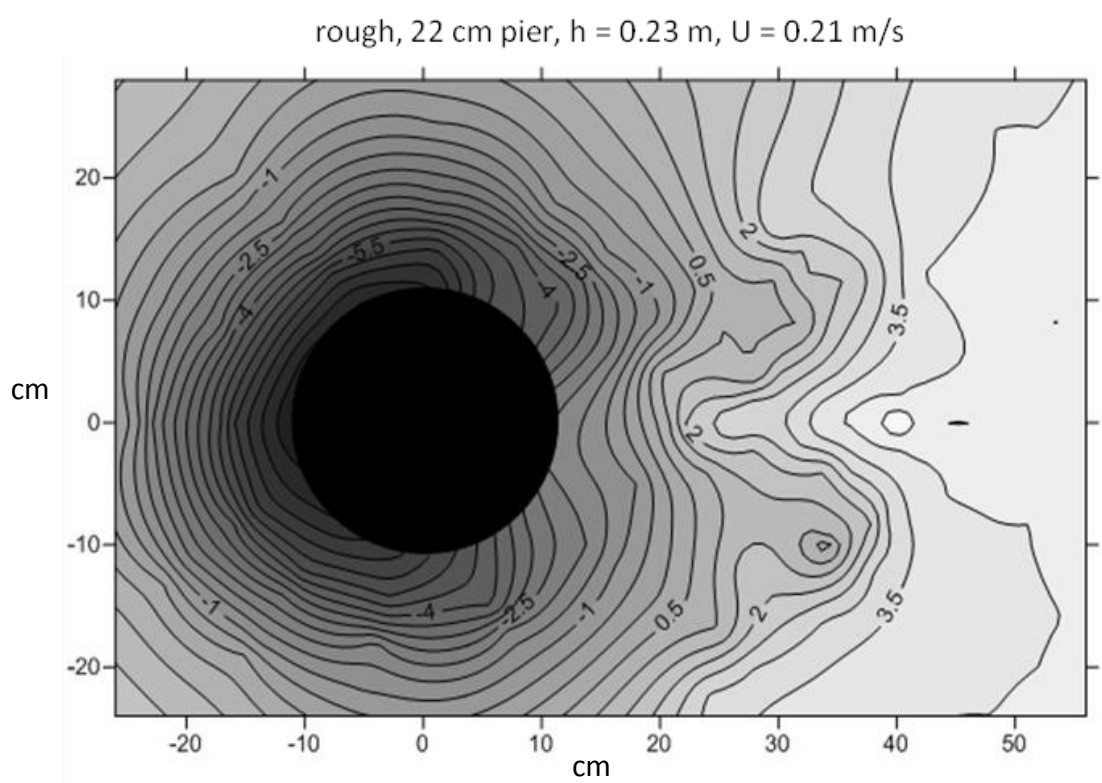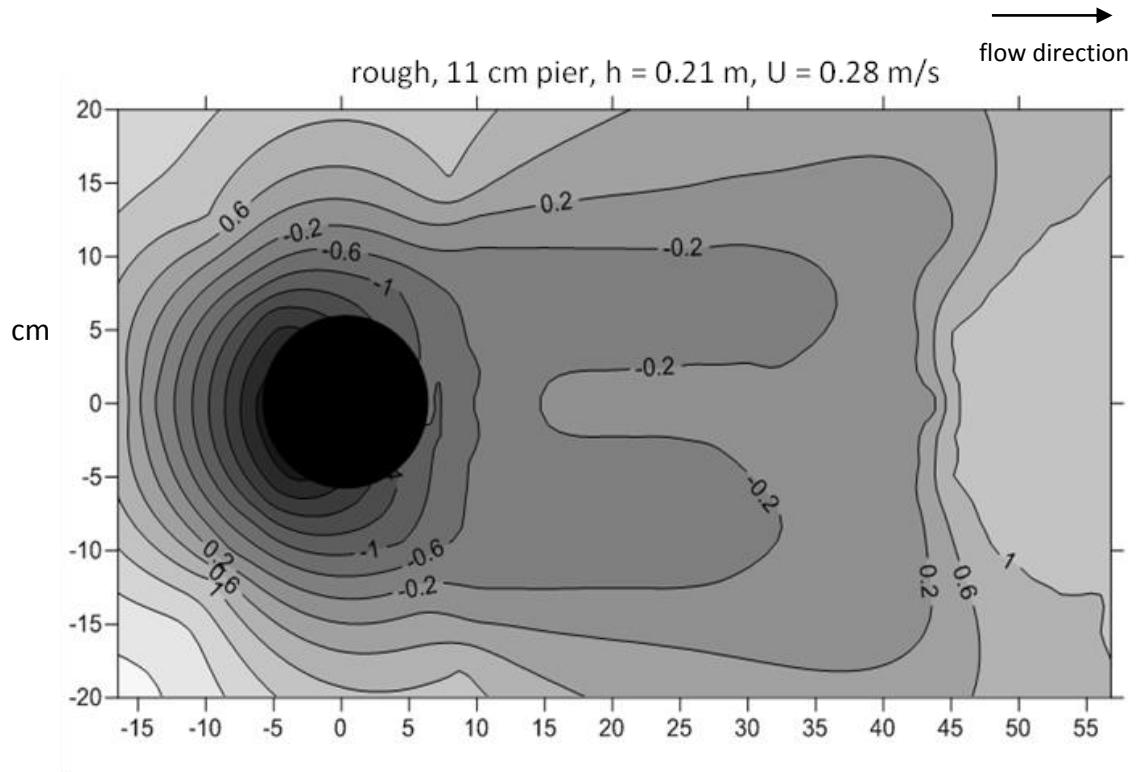
Figure 46. Scour pattern for 11 cm and 22 cm pier, $D_{50} = 0.47$ mm, under rough ice cover channel condition.

rough, 11 cm pier, h = 0.21 m, U = 0.28 m/s

flow direction

cm

cm

cm
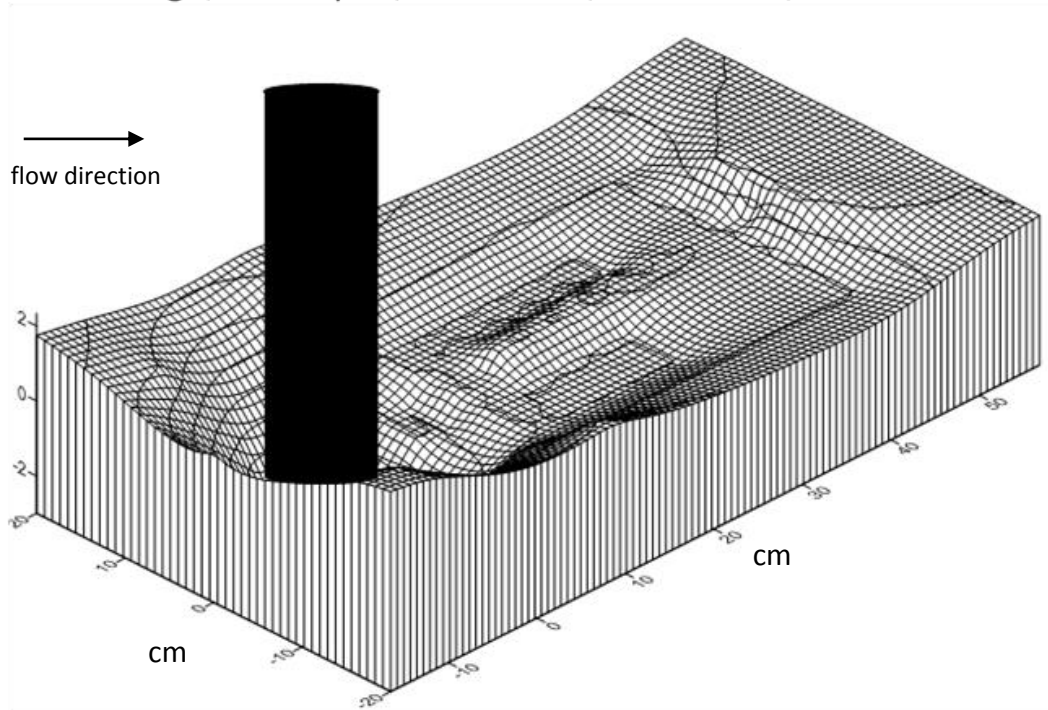
rough, 22 cm pier, h = 0.23 m, U = 0.21 m/s

cm

cm

cm
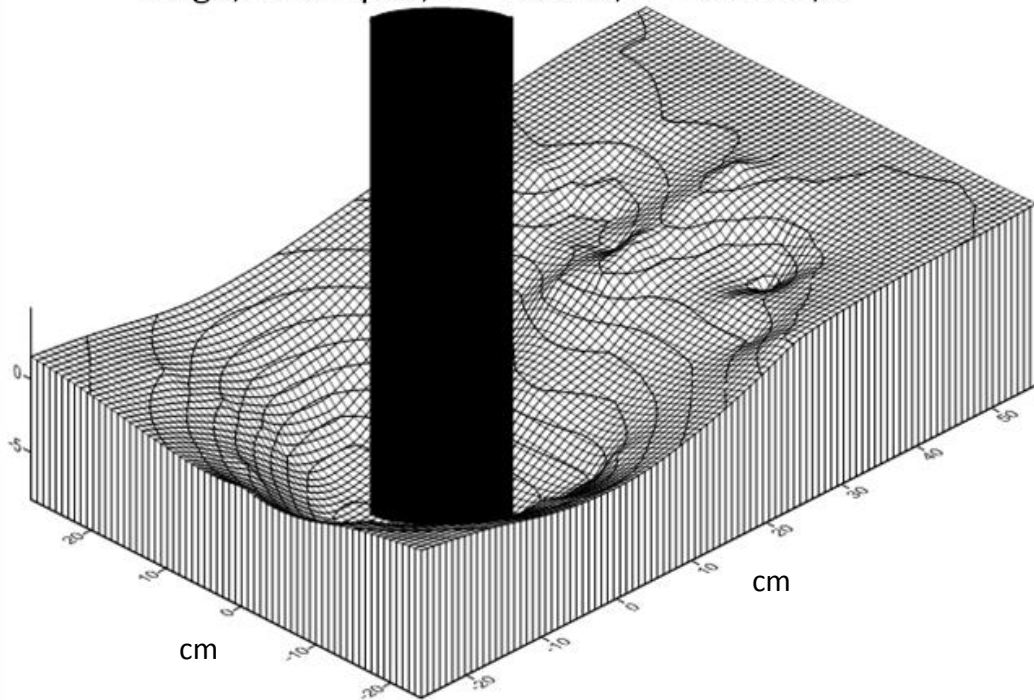
Figure 47. Scour pattern for 11 cm and 22 cm pier, D_{50} = 0.47 mm, under rough ice cover condition.

5.6 Scour profiles

The scour holes from each experiment were manually contoured in centimeter increments. The scour profiles, Figure 48, Figure 49 and Figure 50 illustrate the side view of the scour hole for representative experimental runs. The purpose of this section is to illustrate scour and deposition patterns under open, smooth and rough cover conditions. Scour profiles were measured for each experimental run; however for the sake of avoiding repetition, scour profiles presented here are a representative subset of the entire 54 run data set.

The following is a summary of scour and depositional morphology around the 11 and 22 cm piers as shown in Figure 48, Figure 49 and Figure 50. For all the cross sections the maximum scour depth is located at the upstream face of the pier at an angle of 90 degrees to approach flow. This is due to the downflow and resulting horseshoe vortex within the scour hole. Dey and Raikar (2007) found that within a scour hole there is a higher magnitude of turbulence that increases as the scour hole grows larger. The horseshoe vortices along with turbulent intensities located within the scour hole at the pier face are responsible for the location of the maximum scour depth. Additionally, as previously discussed, the smaller the grain size the larger the maximum scour depth as indicated by the differences in the profiles between the three D_{50}s.

There is also a decrease in scour depth located on the downstream side of the pier. As flow passes the sides of the pier, the flow separates and wake vortices form. The wake vortices are transferred downstream by the approach flow and are responsible for transport of sediment that is already entrained by the downflow and horseshoe vortex (Melville and Coleman, 2000). The strength of the wake vortices are typically less than the horseshoe vortices and therefore cannot transport the same sediment load as the horseshoe vortex. Since the wake vortices are

weaker behind the pier, sediment deposition may occur downstream of the pier. This is most evident in Figure 50 for the 22 cm pier. The amount of scour or deposition that occurs in front and behind the bridge pier is a balance between the strength of the horseshoe vortices and wake vortices. A larger pier size, flow depth, approach velocity and rougher channel cover all lead to increased scour depth. As scour depth increases, there is more sediment for the wake vortices to transport away from the pier base.

Scour mitigation at bridge sites often involves the placement of riprap around the pier base as a scour countermeasure. Riprap can act as a resistant armour layer to the hydraulic shear stress and provide protection to the smaller erodible sediments underneath (Deng and Cai, 2010). Lauchlan (1999) found that placing riprap at a specified depth below the bed surface improved the performance of the riprap layer. For this study, the average scour hole slope ranged from 22-25.5 percent (Table 14), with a standard deviation of up to 13 percent. As bed-form undermining (where the riprap layer is undermined) is a dominant failure mechanism (Lauchlan, 1999) it is important to understand the ranges in possible scour hole slope for successful installation of riprap. Also highlighted in this section was that the maximum scour depth occurs at the upstream pier face under all channel covers which is also important for successful installation of riprap as a scour countermeasure.
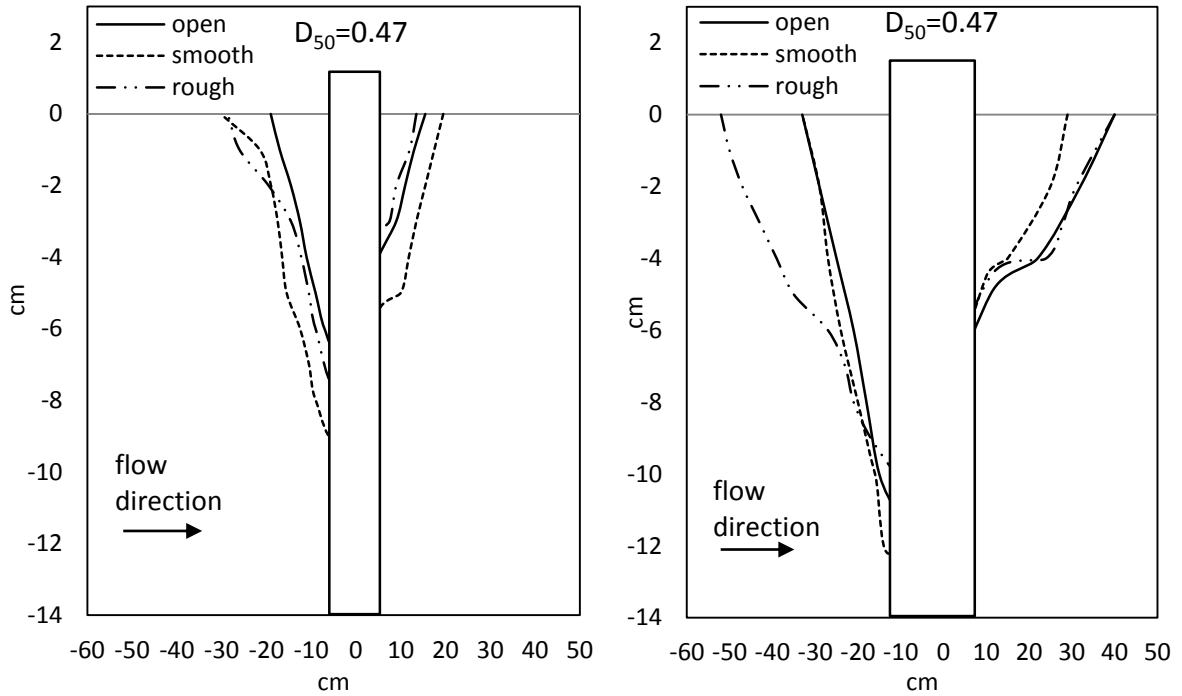
Figure 48. Scour profile for 11 (left) and 22 (right) cm pier under open, smooth and rough channel conditions for D_{50}=0.47 mm. Scour depth measurements subject to +/-0.02 cm error.
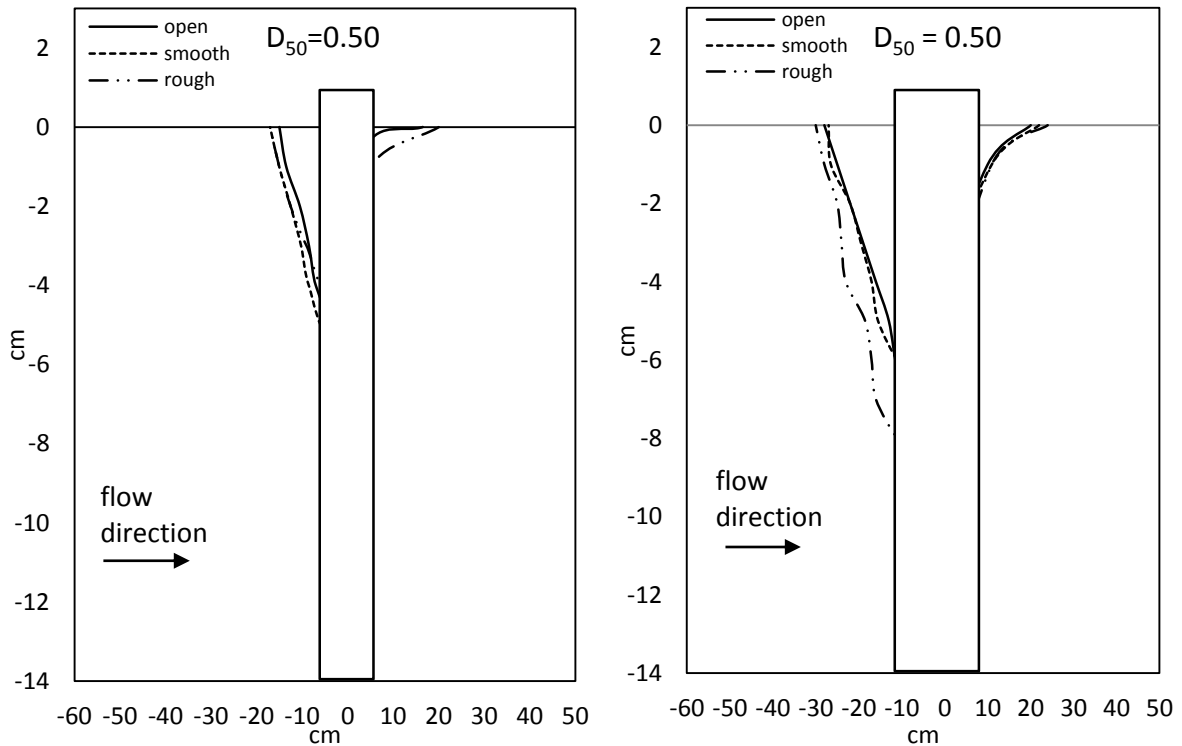
Figure 49. Scour profile for 11 (left) and 22 cm (right) pier under open, smooth and rough channel conditions for D_{50}=0.50 mm. Scour depth measurements subject to +/-0.02 cm error.
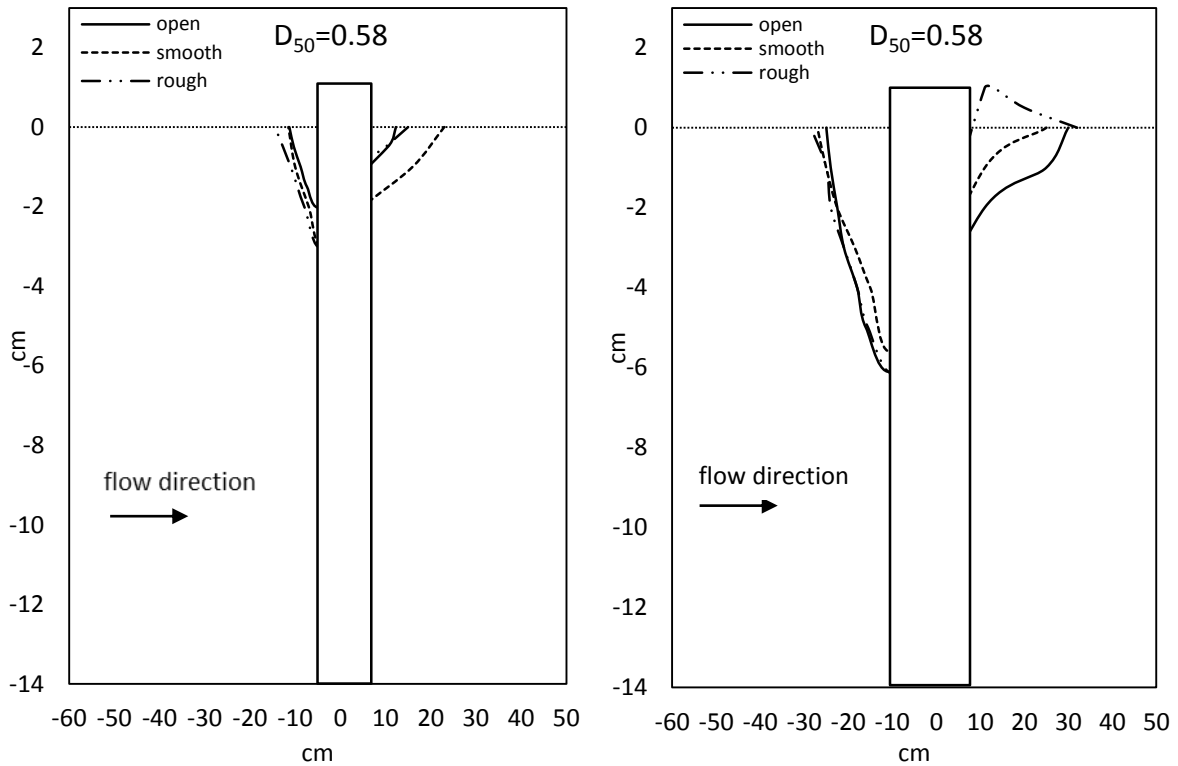
Figure 50. Scour profile for 11 (left) and 22 (right) cm pier under open, smooth and rough ice conditions for $D_{50}= 0.58$ mm. Scour depth measurements subject to +/-0.02 cm error.

Table 14. Slope of scour hole at upstream pier face for each run.

		slope (%), 11 cm pier			slope (%), 22 cm pier		
	open	20.4	25.81	17.7	24.0	11.2	16.4
D_{50}=0.58 mm	smooth	26.5	26.1	12.5	6.25	9.1	20.4
	rough	30.0	31.3	18.2	21.1	7.1	-
	open	15.4	34.5	30.0	22.3	9.4	16.1
D_{50}=0.50 mm	smooth	29.4	26.3	14.7	22.2	8.8	12.5
	rough	18.2	32.3	23.5	28.6	12.1	18.2
	open	38.1	34.2	22.4	20.2	20.0	33.3
D_{50}=0.47 mm	smooth	54.8	41.9	32.0	9.7	36.4	14.9
	rough	38.9	42.4	28.8	20.0	33.3	30.8
*average and standard deviation calculations based upon open, smooth and rough cover inclusive of pier size and sediment grain size.							
	open		22.85	standard deviation	open		8.31
average	smooth		22.46		smooth		13.08
	rough		25.57		rough		9.37

93

5.7 Armour layer analysis

In the flume literature, very few studies use natural or non-uniform sediment due to its complexity. However, since river beds are composed of a mixture of different sediment sizes it is more representative of natural systems to use non-uniform sediment in laboratory flume experiments. In an experimental flume environment, an armour layer is formed when non-uniform sediment is exposed to a constant discharge and no sediment is input to the system. Initially, bed degradation occurs, the bed decreases in slope and the sediment transport rate is at its maximum, gradually decreasing as time passes (Aberle and Nikora, 2006; Mao et al., 2011). Finer bed materials are transported faster than coarse materials under the same flow conditions; the coarse material typically rolls and jumps along the river bed until such point that hydraulic conditions cause it to become stationary. This process is repeated and the river bed sediments effectively become coarser acting as a protective layer for underlying finer material (Proffitt, 1980). The coarser sediments form a static armour layer when the flow entrains only the finer elements of non-uniform bed material (Church et al., 1998). The armouring process depends on the flow velocity and the grain size distribution of the bed mixture (Church et al., 1998).

The armour layer that developed within the scour hole was measured for each experimental run and the average armour layer D_{50} is provided in Appendix C. Figure 51, Figure 52 and Figure 53 present a subset of the experimental data and are examples of the armour layer grain size distribution for three individual experiments for each of the three D_{50}s. The armour layer generated in D_{50}=0.58 mm is coarser than the armour layer for D_{50}=0.47 mm and 0.50 mm (Figure 54). As the D_{50} decreases, more fine sediments make up the bed material and the sediment size in the armour layer decreases. Smaller particles in the armour layer will

provide less scour protection around the pier and result in a larger local scour depth. Figure 55 presents armour layer size and scour depth under the 11 and 22 cm piers. As indicated in Figure 55 armour layer size does not discriminate against pier size. Both the 11 cm and 22 cm piers have similar ranges in armour layer size. This is an important note as while pier size does affect scour depth (Figure 32, Figure 33, and Figure 34), the size of the armour layer that forms around a pier is dependent on the median size of bed material rather than the change in flow vortices with pier size. When measuring median size of the armour layer it should be noted that the non-uniform nature of the three experimental sediments presents large variation in geometric standard deviation (Appendix C). The armour layer D_{50} presented in this section is subject to both systematic and random error. Systematic uncertainty arises in the methods of armour layer sampling, namely the top 5 mm of the armour layer was sampled based upon visual observation. Slight differences would arise from each sample depth and sampling area within the pier scour hole. The upstream, side and downstream areas of the scour hole were sampled, however, slight differences in each sample taken would produce systematic error. Random error arises due to the variation in the transport of non-uniform sediment. Depending on the individual grain embedded depth, turbulence and shear stress, each experimental flume run would result in different fluid forces for sediment transport and subsequent armour layer development. The random error is represented by the geometric standard deviation values for each armour layer sample as indicated in Appendix C.

Under all channel covers, the scour depth decreases as the armour layer size increases. Similar results were also found by Raudkivi and Ettema (1985) and Dey and Raikar (2007). Both studies found that bed armouring acts to reduce pier scour development compared to the expected scour development if no bed armouring layer was present. Chiew and Melville

(1989) also investigated scour in non-uniform sediments. The authors found that local scour in non-uniform sediments was less than that of uniform sediments due to the formation of an armour layer. Raudkivi and Ettema (1983) also found that as the standard deviation of sediment increases, the rate of scouring and final equilibrium depth decreases. They found that the decrease in equilibrium scour depth was due to the formation of an armour layer, which was a significant process for standard deviation values greater than 1.4.

Scour mitigation at bridge sites often involves the placement of riprap around the pier base as a scour countermeasure. Riprap can act as a resistant armour layer to the hydraulic shear stress and provide protection to the smaller erodible sediments underneath (Deng and Cai, 2010). Riprap is the most common and cost effective scour countermeasure used today. The main drawback in using riprap as a scour countermeasure is that once in place, it is difficult to monitor the riprap placement and it may move allowing finer material to erode. Studies by Lagasse et al. (2007) and Lauchland and Melville (2001) both recommend rip-rap be placed at a depth below the average bed level in order to act as an effective countermeasure.

The findings in this study support previous research indicating that as armour layer size decreases pier scour depth increases. The presence of an ice cover did not however influence armour layer size for D_{50}=0.50 and 0.47 mm (Table 15). The average armour layer size for D_{50}=0.47 mm remained constant while average armour layer size for D_{50}=0.50 mm varied by 0.12 mm. Of note however, under D_{50}=0.58 mm the average armour layer size did increase with channel cover roughness by up to 0.67 mm (Table 15). Since all sediments used were non-uniform, it is unclear as to why the average armour layer size varied under D_{50}=0.58 mm but not under the other two sediments used. Since the critical bed shear velocity would be

slightly different for each run due to the initial sediment arrangement, the process of armour

layer development would be different for each experimental run.
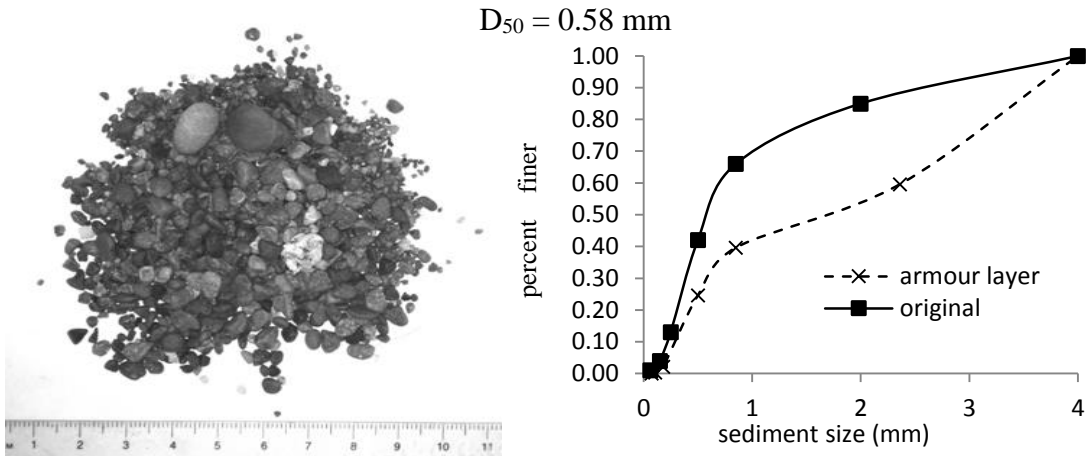
$$D_{50} = 0.58 \text{ mm}$$

Figure 51. Example of armour layer and related distribution curve for $D_{50} = 0.58$ mm.
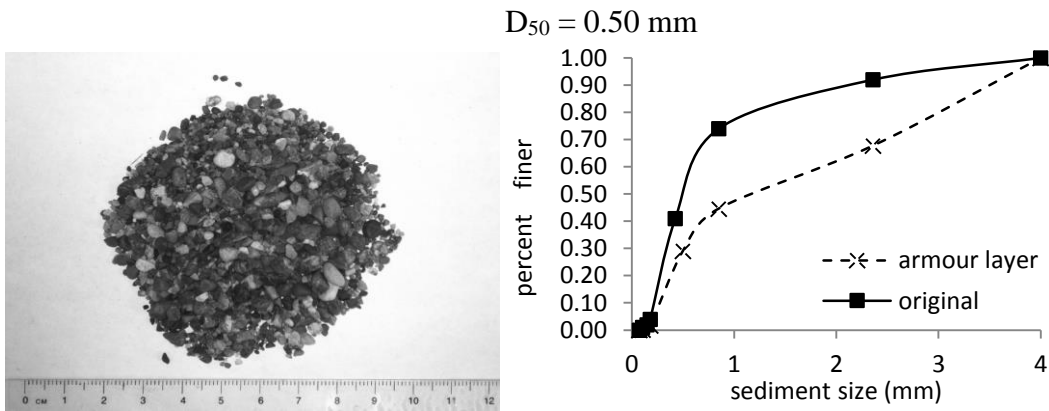
$$D_{50} = 0.50 \text{ mm}$$

Figure 52. Example of armour layer and related distribution curve for $D_{50} = 0.50$ mm.
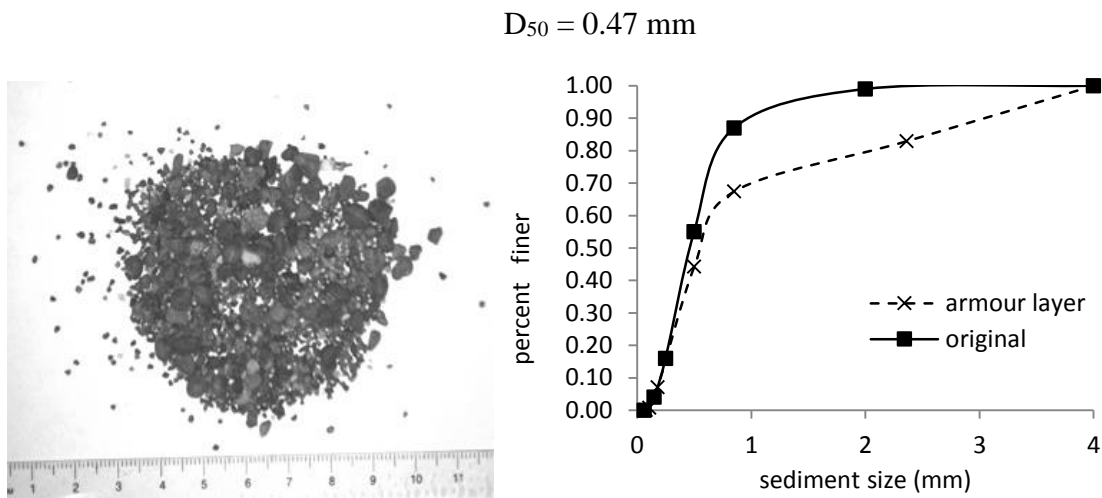
$$D_{50} = 0.47 \text{ mm}$$

Figure 53. Example of armour layer and related distribution curve for $D_{50} = 0.47$ mm.
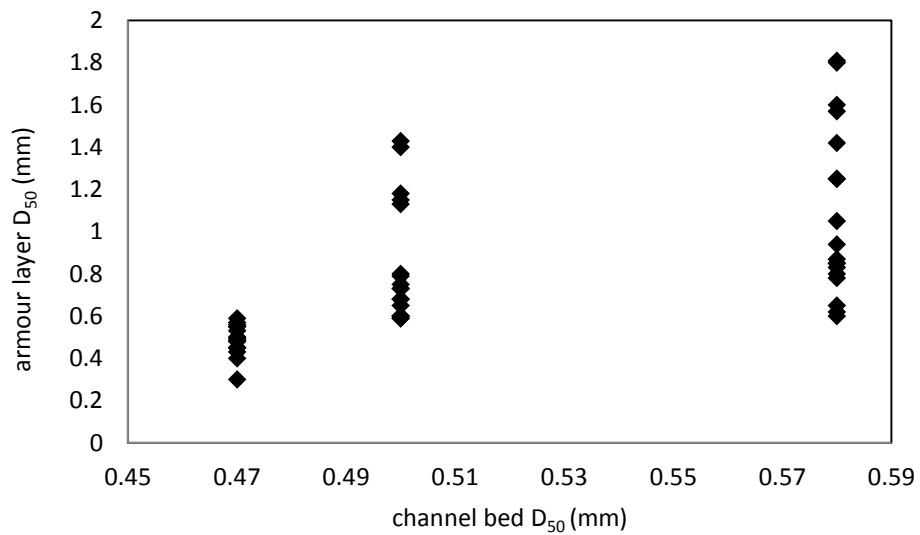
Figure 54. Variation of scour hole armour layer size with median bed grain size. The average geometric standard deviation for $D_{50} = 0.47$, 0.50, 0.58 mm is 2.57, 3.20 and 2.96 mm respectively.
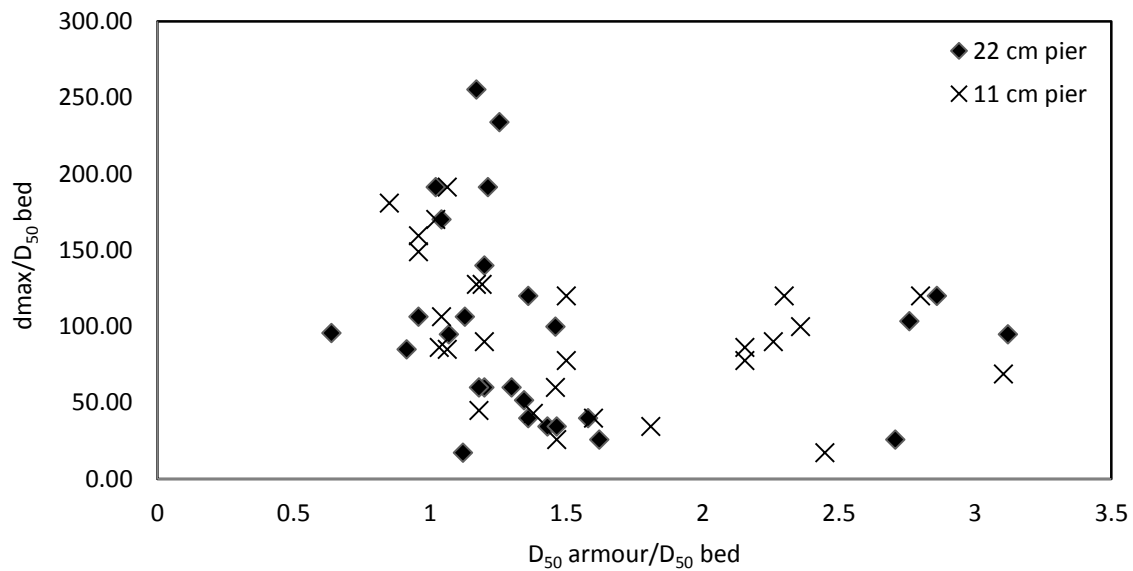
Figure 55. Variation of maximum scour depth and average scour hole armour layer size under 11 and 22 cm pier width.

Table 15. Average size of scour hole armour layer for each bed material and channel cover.

median sediment size channel bed (mm)	channel cover		
	open	smooth	rough
	median sediment size in scour hole armour layer (mm)		
$D_{50} = 0.58$	0.75	1.09	1.42
$D_{50} = 0.50$	0.87	0.88	0.76
$D_{50} = 0.47$	0.50	0.50	0.50

5.8 Scour hole velocity profiles

One of the key features of this thesis is that the scour hole velocity profiles were measured under ice cover. Previous work by Unger and Hager (2007), Graf and Istiarto (2002) and Kumar and Kothyari (2012) have investigated scour hole velocity profiles for open channel flow, but to my knowledge this is the first study to investigate scour hole velocity flow fields under ice cover.

Scour hole velocity profiles were measured for depths varying from 22-24 cm under the two tailgate flume configuration for both the 11 and 22 cm piers. Velocity measurements were taken at the end of the experimental run at which time the scour hole was fully developed. Scour hole velocity profiles for 10 cm depths (1 tailgate) were unavailable due to limitations of the ADV. Of note, while it is expected that scour hole velocity will vary slightly under various D_{50}s due to the variation in the size of the armour layer, the purpose of this section is to highlight the overall patterns and distribution of the velocity profile between open, smooth and rough channel covers. Therefore, the focus of this section is examining the differences in scour hole velocity profiles between open, smooth and rough channel conditions. As the ADV measures velocity in three dimensions, the velocity profiles presented in this section comprise the streamwise (U_x), lateral (U_y) and vertical (U_z) velocity components. The following is a summary of the profile patterns for the individual velocity components under each channel cover.

Streamwise velocity, U_x:

Figure 56 and Figure 57 represent scour hole velocity profiles for individual runs under the 22 and 11 cm piers respectively for various channel covers. For the streamwise (x) velocity component the scour hole profiles take on a logarithmic pattern. For both the 11 and 22 cm piers, the streamwise velocity for rough cover is generally higher than the scour hole velocity for smooth and open channel conditions. For the 22 cm pier, the streamwise velocity for rough cover is between 15-47 and percent higher than the scour hole velocity for open channel conditions (Table 16). This is most clearly represented for the 22 cm pier configuration under D_{50}=0.58 mm and 0.47 (Figure 56). For both pier sizes and channel conditions the streamwise

velocity is smallest in the scour hole and increases towards the water surface. Within the scour

hole, streamwise velocity decreases with scour depth, eventually reaching negative values.

This is indicative of flow reversal that occurs due to the horseshoe vortex that is located at the

pier face in the scour hole. Since the horseshoe vortex and downflow increase with pier size

(Shen et al., 1969) the patterns in the scour hole flow field are most obvious under the 22 cm

pier configuration (Figure 56).

Table 16. Average velocity measured for each profile presented in Figure 56 and Figure 57. In addition, the percent the velocity values are greater or less than open channel velocity are presented. Data are missing due to ADV error for D_{50}=0.47 mm under smooth cover conditions.

median sediment size channel bed	channel cover and velocity component (cm/s)								
	open U_x	smooth U_x	rough U_x	open U_y	smooth U_y	rough U_y	open U_z	smooth U_z	rough U_z
	11 cm pier								
$D_{50} = 0.58$ mm	8.5	14.8	17.8	4.7	-2.6	-5.9	-1.7	-4.9	-4.9
% +/- open U_x		+43	+52		-36	-56		-65	-65
$D_{50} = 0.50$ mm	10.6	11.7	11.4	-3.4	-1.2	4.7	-6.7	-7.6	-6.2
% +/- open U_x		+9.5	+7.1		+35	+58		-12	+7.3
$D_{50} = 0.47$ mm	9.4	-	13.2	-1.1	-	-4.6	-5.8	-	-4.3
% +/- open U_x			+29			-76			+26
	22 cm pier								
$D_{50} = 0.58$ mm	6.6	7.9	9.8	-1.3	0.2	1.4	-3.6	-3.1	-0.7
% +/- open U_x		+16	+33		+13	+51		+14	+80
$D_{50} = 0.50$ mm	4.9	8.9	9.1	-0.4	-2.7	3.4	-3.2	-1.9	-1.7
% +/- open U_x		+45	+47		-85	+89		+61	+47
$D_{50} = 0.47$ mm	6.3	7.4	9.2	-3.5	-2.9	-0.7	-4.3	-4.2	-4.2
% +/- open U_x		+15	+32		+18	+80		+2.4	+2.4

Lateral velocity, U_y:

For the lateral (y) velocity component, there does not appear to be any pattern in flow

for both the 11 cm and 22 cm pier. The lateral velocity profile appears turbulent and changes

between positive and negative values along the entire profile.

Vertical velocity, U_z:

For the vertical velocity component (z) the scour hole profiles exhibit patterns in the shape of the letter C. Figure 56 represents the C-shaped profile to a greater extent than the profiles for the 11 cm pier (Figure 57). The downward velocity is generally greatest under rough cover conditions and smallest under open channel conditions (Table 16). In examining the C-shaped profile, the smallest velocity typically occurs at the transition zone between the channel bed and scour hole. From the channel bed to transition zone the velocity decreases, while from the transition zone to the water surface the velocity increases.

Discussion:

For open channel flow, the logarithmic and C-shaped scour hole velocity distributions for streamwise and vertical velocity are similar to those found by Kumar and Kothyari (2012). Under open channel conditions the horseshoe vortex and downflow increase with pier size (Shen at al., 1969) therefore patterns in the scour hole flow field are most obvious under the 22 m pier configuration. Under the experimental conditions for this study, it was found that the streamwise and vertical (U_x, U_z) velocity profiles for smooth and rough ice cover have a similar distribution and pattern to open channel flow, however, ice cover leads to higher velocity values. The streamwise and downward velocities at the pier face are greater under ice cover than open channel flow. For all sediment D_{50}s under the 22 cm pier, the average rough cover velocity is 37 percent greater and the average smooth cover velocity is 15 percent greater than the open channel velocity (calculated from Table 16). For all sediment D_{50}s under the 11 cm pier, the average rough cover velocity is 29 percent greater and the average smooth cover velocity is 26 percent greater than the open channel velocity. As ice cover shifts the location

of maximum velocity towards the channel bed (Sui et al., 2010), while also increasing the maximum velocity, the overall bulk velocity value is generally higher under ice cover than open channel flows.

A greater flow down the face of the pier to the riverbed can lead to greater scour around the pier base. Under open channel conditions, approaching flow velocity meets the pier face and flows downward to the channel bed or upward to form a bow wave. Under ice cover conditions, the extent of the upward flow and bow wave is diminished due to the ice cover boundary. This causes increased downflow at the pier face resulting in a greater capacity for sediment transport. These conditions described above of increased downflow under ice cover are consistently present under the 22 cm pier for the vertical (U_z) velocity component. For all sediment D_{50}s under the 22 cm pier, the average rough cover vertical velocity is 43 percent greater and the average smooth cover vertical velocity is 26 percent greater than the open channel velocity (calculated from Table 16). The larger scour hole velocity under ice cover supports the findings of greater pier scour depth under ice cover given a consistent armour layer size in comparison to open channel conditions.
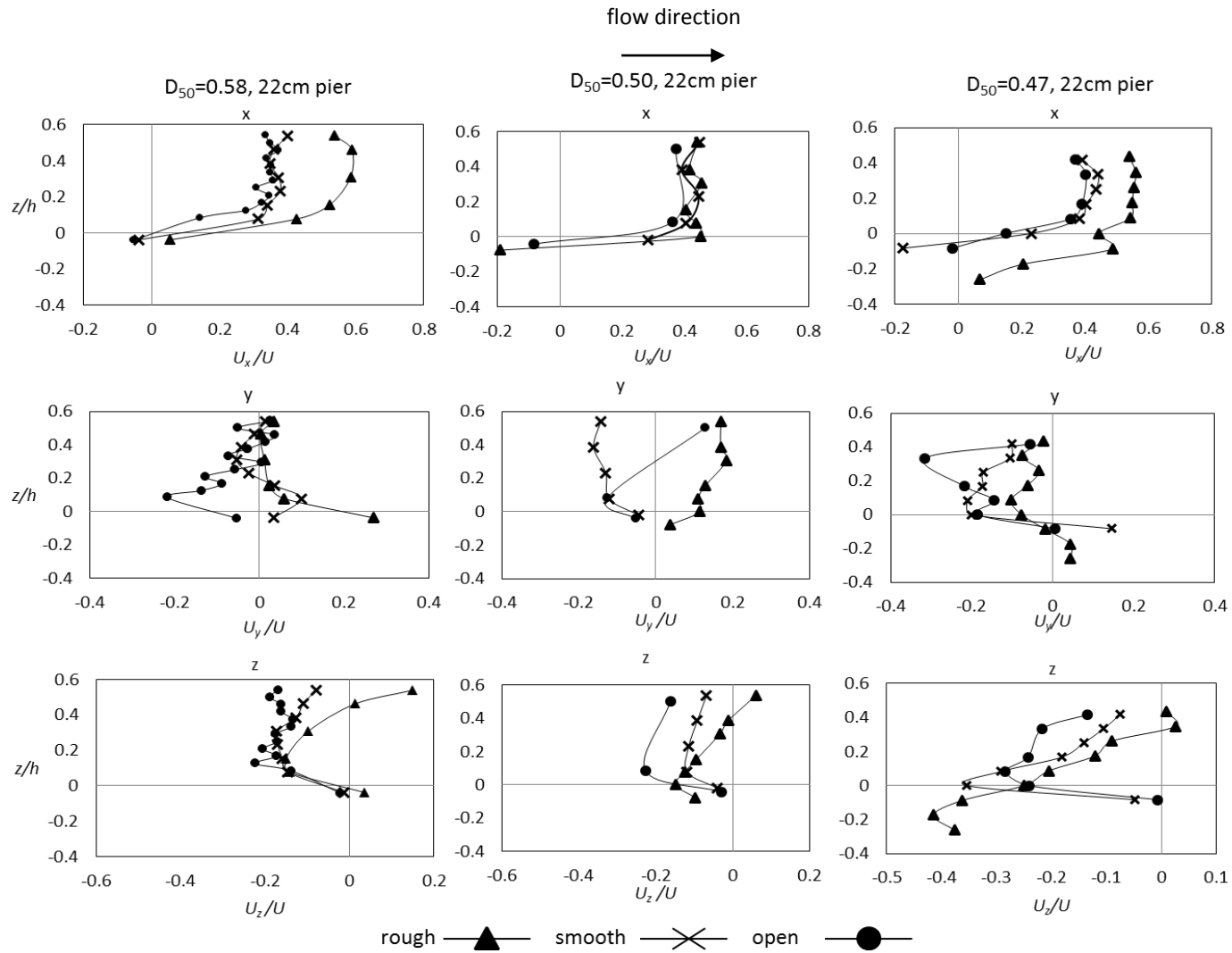
 Figure 56. Scour hole velocity profiles for the streamwise (Ux), lateral (Uy) and vertical (Uz) velocity components under open, smooth and rough ice cover for 22 cm pier. All profiles were measured under the two tailgate flume position with water depths from 22-24 cm. ADV measurements are accurate to +/- 0.25 cm/s.
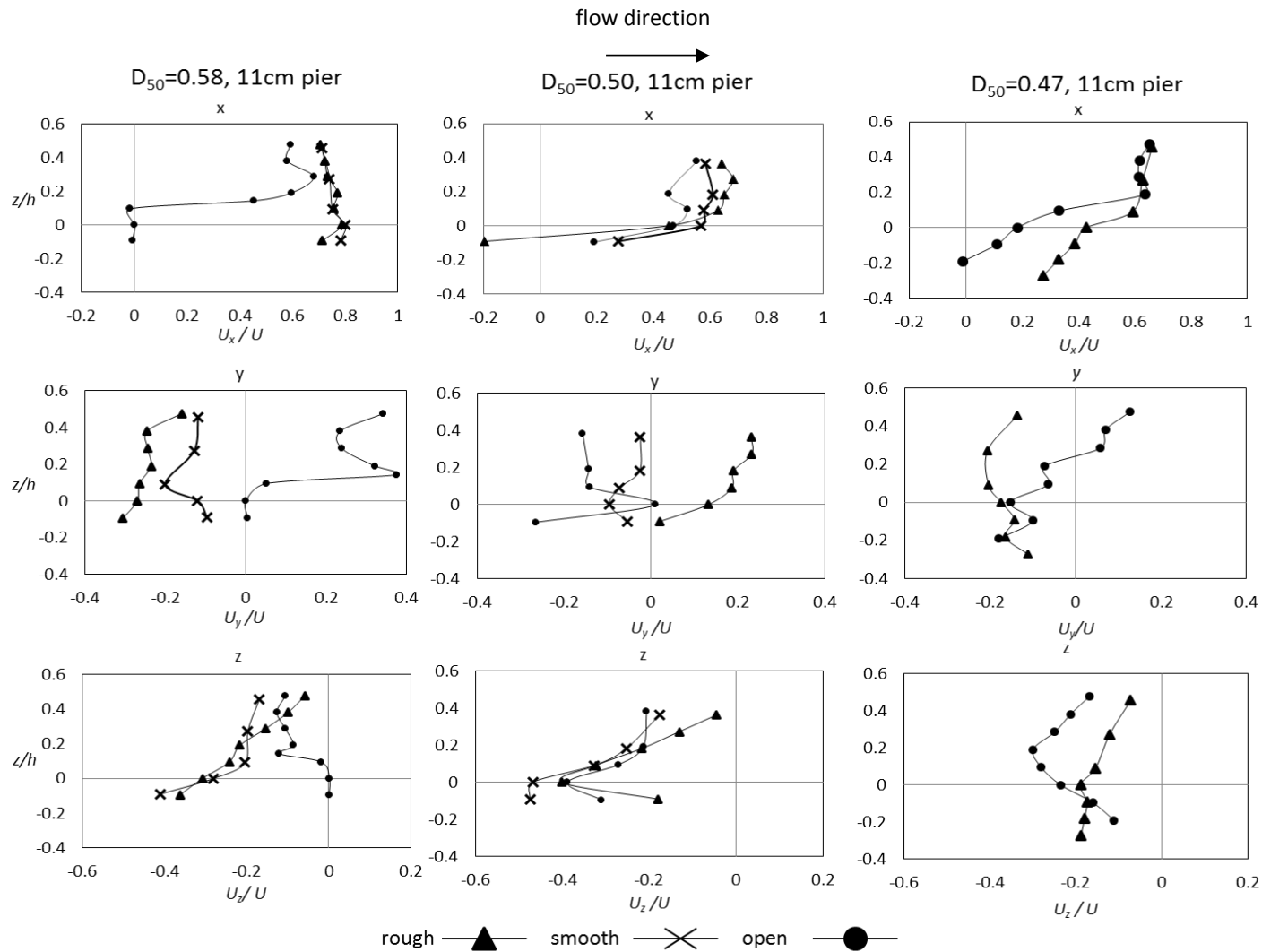
Figure 57. Scour hole velocity profiles for the streamwise (Ux), lateral (Uy) and vertical (Uz) velocity components for 11 cm pier. All profiles were measured under the two tailgate flume position with water depths from 22-24 cm. Smooth cover velocity profiles for $D_{50}=0.47$ mm are missing due to ADV file error. ADV measurements are accurate to +/- 0.25 cm/s.

5.9 Dimensional Analysis

Dimensional analysis is the relationship between various physical quantities by identifying their dimensions. The dimension of any physical quantity is simply the actual physical dimensions that create it. In order for engineers to understand pier scour the parameters and associated dimensions responsible for local scour must be defined. The following are parameters that are associated with local pier scour as suggested by Ozalp (2013) and Melville and Coleman (2000). The parameters are classified in terms of time (T), length (L) and mass (M).

Table 17. Parameters associated with local pier scour.

Parameters describing flow		Units	Dimensions
g	gravitational acceleration	m/s^2	LT^{-2}
H	approach flow depth	m	L
U	approach flow velocity	m/s	LT^{-1}
U_*	shear velocity	m/s	LT^{-1}
ρ_w	density of water	kg/m^3	ML^{-3}
ν	kinematic viscosity of water	m^2/s	$L2T^{-1}$
Parameters describing the flume			
s	channel slope	-	-
B	channel width	m	L
n_i	Manning's coefficient for ice cover roughness	-	-
Parameters describing channel bed material			
ρ_s	sediment density	kg/m^3	ML^{-3}
D_{50}	median sediment size	mm	L
σ_g	standard deviation of sediment size	-	-
C	cohesion	kg/m s^2	$ML^{-1}T^2$
n_b	Manning's coefficient for channel bed	-	-
D_{50a}	median sediment size of the armour layer	mm	L
Parameters describing bridge pier			
b	pier diameter	m	L
K_1	pier shape factor	-	-
K_r	pier surface roughness	-	-
K_2	angle of attack	-	-
Time			
t	flow duration	min	T

The above parameters associated with local pier scour can be presented by the following relationship, where d_{max} represents the maximum scour depth:

$$d_{max} = f(\ g,\ H,\ U,\ U_*,\ \rho_w,\ \nu,\ s,\ B,\ n_i,\ \rho_s,\ D_{50},\ \sigma_g,\ C,\ n_b,\ D_{50a},\ b,\ K_1,\ K_r,\ K_2,\ t)\ = 0 \qquad 5.7$$

Under dimensional analysis the following parameters from equation 5.7 are considered:

$$\frac{d_{max}}{d} = f\left(\frac{U}{\sqrt{gH}}, \frac{UD_{50}}{\nu}, \frac{D_{50}}{H}, \frac{U_*}{U}, \frac{D_{50}}{B}, \frac{D_{50a}}{D_{50}}, \frac{\rho_s - \rho_w}{\rho_w}, \frac{Ut}{B}, \frac{n_i}{n_b}, \sigma_g, \frac{C}{\rho U^2}, \frac{b}{B}, \frac{b}{H}, s, K_1, K_r, K_2\right) \qquad 5.8$$

In considering the experimental conditions of this study equation 5.8 can be simplified by the following conditions:

(a) the flume has a constant slope and channel width so the s and B terms are ignored

(b) cylindrical piers are used which are smooth, and the angle of attack for all experiments is zero, so the K_1, K_r and K_2 terms are ignored

(c) the bed materials remain constant for each experimental set, so the σ_g term is ignored and the $\frac{n_i}{n_b}$ term is considered instead.

(d) the densities of the flume water and sediment are constant for each experimental subset so the $\frac{\rho_s - \rho_w}{\rho_w}$ is ignored.

(e) the bed material is non-uniform and considered non-cohesive (C = 0) so the $\frac{C}{\rho U^2}$ is ignored.

(f) after 24 hrs of experimental run time, an armour layer is formed and equilibrium scour depth is reached; therefore scour time, $\frac{Ut}{B}$, is ignored.

(g) for each experimental subset, the $\frac{U_*}{U}$ is defined in relation to $\frac{D_{50}}{H}$ as it depends on approach flow depth.

Given the above conditions, equation 5.8 is simplified and the following parameters are related

to scour depth under the experimental conditions of this study:

$$\frac{d_{max}}{d} = f\left(\frac{U}{\sqrt{gH}}, \frac{UD_{50}}{\nu}, \frac{D_{50}}{H}, \frac{D_{50}}{B}, \frac{D_{50a}}{D_{50}}, \frac{n_i}{n_b}, \frac{b}{B}, \frac{b}{H}\right) \qquad 5.9$$

Where $\frac{U}{\sqrt{gH}}$ is the Froude number, $\frac{UD_{50}}{\nu}$ is the particle Reynolds number, $\frac{D_{50}}{H}$ and $\frac{D_{50}}{B}$ is the

relationship between median sediment grain size, flow depth and pier width, $\frac{D_{50}}{D_{50a}}$ represents

the impact of sediment composition on armour layer particle size, $\frac{n_i}{n_b}$ represents the ice cover

roughness and the channel bed roughness and $\frac{b}{B}$ and $\frac{b}{H}$ is the pier diameter in relation to

channel width and water depth. Since three types of sand are used for flume experiments, the

densimetric Froude number can also be used in addition to the Froude number, written as:

$$F_o = \frac{U}{\sqrt{\frac{gD_{50}(\rho_s - \rho)}{\rho}}} \qquad 5.10$$

Also of interest in this research is the specific particle Reynolds number, which is indicated by

the shear velocity U_*, so the shear Reynolds number is substituted for the Reynolds number,

written as:

$$Re_* = \frac{U_* D_{50}}{\nu} \qquad 5.11$$

In the following sections, the parameters in equations 5.9 will be compared to maximum scour

depth through correlation and regression analysis.

5.10 Correlation of scour depth versus the Froude number

The ability of an object to move through water will depend on its size (object length and area) as well as the relative velocity and depth of water. The Froude number, $U/\sqrt{gH}$, represents the ratio of fluid inertial forces to fluid gravitational forces. The greater the Froude number, the greater the resistance exerted by water flow on the river bed material. It is standard engineering practice to relate pier scour to flow depth, flow velocity, pier size and the Froude number (Molinas, 2003). One of the first studies to document the positive relationship between Froude number and scour depth was Aziz (1983). The author found pier scour was dependant on both flow depth and velocity and pier scour increased with increasing Froude number. Wu et al. (2014) also documented that the Froude number increased with abutment scour depth under ice cover and open channel flow. Of note however, it is important to consider that the Froude number used in laboratory experiments may be larger than that for similar field conditions as pointed out by Melville and Coleman (2000). Since the flume sediment relative to pier size is larger than the prototype, the flow velocity required for incipient motion may be larger than the velocity derived from Froude scaling of prototype flow (Melville and Coleman, 2000). As such, the Froude number used in flume experiments may be larger than that for field conditions, leading to overestimation of pier scour. While scaling issues related to the Froude number are discussed here, further scaling issues are addressed in Chapter 6. As the Froude number incorporates flow depth and velocity, and scour depth is dependent on flow depth and flow velocity, the relationship between scour depth and the Froude number is examined in this section.

Since the Froude number is a dimensionless variable, it was plotted against the dimensionless maximum scour depth (d_{max}/H) in Figure 58. For all experiments, there is a positive relationship between the Froude number and maximum scour depth (Figure 58). To further investigate variation in Froude number with scour depth, rough ice cover and open channel conditions are compared in Figure 59; however, only open channel and rough cover were compared for all three D_{50}s since including smooth cover created a visually busy graph. The relationship between Froude number and maximum scour depth under smooth ice cover for all three D_{50}s is presented in Figure 60.
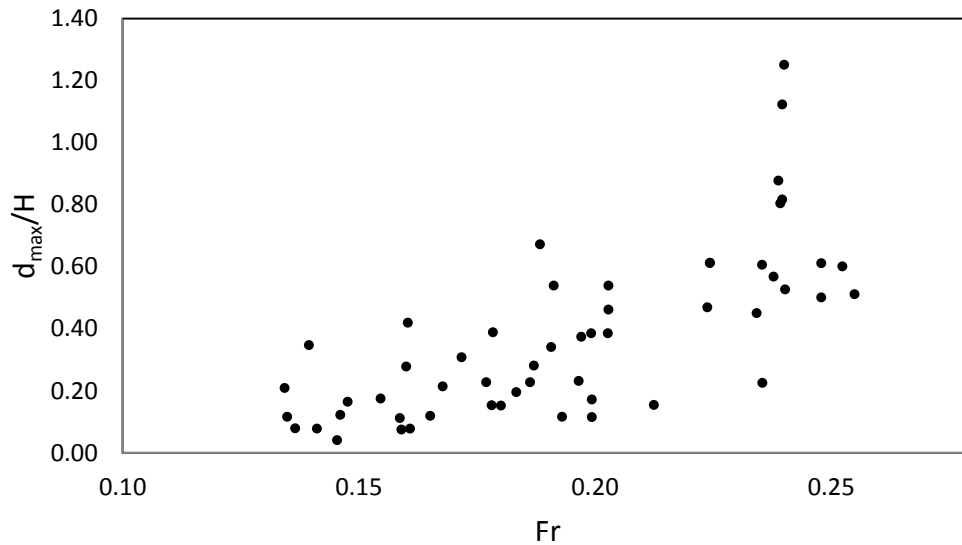
Figure 58. Variation of maximum scour depth with Froude number for all experimental runs.
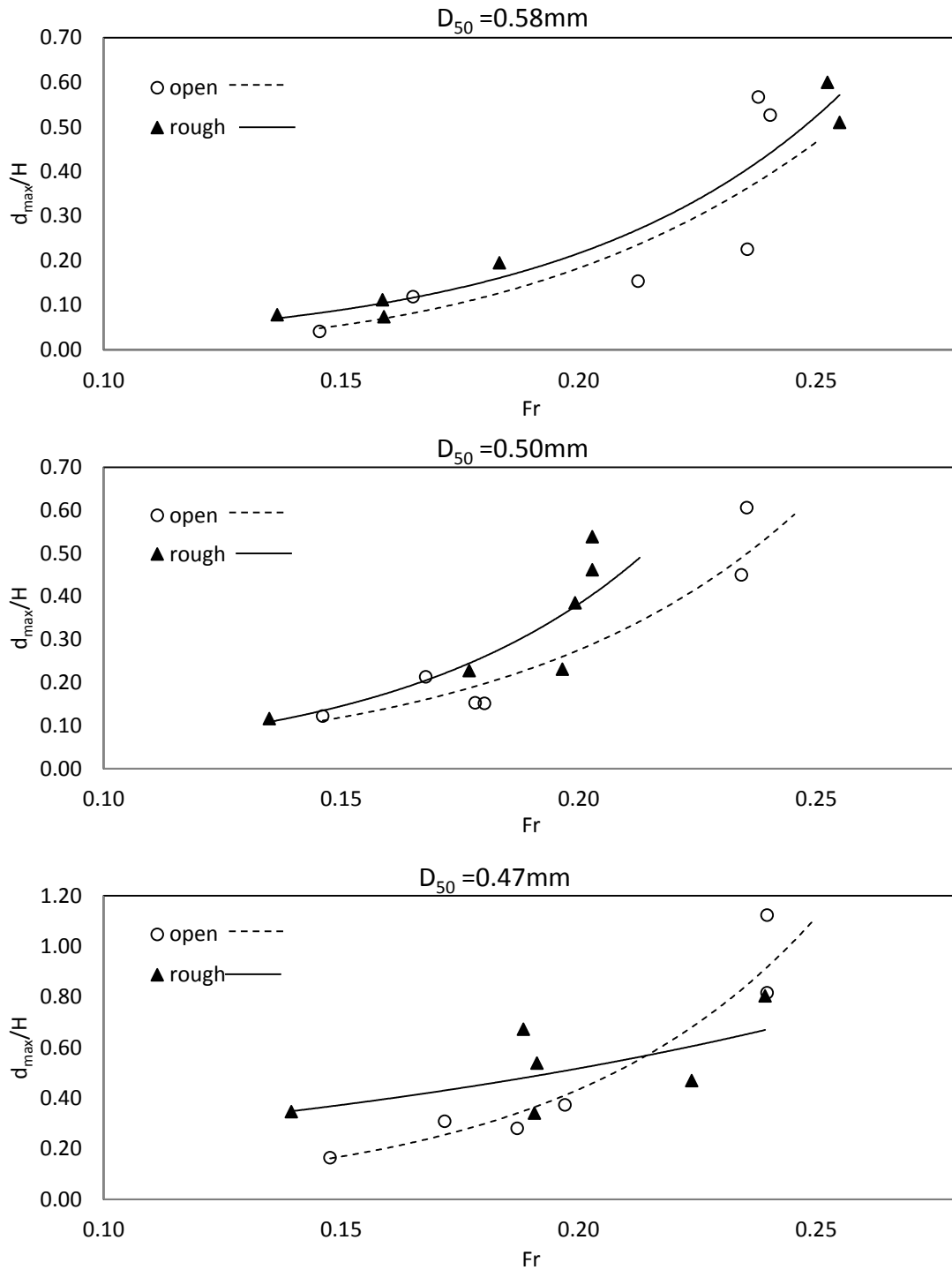
Figure 59. Variation of maximum scour depth with the Froude number under open and rough cover for all three sediment sizes.
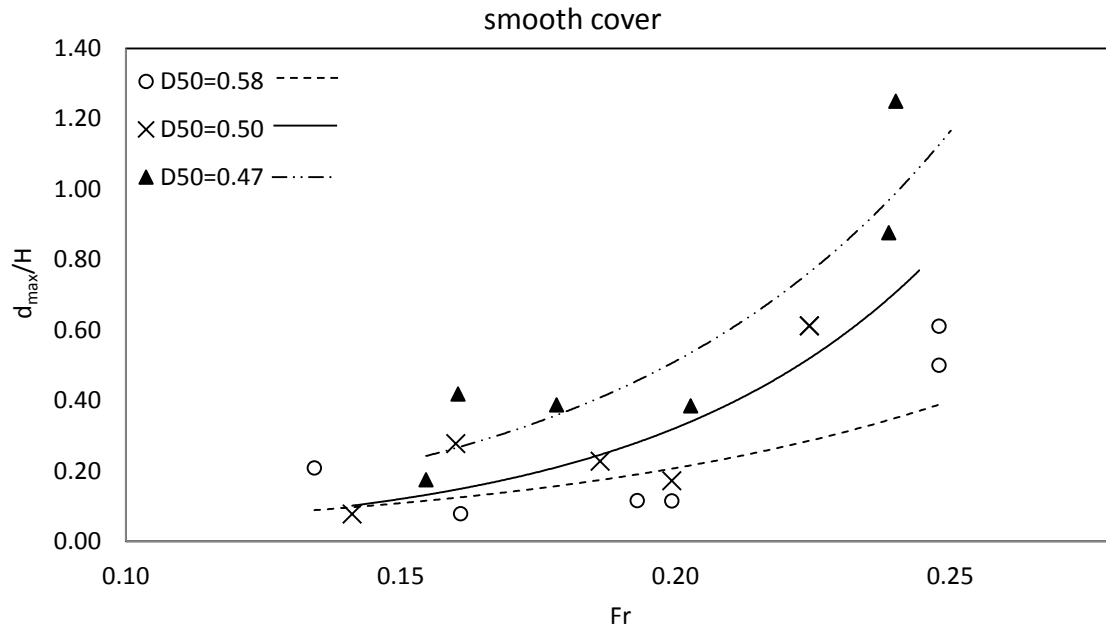
Figure 60. Variation of maximum scour depth with Froude number for smooth channel cover under various sediment sizes.

Generally, under the same Froude number, maximum scour depth is greater under rough ice cover conditions (Figure 59). This is clear for D_{50}=0.58 and 0.50 mm; however, under D_{50}=0.47 mm maximum scour depth is not greater under ice cover conditions for Froude>0.22 (Figure 59). There is also a large range in measured scour depth exhibited for D_{50}=0.50 mm, rough cover at Fr~0.20 and for D_{50}=0.47 mm, rough cover, around Fr~0.19. Under smooth ice cover, maximum scour depth also increases with Froude number. For smooth ice cover conditions, under the same Froude number, the largest scour depth occurs under D_{50}=0.47 mm, while the smallest scour depth occurs under D_{50}=0.58 mm (Figure 60).

The large range in measured scour depth exhibited for D_{50}=0.50 mm, rough cover at Fr~0.20 and for D_{50}=0.47 mm, rough cover, around Fr~0.19 is most likely due to variation in the initial non-uniform sediment arrangement and subsequent armor layer development. In

general, under uniform sediment, an ice cover will increase resistance and turbulence and therefore potential for sediment transport – which supports the trend of larger scour depths under rough ice cover then open channel under the same Froude number. However, for the same Froude number, non-uniform sediment transport processes will vary according to initial sediment arrangement and interactions between sediment grains.

In order to incorporate sediment size in relation to the Froude number, the densimetric Froude number, F_o, can be used as the mass density of sediment is considered (Equation 5.10). Hodi (2009) conducted a series of flume experiments using uniform sediment, D_{50}=0.85 mm, investigating pier scour under F_o = 2.1 and 2.5 under 10, 20 and 30 mm piers. The author found that when the pier size is held constant and F_0 increases from 2.1 to 2.5 the area of scour increases significantly. For this study, in order to investigate if the F_o has a relationship with scour depth, the dimensionless scour depth is plotted against the densimetric Froude number in Figure 61. As indicated by Figure 61, relating the scour depth to the densimetric Froude number provides no guidance when applied to non-uniform sediment. The scatter is large and no significant relationship is present. When the same velocity is applied to both a uniform and non-uniform sediment of the same D_{50}, each sediment will have different critical velocities due to the arrangement and interactions of individual bed grains.

Molinas and Wu (1998) point out that a single sediment size such as the D_{50} does not reflect the range in non-uniform sediment sizes nor the impact various size fractions have on transport calculations. The authors evaluated commonly used sediment transport formulas for bed-material load of non-uniform sediment and found that the transport formulas gave considerable scatter for bed-material load relationships. As a result, Molinas and Wu (1998) developed a size gradation compensation factor, which is a function of the geometric standard

deviation and flow conditions. They included this in the original transport formulas and found that agreement between the measured and computed bed-material concentrations improved.

As indicated by Molinas and Wu (1998), the D_{50} value in the densimetric Froude number does not adequately represent the sediment composition and therefore the F_o does not present a strong relationship with pier scour depth for non-uniform sediment. This study does however indicate that there is a relationship between scour depth and the Froude number. For $D_{50}= 0.58$ and 0.50 mm, under the same Froude number, rough ice cover produces a greater scour depth then open channel conditions. Even though flume scaling under Froude similarity may lead to overestimation of pier scour, it is still important in bridge design to note that ice cover may produce a larger scour depth in comparison to open channel conditions under the same Froude value.
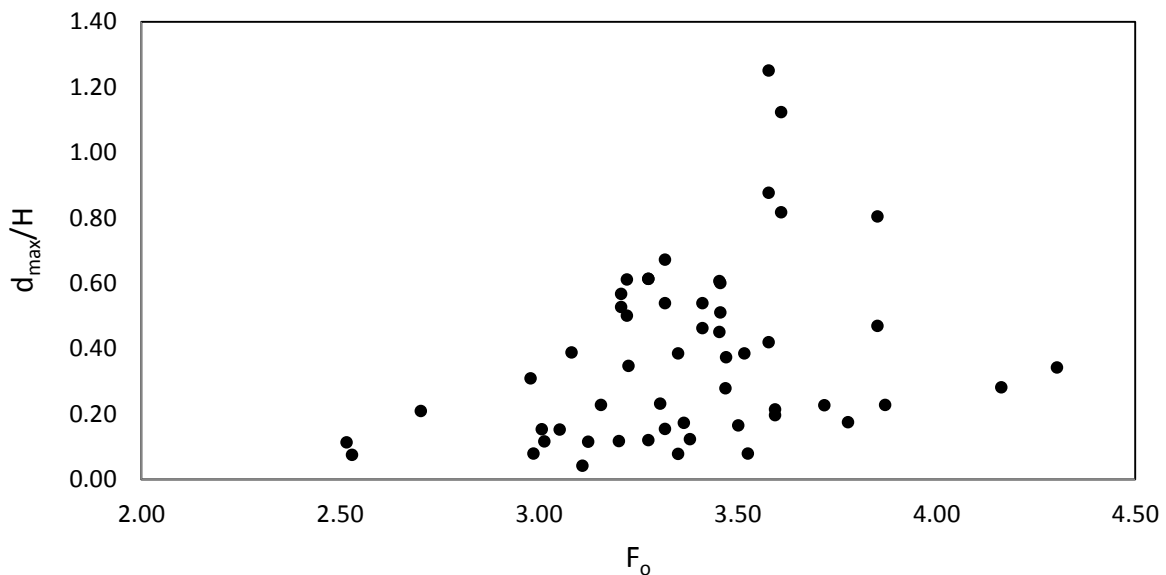
Figure 61. Variation of dimensionless maximum scour depth with densimetric Froude number for all experiments.

5.11 Correlation of scour depth versus shear stress – incipient motion

A sediment grain will move when the shear stress acting on it is greater than the resistance of the particle to movement. The magnitude of shear stress required to move a particle is known as the critical shear stress (T_{cr}). The resistance of the particle to movement and entrainment will vary depending on the particle size, its orientation, particle size relative to surrounding particles and embedment. The relationship between the dimensionless shear stress and the Reynolds number is known as the Shields Diagram which is often used for predicting incipient motion of sediment. The critical Shields value, also called the dimensionless shear stress, τ_*, used to calculate the initiation of motion of sediment is given by the following equation:

$$\tau_* = \frac{\rho U_{*c}^2}{g \Delta \rho D_{50}}$$ 5.12

where ρ is the fluid density, $\Delta \rho$ is the difference between the fluid density and sediment density, U_{*c} is the critical shear velocity, g is gravity, and D_{50} is the median sediment size of bed material. The logarithmic velocity distribution assumption is one of the generally accepted methods for calculating the shear velocity based on the Prandtl and Einstein correction factor (Einstein, 1950).

$$U_{*C} = \frac{\bar{u}}{5.75 \log_{10}\left(\frac{12.27 \chi R_h}{D_{50}}\right)}$$ 5.13

where R_h is the channel hydraulic radius, $\bar{u}$ is the average cross sectional velocity, D_{50} is the median bed grain size and χ is the Einstein multiplication factor, $\chi = 1$. For ice covered flow,

the ice cover can be included under the channel hydraulic radius. In practice, the shear

Reynolds number is usually used to study sediment incipient motion, which is given by:

$$R_e^* = \frac{U_{*c}D}{v} \qquad\qquad 5.14$$

in which, U_{*c} is the critical shear velocity, D is the grain size diameter and v is the kinetic

viscosity of the fluid. Since the sediment used here is the non-uniform sediment, the grain size

diameter will be replaced by D_{50}, then the above equation can be written as following,

$$R_e^* = \frac{U_{*c}D_{50}}{v} \qquad\qquad 5.15$$

The calculated dimensionless shear stress versus Reynolds number is presented in

Figure 62. Under all sediment sizes, as the dimensionless shear stress increases so does the

shear Reynolds number. For the same shear Reynolds number, the finest sediment $D_{50}=0.47$

has the highest dimensionless shear stress. The greater dimensionless shear stress, the greater

the capacity for sediment transport. With a higher proportion of finer particles in non-uniform

sediment, high dimensionless shear stress values will lead to greater sediment transport. For

the same dimensionless shear stress, the coarser the bed material, the larger the shear Reynolds

number. A larger Reynolds number for coarser sediment particles indicates a larger shear

velocity is required for incipient motion of sediment.

Figure 63 presents the maximum scour depth as it relates to dimensionless shear stress

for both the 11 and 22 cm pier. As the maximum scour depth increases the dimensionless

shear stress increases correspondingly. Figure 63 also indicates that, for dimensionless shear

stress>0.030, the 22 cm pier will produce a greater maximum scour depth. This supports

findings by Breusers et al. (1977) that the dimension of the horseshoe vortex is a function of

pier diameter. With a larger horseshoe vortex, the sediment transport capacity is greater hence the larger maximum scour depth for the larger 22 cm pier.

Figure 64 and Figure 65 present the maximum scour depth in relation to dimensionless shear stress for open channel and rough ice cover conditions. For both open channel and ice covered conditions the maximum scour depth and dimensionless shear stress increase correspondingly. This positive trend is expected as increasing dimensionless shear stress allows for greater sediment transport and larger scour hole development. For both the 11 and 22 cm piers, under the same dimensionless shear stress open channel conditions produce a larger scour hole. In other words, under rough ice cover conditions less dimensionless shear stress is required for sediment transport and scour hole development.
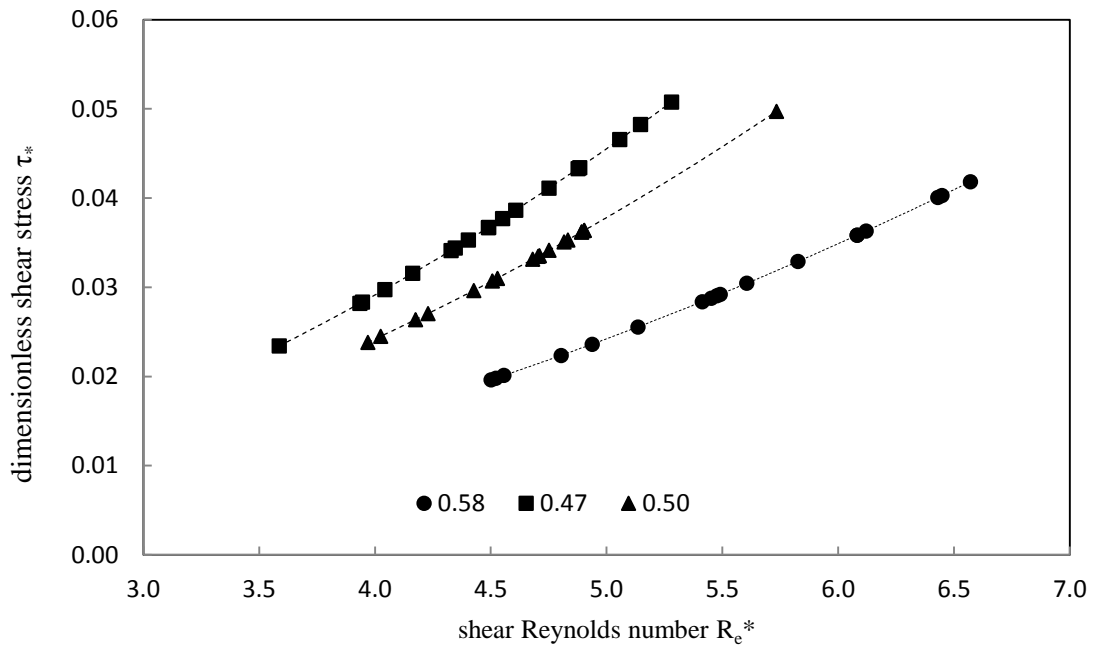
Figure 62. The variation of shear Reynolds number with dimensionless shear stress
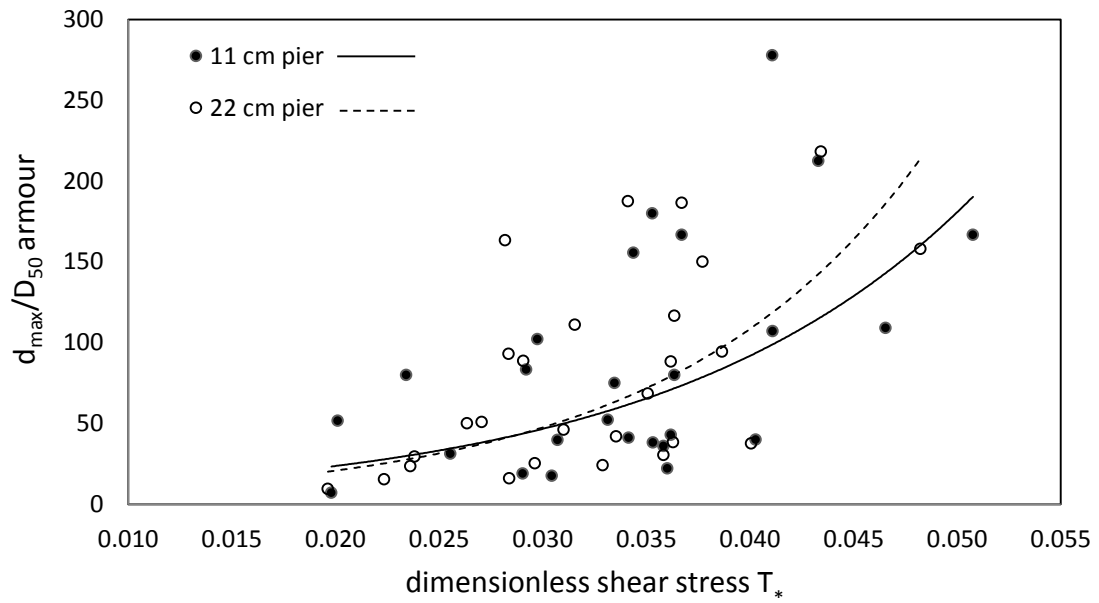
Figure 63. Variation of maximum scour depth with dimensionless shear stress around 11 and 22 cm pier.
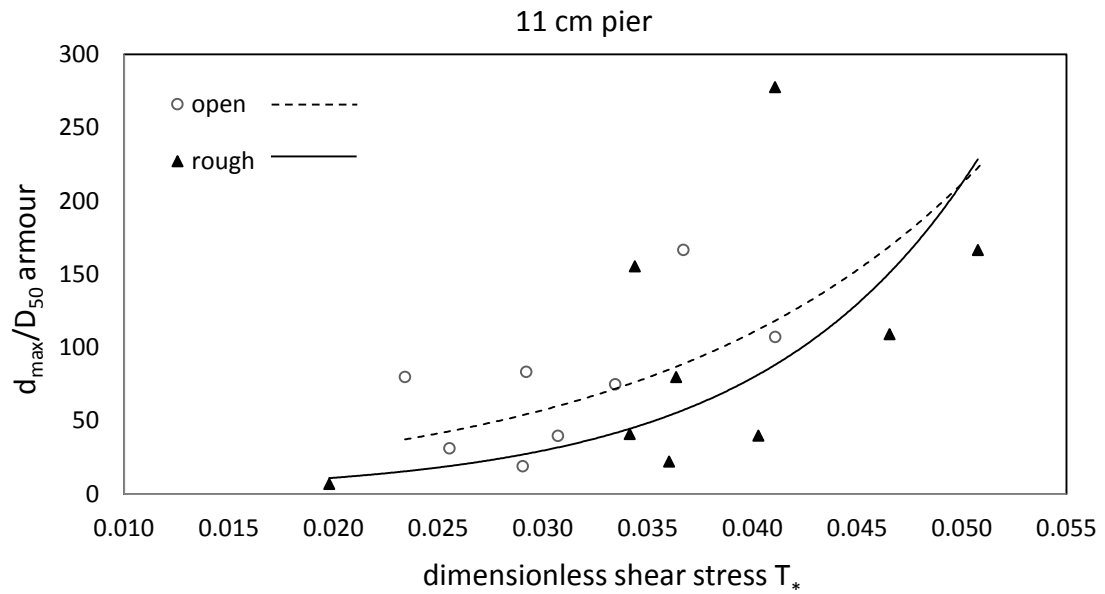
Figure 64. Variation of maximum scour depth with dimensionless shear stress under rough ice cover and open channel conditions for 11 cm pier.
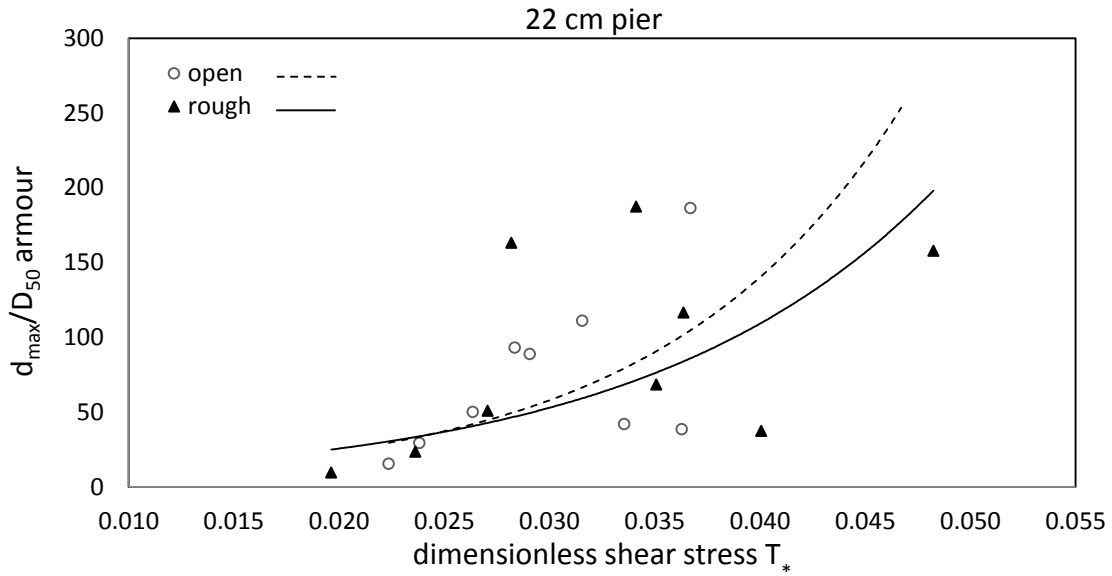
Figure 65. Variation of maximum scour depth with dimensionless shear stress under rough ice cover and open channel conditions for 22 cm pier.

5.12 Multiple Regression Analysis

A basic linear regression model assumes that the contributions of various independent variables to the prediction of the dependant variable are additive. Given that two independent variables (X_1 and X_2) may contribute additively to the dependant variable (Y), the prediction equation would be as follows,

$$Y(t) = b_0 + b_1X_1(t) + b_2X_2(t) \qquad\qquad 5.16$$

where if all things are equal and X_1 increases by one unit, then Y is expected to increase by b_1 units. When there is an absolute change in Y that is proportional to the absolute change in X_1, then the coefficient b_1 represents the constant of proportionality. For this study the dependant variable is the maximum scour depth and the independent variables can be written as follows,

$$\frac{d_{max}}{H} = f\left(\frac{U}{\sqrt{gH}}, \frac{UD_{50}}{\nu}, \frac{D_{50}}{H}, \frac{D_{50}}{B}, \frac{D_{50a}}{D_{50}}, \frac{n_i}{n_b}, \frac{b}{B}, \frac{b}{H}\right) \qquad\qquad 5.17$$

For this study, the maximum scour depth is affected multiplicatively by the independent variables, meaning that the percentage change in Y should be proportional to the percentage change in X_1 and X_2 and so on (unlike linear regression where the change is additive). Since linear regression is not appropriate for this situation, a multiplicative regression model should be applied,

$$Y(t) = b_0(X_1(t)^{b_1})(X_2(t)^{b_2}) \qquad\qquad 5.18$$

where Y is proportional to the product of X_1 and X_2 which are each raised to some power based upon the data set. For analysis purposes and equation development, a multiplicative model can be converted into an equivalent linear model by taking the natural logarithm as follows,

$$LN\ [Y(t)] = LN[b_0(X_1(t)^{b_1})(X_2(t)^{b_2})] \qquad\qquad 5.19$$

where the coefficients b_1 and b_2 can be positive or negative and will provide the direction and magnitude of the effect of the associated variable, X_1 or X_2 on Y.

In order to gain a better understanding of the impact of various dimensionless hydraulic parameters on maximum scour depth, a multiplicative regression model was applied and the natural logarithm was used in order to present linear graphical analysis. Using multiplicative regression provides a quantitative description into the dependence of maximum scour depth on the Froude number, sediment grain size, pier size, ice cover and armour layer size. Various parameter combinations from equation 5.17 were explored through regression analysis since for example sediment D_{50} is presented by both D_{50}/H and D_{50}/B. Not all parameter

combinations produced strong regression models and therefore are not included in the sections following but rather in Appendix D. Reasons that parameter combinations did not produce strong regression models are as follows:

(a) the regression model produced regression coefficients that did not support findings from previous sections in this study. For example, the regression coefficient for sediment D_{50} would be positive, when in fact findings under section 5, indicate that sediment D_{50} actually decreases with increasing scour depth.

(b) the regression model produced supported findings of this study however a stronger correlation was found using various other parameters. For example, it was found that the parameters D_{50}/H and D_{50}/B both typically produced valid regression models, however, for the most part, D_{50}/B would produce a stronger correlation.

The following sections present the regression models for maximum scour depth as it relates to open channel conditions, ice covered conditions and armour layer development.

Scour depth under open channel conditions:

Using principals of dimensional analysis described in section 5.9, the maximum scour depth around the 11 and 22 cm piers under open channel flow can be described by the following variables:

$$\frac{d_{max}}{H} = A \left(\frac{U}{\sqrt{gH}} \right)^a \left(\frac{D_{50}}{B} \right)^b \qquad 5.20$$

where $U/\sqrt{gH}$ is the Froude number and D_{50}/B is the change in sediment size with pier width. By using regression analysis the following equations were derived from open channel experiments (Figure 66 and Figure 67).

For 11 cm pier:

$$\frac{d_{max}}{H} = 5\text{E}^{-11} \left(\frac{U}{\sqrt{gH}}\right)^{3.26} \left(\frac{D_{50}}{B}\right)^{-3.36} - 0.019 \qquad\qquad 5.21$$

For 22 cm pier:

$$\frac{d_{max}}{H} = 4\text{E}^{-16} \left(\frac{U}{\sqrt{gH}}\right)^{4.03} \left(\frac{D_{50}}{B}\right)^{-4.93} - 0.017 \qquad\qquad 5.22$$

For both the 11 and 22 cm piers, the D_{50}/B regression coefficients indicate that as sediment size decreases the maximum scour depth increases. This trend supports findings in section 5.1 (scour depth versus sediment size) of this thesis. Finer channel particles require less shear stress for incipient motion and can produce a larger maximum scour depth. Both Froude regression coefficients for equations 5.21 and 5.22 indicate that as the Froude number increases the maximum scour depth also increases. This is also confirmed in section 5.9 (correlation of flow depth with Froude number). The greater the Froude number, the greater the resistance exerted by water flow on the river bed material; therefore, there is a positive relationship between Froude number and scour depth (Aziz, 1983). Similarly, Wu et al. (2014) also documented that the Froude number increased with abutment scour depth under open channel flow. The R^2 value for the 22 cm pier, Figure 67, is also greater than the R^2 value for the 11 cm pier, Figure 66, indicating a stronger correlation.

Using dimensional analysis, the pier size can also be incorporated into the regression model given by the following equation,

$$\frac{d_{max}}{H} = A\left(\frac{U}{\sqrt{gH}}\right)^a \left(\frac{D_{50}}{B}\right)^b \left(\frac{b}{B}\right)^c \qquad\qquad 5.23$$

where *b/B* is the change in pier size with channel width. Through regression analysis, the following equation was derived for open channel conditions, representing the change in maximum scour depth with flow Froude number, sediment D_{50} and pier size (Figure 68).

$$\frac{d_{max}}{H} = 2E^{-13}\left(\frac{U}{\sqrt{gH}}\right)^{3.77} \left(\frac{D_{50}}{B}\right)^{-4.15} \left(\frac{b}{B}\right)^{0.03} - 0.014 \qquad\qquad 5.24$$

For equation 5.24, the Froude regression coefficient of 3.77 indicates that maximum scour depth increases with Froude number, the D_{50} coefficient of -4.15 indicates that as sediment D_{50} decreases scour depth increases, and the pier size coefficient of 0.03 indicates that as pier size becomes larger, scour depth also increases. Here, when comparing the two positive regression coefficients, the Froude coefficient (3.77) is larger than the pier size coefficient (0.026); this indicates that the value of the Froude number has a greater influence on scour depth than the pier size. In addition, the sediment D_{50} has the largest regression coefficient (4.15) indicating that the sediment size has the largest influence on scour depth.

11 cm pier, open channel

$$d_{max}/H = 5E\text{-}11\ X - 0.019$$

$$R^2 = 0.8456$$

$$X = \left(\frac{U}{\sqrt{gH}}\right)^{3.26} \left(\frac{D_{50}}{B}\right)^{-3.36}$$
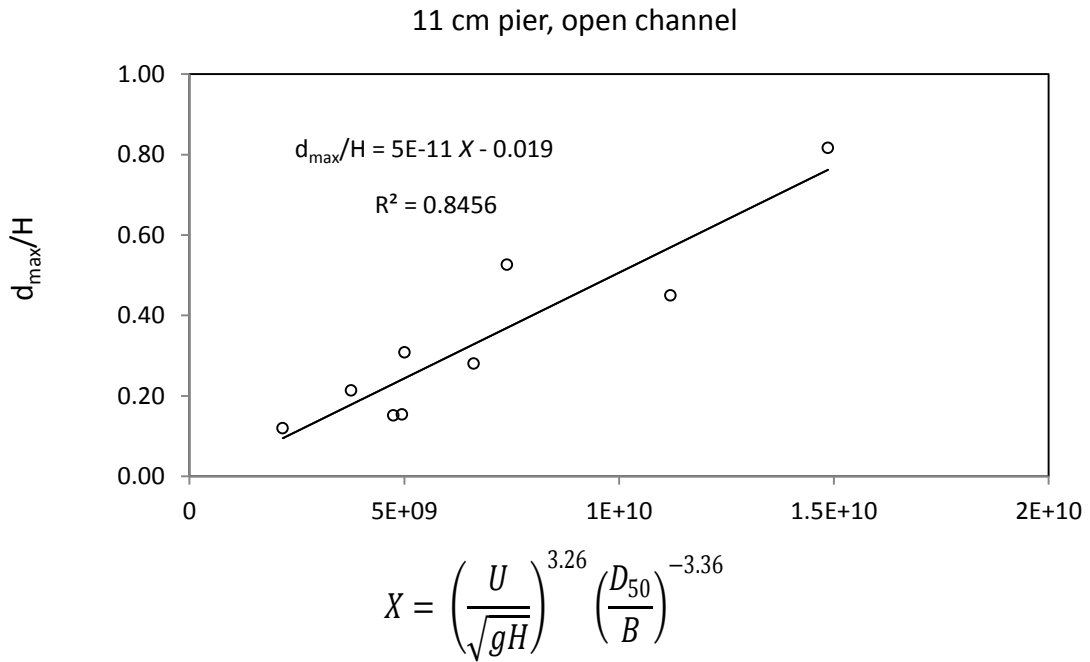
Figure 66. Variation of scour depth for 11 cm pier under open channel conditions.

22 cm pier, open channel

$$d_{max}/H = 4E\text{-}16\ X - 0.017$$

$$R^2 = 0.90$$

$$X = \left(\frac{U}{\sqrt{gH}}\right)^{4.03} \left(\frac{D_{50}}{B}\right)^{-4.93}$$
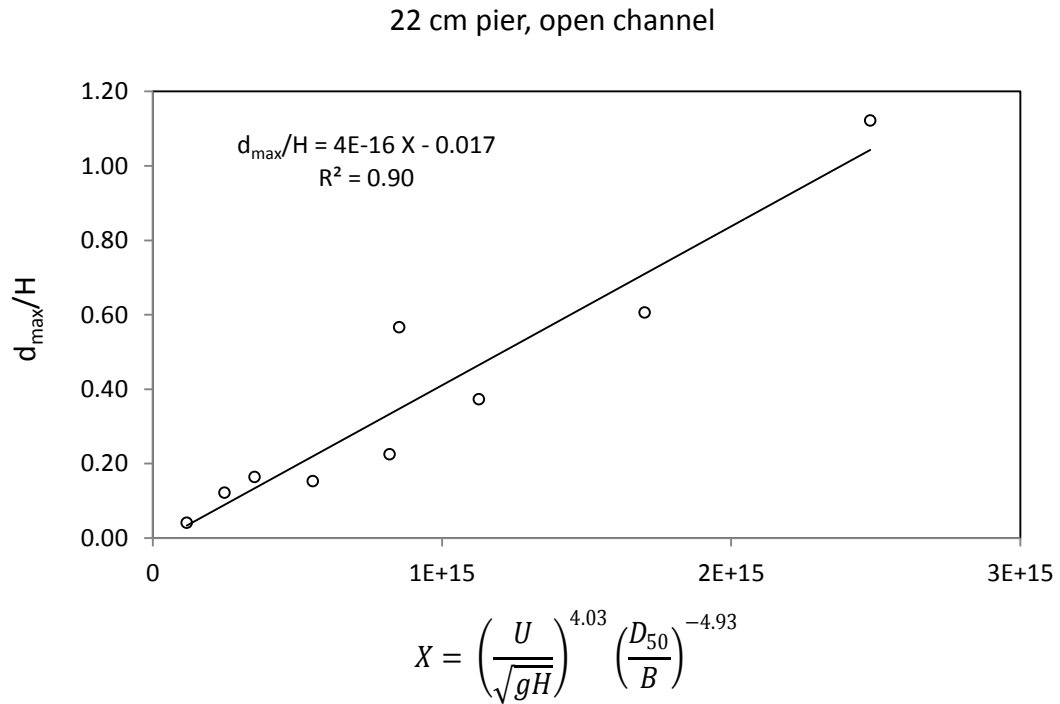
Figure 67. Variation of scour depth for 22 cm pier under open channel conditions.

$$X = \left(\frac{U}{\sqrt{gH}}\right)^{3.77} \left(\frac{D_{50}}{B}\right)^{-4.15} \left(\frac{b}{B}\right)^{0.026}$$
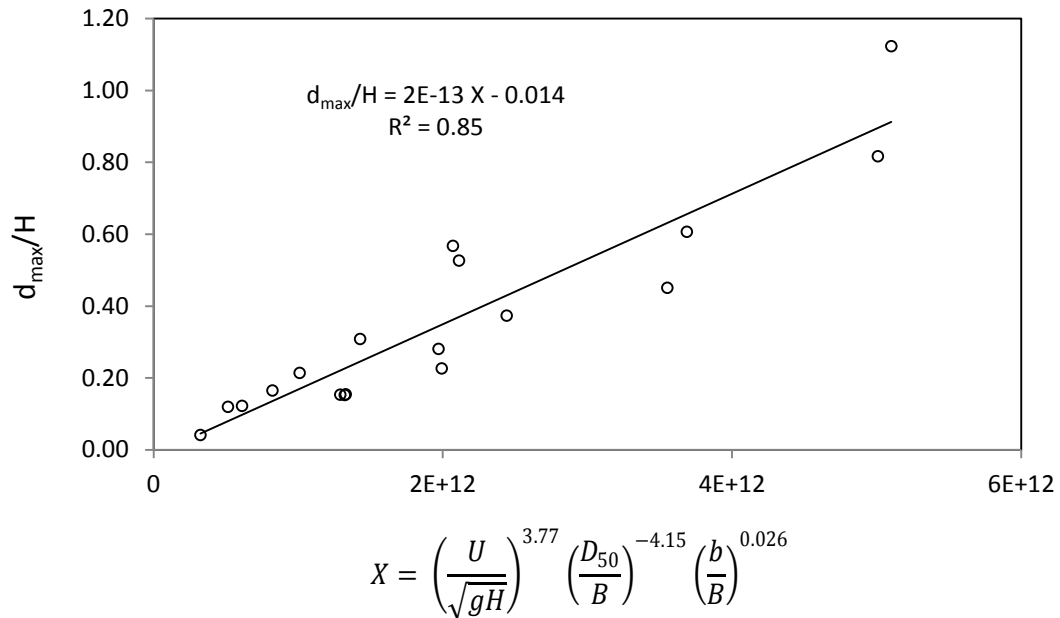
Figure 68. Variation of scour depth in relation to Froude number, median bed sediment size and pier width under open channel conditions.

Scour depth under ice conditions:

Using dimensional analysis, the maximum scour depth around the 11 and 22 cm piers under ice cover can be described by the following variables:

$$\frac{d_{max}}{H} = A \left(\frac{U}{\sqrt{gH}}\right)^a \left(\frac{D_{50}}{B}\right)^b \left(\frac{n_i}{n_b}\right)^c \qquad 5.25$$

where n_i/n_b is the ice cover roughness compared to the channel bed roughness. In order to calculate the roughness coefficients for the channel bed and ice cover, equations from the literature were examined. Li (2012) analyzed large sets of field data and found that Manning's coefficient for ice cover for ice covered rivers averages from 0.013 to 0.040 during the winter. The following equation was used to calculate the Manning's coefficient for rough ice cover (Li, 2012):

$$n_i = 0.039 \, k_s{}^{1/6} \qquad\qquad 5.26$$

where k_s is the average roughness height of the ice underside in meters. Using equation 5.26 the Manning's coefficient for rough ice cover was calculated as 0.021. This value also coincides with findings by Carey (1966) and Hains and Zabilansky (2004). The height of roughness of the ice underside was based upon the 2.5 cm Styrofoam cubes that were attached to the original 1.2 m x 2.4 m (4 x 8 foot) Styrofoam sheet. For smooth ice cover, the Manning's coefficient was based upon the Manning's value for smooth concrete, and the value of 0.013 was used (Mays, 1999). To calculate channel bed roughness for non-uniform sediment the following equation was used (Hager, 1999):

$$n_b = 0.039 \, D_{50}{}^{1/6} \qquad\qquad 5.27$$

Based upon equation 5.27, the channel bed roughness for the various D_{50}s in this study were calculated as follows: D_{50}=0.58 mm $n_b = 0.0113$, D_{50}=0.50 mm $n_b = 0.0110$, D_{50}=0.47 mm $n_b = 0.0109$. By using regression analysis the following equations were derived for ice covered experiments (Figure 69 and Figure 70).

For 11 cm pier ice cover conditions:

$$\frac{D_{max}}{H} = 3\text{E}^{-12} \left(\frac{U}{\sqrt{gH}}\right)^{2.05} \left(\frac{D_{50}}{B}\right)^{-3.52} \left(\frac{n_i}{n_b}\right)^{-0.39} - 0.024 \qquad\qquad 5.28$$

For 22 cm pier ice cover conditions:

$$\frac{D_{max}}{H} = 2\text{E}^{-14} \left(\frac{U}{\sqrt{gH}}\right)^{3.55} \left(\frac{D_{50}}{H}\right)^{-4.31} \left(\frac{n_i}{n_b}\right)^{0.85} + 0.066 \qquad\qquad 5.29$$

Just as for open channel conditions, the D_{50}/H regression coefficients for ice cover indicate that as sediment size decreases the maximum scour depth increases. For both equations 5.28 and 5.29, the Froude regression coefficients indicate that as the Froude number increases the maximum scour depth also increases. The n_i/n_b regression coefficients however do not indicate similar trends for both the 11 and 22 cm piers. The ice cover roughness coefficient for the 22 cm pier indicates that as the ice cover roughness increases the scour depth will also increase (Figure 70). Opposite is indicated by the roughness coefficient for the 11 cm pier (Figure 69). This discrepancy reflects the findings outlined in section 5.3 'scour depth versus channel cover' where rough ice cover resulted in greater scour depth then open channel conditions for 60 percent of experiments and smooth ice cover produced greater scour depth then open channel conditions for 53 percent of experiments. Various other parameters were tested for this regression model as indicated in Appendix D, however for the n_i/n_b parameter an appropriate model could not be found.

Using dimensional analysis, pier size was also incorporated into the regression model given by the following,

$$\frac{d_{max}}{H} = A \left(\frac{U}{\sqrt{gH}}\right)^a \left(\frac{D_{50}}{B}\right)^b \left(\frac{n_i}{n_b}\right)^c \left(\frac{b}{B}\right)^d \qquad 5.30$$

By using regression analysis the following equation was derived for ice covered experiments taking into consideration pier size (Figure 71).

$$\frac{d_{max}}{H} = 4\text{E}^{-13}\left(\frac{U}{\sqrt{gH}}\right)^{2.87}\left(\frac{D_{50}}{B}\right)^{-3.89}\left(\frac{n_i}{n_b}\right)^{0.15}\left(\frac{b}{B}\right)^{0.03} - 0.011 \qquad 5.31$$

In equation 5.31, the regression coefficient for the Froude number and pier size are both positive, indicating that both parameters have a positive relationship with maximum scour depth. The Froude coefficient, 2.87, is larger than the pier size coefficient, 0.03, indicating that the Froude value has a greater impact on scour depth than pier width under ice cover conditions. Additionally, under the regression model in equation 5.31, the coefficient for the ice roughness parameter is positive, indicating that as ice cover roughness increases so does scour depth. As over 50 percent of experimental runs measured a greater scour depth under ice cover, theoretically, the coefficient should be positive; however, as previously mentioned, smooth and rough ice cover only produced a greater scour depth than open channel flow for 57 and 60 percent of experiments, therefore the coefficient value is small. The ice cover condition does not always produce a greater scour depth due to variations in non-uniform sediment transport and subsequent armour layer development, as discussed in section 5.3, 'scour depth versus channel cover'. To further explore the effects of the armour layer on scour depth, the next section includes the armour layer in regression analysis.

11 cm pier, smooth + rough ice cover

$$d_{max}/H = 3E\text{-}12\ X - 0.024$$
$$R^2 = 0.70$$
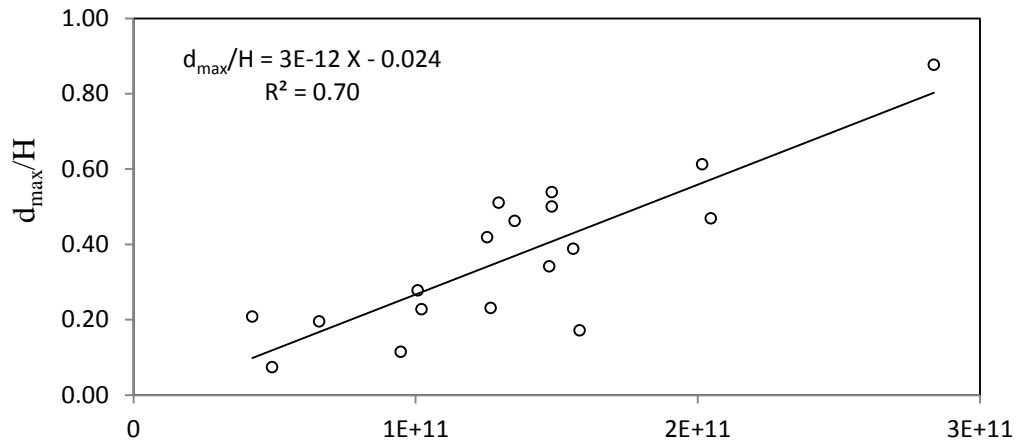
$$X = \left(\frac{U}{\sqrt{gH}}\right)^{2.05} \left(\frac{D_{50}}{B}\right)^{-3.52} \left(\frac{n_i}{n_b}\right)^{-0.39}$$

Figure 69. Variation of scour depth for 11 cm pier under ice covered conditions.

22 cm pier, smooth + rough ice cover

$$d_{max}/H = 2E\text{-}14\ X + 0.066$$
$$R^2 = 0.73$$
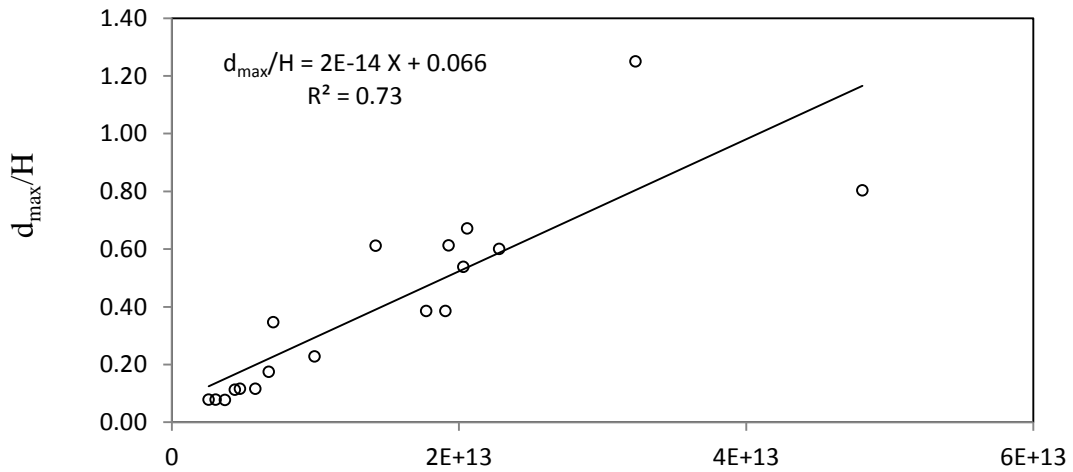
$$X = \left(\frac{U}{\sqrt{gH}}\right)^{3.55} \left(\frac{D_{50}}{B}\right)^{-4.31} \left(\frac{n_i}{n_b}\right)^{0.85}$$

Figure 70. Variation of scour depth for 22 cm pier under ice covered conditions.

smooth + rough ice cover

$d_{max}/H = 4E\text{-}13\ X - 0.011$

$R^2 = 0.76$

$$X = \left(\frac{U}{\sqrt{gH}}\right)^{2.87} \left(\frac{D_{50}}{B}\right)^{-3.89} \left(\frac{n_i}{n_b}\right)^{0.15} \left(\frac{b}{B}\right)^{0.03}$$
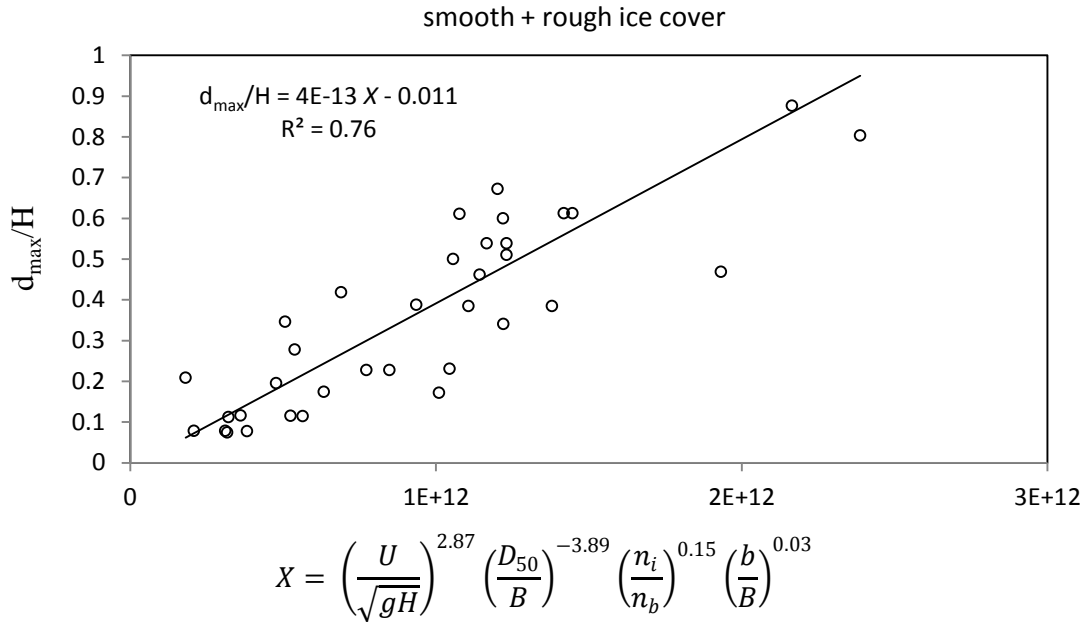
Figure 71. Variation of scour depth in relation to Froude number, median bed sediment size, ice cover roughness and pier width.

Effect of armour layer on maximum scour depth:

Using principals of dimensional analysis and taking into consideration the armour layer, the maximum scour depth under open channel conditions and ice cover can be described by the following variables:

For open channel conditions:

$$\frac{d_{max}}{H} = A\left(\frac{U}{\sqrt{gH}}\right)^{a} \left(\frac{D_{50}}{B}\right)^{b} \left(\frac{b}{B}\right)^{c} \left(\frac{D_{50}armour}{D_{50}channel}\right)^{d} \qquad 5.32$$

For ice cover conditions:

$$\frac{d_{max}}{H} = A\left(\frac{U}{\sqrt{gH}}\right)^{a} \left(\frac{D_{50}}{H}\right)^{b} \left(\frac{n_i}{n_b}\right)^{c} \left(\frac{D_{50}armour}{D_{50}channel}\right)^{d} \left(\frac{b}{H}\right)^{e} \qquad 5.33$$

where $D_{50}\ armour/D_{50}channel$ is the armour layer size relative to the channel D_{50}. By using regression analysis the following equations were derived from open channel and ice covered experiments (Figure 72, Figure 73).

For open channel conditions:

$$\frac{d_{max}}{H} = 3\text{E}^{-13} \left(\frac{U}{\sqrt{gH}}\right)^{3.79} \left(\frac{D_{50}}{B}\right)^{-4.08} \left(\frac{b}{B}\right)^{0.01} \left(\frac{D_{50}armour}{D_{50}channel}\right)^{-0.21} - 0.0096 \qquad 5.34$$

For ice cover conditions:

$$\frac{d_{max}}{H} = 20.58 \left(\frac{U}{\sqrt{gH}}\right)^{3.54} \left(\frac{D_{50}}{H}\right)^{-0.33} \left(\frac{n_i}{n_b}\right)^{0.25} \left(\frac{D_{50}armour}{D_{50}channel}\right)^{-0.47} \left(\frac{b}{H}\right)^{0.05} + 0.0254 \qquad 5.35$$

In this case, the interest is in comparing the regression coefficients for armour layer D_{50} as they relate to maximum scour depth. For both open channel and ice covered conditions the armour layer regression coefficients are negative indicating that as armour layer D_{50} size decreases, scour depth increases. This correlation supports results of this study outlined in section 5.7 'armour layer analysis'. Bed armouring acts to reduce pier scour development compared to the expected scour development if no bed armouring layer was present. For non-uniform sediments, local scour is typically less than that of uniform sediments due to the formation of an armour layer (Chiew and Melville, 1989). The negative regression coefficient for the armour layer parameter also aligns with the negative regression coefficients for sediment D_{50} for open channel and ice cover conditions (D_{50}/B and D_{50}/H for equations 5.34 and 5.35 respectively). As previously discussed, this study found that scour depth increases as sediment D_{50} decreases; the D_{50} coefficients in equations 5.34 and 5.35 also support this trend. Considering all the regression coefficients in equations 5.34 and 5.34, the Froude number, sediment D_{50} and armour layer D_{50} appear to be the most important parameters affecting

maximum scour depth, while ice cover roughness and pier size typically have smaller regression coefficients indicating a smaller influence on maximum scour depth.

Also of note, the correlation in Figure 73 is weaker than the correlation in Figure 72. As the number of independent variables increase in regression analysis the number of scaling issues also increases. Using dimensional analysis and multiple regression, a number of parameter combinations were examined investigating the effects of the armour layer on maximum scour depth. The parameter combinations that produced strong regression models are presented in Figure 72 and Figure 73, while remaining regression models can be found in Appendix D.

$$X = \left(\frac{U}{\sqrt{gH}}\right)^{3.79} \left(\frac{D_{50}}{B}\right)^{-4.08} \left(\frac{b}{B}\right)^{0.01} \left(\frac{D_{50}\,Armour}{D_{50}\,Channel}\right)^{-0.21}$$
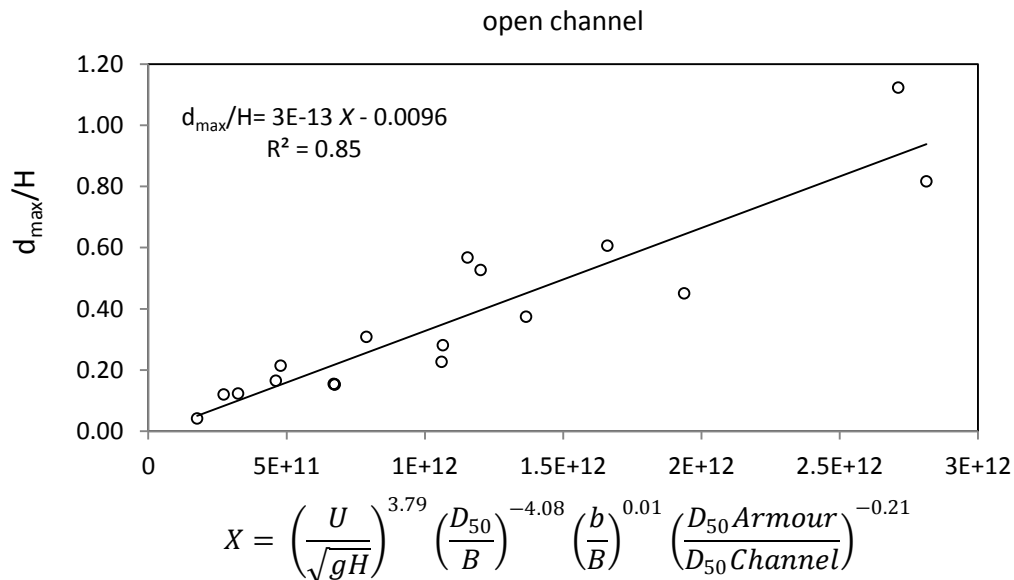
Figure 72. Variation of maximum scour depth in relation to Froude number, median sediment size, pier size and armour layer under open channel conditions.

$$X = \left(\frac{U}{\sqrt{gH}}\right)^{3.54} \left(\frac{D_{50}}{H}\right)^{-0.33} \left(\frac{n_i}{n_b}\right)^{0.25} \left(\frac{D_{50}Armour}{D_{50}Channel}\right)^{-0.47} \left(\frac{b}{H}\right)^{0.05}$$
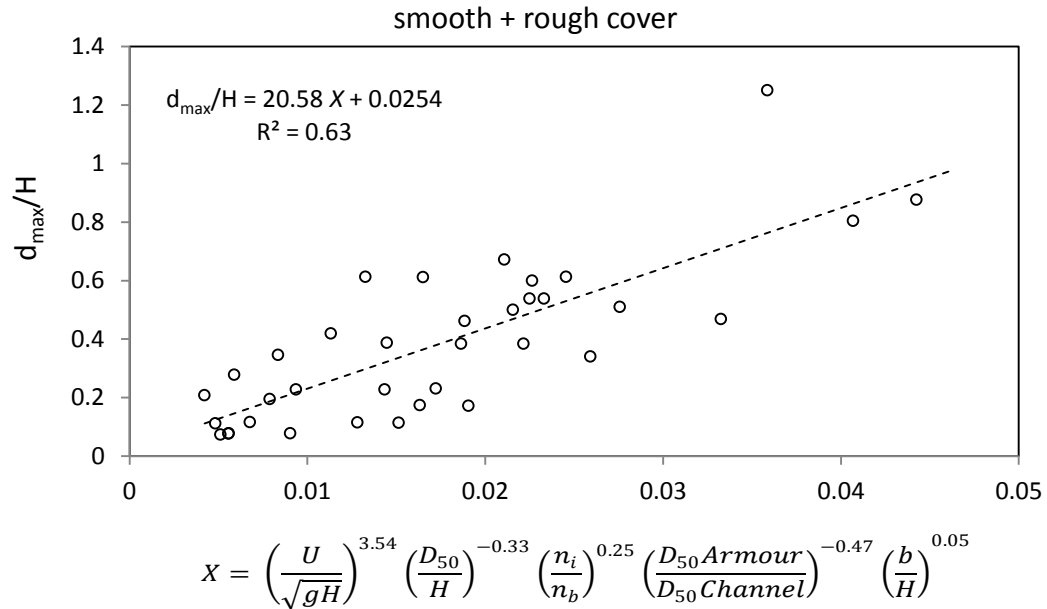
Figure 73. Variation of maximum scour depth in relation to Froude number, median sediment size, ice cover roughness, armour layer and pier size.

5.13 Summary and conclusions

The purpose of this chapter was to examine various hydraulic parameters as they relate to pier scour. In doing so, 54 flume experiments were completed investigating pier scour under open, smooth and rough ice cover conditions. In order to avoid repetition, a summary of major findings is not provided here, but rather in the conclusion section of this thesis (Chapter 7).

In order to address whether the findings of this study are useful and relevant to bridge design a critical analysis of bridge research and management is undertaken in the next section of this thesis. In order to assess the validity of the physical experiments conducted, scaling issues associated with physical models must be explored. This is an important consideration for this study as exact similitude between a model and prototype has not yet been achieved in any known study. The results presented in Chapter 4 and Chapter 5 are all subject to scaling effects and experimental results typically cannot be translated directly to real world

applications. However, parameter relationships presented in the multiple correlation analysis do present possible causal relationships to scour hole formation. In conducting a critical assessment of bridge research and design, the goal is to investigate and highlight current approaches to bridge research and highlight areas of current bridge manuals where this research addresses knowledge gaps.

6.0 CRITICAL ASSESSMENT OF BRIDGE RESEARCH AND DESIGN

6.0 Introduction

To critically assess something means to examine and judge something in order to assess its worth. In academia critical analysis involves interpretation and evaluation of a body of work which often takes the form of an essay. Academics are often asked to explain how their research is applicable in the real world, as the dissemination of information from academia to industry and government can range from open and effective to difficult and confusing (Rynes et al., 2001). Armstrong (2004) argued that only 3 percent of published papers in climate and population forecasting contained useful knowledge that could contribute to better decision making. The author proposed that universities could ask faculty to write short reports on: what they discovered, how they made the discovery, and how the findings will lead to better decision making.

As researchers have investigated pier scour for the past 50 years and published hundreds of journal articles, one must question what further contributions this thesis can offer the field of scour research or is it merely an 'exercise in academia'. Secondly, can information presented in this thesis be used or incorporated into bridge design or form the groundwork for further studies relating river ice and pier scour.

The purpose of this chapter is to examine the various research components that involve bridge scour research, namely flume work, scour equation development and computational fluid dynamics, and assess where components of this thesis work relate and the overall usefulness in current day practices. Bridge standards in North America along with scour prevention practices are then reviewed in order to gain insight as to how academic bridge research is used and applicable to real world bridge design problems around pier scour.

6.1 The use of flume experiments and their relation to field conditions

Both physical hydraulic modeling in a laboratory and numerical computer modeling are the standard techniques used to evaluate bridge design and scour. Physical models fulfill an important role in hydraulic analysis by verifying solutions that cannot be obtained by numerical methods. Physical hydraulic models for bridge scour research consist of hydraulic flumes. The model component is a small scale replica of a bridge pier or abutment while the prototype is the fully functional real world bridge pier or abutment.

6.1.1 Similitude theory and scaling

This section addresses scaling principles that were considered under Chapter 3. Similitude is the relationship between prototype and model with geometrically similar boundaries (Zevenbergen et al., 2012). In the realm of fluid mechanics there are three types of similitude: geometric, kinematic and dynamic.

(a) geometric similarity involves x, y, z length scales and imposes that the corresponding lengths between the model and prototype have the same ratios.

(b) kinematic similarity requires that the length and time scales be similar between the model and the prototype. Under kinematic similarity streamline patterns for water flow around a pier model and pier prototype would be similar. In order for flow-field similitude the geometric scale relating to the point of the stagnation head along the face of the pier must be scaled directly with the pier size (Ettema et al., 1998). The stagnation head refers to the point in which the water hits the pier face and the fluid velocity becomes zero. When this occurs the kinetic energy is converted into pressure energy.

(c) dynamic similarity occurs between the model and prototype when the forces at corresponding points are similar. Fluid forces that are considered in dynamic similarity are inertia, viscosity, gravity, surface tension, pressure and the elastic compression force. This similarity is the hardest to achieve in fluid mechanics since all non-dimensional numbers between model and prototype relevant to the flow must be preserved. For perfect dynamic similarity the following equations must be identical for model and prototype (Heller, 2011).

The ratio of the inertial force to the gravity force is represented by the Froude number as:

$$Froude\ number\ F = \left(\frac{U}{\sqrt{gh}}\right)_M = \left(\frac{U}{\sqrt{gh}}\right)_P \qquad 6.1$$

where M is the model and P is the prototype. The ratio of the inertial force to the viscous force for the model and prototype is represented by the Reynolds number written as:

$$Reynolds\ number\ R = \left(\frac{UR}{v}\right)_M = \left(\frac{UR}{v}\right)_P \qquad 6.2$$

The ratio of the inertial force to the surface tension is known as the Weber number:

$$Weber\ number\ W = \left(\frac{\rho U^2 L}{\sigma}\right)_M = \left(\frac{\rho U^2 L}{\sigma}\right)_P \qquad 6.3$$

where L is the characteristic length and σ is the surface tension. The ratio of inertial force to elastic force is represented by the Cauchy number:

$$Cauchy\ number\ C = \left(\frac{\rho U^2}{E}\right)_M = \left(\frac{\rho U^2}{E}\right)_P \qquad\qquad 6.4$$

where E is Young's modulus, also known as the tensile modulus representing the elastic force. The ratio of the pressure force to inertial force is represented by the Euler number:

$$Euler\ number\ E = \left(\frac{P}{\rho U^2}\right)_M = \left(\frac{P}{\rho U^2}\right)_P \qquad\qquad 6.5$$

where P is the pressure.

If a hydraulic model were to have perfect geometric, kinematic and dynamic similitude than the model would be the same size as the prototype. Perfect scaling is however not possible. Take for example studying the flood stages of the Mississippi River which is 2,092 km long, 0.4 km wide and 6 m deep. Construction of a downscaled physical model of the Mississippi with a length of 100 m would cause the model depth to decrease to a miniscule scale of 0.0286 cm. In this case the effects of surface tension (cohesion of water molecules) would be exaggerated in the model in comparison to the prototype (Grabel, 2001).

In order to minimize scale effects, the most common practice in flume studies is to follow a set of limiting criteria (rules of thumb). Limiting criteria for scour studies involve maximum and minimum ratios for pier width, flume width and sediment grain size as outlined in Table 7, section 3.6, 'Flume scaling and pier selection'. The limiting criterion that was not met for all experiments in this thesis was the ratio pier width to flow depth (b/H). The ratios were all less than 4, indicating that the resulting experimental scour depths cannot be considered independent of flow depth. Melville and Coleman (2000) state that if the ratio of pier width to flow depth (b/H) is between 0.7-5.0 then local pier scour is dependent on both

flow depth and pier width, while if b/h is less than 0.7 than local pier scour depth is dependent only on pier width. For this thesis, the ratios of pier width to flow depth range from 0.42 to 2.2 as indicated in Table 7, Chapter 3. While the purpose of this thesis was not to investigate scour depth in relation to flow depth, this scaling is present in the design of the flume experiments. In order to investigate scour depth under various channel covers all the while having flow depth as a scaling issue, the experiment parameters (depth, velocity and pier size) remained constant with only the channel cover changing (as outlined in Table 8, Chapter 4). With all flow and bridge parameters remaining constant, the impact of ice cover could be investigated.

While flume scaling guidelines (rules of thumb) were followed in this thesis (with the exception of flow depth to pier width ratio), the importance of kinematic and dynamic similarity must be discussed. As indicated by (Heller, 2011) the most common and important similarity criterion applied to open channel hydraulics is Froude similarity. Under Froude similarity, the additional force ratios outlined in equations 6.2-6.5 cannot be identical between the model and prototype. The additional flow forces such as surface tension, elasticity and pressure are therefore not considered and represent scale effects, however these scale effects are small and often considered negligible (Heller, 2001; Zevenbergen et al., 2012).

While Froude similarity was considered in this thesis, in doing so the similitude of particle mobility is affected. Similitude of particle mobility (U/U_c) and similitude of the Froude number ($U/\sqrt{gD}$ with b/H) cannot occur simultaneously (Ettema et al., 1998). The natural scale to which river bed particles can be scaled does not allow for both criteria to be satisfied. The majority of flume experiments use particles that are comparable in size to natural

river bed sediments (D_{50} from 0.25-4.00 mm); therefore the ratio of pier diameter (b) to particle diameter (D_{50}) is always larger in the prototype than the physical model (Table 18). Due to the similar size of river bed particles for model and prototype, larger approach velocity values are required to satisfy incipient motion (U/U_c) similitude than Froude number ($U/\sqrt{gD}$) similitude. The result of using larger approach velocities to satisfy incipient motion similitude leads to larger values of scour depth than those naturally occurring at bridge piers in actual rivers (Ettema et al., 1998). In this thesis the flume was designed with the goal of obtaining subcritical flows (Froude number < 1) and incipient motion. As previously indicated, flume testing was undertaken using three tailgates (30 cm water depth) and under this depth, velocity could not be adjusted for incipient motion to occur. In addition under the two tailgate configuration the small pier was always placed in the upstream sandbox since under such channel conditions in the downstream window no scour/incipient motion would occur. Due to the design of the gravity flow water system, the flume velocity was adjusted to obtain particle mobility similitude all the while retaining a Froude number < 1.

In the design of this experimental study, geometric similitude was considered by following the flume scaling guidelines and dynamic similitude was considered by the Froude number and occurrence of incipient motion. As indicated in Mount (1995) the Reynolds number is used to characterize whether flow is turbulent or laminar while the Froude number characterizes whether the flow is subcritical versus supercritical. Using the Reynolds and Froude numbers virtually all flow falls into one of four categories:

1. subcritical-laminar ($F_r < 1$, $R_e < 500$), rare in rivers, more common in groundwater or very slow moving deep water.

2. supercritical-laminar ($F_r > 1$, $R_e < 1$), rare in rivers, occurs in sheetwash and in fast moving water that forms a thin moving layer over smooth rocks.

3. subcritical-turbulent ($F_r < 1$, $R_e > 2,000$), most common flow condition in rivers where inertial forces exceed viscous forces.

4. supercritical-turbulent ($F_r > 1$, $R_e > 2000$), found in high gradient, shallow rivers with high velocities, spatially limited.

For the purpose of discussing similarity, a reach of the Nechako River, including the John Hart Highway Bridge around Prince George was used as a real world comparison for how representative the experimental flume used in this research is of real river channels. Of note however, the flume was not built or scaled to the Nechako River or Hart Highway Bridge, this example is merely used for the purpose of highlighting a real world bridge and channel configuration. The reach of the Nechako around Prince George is subject to annual ice events and the channel is composed of fine sediment. As indicated in Table 18, the Froude and Reynolds numbers for the flume fall within the most common flow conditions found in rivers and streams. The flow in the flume was turbulent ($R_e > 2,000$) and subcritical ($F_r < 1$). Subcritical flow can be described as slow, deep flow where ripples can travel upstream. Reynolds turbulent flow is always irregular with eddies and vortices that can occur on many scales. Froude values for the flume and Nechako were similar, while Reynolds numbers for the Nechako were considerably larger due greater inertial components of velocity and hydraulic radius. Also, as previously mentioned, the ratio of pier width to sediment D_{50} is

much larger for the Nechako and all natural rivers in comparison to the flume setup. This is due to the fact that for this study, flume experiments use sediments that are comparable in size to natural low gradient rivers. (Here, only natural low gradient rivers are used for comparison as high gradient mountain streams are not considered for bridge experiments).

Summary: While there is a long standing practice of using physical hydraulic models to investigate sediment transport around bridge structures, there is currently no known study that successfully models such phenomena without scale effects (Heller, 2011). The design and construction of the flume and experiments undertaken in this thesis were subject to scale effects; the scale effects of flow depth to pier width were addressed while the scale effects of sediment size could not be avoided. Many scour equations are developed from physical model tests in flumes; therefore, scour equation development has evolved and is addressed in the next section.

Table 18. Similarity parameters. Water Survey Canada data for March 4, 2014 was used to calculate Froude and Reynolds numbers, WSC Station 08JC002, Isle Pierre.

Parameter	Flume environment		John Hart Highway Bridge, Nechako River, Prince George
Pier width	0.11 m pier	0.22 m pier	1.22 m
Channel width	2 m	2 m	240 m
Channel depth	0.10 m, 0.13 m, 0.21 m	0.10 m, 0.13 m, 0.21 m	1.243 m
D_{50} (mm)	0.47, 0.50, 0.58	0.47, 0.50, 0.58	assume 0.50
Froude number	0.17-0.26	0.15-0.26	0.26-0.29
Reynolds number	15,400-31,400	15,700-34,000	926,721
Pier width:D_{50}	189, 220, 234	379, 440, 468	2,103

6.1.2 Scour equation development and field data

The process of developing and validating equations for pier scour depends entirely on how representative the equations are of the real world system. Experimental flumes are subject to scale effects and can over simplify river channel morphology and hydrology. As a result, pier scour equations can underestimate or overestimate scour hole development. Over the past 30 years numerous studies have developed pier scour equations for open channel flow. In Table 19 are the most commonly cited equations for computing pier scour under open channel conditions.

Table 19. Pier scour equations with associated author and study.

Author	Equation
Colorado State University (CSU) equation (FHWA, 1993):	$$d_s = 2.0 H k_1 k_2 k_3 \left(\frac{b}{H}\right)^{0.65} F_r^{0.43}$$
where d_s is scour depth, H is flow depth upstream of the pier, k_1 is correction factor for pier nose shape, k_2 is correction factor for angle of attack flow, k_3 is correction factor for bed condition, b is the pier width and F_r is the Froude number.	
Melville and Sutherland (1988):	$$d_s = k_1 k_d k_y k_\alpha k_s b$$
where k_1 is the flow intensity factor, k_d is the sediment size factor, k_y is the flow depth factor, k_α is the pier alignment factor, k_s is the pier shape factor and b is the pier width.	
Shen (1969):	$$d_s = 0.00022 \left(\frac{Ub}{v}\right)^{0.3}$$
where U is the approaching flow velocity, b is the pier width and $v = 1.0 \times 10^{-6}$ m^2/s	
Froehlich (1989):	$$d_s = 0.32 b \emptyset F r^{0.2} \left(\frac{b_e}{b}\right)^{0.62} \left(\frac{H}{b}\right)^{0.46} \left(\frac{b}{D_{50}}\right)^{0.082}$$
where $\emptyset$ is the shape coefficient based on the shape of the pier nose, F_r is the Froude number, b_e is the width of the bridge pier projected normal to the approach flow, b is the pier width, H is the flow depth and D_{50} is the median sediment size.	
Breusers et al. (1977):	$$d_s = b f k_1 k_2 [2 \tan H (H/b)]$$ $$f = 0 \ for \ \frac{U}{U_c} \geq 0.5$$ $$f = \frac{2U}{U_c} - 1 \ for \ 0.5 < \frac{U}{U_c} \leq 1$$ $$f = 1 \ for \ U/U_c > 1$$
where b is pier width, k1 and k2 are the correction factors for the pier nose shape and angle of attack respectively, H is the flow depth just upstream of the pier, V is the approach flow velocity, Vc is the critical velocity.	
Jain and Fischer (1979):	if (F_r - F_{rc}) > 2 $$d_s = 2.0 b (F_r - F_{rc})^{0.25} (\frac{H}{b})^{0.5}$$ if ($F_r - F_{rc}$) < 0 $$d_s = 1.85 b (F_{rc})^{0.25} (\frac{H}{b})^{0.5}$$
where F_r is the Froude number, F_{rc} is the critical Froude number calculated by $U_c/(gH)^{0.5}$. If $0 < (F_r - F_{rc}) < 0.2$, the largest commuted scour depth is used.	

As field data measurements of pier scour are very limited, large uncertainty exists around how accurate laboratory equations are in predicting pier scour. Johnson (1995) examined the above listed bridge pier scour equations and tested them on four sets of field data (Dongguang et al., 1993; Froelich, 1988; Jain and Modi, 1986; Zhuravlyov, 1978). The field data sets included pier width, flow depth, flow velocity, median particle size, pier-shape coefficient and observed scour depth. Johnson (1995) found that the equation developed by Shen (1969) performed best at low Froude numbers. The scour depth equation developed by Breuser et al. (1977) performed best for ranges of U/U_c greater than 0.5. For low H/b ranges Breuser et al. (1977) and Shen et al. (1969) performed best, while for H/b > 1.5 the Colorado State University equation performed best. Similarly, Mohamed et al. (2005) also used pier scour field data from Pakistan, Canada and India to test the accuracy of the above equations. Mohamed (2005) found that the Melville and Sutherland and the Jain and Fisher equations generally over predicted scour depth while the Colorado State University equation gave reasonable predictions of scour depth.

The most extensive study to evaluate scour equations based upon field data is that by Landers and Mueller (1996). A total of 139 field pier scour measurements were obtained at high flow in clear water conditions by the United States Geological Survey (USGS) and various state departments. After comparing computed (CSU, Froehlich, Shen scour equations) and observed scour depths the author's concluded that none of the selected equations estimated scour depth for the selected field conditions. Many of the scour equations tested over-predicted scour depths but would also under predict very large scour depths.

One of the main issues in estimating local scour depth around bridge piers is trying to identify the relationship between pier width and scour depth. Some studies have found a linear

145

relationship between scour depth and pier width (Landers and Mueller, 1996) while other studies report that there is not a linear relationship between pier width and scour depth unless complete geometric similitude is obtained between pier size, flow and bed particles (Ettema et al., 1998). These discrepancies in combination with flume scaling issues mentioned above are the cause of much scepticism about hydraulic flume experiments and scour equation development. As a result bridge engineers and scientists have to use a variety of measures to arrive at satisfactory pier scour equations for bridge design.

For guidance on evaluating pier scour, a commonly referenced document is the Evaluating Scour at Bridges, Hydraulic Engineering Circular No. 18 (HEC-18) Manual developed in the United States. This manual presents the current state of knowledge regarding bridge design and construction. The HEC-18 manual also provides guidelines for: designing new and replacement bridges to resist scour, evaluating existing bridges for vulnerability to scour and inspecting bridges for scour. The HEC-18 manual is currently in its fifth edition. In conjunction with the HEC-18 manual, the US Department of Highways also developed HEC software packages that accompany the HEC-18 manual. The CSU pier scour equation is used in the HEC software programs for calculating pier scour. Hence, the most widely used and accepted pier scour equation is the CSU equation. As outlined in the Federal Highway Administration (FHWA) HEC-18 manual, the following options are available to bridge engineers:

(a) bridge engineers can use a chosen pier scour equation to calculate an upper estimate of scour depth.

(b) engineers can continue to use the leading pier-scour equation based upon HEC-18, currently the Colorado State University pier scour equation.

(c) engineers can use a pier scour equation that was empirically developed based upon field measurements.

While it was not an objective of this thesis to develop a pier scour equation for ice covered conditions, it is of interest whether or not the currently used CSU scour equation can accurately calculate the scour depths measured in this thesis. Open channel scour depths were calculated using the CSU equation and compared to flume scour depths as indicated in Table 20. The maximum scour depth as calculated by the CSU equation is consistently larger than the maximum scour depths measured from this study. This further reinforces that the experimental flume used in this study was subject to scale effects that must be taken into consideration when interpreting experimental results. This is similar to findings by Mohamed et al. (2005) where the authors found the CSU equation over predicted scour depth when compared to laboratory flume data. Of note however, Mohamed et al. (2005) also compared CSU calculated scour depth to measured scour depths from field data; the authors found that the CSU equation gave a reasonable estimate of local field scour depth. Johnson (1995) also found that the CSU equation performed well for very low Froude numbers ($F_r < 0.1$); however, for Froude numbers $0.25 < F_r < 0.5$ the CSU equation did not perform well when applied to field data. Mueller (1996) also compared field data to CSU calculated scour depth and found that the CSU frequently over predicted the observed scour depth.

Table 20. CSU calculated and measured maximum scour depths for open channel flow. Measured scour depths are from open channel flow conditions for this study.

	11 cm pier	22 cm pier
Measured	2 – 8 cm	2 – 11 cm
CSU calculated	12 – 14.5 cm	19 – 22 cm
% CSU greater then measured	43 – 87 %	50– 90 %

Summary: Just as found in other studies (Johnson, 1995; Mohamed et al., 2005; Mueller, 1996), the CSU equation also over predicts scour depth when compared to scour depth as measured in this thesis. Studies that have compared scour equations to field and laboratory data typically find that most scour equations will overestimate scour depth however, under various hydraulic conditions equations from Table 19 have also underestimated scour depth (Johnson and Ayyub, 1996; Ataie-Ashtiani and Beheshti, 2006; Lu et al., 2008). Any equation that underestimates scour depth is typically not considered in bridge design as it is better to overestimate scour depth then to underestimate it in the interest of public safety. The CSU equation is recommended by the FHWA as it most consistently represents scour depth or overestimates scour depth and is used as a conservative measure (Deng and Cai, 2010).

6.2 The use of CFD as it relates to bridge construction

Bridge engineers include a safety margin in bridge design in order to compensate for variations in building materials, unknown vehicular loadings and flood events. Prior to the use of modern bridge codes and computer software programs, precise calculations regarding scour and loading conditions were not always possible. Since many bridges in North America were built in the post World War II era many bridges were not constructed under modern day bridge codes. Hydraulic issues remain the leading factor in bridge failure (Zevenbergen et al., 2012).

Prior to computers, equations governing fluid flow were solved by hand but now the process is completed by computer software. The advantage of computer models is that they do not suffer from the scale effects that physical models do (Yang, 2005). The ultimate goal of numerical modeling is to replace the need for costly physical models; at present the scientific community is still a long way from adequately capturing flow routines that physical models display. The process of modeling fluid flow is referred to as computational fluid dynamics (CFD). In order to simulate the path a fluid takes numerical equations that describe the flow routing are selected and solved.

There are four general steps that are followed when operating CFD programs:

(1) the geometry of the problem must be defined which is completed using pre-processing software. The boundary and initial conditions must be set.

(2) a mesh is generated. In doing so the geometry domain is divided into finite elements. Mesh generation can be unstructured or structured. Unstructured meshes involve filling geometry with control volumes in an irregular fashion whereas structured meshing involves creating regular control volumes throughout the entire domain.

(3) the solver is specified and resulting algebraic equations are solved. Appropriate solvers is still an active area of research as the topic of convergence is explored (Davidson, 2002).

(4) the solution is examined to obtain the desired information. This step can often involve post-processing software that can load and display complex illustrations of vector flow, field data or contour lines. The data set can be quite large with up to a million points or more, so post-processing can be time consuming especially when comparing to field or experimental data sets.

There are a number of CFD software packages available on the market today; the most common CFD models are FLOW-3D and FLUENT. Both software programs are highly sophisticated and widely used in industry and academic publications for solving fluid flow around bridge piers.

6.2.1 Critical assessment of FLUENT for use in this thesis

FLUENT was originally selected for use in this thesis to simulate flow and scour hole depth around bridge piers under ice cover. The objective was to recreate flume boundary conditions and validate the software against experimental flume results; however, after review and software trial it was decided that using FLUENT was not a viable endeavor. The following sections outline a brief description of the FLUENT software and describe why FLUENT was not used in this thesis. The purpose of this section is to shed light on the capabilities of CFD as they relate to hydraulic problems.

FLUENT is owned and distributed by ANSYS Incorporated – a large engineering simulation software company based in the United States. Most academic research groups purchase a short term use licence renewable on an annual basis. Since FLUENT simulates complex 2D and 3D flows the software cannot be run on a standard desktop computer. For this reason FLUENT is operated out of high performance computing (HPC) centres. A one year license for FLUENT was purchased and installed at UNBC's HPC laboratory.

Pre-processing with FLUENT was initiated by using FLUENT's meshing mode. Meshing requires building geometry by the user for the flume environment, the pier and associated ice cover through manual input. Depending on the complexity of the mesh this process takes between 3-6 months. While the FLUENT code was written to satisfy the

requirements of setting up a mesh for open channel flow, there is no provision written in the program code to create an ice covered channel. Boundary conditions can be set for the channel bed and channel sides as is normal for open channel CFD modelling. In order to create an ice cover for a channel the only option is to create a boundary for the channel surface similar to those created for the channel bottom and sides. The problem this inherently presents is that ice acts much differently than conditions set for the side or bottom of a channel. Specifically, ice cover floats, creating dynamic forces from buoyancy different from that of the channel bed and sides. The options for boundary conditions in FLUENT are creating slip or no-slip boundaries with a specified roughness. A no-slip boundary condition is most appropriate for defining an ice cover as flow velocity is expected to approach zero as it contacts the ice cover. Boundary roughness is specified by roughness height K_s and a roughness constant C_s. The roughness height in FLUENT is typically specified as the D_{50} of the bed material; however, in the instance of defining an ice cover the roughness height would be the height of the Styrofoam cubes used to create the flume rough ice cover and K_s would equal zero for the smooth ice cover. The roughness constant, C_s, is typically set to 0.5 when modeling uniform sand-grain roughness; currently there is no guideline for choosing C_s for other types of roughness (Fluent Inc. 2006). It is suggested that for other roughness types the value of C_s should increase, however to select an appropriate C_s value to represent rough ice cover, flow field results would have to be compared with experimental results and calibration procedures would have to be undertaken.

While it is unknown if an appropriate roughness constant, C_s, can be found for ice cover, the main limiting feature in using FLUENT to model ice covered channels is that boundaries can only be specified to move in the x or y directions. A wall or boundary can be

defined as moving or stationary. Moving walls are defined by velocities specified in either the x or y direction but problems where the wall has a motion normal to itself cannot be simulated using FLUENT (Fluent Inc. 2006). The ice cover in the flume environment was stationary in the x and y direction due to the experimental design. However the ice cover used in this study moved in the z direction continuously throughout the entire experimental period as the Styrofoam floated in the flume channel. With an average of 1 million points in a generated mesh, the micro-scale flow environment around ice cover and bridge piers is sensitive to even minor changes in boundary roughness and movement. Being able to accurately define ice cover is the main key to successful flow field simulation using FLUENT. Flow simulation needs to accurately represent flume flow fields in order for scour hole depth and sediment transport to be modeled. Without the provisions to accurately define the flume ice cover in conjunction with the allotted time of 18-24 months required to set up, calibrate and run FLUENT (the time required to learn the FLUENT software is significant, typical CFD projects are undertaken during the course of Master's or PhD degrees: Acharya, 2011; Ali and Karim, 2002; Escauriaza, 2008; Inkratas, 2007; Ou, 2007; Yang, 2005; Zhang, 2005) it was assessed that use of FLUENT in this thesis was not appropriate.

It should be noted however that one study has used FLUENT to simulate flow in an ice covered channel; however, no winter field data was used for verification of results so the accuracy of the entire study cannot be verified. Inkratas (2007), completed his master's thesis on modeling 3-dimensional flows in a scour hole of the Mackenzie Delta, Canada, using FLUENT. There are a number of natural scour holes in the Mackenzie Delta and proposed gas pipeline crossings have questioned the stability of the scour holes. Two publications were produced from the Inkratas (2007) Thesis: that by Gharabaghi et al. (2007) (supervisor) and

Inkratas et al. (2009). In the first study, looking only at open channel conditions, Gharabaghi et al. (2007) investigated a 30 m deep scour hole in the Mackenzie Delta. FLUENT was set up and calibrated against open channel flow data gathered by Environment Canada using an acoustic Doppler current profiler (ADCP). The scour hole flow field was simulated by FLUENT with a correlation coefficient of 0.68 between the field and simulated velocity values. In the second study, Inkratas et al. (2009) used the open channel model parameter set-up from Gharabaghi et al. (2007) with the addition of a no-slip boundary condition set to represent ice cover. FLUENT simulated a velocity flow field in and around the scour hole; however, there were no field data to calibrate and validate against (since collecting field data during ice events on the Mackenzie Delta is too dangerous). The accuracy and validity of FLUENT in modeling flow fields under ice cover is not known from the latter study since there are no winter field data to validate against. In addition, the flow fields under ice cover were simulated based upon open channel correlation accuracy of 0.68; in doing so, it is suspected that compounding errors would be present in numerical results. After review and software trial it was decided that using FLUENT was not a viable endeavor for use in this thesis.

6.2.2 CFD programs used for hydraulic design of bridges

In North America, the most widely used program for hydraulic bridge design is the Hydrologic Engineering Center River Analysis System, HEC-RAS, software package by the FHWA. HEC-RAS is capable of modeling steady and unsteady flow, sediment transport and water quality. The software performs one-dimension hydraulic calculations for natural and constructed channels. HEC-RAS can output surface profile and cross section information such as channel depth, channel width and total discharge. The model is also capable of producing

rating curve information and estimates of various return periods. Sediment transport potential is calculated based on grain size fraction.

The HEC-RAS model also allows for input of ice data at bridges when calculating water surface profiles. Model users can input ice information with either the presence of a bridge stipulated or left absent from the model set up. Ice cover at bridges can be input as a constant thickness or a dynamic thickness. In the case of constant thickness, the model uses the ice thickness immediately upstream of the bridge; in the case of dynamic thickness the model calculations will be performed at the bridge cross section. Input of ice data, discharge, surface profiles and cross section information can be used in HEC's pier scour software package HEC-18.

The HEC-18 software for pier scour can calculate scour depth in 1-dimension. The software is set up for the river in which multiple cross sections are entered, a water surface profile is generated and used for calibration. A design event is selected (100 year flood) and the Colorado State University (CSU) equation is used to compute pier scour under both live-bed and clear water conditions. Presently there is no provision in the CSU equation for calculating pier scour under ice cover. Often modellers do not incorporate the presence of ice at bridges since historically observed jams did not contact the low bridge steel (Brunner, 2010). The HEC manual states that "little is known about the ways in which a river ice jam interacts with the various components of a bridge" (Arneson et al., 2012, p.118).

6.2.3 Success and limitations of CFD

It is accepted that a well-developed numerical model can assist design engineers in identifying crucial cases in which tests should be conducted (Yang, 2005). As scaling effects

are not present in numerical modeling the governing equations which best simulate the experimental environment will be of use to the engineering community in design of bridge structures.

However, the inability of current CFD software to accurately solve turbulent and unsteady flow is a significant limitation. Turbulence can occur at a fine scale so a spatial grid small enough to capture even the smallest length scale of turbulence is required. Computational resources and issues of time efficiency arise when addressing turbulent flow with CFD. In order to solve turbulence CFD programs employ turbulence models that use the Reynolds-average equations. The Reynolds-average equations represent fluid motion over a larger time scale than that of actual instantaneous turbulent time scales. In using time-averaged scales to represent instantaneous scales for turbulence, modeling inaccuracies can occur and users of CFD software must be aware of these limitations. Since there is no standard turbulence model that is accepted for use in CFD the selection of turbulence model depends on the level of accuracy required, computational resources and the actual physics of flow (FLUENT, 2006).

As an alternative to CFD, large eddy simulation can be used to address turbulence modeling by solving large eddy motion by using the Navier-Stokes equations for fluid. Large eddy simulation solves large scale eddies which are assumed to be dependent on the flow geometry. In solving for the large eddies, eddies at the smallest scale are implicitly included in solving for the largest eddies.

The second main limitation in CFD is the inability to accurately model multi-phase flows. A multi-phase flow consists of phases which do not chemically relate to each other. The phases have separate volume fractions and velocity fields. The flume experiment set up

for this thesis is an example of multi-phase flow: water flow, sediment transport and air flow. There are a number of models set up to handle multiphase flows, the most common being the Euler-Euler approach and the Euler-Lagrange approach. Under the Euler-Lagrange approach it is assumed that the first phase is fluid and is treated as a continuum by solving the time-averaged Navier-Stokes equations. The second phase is a dispersed phase solved by tracking a number of particles through the calculated flow field. The second phase always occupies a lower volume fraction than the first phase and particle interactions are neglected (Zhang, 2009). In the Euler-Euler approach the phases are treated as interconnected continua. Under this approach interactions between sediment particles are considered. Each phase is divided into fractional volumes, continuous through space and time with their total sum equal to one. The FLUENT user manual also states that the Euler-Lagrange model is appropriate for particle laden flows (FLUENT, 2006). The multiphase models do not however incorporate particle shape, deformation rate or particle coalescence and therefore do not accurately represent non-uniform sediment. The inability of FLUENT to accurately simulate non-uniform sediment transport was also a key factor considered in deciding FLUENT was not a viable endeavor to pursue in this thesis.

Summary: As Davidson (2002) points out, the use of CFD remains in the hands of specialists. Significant expertise in transport phenomena, turbulence and multiphase flows is required in order to properly select a modeling approach and define boundary conditions. Additionally, one must have a high understanding of the relationship between mesh quality, convergence and solution accuracy which all rely on CFD code and ultimately overall efficiency of the modeling process (Davidson, 2002). CFD also requires significant time investment for

meshing and post-processing meaning that solutions cannot be calculated in the short term. (For example, the time required to learn the FLUENT software is significant, the user manual is 2,426 pages in length). Typical CFD projects are undertaken during the course of Master's or PhD degrees (Acharya, 2011; Ali and Karim, 2002; Escauriaza, 2008; Inkratas, 2007; Ou, 2007; Yang, 2005; Zhang, 2005) where multiple years can be spent on simulating one specific problem.

6.3 Bridges in Canada

6.3.1 Governing bodies and financial management

In Canada bridges are managed by three main administrative levels: federal, provincial and municipal governments. However, some bridges are also managed by private forestry and mining companies.

Federal bridge management in Canada is undertaken by Transport Canada and the Federal Bridge Corporation Limited (FBCL). Transport Canada and the FBCL provide management of intraprovincial, interprovincial and international bridges and associated structures. Specifically, the FBCL manages the Jacques Cartier, Champlain, Seaway International, Sault Ste. Marie and Thousand Islands Bridges. All of these bridges are located in Ontario and provide important trade routes and links between Ontario, Michigan and New York. The Confederation Bride, connecting Prince Edward Island and New Brunswick, is managed by Strait Crossing Development Incorporated, a private sector developer that is responsible for operating and managing the bridge until 2032; at such time operations will be transferred to the Government of Canada.

Provincial bridge management is undertaken by the ministry or department of transportation within each province. Presently, provinces and territories (except for Ontario) do not have a provincial regulation for bridge inspection. (Provinces typically have written policies but no enforceable legislation). Provinces generally download the responsibility of bridge management to local municipalities.

Municipalities are the largest and most important bridge owners in all provinces and territories of Canada. Each province and territory has a different bridge management system that municipalities use. For instance, Alberta uses BEADS, the Bridge Expert Analysis and Decision Support system and for the past 20 years British Columbia has been using BMIS, The Bridge Management Information System. British Columbia, Alberta, Ontario, Quebec and Prince Edward Island all have computerized bridge management systems while the remaining province and territories manually enter bridge data to spreadsheets to create an inventory database. Bridge management in Canada is a challenge since not all provinces and territories have central databases of bridges. Already established databases are often lacking records, reports and inspections for bridges (Khanzada 2012).

Building Canada Fund

The Building Canada Fund, introduced in 2014, provides a total of $53 billion towards infrastructure investment over the next 10 years (2014-2024). This is the largest provision of infrastructure funding in Canadian history. This funding is divided amongst the provinces and territories for infrastructure improvements. The Building Canada Fund consists of a number of funding categories:

(a) Federal Gas Tax Fund: the federal Gas Tax Fund was introduced in Canada's Economic Action Plan for 2013. The Gas Tax Fund is legislated and set to operate over the next 10 years and provide a projected $2 billion per year to municipalities for infrastructure needs. Funding is dispersed twice per year to provinces and territories who then allocate funding to municipalities to support local infrastructure priorities. Municipalities are allowed to borrow against future allocations in order to invest in long term infrastructure projects.

(b) P3 Fund: the pubic-private partnerships (P3s) are long term infrastructure projects where a private sector company assumes responsibility for construction of infrastructure projects in Canada. P3 projects consist of rapid transit system improvements, airport improvements to infrastructure projects. A total of $1.5 billion has been allocated for P3 projects.

(c) National Infrastructure Component: a total of 4 billion dollars is allocated for projects of national significance. Projects considered are those that provide the greatest economic impact such as: port infrastructure, major roads, public transit and airports.

(d) National and Regional Projects: a total of $10 billion is being given to provinces and territories over the next 10 years for infrastructure projects at the regional level. Eligible projects can be anything from wastewater treatment plants to public transit to highways and bridges. Funding is allocated to province and territories based upon per-capita calculations.

As mentioned, bridge responsibility typically falls onto municipalities. As the Canadian government recently rolled out a large infrastructure funding package, the Building Canada

Fund, it is up to local municipalities to plan and lobby for funding in order to adequately maintain bridges or replace bridges as deemed necessary.

6.3.2 Construction standards

The Transportation Association of Canada (TAC) is an organization independent from government that offers idea exchange, technical guidelines and best practices for transportation needs in Canada. The association considers itself a neutral forum that does not set transportation standards but acts as a source for technical documents and national guidelines.

In Canada, the legal mandate for construction standards of highways and bridges is the responsibility of the provincial and territorial governments. Prior to 2000 there was three design codes used across Canada for bridge construction: the Ontario Ministry of Transportation's Bridge Design Code OHBDC-91-01, the Canadian Highway Bridge Design Code used by all province and territories except Manitoba and Ontario, and the bridge code published by the American Association of State Highway and Transportation, which was used by the province of Manitoba. In 2000, the Canadian Highway Bridge Design Code amalgamated the previous Canadian code with the Ontario code to produce one bridge design code across Canada. Since then it has been updated and the latest code is the CAN/CSA-S6 Bridge Design Code. The Canadian Bridge Code is written and produced by numerous expert committees from across the country; it is distributed through the TAC. In Section 1.9 of the Canadian Bridge Code it specifies that hydraulic design of bridges must comply with the regulatory authority (local province regulations) or in their absence the TAC's Guide to Bridge Hydraulics (TAC, 2004).

There are a number of manuals issued by the TAC that specify various construction standards for steel, concrete bridge applications, acceptable loads, surface design and hydraulic design. As is relevant to this thesis, only the standards pertaining to hydraulic design of Canadian bridges will be discussed here.

The following guidelines are specified in the CAN/CSA-S6 code book and the TAC Guide to Bridge Hydraulics (TAC-GBH), and must be considered in the design and construction of a bridge.

(a) the opening should be large enough to avoid backwater effects and not cause realignment of natural flows (Chapter 4).

(b) hydraulic performance of existing structures near the build site must be reviewed (Chapter 3).

(c) the bridge should be able to withstand design discharge and severe ice conditions if applicable without compromising the structural integrity of the bridge (Chapter 4).

(d) climate change and variability should be considered in evaluating bridge design floods. Regression analysis of two or more close-by stations is recommended (Chapter 3).

(e) computation of water surface profiles and hydraulic properties can be modeled with common software such as HEC-RAS (Chapter 4).

(f) scour estimates based upon models such as HEC-RAS should not be relied upon without independent checks since scour is a complex phenomenon and is not adequately represented in these models (Chapter 4).

In the TAC-GBH, Chapter 4, Section 4.5, 'Local Scour due to Piers and Abutments', the manual offers two suggested methods for measuring local pier scour. Specifically, Melville's

(1997) "curves and formulas… [where] pier diameter is usually the primary parameter affecting scour depth" (p. 81) and the US FHWA procedure based upon the CSU equation (Richardson and Davis, 1995). Under Melville's (1997) method, which is a slight modification of the Melville and Sutherland (1988) equation listed in Table 19, the following procedure is suggested (p. 84):

- Step 1: Determine effective pier width or diameter b.

- Step 2: Determine depth of approach flow under design or other desired flow conditions, allowing for general scour if appropriate. For a pier on a floodplain use local depth of floodplain flow.

- Step 3: Using the envelop lines of Figure 74, calculate the scour depth d_s.

- Step 4: Multiple the primary scour depth, d_s, by a set of K factors to obtain the design local scour depth (d_{se}) as presented in the following equation.

$$d_{se} = k_d k_s k_\theta d_s \qquad\qquad 6.6$$

Where d_{se} is the local design scour depth, k_d is the sediment size factor, k_s is the pier shape factor and k_θ is the pier alignment factor.
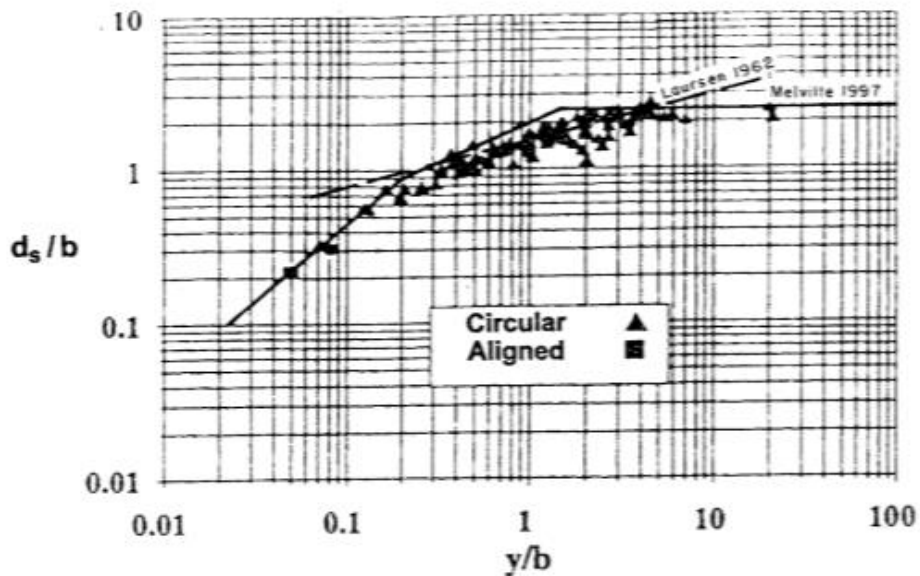
Figure 74. Basic local scour relationship for aligned or circular piers where d_s is scour depth, b is pier width and y is approach flow depth. Data represented in the above figure were measured from uniform sediments. Data are also independent from sediment size effects as $b/D_{50}>50$, (taken from Melville, 1997; TAC, 2004).

The second method for calculating scour depth as outlined in the TAC-GBH is based upon the CSU equation (Richardson and Davis, 1995) written as:

$$d_s = 2.0yk_1k_2k_3 \left(\frac{b}{H}\right)^{0.65} F_r^{0.43} \qquad 6.7$$

where $k_1k_2k_3$ are correction factors for pier shape, angle of attack and bed condition respectively. The Guide notes that for the CSU equation, scour depth increases with Froude number and does not represent grain size; therefore, with uniform bed materials scour depth may be greater for steep rivers with larger bed materials. The TAC-GBH recommends the use of Melville's method rather than the CSU equation as the CSU equation "contains no explicit factor representing grain size exclusive of armouring considerations" (p.85).

Specific consideration is given to effects of ice and the Guide states:

(a) Investigation of ice conditions and ice history must be completed by examining: dates of break-up and freeze-up, published and unpublished reports of ice problems and a search for local physical evidence of high ice conditions.

(b) Scour can occur during an ice jam break-up event due to increased flow velocities. Additionally, ice jam runs can transport and deposit piles of rocks and boulders. This is an important consideration since riprap is often placed around bridge piers as a scour countermeasure. The Guide states that riprap should have a diameter that is at least equal to the ice thickness. In the instance of ice or debris accumulations, the TAC-GBH provides the following equation, slightly modified from Melville (1997):

$$b_e = \frac{[0.5tb_a + (y - 0.5t)b]}{H} \qquad\qquad 6.8$$

where b_e is the equivalent width or diameter of pier with drift accumulation, b_a is the width or diameter of drift accumulation, b is the pier diameter, t is the thickness of drift accumulation and H is the approach flow depth. Here the equivalent width or diameter of pier shall be used in place of pier width in the Melville (1997) or CSU (Richardson and Davis, 1995) equations.

Lastly, since there are three series of manuals that govern bridge hydraulic standards (CAN/CSA-S6, TAC guide to bridge hydraulics and individual provincial manuals) it is up to the regulatory authority and bridge owner to reference appropriate manuals for hydraulic design floods. The TAC manual dedicates an entire chapter regarding methodology for

calculating return periods. As each province is different in geography and hydrology, different

return periods may be used for bridge design floods (Table 21).

Table 21. Bridge design flood frequencies as stipulated by the various Canadian Bridge Design manuals. Provincial guidelines were taking from the TAC manual, Guide to Bridge Hydraulics, with reference to Watt et al. (1989).

Manual	Hydraulic design flood frequency, years	Scour design flood frequency, years	Check flood frequency, years
CAN/CSA-S6	50 unless otherwise specified by regulatory authority	refer to TAC manual	at least twice the normal design flood unless otherwise specified by the regulatory authority.
TAC Guide to bridge hydraulics	refer to appropriate provincial manuals	1.7 times the 100- year peak	500
Province	**Type of structure**		**Return period, years**
British Columbia	bridges low volume road bridges *low volume roads = 500 vehicles per day or less		200 100
Alberta	main highways secondary highways local roads		100 50 25
Saskatchewan	major bridges others		100 50 or less
Manitoba	main crossings		100-50
Ontario	spans > 6 m freeways arterials local roads		100 100 50 25
Quebec	spans < 6 m bridges & highways main roads secondary roads		50/25/10 100 50 25
Newfoundland	TransCanada highway other roads		100 50

6.3.3 Bridge maintenance

In Canada there are four manuals used for bridge inspections: the British Columbia Bridge Inspection Manual, Alberta's Bridge Inspection and Maintenance Manual, Quebec's Manual d'inspection des structures and Ontario's Structure Inspection Manual. Currently, the Yukon and Northwest Territories use Alberta's manual while Saskatchewan, Manitoba, New Brunswick, Prince Edward Island and Nova Scotia are using the Ontario manual (Khanzada, 2012). Each manual stipulates inspection and maintenance standards. Inspections vary between provinces, with most provinces conducting bridge inspections every 2 years and British Columbia inspecting every year. Underwater inspections are completed by all provinces except Alberta, Saskatchewan and the Northwest Territories. This is a cause for concern since it is estimated that 60 percent of bridge failures result from scour (Khanzada, 2012).

All provincial governments have in-house bridge managers which partake in routine inspections and report writing. All inspections and reports are done to the standard of the associated provincial inspection manual used. British Columbia has privatized the maintenance of bridges and highway systems; maintenance contractors are hired within each management district to observe and conduct routine maintenance. The Yukon and Northwest Territories hire engineering firms to conduct bridge inspections. Most bridge inspections are based upon visual observations with limited physical testing such as tapping of concrete. Bridges in some provinces such as Ontario are graded on a scale of excellent, good, fair and poor, while other provinces such as Alberta rank bridges on a scale of 1 to 9. In all provinces bridge inspections must be completed under the supervision of an engineer. Bridge inspector

training is provided in-house by each province except for New Brunswick where training is sought through the United States Federal Highways Administration.

6.4 Bridges in the United States

6.4.1 Governing bodies

Bridges in the United States are regulated by the Department of Transportation (DOT), Federal Highway Administration (FHWA). The FHWA provides stewardship, research and development for the countries' highways and bridges along with research programs to support design and construction practices. Within the FHWA there are three bridge and structures research and development teams that conduct and manage research in the following areas:

(a) Design and construction: reviews use of structural materials (steel, wood, concrete), shallow and deep foundations, river hydraulics, aerodynamics, bridge security and extreme events (floods, seismic).

(b) Infrastructure management: investigates tools and practices for bridge inspections and monitoring, improving bridge durability and preservation.

(c) Long-term bridge performance: this team looks at developing data and knowledge to understand bridge performance under a variety of conditions.

The FHWA main research centre is the Turner-Fairbank Highway Research Center based in Virginia. The centre has 20 laboratories and support facilities. The center reviews and tests solutions to transportation topics such as: concrete coatings and corrosion, stream stability and bridges, pavement testing, steel and timber structures, and bridge durability and

loads. The facility has over 100 scientists and engineers trained in transportation related disciplines. To assist with technology transfer along with national and international collaboration the center also employs a team of support professionals focused on information dissemination.

In addition to the Turner-Fairbanks Highway Research Center, the FHWA also directs a number of transportation research initiatives outlined as follows.

University Transportation Centers: the main research program under the FHWA is the allocation of University Transportation Centers (UTC). This program began in 1987 under the Surface Transportation and Uniform Relocation Assistance Act and established funding that is allocated on a competitive basis to Universities located in each of the 10 standard federal regions. To qualify, a UTC must be located within the United States, comprise a single or consortium of universities and must obtain matching funding from non-federal sources. The most recent allocation of funding came from the Moving Ahead for Progress in the 21st Century Act, July 2012, which authorized $72.5 million per year from federal funds to be allocated for up to 35 UTCs in the United States. During 2013 all of the grants were competitively selected and research is currently being conducted. The UTCs provide the main transportation knowledge base outside of the Department of Transportation.

Small Business Innovation Research Program: the FHWA also invests in technological innovation regarding bridge infrastructure through the Small Business Innovation Research Program (SBIR). This program awards contracts to small businesses to research and develop

technological solutions to various transportation challenges. Each year the SBIR solicits proposals on a number of transportation topics that are needed by the FHWA.

State Planning: each state must also set aside 2 percent of funding they receive from core federal-aid programs to fulfill State planning and research activities. Transportation research activities must include practical application of technology and investigating new areas of knowledge.

Exploratory Advanced Research Program: the Exploratory Advanced Research Program (EAR) is based upon legislation that outlines the need to conduct transportation research on a long time scale and in high risk areas. Projects typically funded through the EAR highlight new technology and involve projects that are not likely completed within 10 years. The FHWA appoints expert panels consisting of State, Federal, academic and international transportation experts to scope topics and ensure technical quality of sponsored research. An example of technology research produced by the EAR is the use of self-powered wireless sensors for real-time monitoring of potentially dangerous cracks in steel bridges. This project, competed in 2013, is expected to increase cement crack detection awareness. Prior to 2012, approximately $14 million per year was allocated for exploratory advanced research; under the current Moving Ahead for Progress in the 21st Century Act 2013, funding for the program continues.

National Cooperative Highway Research Program: the National Cooperative Highway Research Program (NCHRP) was created in 1962 to disseminate information and conduct independent transportation research across the country. Each State receives planning and research funds, and is expected to contribute 5.5 percent of their funds to the NCHRP to ensure

its operation. Each year the American Association of State Highway Transportation Officials (AASHTO) solicits proposals on transportation issues from private and public organizations (universities, non-profit institutions, consulting firms). A technical review panel is formed and contracts are awarded. Research findings are published in the NCHRP report series. Annual funding under this program is approximately $37 million per year.

6.4.2 Construction standards

The AASHTO is a non-profit organization that represents highway and transportation departments in all 50 states. The AASHTO acts as a liaison between the states and the federal government. The role of the AASHTO is to provide and set technical standards for all design and construction of bridges and highways. The AASHTO has a number of committees that consists of state transportation representatives; the committees meet annually to address planning, design and construction of transportation infrastructure. Specifically, the Committee on Bridges and Structures provides key standards manuals on topics such as bridge element inspection, seismic design and bridge construction specifications.

There are a number of manuals issued by the AASHTO that specify various construction standards for bridges, concrete bridge applications, acceptable loads, surface design and hydraulic design. As is relevant to this thesis, only the standards for hydraulic design will be discussed here.

The following standards were taken from the Hydraulic Design of Safe Bridges manual (Zevenbergen et al., 2012). Bridge engineers have a variety of choices when deciding the site and location of a new bridge. The following hydraulic components must be considered:

(a) the level of service the bridge will incur. If the bridge is in a remote area with low traffic then the bridge can be designed with a lower hydraulic capacity; this enables construction costs to be low. Alternatively, if the bridge is expected to have a high volume of traffic and significant economic costs would incur if the bridge was out of service then the bridge is designed with a higher hydraulic capacity.

(b) the bridge must provide enough hydraulic capacity to avoid excessive backwater so to prevent adverse floodplain impacts. The design, geometry and occurrence of piers must not lead to an increase in backwater over existing conditions. In the case of bridge replacement over an existing floodplain crossing the backwater must not exceed 1 foot (0.3048 m).

(c) the bridge must provide enough hydraulic capacity to prevent excessive velocity and shear stress within the bridge waterway.

(d) the bridge must have a freeboard for a 50 year flood for low-traffic routes, and a freeboard for a 100-year flood for high traffic routes. Under the Federal Emergency Management Agency, the floodplain regulations state that any bridge element must not cause in increase in the 100-year flood water surface elevation compared to existing conditions.

Specific consideration is given to effects of ice in the Hydraulic Design of Safe Bridge Manual (Zevenbergen et al., 2012). The guidelines indicate that:

(a) the bridge design team should conduct site-specific analysis to see if ice events are relevant.

171

(b) if ice forces are deemed relevant, the hydraulic engineer involved must provide the bridge

   designer with information regarding ice forces. In doing so the hydraulic engineer can

   model simulations of ice jam situations using HEC-RAS. The model allows user input of

   ice cover thickness, ice cover Manning's n value and maximum mean velocity under ice

   cover.

The latest edition of the HEC-18 manual outlines the recommended minimum scour design

flood frequencies:

Table 22. Bridge design flood frequencies as stipulated in FHWA HEC-18 manual (Zevenbergen et al., 2012).

Hydraulic design flood frequency, Q_D	Scour design flood frequency, Q_S	Scour design check flood frequency, Q_C
Q_{10}	Q_{25}	Q_{50}
Q_{25}	Q_{50}	Q_{100}
Q_{50}	Q_{100}	Q_{200}
Q_{100}	Q_{200}	Q_{500}

The flood frequencies for scour are larger than the hydraulic design flood frequencies

since there is a 39.5 probability of exceedance that during a 50 year design life a bridge will

experience a flood that is greater than the Q_{100} level (Zevenbergen et al., 2012). The same

rationale goes for the check flood levels being larger than the scour design flood frequency.

In bridge design it is generally accepted that rare floods do occur and bridges may incur

occasional damage; however, major damage or collapse can cause significant economic loss,

social impacts and safety hazards. For these reasons, there is a higher hydraulic standard for

design of bridge foundations in comparison to design of bridge hydraulic capacity. Lastly, the

HEC-18 manual states that all bridge foundations must have a minimum factor of safety of 1.0 under the scour design check flood conditions (Table 22).

6.4.3 Bridge maintenance

As bridges in the United States continue to age and deteriorate, it is increasingly important that bridges are inspected and maintained. The DOT oversees the National Bridge Inspection Standards (NBIS) which form minimum nationwide requirements for bridges. The NBIS originated in 1971 after the Silver Bridge collapsed in the Ohio River in 1967 during rush-hour killing 46 people. The NBIS is a set of Federal regulations that outlines inspection procedures, inspection frequency, qualified personnel, inspection reports and maintenance of bridge inventory. Since 2000, approximately 59,000 bridges have been replaced and rehabilitated under this federal regulation. A national Bridge Inspection Training Program exists and bridge inspectors enter their data into the National Bridge Inventory (NBI). The training program consists of many courses up to 2 weeks long regarding inspection safety, inspection standards, stream stability, scour, underwater bridge inspection and bridge maintenance.

It is the responsibility of each bridge inspector to: (a) provide a thorough bridge inspection of conditions and defects and to (b) report deficiencies to supervisors and engineers that may impact public safety or integrity of the structure and (c) provide recommendations to close a bridge if necessary. Bridge inspections also serve to investigate minor problems that can be upgraded before they lead to major repairs. It is also recognized that bridge inspectors play a key role in maintaining and adding data to the National Bridge Inventory. Issues such as abutment tilt may only be captured after looking at multiple years of historic data. Once a

bridge inspection is completed it becomes a legal document. Bridge inspectors are required to be registered engineers and have completed the FHWA bridge inspection training program.

6.5 In situ scour measurement technology and countermeasures

As scour is one of the major causes of bridge failures (Lin et al., 2010), it is important that time and money is allocated to technology for measuring and monitoring pier scour. In addition to providing public safety, scour monitoring technology can also provide hydraulic data for engineers in which scour equations can be improved upon. Real world scour data can also be used to investigate scaling issues that arise from physical modeling. Scour monitoring systems can also reduce operating costs of transportation departments as field inspections and underwater inspections can be reduced. Over the years a number of studies have investigated and developed scour monitoring systems (Ballio and Radice, 2003; Lu et al., 2008; Yu, 2009) and the Hawaii DOT funded a sonar project which measured bridge scour in order to validate scour equations included in the HEC-18 manual. Reliable scour monitoring technology is essential for decision making and public safety: for instance, during 1994 flooding in Georgia, 2100 bridges were monitored and 1000 were closed and no lives were lost as a result of bridge failures (Schall and Price, 2004).

Not all bridge sites are optimal for installation of scour monitoring equipment. High flow conditions, high sediment concentration, low bridge clearance, severe water temperature, floating debris and ice accumulation cause interference and damage to monitoring equipment. In a survey conducted by Hunt (2005) debris and ice flows were shown to be responsible for 26 and 13 percent of all damage to monitoring systems. The following is an outline of the most successful and currently used scour monitoring technology.

SONAR: sound navigation and ranging (SONAR) technology works by sending an acoustic pulse from a transmitter mounted to a bridge pier. The acoustic pulse travels through the water and is reflected when it hits the river bed. The reflected pulse is captured by the receiver and the time elapsed is calculated. The distance from the transmitter to the river bed can be calculated by measuring the elapsed time and acoustic signal travel speed. ETI Instrument Systems Inc. and Nortek are scientific instrumentation companies with offices in North America and Europe. They currently offer a SONAR scour monitoring technology as indicated in Figure 75.

Magnetic Sliding Collar: the magnetic sliding collar consists of a vertical pipe that is driven into the river bed typically on the upstream side of the pier. A collar is installed around the vertical pipe and rests on the riverbed. The collar moves down the vertical pipe in the event of scour. Magnets are attached to the collar which create a magnetic field. Inside the pipe is a magnetic sensor which can detect the position of the magnetic collar. The design is robust and can survive flood conditions; however the main limitation in this technology is that the collar becomes buried during deposition events.
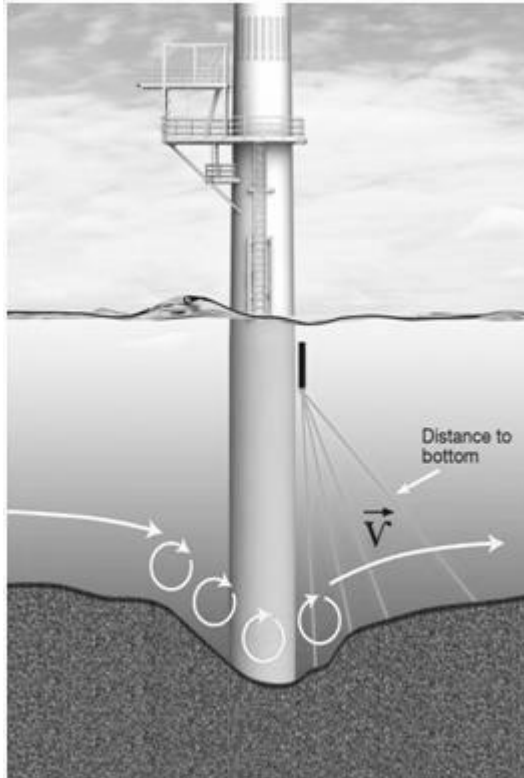
Figure 75. SONAR scour monitoring equipment (NORTEK, 2014).

Float-Out Transmitter: a simple yet effective scour measuring device is the float-out transmitter. The device consists of a buoyant container with an internal transmitter. The container is buried at scour-prone locations around bridge piers. Should significant scour occur, the device will float to the water surface and activate the internal transmitter which will send a signal to a receiver that is mounted on the bridge. If significant scour occurs during ice events the float-out device will be stuck under the ice cover and signal transmission may not be successful.

Each bridge site can have a unique scour environment that must be considered prior to selecting potential scour monitoring technology. Sonar systems are ideal for bridge sites that have little debris while float-out transmitters and magnetic collars are better suited for debris

176

laden channels. In regards to a scour sensor that would be optimal for channel ice conditions presented in this thesis, either a sonar-type system or sliding collar would be suitable for measuring scour under ice conditions. A sonar-type system would have to be mounted on a bridge pier at a suitable level to avoid ice interference and damage. A sliding collar would be significantly less in cost than installing sonar technology and would avoid damage from surface water ice. Installing a magnetic collar would however only be useful if it is not buried by sediment deposition.

6.6 Evaluation of this study in the context of current day bridge design

As discussed, bridge design and construction has an extensive history involving both academic and government institutions in Canada and the US. As researchers have investigated pier scour for the past 50 years and published hundreds of journal articles, one must question what further contributions this thesis can offer the field of scour research or is it merely an 'exercise in academia'. Secondly, can information presented in this thesis be used or incorporated into bridge design or form the groundwork for further studies relating river ice and pier scour. The following is an overview of (a) knowledge gaps in TAC-GBH, (b) an explanation of what this study contributes to the field of bridge design and (c) how this study can be communicated to Engineers working in bridge design.

In reviewing the TAC-GBH, it is evident there are knowledge gaps regarding ice induced pier scour. There are no equations in the Guide regarding how to calculate pier scour under ice cover. The issues of floating ice, ice jamming and floating debris are reviewed over pages 97-108, while specific attention is given to ice induced pier scour in the following statements:

- "Ice jams and accumulations in the vicinity of bridges may cause or contribute to general and local scour by inducing high velocities in the obstructed cross-section" (p.97).

- "Jams may affect bridges… [by] their formation or release that may cause or aggravate river-bed scour" (p.98).

- "Scour during breakup can occur as a result of high velocities during an ice run, or because the toe of a jam forms in the vicinity of a bridge. A worst case scenario would be a grounded jam, with all flow passing under the toe within the scour depression." (p.103).

- "Accumulation of debris against…piers…can significantly increase the potential for local scour, as the stream flow is forced downwards under the accumulation or as the accumulation causes the flow to impinge obliquely on submerged pier shafts and foundations" (p. 105)

While the TAC-GBH states ice cover and jamming may result in greater scour, no literature or data are referenced to support these statements. The Guide suggests the above statements are issues to consider during pier design. In considering debris accumulation around piers, the Guide does provide equation 6.8 in order to calculate a larger pier width due to debris. The TAC-GBH also suggests that in order to protect bridge piers from increased ice induced scour, "rip-rap should [be placed and] have a diameter at least equal to the ice thickness" (p.103); again, no literature is referenced to support this suggestion. While no literature is referenced in the ice section of the TAC-GBH, it is assumed that currently bridge engineers review the site specific channel hydraulics and design piers taking in account the historical evidence of

ice jam occurrence and install rip-rap as appropriate. In section 4.4.8, the TAC-GBH states that due to the "inherent uncertainty of scour estimates and the high risk of public safety usually associated with foundation undermining, bridge foundations should be designed or upgraded to provide an adequate margin of safety against scour failure. It is difficult to give general guidance because scour estimates interact with various design features and other considerations" (p. 93). In addressing scour uncertainty the Guide states that extra attention should be given to extreme flows exceedance probabilities, seriousness of consequences of total or partial pier failure and experience of the designer in comparable situations (p.94). While the TAC-GBH does acknowledge the uncertainty in channel hydraulics and the literature on river ice processes is referenced (Ashton, 1986; Beltaos, 1995; Gerard, 1989; USACE, 1982), there is still a large knowledge gap surrounding how river ice processes interact with bridge infrastructure and the process of pier scour.

Taking into consideration the above mentioned knowledge gaps, the following points are the main results of this study that contribute to the field of bridge design and address the knowledge gaps in the TAC-GBH.

1. This study found that in non-uniform sediments, ice cover can produce a 20-37 percent larger scour depth than compared to open channel flow (Figure 35-37, Chapter 5). The variation in scour depth will depend upon the range in bed sediment size which will influence the formation of an armour layer (p. 74, Chapter 5). The TAC-GBH does suggest that ice cover leads to greater pier scour by inducing higher velocities; however there is no reference quantifying or explaining this phenomenon. Chapter 5, Section 3.5 of this study addresses this knowledge gap, confirming that ice cover does in fact increase pier scour.

2. The second main result of this study was that under ice cover, armour layer formation can lead to a decrease in scour depth (Chapter 5, Section 5.7). Smaller particles in the armour layer will provide less scour protection around the pier and result in a larger local scour depth. This indicates that an armour layer will provide scour protection as long as the critical bed shear velocity is not large enough to cause incipient motion of the armour layer. This study also confirms that under ice cover, the greatest scour depth always occurs at the pier face (Figure 42-47, Chapter 5); therefore implying that rip-rap size and placement must be designed to withstand scour hole velocities at the pier face. The TAC-GBH has an entire chapter on scour mitigation measures (Chapter 5, p. 115-145); however, all guidelines are based upon open channel flow conditions. For example, to ensure incipient motion does not occur when selecting rip-rap size around piers, the TAC-GBH states that the "local design velocity V should generally be at least 50 percent greater than the velocity approaching the pier" (p. 131). The TAC-GBH addresses ice cover once when stating that the safety factor (S) of 1.1 is normally used when calculating rip-rap size, except "where there is ice or debris impact" (p.129), a higher value may be used.

3. The third main result of this study was that the downflow and turbulence within the scour hole is greater under ice cover than open channel conditions. Scour hole velocity under rough ice cover is 29-37 percent greater than compared to open channel scour hole velocity (Figure 56-57, Chapter 5). These findings address the knowledge gap around calculating rip-rap sizes for bridge piers under ice cover. Local design velocities are currently estimated under ice cover conditions and rip-rap size is calculated based upon design velocities. This study provides evidence that scour hole velocity under ice cover is 29-37 percent greater

than open channel conditions (Chapter 5, Section 5.8) which can provide supporting evidence for greater certainty in rip-rap design.

As discussed, this study addresses current knowledge gaps in the pier scour literature and also provides supporting evidence to address unknowns in the TAC-GBH. While this is the first study to measure under ice scour depth and scour profiles with armour layer formation, realistically further research is required before bridge engineering committees will find confidence in study results. Additional research exploring a range of flow velocities and depths as they relate to pier scour under ice cover is required. Also, pier scour under ice over for a greater range in sediment D_{50} should also be examined.

In the United States and Canada, Bridge Design Codes are written by various committees comprised of professionals whom specialize in a specific bridge construction area. Bridge hydraulic committees are made up of engineers working in academia, private industry and local governments. Annual meetings are held to discuss code revisions and ongoing research. The code and reference manuals typically have 2-3 leading authors. Recommendations and standards are written based upon citing academic and professional literature. For example, in both the Canadian and US bridge manuals, the CSU pier scour equation is recommended as a scour equation based upon 20 years of research using the equation. Whether or not academic work will be recognized by bridge committees depends on (a) whether the academic work is titled effectively and found in a search of the literature (b) whether the study is designed well and actually builds on knowledge gaps in the current bridge manuals and (c) whether the study is repeatable and well respected in the field of literature. Given that this study does contribute valuable evidence that scour processes around bridge piers is different under ice cover, communicating study results to the engineering

community is important. Publication plans are discussed in the conclusion section of this thesis (Chapter 7), and are the avenue in which study results will be communicated to the bridge design community.

6.7 Conclusion and recommendations

The purpose of this chapter was to examine the various components that involve bridge scour research, namely flume work, scour equation development and computational fluid dynamics and assess where components of this thesis relate and are useful in current day practices. Additionally, bridge standards in North America along with scour prevention practices were reviewed in order to gain insight as to whether academic bridge research is used and applicable to real world bridge design problems around pier scour. The following points are the conclusions drawn from this critical assessment:

(1) While there is a long standing practice of using physical hydraulic models to investigate sediment transport around bridge structures, there is currently no known study that successfully models such phenomena without scale effects. For the experimental flume used in this study, issues around dynamic similitude arise because flume bed material relative to pier size is larger than the real world prototype. In addition, similitude of particle mobility and similitude of the Froude number cannot occur simultaneously. Also, non-cohesive sediments are traditionally used in flumes whereas that is not the case in natural river systems. The design and construction of the flume and experiments undertaken in this thesis were subject to scale effects. The scale effects of flow depth to pier width were addressed by only changing one parameter, that being channel cover, while all other parameters remained constant. The scale

effects of incipient motion were investigated at specific Froude numbers < 1, and the scale effects of sediment size could not be avoided.

(2) The success of developing and validating equations for pier scour depends entirely on how representative the equations are of the real world system. Experimental flumes are subject to scale effects and can over simplify river channel morphology and hydrology. As a result, pier scour equations can underestimate or overestimate scour hole development. The most commonly used pier scour equation is the CSU equation. As found in numerous studies, for open channel flow conditions, the CSU equation also overestimated scour depth as measured in flume experiments conducted in this thesis. As flume studies are always subject to scale effects, scour equations should be developed with a focus on replicating field data sets rather than flume data sets. In order for this to occur, substantial funding and effort must be directed towards developing field data sets for a variety of bridge environments. As discussed, scour measurement and monitoring technology such as SONAR is currently used, however during construction, firms must partner with both private and academic bridge engineers in order for planning and financial investment towards scour monitoring equipment.

(3) The use of the CFD program FLUENT was assessed and it was decided that FLUENT was not appropriate for use in this thesis due to the inability to accurately model a floating ice cover. In addition, current CFD practices are limited due to the inability to accurately solve turbulent, unsteady and multi-phase flows.

(4) Bridge management in the United States is highly organized with nationwide construction standards and substantial federal funding backing numerous research institutions. The DOT manages a National Bridge Inventory which provides a snap shot of bridges in the United States. Canada on the other hand downloads bridge responsibility to local municipalities who typically contract out bridge construction and management to private companies. (In doing so liability is also passed from the government to private companies). Canada also operates under numerous bridge codes and data systems. Each province has its own bridge code (adapted from the CAN/CSA-S6 code) and various computer management systems ranging from provincial software programs such as Alberta's BEADS, to relying on pen and paper filing systems. Having various bridge codes for each province may be appropriate considering varying Canadian topography and hydrology; however, there is a need to develop sufficient bridge management software that can provide an understanding of the current state of bridges in Canada.

(5) In reviewing the Bridge Design Manuals, it is evident there is still a large knowledge gap surrounding how river ice interacts with bridge infrastructure and the process of pier scour. There are no equations regarding how to calculate pier scour under ice cover. When ice cover or debris accumulations are part of the channel dynamics, the TAC-GBH recommended that the factor of safety be greater than 1.1 when designing rip-rap sizes. This study addresses current knowledge gaps by providing evidence that (a) pier scour is greater under ice cover than open channel conditions, (b) under ice cover, armour layer formation can lead to a decrease in scour depth, and (c) the downflow and turbulence within the scour hole is greater under ice cover than open channel conditions.

7.0 CONCLUSIONS AND FUTURE RESEARCH

7.1 Thesis conclusions

The purpose of this thesis was to gain a better understanding of how ice cover is related to local scour around bridge piers. In doing so, 54 flume experiments were completed investigating pier scour under open, smooth and rough ice cover conditions. In order to assess the current state of bridge design, a critical analysis of bridge research was also conducted. The following are the major conclusions of the experimental flume component of this thesis:

- The average maximum velocity under rough ice cover ranged from 0.36-0.43 of the total depth and for smooth ice cover was 0.41 of the total depth. Channel depth was measured from the channel bed to water surface. This indicates that ice cover causes the maximum flow velocity to move closer to the channel bed in comparison to open channel conditions.

- Turbulent intensities and Reynolds stresses are affected by the presence of simulated smooth and rough ice cover. Both turbulent intensity and Reynolds stresses are greater under ice cover then open channel conditions.

- The smallest sediment size, D_{50} = 0.47 mm yielded the largest pier scour depth under all channel covers. The largest sediment size, D_{50} = 0.58 mm, yielded the smallest pier scour depth under all channel covers. This indicates that less shear velocity is required for incipient motion of smaller D_{50}s.

- The average maximum scour depth for the 22 cm pier was 29, 12 and 25 percent larger than the 11 cm pier for rough, smooth and open channel conditions respectively.

- Scour depth is greater under rough ice cover compared to open channel conditions for 60 percent of experiments. Scour depth is greater under smooth ice cover compared to open channel conditions for 53 percent of experiments. The average rough and smooth ice cover scour depths are 37 and 20 percent greater than open channel scour depth.

- The streamwise and downward velocities at the pier face and within the scour hole are greater under ice cover than open channel flow. For all sediment D_{50}'s under the 22 cm pier, the average rough cover velocity is 37 percent greater and the average smooth cover velocity is 15 percent greater than the open channel velocity. For all sediment D_{50}'s under the 11 cm pier, the average rough cover velocity is 29 percent greater and the average smooth cover velocity is 26 percent greater than the open channel velocity.

- Regardless of cover condition, the location of maximum scour depth is always at the pier face. Scour depth decreases towards the downstream side of the pier. Downstream sediment deposition is greater for the 22 cm pier under all channel covers.

- Under all channel conditions there is a positive relationship between maximum scour depth and Froude number. Under the same Froude number, maximum scour depth is greater under rough ice cover conditions.

- Relating the scour depth to the densimetric Froude number provides no guidance when applied to non-uniform sediment since the densimetric Froude number does not adequately represent sediment nonuniformity. When scour depth and the densimetric Froude number are compared through linear correlation, the scatter is large and no significant relationship is present.

- Under all sediment sizes, the dimensionless shear stress increases with an increasing shear Reynolds number. For the same scour depth, less dimensionless shear stress is needed under rough ice cover compared to open channel conditions.

- As sediment D_{50} increases so does the D_{50} of the scour hole armour layer. Under all channel covers, the scour depth decreases as the armour layer size increases.

- Results of multiple regression analysis indicate that the most important factors to consider when examining pier scour under ice cover are: the Froude number, sediment D_{50}, and armour layer D_{50}.

The following are the major conclusions of the critical assessment component of this thesis:

- The major scaling issues present in this study are that of dynamic similitude because flume bed material relative to pier size is larger than the real world prototype. In addition, Reynolds similitude cannot be satisfied while meeting Froude similitude.

- Since flume studies are always subject to scale effects, in order for pier scour equations to become more accurate, scour equations should be developed with a focus on replicating field data sets rather than flume data sets.

- CFD projects require significant expertise, training, finances and time. Current CFD practices are limited due to the inability to accurately solve turbulent, unsteady and multi-phase flows all the while modeling a floating ice cover.

- Bridge management in the United States is highly organized with nationwide construction standards and a National Bridge Inventory. Bridge management in Canada is governed by numerous bridge codes and software management systems.

- Whether or not this thesis work will be referenced in present day bridge design literature is dependent upon the success of publishing this work in a well-respected engineering journals and whether bridge committees come across this work in their search of the bridge literature.

7.2 Study limitations

As with most hydraulic engineering research, the success of many laboratory experiments is related to the design and financial support for a study. Hydraulic flumes are located in university labs all over the world and are an important piece of infrastructure when studying river and ocean processes. Hydraulic flumes are typically designed by an engineering company and contracted out to a construction company or the facilities department of a university. This study required building a hydraulic flume as use of a flume at another institution was not possible. The design of the hydraulic flume for this study was completed by using (a) information found in the literature, (b) calculations regarding hydraulic head and flow velocities, and (c) trial and error in testing design flows. Construction of the hydraulic flume was completed by graduate students, a member of the university facilities department and hiring of local contractors for initial site excavation and concrete removal. Provincial and federal approval was required as construction occurred in the riparian area of the Quesnel River. No professional contractor or design support was available and existing infrastructure was an old fish spawning channel; as a result, the constructed hydraulic flume, budgetary provisions and remote location presented study limitations which are listed as follows:

- The flume velocity was regulated by gravity fed water valves that could only open by quarter revolutions at a time. This limited the precision and range of experimental flow velocity. Due to the inability to set specific approach velocities, parameters such as incipient motion velocity for each sediment were not measured.

- The Sontek 10 MHz ADV was large and measured a flow volume 10 cm from the measuring head. Alternatively, if funding permitted, Sontek's 16 MHz micro ADV would have been suitable as the flow volume is measured 5 cm from the instrument head allowing for increased precision in flow measurements. It is also assumed that the ADV somewhat interferes with the natural flow dynamics by simply being present in the water while under natural circumstances it would not be. Using a smaller ADV would reduce impact to flow dynamics. Turbulence, Reynolds stresses and the location of flow reversal within the scour hole are all analyzed based upon the output of the ADV measurements. Using Sontek's 16 MHz micro ADV would enable additional measurements of the scour hole flow profile and ultimately a greater understanding of scour hole flow dynamics.

- Due to the size of the flume and finances available, sand from local quarries was used which yielded a fairly small range in D_{50}s for this study (D_{50}s of 0.47 mm, 0.50 mm and 0.58 mm). The quarries in the area only offered a limited range in D_{50}; using larger bed material would have provided more information around how scour depth varied under a larger armour layer. The sand itself was not expensive, but rather high costs were associated with transporting the sand to the remote field location of Likely, BC, where the hydraulic flume was located. Also, since the flume required an entire dump truck load of

sand to fill the experimental sandbox area, additional time and labour was needed to move

sand in and out of the flume.

- The accuracy and extent of scour hole and sediment ridge contouring was limited by using

   manual measuring techniques. It is standard in the flume literature to use a bed profiler to

   map and display changes in scour and bed morphology. Funding limitations did not allow

   for such technology. Use of a bed profiler would increase the accuracy of scour depth

   measurements and also allowed for measurement of dune and ripple formation around the

   bridge pier.

7.3 Strengths of study and contributions to science

   Even though the flume construction and operational budget presented study limitations,

aspects of the flume design mirrored natural river systems more closely in comparison to some

smaller laboratory flumes. The size of the flume experimental section (40m x 2m), was most

likely more representative of natural river systems in comparison to shorter flumes used in the

literature (16 m x 0.60 m). The experimental section of the flume prior to the first sandbox

was 11.3 meters; this also allowed for flow to fully develop prior to passing the bridge pier.

Also, non-uniform sediment was used which is more representative of natural river systems in

comparison to uniform sediment.

   Overall, this study expanded on current knowledge of how ice cover influences scour

around bridge piers. In the current issue of the TAC-GBH there is limited guidance on how to

address ice cover in bridge design and construction. It is anticipated that this study will be

written up in a series of publications that can addresses the knowledge gaps in the TAC-GBH. The following is a brief outline of publications plans.

(1) Title: *The impacts of ice cover on local scour around bridge piers – an experimental study.*

Summary: The average maximum velocity under rough and smooth ice cover was greater than open channel conditions. Ice cover causes the maximum flow velocity to move closer to the channel bed, which leads to greater scour depths under ice cover conditions. There is also a positive relationship between the Froude number and maximum scour depth. Taking into account the ice cover velocity profile and Froude number, the resulting scour hole geometry is greater compared to open channel conditions.

(2) *Investigation of 3D scour hole flow field around bridge piers under ice cover.*

Summary: The scour hole flow field under ice cover is significantly different than that under open channel conditions. The streamwise and downward velocities at the pier face and within the scour hole area greater under ice cover than open channel conditions. Both turbulent intensity and Reynolds stresses are greater under ice cover then open channel conditions. The scour hole flow field under ice cover provides evidence as to the processes that lead to greater scour depth under ice cover.

(3) Title: *Investigation of armour layer development around bridge piers under ice cover*.

Summary: It was found that armour layer development was different for all 3 channel covers: open, smooth and rough ice cover. Armour layer development appears to be related to the sediment D_{50} rather than the channel cover. As sediment D_{50} increases so does the D_{50} of the scour hole armour layer. Under all channel covers, the scour

depth decreases as the armour layer size increases. Dimensional analysis and regression are used to determine the relationship and dependence between variables.

7.4 Future work

Recommendations regarding possible future work in relation to this thesis are as follows:

- In this study all scour hole profiles were measured using a Sontek 10 MHz ADV flow meter. Future work should measure the scour hole flow field under ice cover with a Sontek 16 MHz micro ADV. A micro ADV would impact the flow to a lesser extent and enable measurements around the entire scour hole. In doing so a greater understanding of the turbulent intensities and Reynolds stresses under ice cover could be investigated.

- In future flume experiments investigating pier scour under ice, using a bed profiler to measure changes in scour morphology would yield greater understanding of sediment transport processes in and around the pier scour hole. Using a bed profiler would also allow for measurement of dune and ripple formation around the bridge pier which may provide useful information for rip-rap placement and scour countermeasure design.

- Future flume experiments investigating pier scour under ice should use larger bed sediment (D_{50}) and explore a greater range in flow velocities. Maintaining an experimental ratio of b/h>5 (Melville and Coleman, 2000) will ensure that resulting scour depth is independent of flow depth and only proportional to pier width.

- Future flume experiments investigating pier scour under ice cover would benefit from pump and water control infrastructure so that flow velocities can be adjusted in small increments. Incremental adjustment of water velocity in addition to the installation of

192

underwater cameras would allow for the study of incipient motion of sediment under ice cover conditions which would build on the previous study by Wang et al. (2008).

- In the TAC-GBH, Melville's (1997) curve is used, Figure 74, to calculate scour depth based upon approach flow depth and pier size. Future flume experiments could expand upon this study and address gaps in the TAC-GBH by investigating the relationship between d_s/b and H/b under ice cover; this would basically recreate Melville's (1997) relationship, except data would represent ice cover conditions. Flume experiments investigating this relationship should be independent from sediment size effects with $b/D_{50}>50$.

8.0 REFERENCES

Aberle, Q. and Nikora, V. Statistical properties of armored gravel bed surfaces. *Water Resources Research*, 42, 2006. DOI. 10.1029/2005WR004674

Acharya, A. 2011. Experimental study and numerical simulation of flow and sediment transport around a series of spur dikes. PhD Dissertation. University of Arizona, Tucson, Arizona.

Alabi, P. 2006. Time development of local scour at a bridge pier fitted with a collar. MSc Thesis. University of Saskatchewan, Saskatoon, Saskatchewan.

Ali, K. and Karim, O. 2002. Simulation of flow around piers. *Journal of Hydraulic Research*, 40(2), 161-174.

Andrey, B. and Gareth, P. 2000. Flume study of the effect of relative depth on the incipient motion of coarse uniform sediments. *Journal of Water Resources Research*, 36(2), 619-628.

Assaad, F., LaMoreaux, P. and Hughes, T. (Eds.) 2004. Field methods for geologists and hydrogeologists. Springer, 377p.

Armstrong, J. 2004. Does an academic research paper contain useful knowledge? *Australasian Marketing Journal*, 12(2), 62-63.

Arneson, L., Zevenbergen, L., Lagasse, P., and Clopper, P. 2012. Evaluating scour at bridges, HEC-18, 5th Edition. FHWA-HIF Report 12-003, Federal Highway Administration U.S. Department of Transportation, Washington, D.C

Ashton, G.D. (ed.) 1986. River and lake ice engineering. Water Resources Publications, Littleton, Colorado.

Ataie-Ashtiani, B., and Beheshti, A.A. 2006. Experimental investigation of clear-water local scour at pile groups. *Journal of Hydraulic. Engineering*, 132(10), 1100–1104.

Ataie-Ashtiani, B. and Aslani-Kordkandi, A. 2013. Flow field around single and tandem piers. *Flow Turbulence and Combustion*, 90, 471-490.

Aziz, I. 1983. Dimensional analysis as applied to scouring around bridge piers in alluvial rivers. *Jernel Teknologi Billiten*, 3, 59-66.

Babaeyan-Koopaei, K. and Valentine, E. 1999. Bridge pier scour in self-formed laboratory channels. Proceedings from the 28th IAHR Congress, Graz, Austria. pp. 22-27.

Ballio, F. and Radice, A. 2003. A non-touch sensor for local scour measurements. *Journal of Hydraulic Research*, 41(1), 105-108.

Barbhuiya A. and Dey, S. 2003. Vortex flow field in a scour hole around abutment. *International Journal of Sediment Research*, 18(4), 310-325.

Batuca, D. and Dargahi, B. 1986. Some experimental results on local scour around cylindrical piers for open and covered flows. Proceedings from the 3rd International Symposium of River Sedimentation, University of Mississippi. pp. 1095-1104.

Beg, M. and Beg, S. 2013. Scour reduction around bridge piers. *International Journal of Engineering Inventions*, 2(7), 7-15.

Beheshti, A. and Ataie, B. 2008. Analysis of threshold and incipient conditions for sediment movement. *Journal of Coastal Engineering*, 55, 423-430.

Beltaos, S. (ed.) 1995. River ice jams. Water Resources Publications, Littleton, Colorado.

Beltaos, S. 2000. Advances in river ice hydrology. *Hydrological Processes*, 14, 1613-1625.

Bong, C. 2012. Incipient motion of sediment in open channels: a comparison between laboratory data and site observation. Proceedings of 2nd International Conference on Water Resources, Malaysia.

Breusers, H., Nicollet, G. and Shen, H. 1977. Local scour around cylindrical piers. *Journal of Hydraulic Resources*, 15(3), 211-252.

Briaud, J., Brandimarte, L., Wang, J. and D'Odorico, P. 2007. Probability of scour depth exceedance owing to hydrologic uncertainty. *Georisk: Assessment and Management of Risk for Engineered Systems and Geohazards*, 1(2), 77-88.

Brunner, G. 2010. River Analysis System User's Manual HEC-RAS, version 4.1. US Army Corps of Engineers, California.

Buffington, J. and Montgomery, D. 1997. A systematic analysis of eight decades of incipient motion studies, with special reference to gravel-bedded rivers. *Water Resources Research*, 33(8), 1993-2029.

Bunte, K. and Abt, S.R. 2001. Sampling surface and subsurface particle-size distributions in wadable gravel and cobble bed streams for analyses in sediment transport, hydraulics, and streambed monitoring. Technical Report RMRS-GTR-74. Fort Collins, CO: U.S. Department of Agriculture, Forest Service, Rocky Mountain Research Station. 428p.

Carey, K. 1966. Observed configuration and computed roughness of the underside of river ice, St Croix River, Wisconsin. Professional paper 550-B. US Geological Survey: Washington, USA, B192–B198.

Chang, H. 1992. Fluvial Processes in River Engineering. Krieger Publishing Company, Florida, 432p.

Chiew, Y.M. and Melville, B.W. 1989. Local scour at bridge piers with non-uniform sediments. Proceedings of the Institution of Civil Engineers, Part 2, 87, 215-224.

Church, M., Hassan M.A. and Wolcott, J.F. Stabilizing self-organized structures in gravel-bed stream channels: field and experimental observations, *Water Resources Research*, 1998, 34(11), 3169-3179.

Clifford, N. and French, J. 1993. Monitoring and modelling turbulent flows: historical and contemporary perspectives. In Turbulence: Perspectives on flow and sediment transport, (Eds. Clifford N., French, J., and Hardisty, J). Wiley: Chichester, 1-34.

Crance, M. and Frothingham, K. 2008. The impacts of ice cover roughness on stream hydrology. Proceedings from the 65th Eastern Snow Conference, Vermont, USA. 149-165.

Davidson, D. 2002. The role of computational fluid dynamics in process industries. *The Bridge,* 32(4), 9-14.

Deng, L. and Cai, C. 2010. Bridge Scour: prediction, modeling, monitoring and countermeasures – review. *Practice Periodical on Structural Design and Construction*, 15(2), 125-134.

Dey, S. and Raikar, R. 2007. Clear-water scour at piers in sand beds with an armor layer of gravels. *Journal of Hydraulic Engineering*, 133, 703-711.

Diplas, P. and. Fripp, J.B. 1992. Properties of various sediment sampling procedures. *Journal of Hydraulic Engineering*, 118 (7), 955-970.

Diab, R., Zanke, U. and Link, O. 2010. 3D turbulent flow field at square pier in a gravel scour hole. International Conference on Fluvial Hydraulics "River Flow 2010" Braunschweig, 691-697.

Dongguang, G., Pasada, L. and Nordin, C. 1993. Pier scour equations used in the People's Republic of China. Report No. FHWA-SA-93-076. FHWA, Washington, DC.

Escauriaza, C. 2008. Three-dimensional unsteady modeling of clear-water scour in the vicinity of hydraulic structures: Lanrangian and Eulerian Perspectives. PhD Dissertation, University of Minnesota, Minneapolis, Minnesota.

Ettema, R. 1980. Scour at bridge piers. PhD Dissertation, Auckland University, Auckland, New Zealand.

Ettema, R. 1984. Sampling armor-layer sediments. *Journal of Hydraulic Engineering*, 10(7), 992-996.

Ettema, R. Braileanu, F. and Muste, M. 2000. Method for estimating sediment transport in ice covered channels, *Journal of Cold Regions Engineering*, 14(3), 130-144.

Ettema, R. Melville, B. and Barkdoll, B. 1998. Pier width and local-scour depth in Stream stability and scour at highway bridges Compendium of stream stability and scour papers ASCE Water Resources Engineering Conferences, (Eds. Richardson, E and Lagasse, P). Nashville, Tennessee, 1991-1998.

Ettema, R. and Muste, M. 2004. Scale effects in flume experiments on flow around a spur dike in flatbed channel. *Journal of Hydraulic Engineering*, 130(7), 635-646.

Federal Highway Administration. 1993. Evaluating scour at bridges. HEC-18, Report No. FHWA-IP-90-017, Federal Highway Administration U.S. Department of Transportation, Washington, D.C.

Faruque, Md. Abdullah Al. 2009. Smooth and rough wall open channel flow including effects of seepage and ice cover. PhD Dissertation, University of Windsor, Windsor, Ontario.

Fluent Inc. 2006. FLUENT 6.3 users guide. Fluent Inc., Canonsburg, PA. p.2428.

Froehlich, D. 1988. Analysis of onsite measurements of scour at piers. Proceedings from ASCE National Hydrology and Engineering Conference, New York, NY.

Froehlich, D. 1989. Local scour at bridge abutments. Proceedings from the 1989 National Conference on Hydraulic Engineering, New York, 13–18.

Garcia, M. (ed.) 2008. Sediment Engineering – Processes, Measurements, Modeling and Practice. ASCE Manuals and Reports on Engineering Practice No. 110.

Gerard, G. 1989. Ice jam floods. Chapter 10 in Hydrology of Floods in Canada: A guide to planning and design, (Ed. Watt, W.E.) National Research Council, Ottawa.

Gharabaghi, B., Inkratas, C., Beltaos, S. and Krishnappan, B. 2007. Modelling of three-dimensional flow velocities in a deep hole in the East Channel of the Mackenzie Delta, Northwest Territories. *Canadian Journal of Civil Engineering*, 34, 1312-1323.

Graebel, W. 2001. Engineering Fluid Mechanics. CRC Press, 752p.

Graf, W. and Istiarto, W. 2002. Flow pattern in the scour hole around a cylinder. *Journal of Hydraulic Research*, 40(1), 13-20.

Guo, J. 2012. Pier scour in clear water for sediment mixtures. *Journal of Hydraulic Research*, 50(1), 18-27.

Hager, W. 1999. Wastewater Hydraulics: Theory and Practice. Springer: Berlin, New York.

Hains D.B. and Zabilansky L. 2004. Laboratory test of scour under ice: data and preliminary results. Cold Regions Research and Engineering Laboratory, ERDC/CRREL TR-04-09: Hanover, NH, USA.

Hains, D. and Zabilansky, L. 2007. Scour under ice: Potential contributing factor in the Schoharie Creek Bridge Collapse. From Current Practices in Cold Regions Engineering, in Proceedings of the 13th International Conference on Cold Regions Engineering, Maine, USA.

Hains, D. 2004. An experimental study of ice effects on scour at bridge piers. PhD Dissertation, Lehigh University, Bethlehem, PA.

Heller, V. 2011. Scale effects in physical hydraulic engineering models. *Journal of Hydraulic Research*, 49(3), 293-306.

Hodi, B. 2009. Effect of blockage and densimetric Froude number on circular bridge pier local scour. MSc Thesis. University of Windsor, Ontario, Canada.

Hoffmans, G. and Verheij, H. 1997. Scour manual. CRC Press, 205p.

Hoque, M. 2009. Hydraulic analysis of ice-covered river flow. Master's Thesis, Concordia University, Montreal, Canada.

Hunt, B.E. 2005. Practices for Monitoring Scour Critical Bridges. *NCHRP Project 20-5 first draft report*, Transportation Research Board, National Research Council, National Academy Press, Washington, D.C.

Inkratas, C. 2007. Stability analysis of a deep hole in the east channel of the Mackenzie Delta, Northwest Territories. MSc Thesis, University of Guelph, Guelph, Ontario.

Inkratas, C., Gharabaghi, B., Beltaos, S. and Krishnappan, B. 2009. 3D modelling of ice-covered flows in the vicinity of a deep hole in the East Channel of the Mackenzie Delta, N.W.T. *Canadian Journal of Civil Engineering*, 36, 791-800.

Jain, S.C. and Fischer, E.E. 1979. Scour around bridge piers at high Froude numbers. Report. No. FHWA-RD-79-104, Federal Highway Administration, Washington, D.C.

Jain, B. and Modi, P. 1986. Comparative study of various formulae on scour around bridge piers. *Journal of the Institution of Engineers (India)*, 67, Part 3.

Johnson, P.A. 1995. Comparison of pier-scour equations using field data. *Journal of Hydraulic Engineering*, 121(8), 626–629.

Johnson, P.A., and Ayyub, B.M. 1996. Modelling uncertainty in prediction of pier scour. *Journal Hydraulic Engineering,* 122(2), 66–72.

Kaless, G. and Mao, L. 2011. Numerical simulation of armour layer development under conditions of sediment starvation. Proceedings from the National Conference of the Italian Association of Agricultural Engineering, Belgirate. 1-7.

Kanellopoulos, P. 1998. Incipient motion under shallow flow conditions. MSc Thesis. Virginia Polytechnic Institute and State University, Blacksburg, Virginia.

Khanzada, K. 2012. State of bridge management in Canada. Master's Thesis. North Dakota State University, Fargo, North Dakota.

Khorsandi, Babak., Mydlarski, L. and Gaskin, S. 2012. Noise in turbulence measurements using acoustic Doppler velocimetry. Journal of Hydraulic Engineering, 138(10), 829-838.

Khwairakpam, P., Ray, S., Das, S., Das, R. and Mazumdar, A. 2012. Scour hole characteristics around a vertical pier under Clearwater scour conditions. *ARPN Journal of Engineering and Applied Sciences*, 7(6), 649-654.

Kumar, A. and Kothyari, U. 2012. Three-dimensional flow characteristics within the scour hole and circular uniform and compound piers. *Journal of Hydraulic Engineering*, 138(5), 420-429

Lagasse, P. 1999. National Research Council, Research Results Digest: 1998 Scanning review of European practices for bridge scour and stream stability countermeasures. Transportation Research Board of the National Academics, Washington, D.C.

Lagasse, P., Zevenbergen, L., Schall, J. and Clopper, P. 2001. Bridge scour and stream instability countermeasures: Experience, selection, and design guidelines. FHWA NHI 01-003: Federal Highway Administration, Hydraulic Engineering Circular No. 23, 2nd ed., U.S. Department of Transportation, Washington, D.C.

Lagasse, P. Clopper, P. Zevenbergen, L. and Girard, L. 2007. Countermeasures to protect bridge piers from scour. National Cooperative Highway Research Program (NCHRP) Report No. 593, Transportation Research Board, Washington, D.C.

Landers, M. and Mueller, D. 1996. Evaluation of selected pier-scour equations using field data. *Transportation Research Record*, 1523, 186-195.

Lau, L. and Krishnappan, B. 1985. Sediment transport under ice cover. *Journal of Hydraulic Engineering*, 3(6), 934-951.

Lauchlan, C. 1999. Countermeasures for pier scour. PhD Thesis. University of Auckland, Auckland, New Zealand.

Lauchlan, C. and Melville, B. 2001. Riprap protection at bridge piers. *Journal of Hydraulic Engineering*, 127(5), 412-418.

Lee, S. and Sturm, T. 2009. Effect of sediment size scaling on physical modeling of bridge pier scour. *Journal of Hydraulic Engineering*, 135(10), 793-802.

Li, S.S. 2012. Estimates of the Manning's coefficient for ice covered rivers, Proceedings of the Institution of Civil Engineers, *Water Management*, 165(9), 495–505.

Lin, Y., Lai, J., Chang, K., Chang, W., Lee, F. and Tan, Y. 2010. Using mems sensors in the bridge scour monitoring system. *Journal of the Chinese Institute of Engineers*, 33(1), 25-35.

Link, O., Pfleger, F. and Zanke, U. 2008. Characteristics of developing scour holes at sand embedded cylinder. *International Journal of Sediment Research*, 23, 258-266.

Lu, J., Hong, J., Su, C., Wang, C., and Lai, J. 2008. Field measurements and simulation of bridge scour depth variation during floods. *Journal Hydraulic Engineering,* 134(6), 810–821.

Mao L., Cooper, J. and Frostick, L. 2011. Grain size and topographical differences between static and mobile armour layers. *Earth surface Processes and Landforms*, 36(10), 1321-1334.

Mays, L.W. 1999. Hydraulic Design Handbook. McGraw-Hill: New York, USA.

Melville, B.W. 1997. Pier and abutment scour: integrated approach. *Journal of Hydraulic Engineering*, 123(2), 125-136.

Melville, B. 2008. The physics of local scour at bridge piers. Proceedings from the 4th International Conference on Scour and Erosion, Tokyo, Japan.

Melville, B. and Chiew, Y. 1999. Time scale for local scour at bridge piers. *Journal of Hydraulic Engineering,* 125(1): 59-65.

Melville, B. and Coleman, S. 2000. Bridge Scour. Water Resources Publications, LLC, Highlands Ranch, Colorado, USA.

Melville, B. and Sutherland, A.J. 1988. Design method for local scour at bridge piers. *Journal Hydraulic Engineering,* 114(10), 1210-1226.

Miranda, K. 2004. Effects of the upstream length of a fixed ice cover on local scour at a bridge pier. MSc. Thesis. Lehigh University, Bethlehem, Pennsylvania.

Mohamed, T., Noor, M., Ghazali A. and Huat, B. 2005. Validation of some bridge pier scour formulae using field and laboratory data. *American Journal of Environmental Sciences*, 1(2), 119-125.

Molinas, A. 2003. Bridge scour in non-uniform sediment mixtures and in cohesive materials: synthesis report. Report No. FHWA-RD-03-083, Federal Highway Administration, McLean, Virginia.

Molinas, A. and Wu, B. 1998. Effect of size gradation on transport of sediment mixtures. *Journal of Hydraulic Engineering*, 24(8), 786-793.

Mostafa, E. 1994. Scour around skewed bridge piers. PhD Dissertation. Alexandria University, Alexandria, Egypt.

Mount, J. 1995. California rivers and streams: the conflict between fluvial process and land use. University of California Press, 359p.

Mueller, D.S. 1996. Local scour at bridge piers in nonuniform sediment under dynamic conditions. Ph.D. Dissertation, Colorado State University, Fort Collins, Colorado.

Muste, M., Braileanu, F., and Ettema, R. 2000. Flow and sediment transport measurements in a simulated ice-covered channel. *Water Resources Research*, 36(9), 2711-2720.

Muzzammil, M., Gangadharaiah, T. and Gupta, A. K. 2004. An experimental investigation of a horseshoe vortex induced by a bridge pier. *Water Management Journal*, Proceedings of the Institution of Civil Engineers, Thomas Telford Journals, London, 157 (2), 109-119. Paper 13904.

Nowell, A. and Jumars, P. 1987. Flumes: theoretical and experimental considerations for simulation of benthic environments. *Oceanography and Marine Biology Annual Review*, 25, 91-112.

Oliveto, G. and Hager, W. 2002. Temporal evolution of clear-water pier and abutment scour. *Journal of Hydraulic Engineering*, 128(9), 811-820.

Olsson, P. 2000. Influence of ice cover on local scour at circular bridge piers: an experimental study. PhD Dissertation, Lulea University of Technology, Lulea, Sweden.

Olufayo, O., Otieno, F. and Ochieng, G. 2010. Sand water storage systems using coefficient of uniformity as surrogate for optimal design: a laboratory study. *International Journal of the Physical Sciences*, 5(6), 1227-1230.

Ou, Z. 2007. Numerical simulation of flow around vertical cylinders. PhD Dissertation, University of Western Australia, Crawley, Australia.

Ozalp, M. 2013. Experimental investigation of local scour around bridge pier groups. MSc Thesis. Middle East Technical University, Cankaya Ankara, Turkey.

Proffitt, G.T. 1980. Selective Transport and Armoring of Non-uniform Alluvial Sediments, PhD Dissertation, University of Canterbury, Christchurch, New Zealand.

Raikar, R. and Dey, S. 2005. Clear-water scour at bridge piers in fine and medium gravel beds. *Canadian Journal of Civil Engineering*, 32, 775-781.

Raikar, R. and Dey, S. 2009. Maximum scour depth at piers in armour-beds. *Journal of Civil Engineering*, 13(2), 137-142.

Raudkivi, A.J. and Ettema, R. 1983. Clear-water scour at cylindrical piers. *Journal of Hydraulic Engineering*, 109(3), 339-350.

Raudkivi, A. J. and Ettema, R. 1985. Scour at cylindrical bridge piers in armored beds. *Journal of Hydraulic Engineering*, 111, 713-731

Richardson, E. and Davies, S. 1995. Evaluating scour at bridges. Rep. No. FHWAIP-90-017 (HEC-18), FHWA, U.S. Department of Transportation, Washington, D.C.

Richardson, E. and Davis, S. 2001. Evaluating scour at bridges, 4th edition. Publication No. FHWA NHI 01-001. p380.

Richardson, E., Simons, D. and Julien, P. 1990. Highways in the river environment publication. HI-90-016, Federal Highway Administration, McLean, Virginia.

Robert, A. and Tran, T. 2012. Mean and turbulent flow fields in a simulated ice-covered channel with a gravel bed: some laboratory observations. *Earth surface processes and landforms*, 37, 951-956.

Rynes, S., Bartunek, J. and Daft, R. 2001. Across the great divide: knowledge creation and transfer between practitioners and academics. *Academy of Management Journal*, 44(2), 340-355.

Schall, J. and Price, G. 2004. Portable Scour Monitoring Equipment. NCHRP Report 515, Transportation Research Board, National Research Council, National Academy Press, Washington, DC.

Shen, H. and Schneider, V. 1969. Local scour around bridge piers. *Journal of the Hydraulics Division,* Proceedings of the American Society of Civil Engineers, 95(6), 1919-1941.

Shen H., Schneider V.R., and Roper A.T. 1966. Analytical Approach to local scour. Proceedings of the 12th Congress, IAHR, Vol. 3, Colorado State University.

Shen, H. and Wang, D. 1995. Under cover transport and accumulation of frazil granules. *Journal of Hydraulic Engineering*, Vol. 121, No. 2, 184-195.

Sheppard, D., Odeh, M. and Glasser, T. 2004. Large scale clear-water local pier scour experiments. *Journal of Hydraulic Engineering*, 130(10), 957-963.

Simons, D.B. and Sentürk, F. 1992. Sediment Transport Technology. Water and Sediment Dynamics. Water Resources Publications, Littleton, Colorado, 897p.

Smith, B. and Ettema, R. 1997. Flow resistance in ice covered alluvial channels. *Journal of Hydraulic Engineering*, 123(7), 592-599.

SonTek. 1997. Pulse coherent Doppler processing and ADV correlation coefficient. SonTek Technical Notes. www.sontek.com

Sontek. 2014. Website: <www.sontek.com> Accessed March 23, 2014.

Speziale, C. 1990. Analytical methods for the development of Reynolds stress closure in turbulence. NASA Contractor Report 182017, ICASE Report No. 90-26, Virginia.

Sui, J., Wang, D. and Karney, B. 2000. Sediment concentration and deformation of riverbed in a frazil jammed river reach. *Canadian Journal of Civil Engineering*, 27(6), 1120-1129.

Sui, J., Wang, J., He, Y. and Krol, F. 2010. Velocity profiles and incipient motion of frazil particles under ice cover. *International Journal of Sediment Research*, 25(1), 39-51.

TAC. 2004. Transportation Association of Canada, Guide to bridge hydraulics, 2nd Edition. Transportation Association of Canada, Thomas Telford Publishing, 181p.

Unger, J. and Hager, W. 2007. Down-flow and horseshoe vortex characteristics of sediment embedded bridge piers. *Experimental Fluids*, 42, 1-19.

USACE. 1982. Ice engineering. Engineer Manual 1110-2-1612, U.S. Army Corps of Engineers, Washington D.C.

Vollmer, A. and Kleinhans, M. 2007. Predicting incipient motion, including the effect of turbulent pressure fluctuations in the bed. *Water Resources Research*, 43, 1-16.

Wang, J., Sui, J., and Karney, B. 2008. Incipient motion of non-cohesive sediment under ice cover – an experimental study. *Journal of Hydrodynamics*, 20(1), 117-124.

Watt, W.E. (Ed). 1989. Hydrology of Floods in Canada, A Guide to Planning and Design. National Research Council of Canada, Ottawa.

Wu, P., Hirshfield, F., Sui, J., Wang, J., and Chen, P. 2014. Impacts of ice cover on local scour around semi-circular bridge abutment. *Journal of Hydrodynamics*, 26(1), 10-18.

Wu, W., Wang, S., and Jia, Y. 2000. Non-uniform sediment transport in alluvial rivers. *Journal of Hydraulic Research*, 38(6), 427-434.

Xu, H., Lu, J. and Liu, X. 2008. Non-uniform sediment incipient velocity. *International Journal of Sediment Research*, 23, 69-75.

Yang C. 2003. Sediment transport, theory and practice. Krieger publishing company, Florida, 396p.

Yang, Q. 2005. Numerical investigations of scale effects on local scour around a bridge pier. MSc. Thesis, Florida State University, Tallahassee, Florida.

Yanmaz, A. 2002. Dynamic reliability in bridge pier scouring. *Turkish Journal of Engineering and Environmental Sciences*, 26, 367-375.

Yu, X. 2009. Experimental Study of an innovative bridge scour sensor. PhD Dissertation. Case Western Reserve University, Cleveland, Ohio.

Zabilansky, L. 1996. Ice force and scour instrumentation for the White River, Vermont. US Army CRREL Special Report, 59p, Hanover, USA.

Zabilansky, L., Hains, M. and Remus, J. 2006. Increased bed erosion due to ice. Proceedings from the 13th International Conference on Cold Regions Engineering, Maine, USA.

Zevenbergen, L., Ameson, L., Hunt, J. and Miller, A. 2012. Hydraulic design of safe bridges. FHWA-HIF Report 12-018-HDS 7.

Zhang, H. 2005. Study of flow and bed evolution in channels with spur dykes. PhD Dissertation, Kyoto University, Japan.

Zhang, L. 2009. 3D numerical modeling of hydrodynamic flow, sediment deposition and transport in stormwater ponds and alluvial channels. PhD Dissertation, Old Dominion University, Norfolk, Virginia.

Zhao, M., Cheng, L. and Zaong, Z. 2010. Experimental and numerical investigation of local scour around a submerged vertical circular cylinder in steady currents. *Coastal Engineering*, 57, 709-721.

Zhuravlyov, M. 1978. New method of estimation of local scour due to bridge piers and its substantiation. Transactions, Ministry of Transport Construction, State All Union Scientific Research Institute on Roads, Moscow, Russia, 4-51.

APPENDIX A - FLUME DATA

The data in this appendix represents the measured experimental flume conditions along with the values of calculated hydraulic parameters for all 54 flume experiments. Data are sorted by cover type rather than run number as that is how is was analyzed and presented in this thesis.

Table 23. Measured experimental data for 54 flume runs.

Date run finished	Run #	Cover	Position in flume	# valves	# Tailgate	D_{50}	$D_{90}^{\wedge 1/6}$	Pier width
						mm	m	cm
Sep-23	1	open channel	upstream	1.25	1	0.58	0.37	11
Sep-26	2	open channel	upstream	2.25	2	0.58	0.37	11
Sep-22	1	open channel	downstream	1.25	1	0.58	0.37	11
Sep-27	4	open channel	upstream	1.25	1	0.58	0.37	22
Sep-28	5	open channel	downstream	2.25	2	0.58	0.37	22
Sep-29	6	open channel	downstream	1.25	1	0.58	0.37	22
Oct-03	10	smooth ice	upstream	1.25	1	0.58	0.37	11
Oct-04	11	smooth ice	upstream	2.25	2	0.58	0.37	11
Oct-05	12	smooth ice	downstream	1.25	1	0.58	0.37	11
Oct-02	9	smooth ice	upstream	1.25	1	0.58	0.37	22
Oct-01	8	smooth ice	downstream	2.25	2	0.58	0.37	22
Sep-30	7	smooth ice	downstream	1.25	1	0.58	0.37	22
Oct-07	14	rough ice	upstream	1.25	1	0.58	0.37	11
Oct-08	15	rough ice	upstream	2.25	2	0.58	0.37	11
Oct-06	13	rough ice	downstream	1.25	1	0.58	0.37	11
Oct-09	16	rough ice	upstream	1.25	1	0.58	0.37	22
Oct-10	17	rough ice	downstream	2.25	2	0.58	0.37	22
Oct-11	18	rough ice	downstream	1.25	1	0.58	0.37	22
Oct-19	20	open channel	upstream	1.25	1	0.47	0.31	11
Oct-20	21	open channel	upstream	2.25	2	0.47	0.31	11
Oct-18	19	open channel	downstream	1.25	1	0.47	0.31	11
Oct-21	22	open channel	upstream	1.25	1	0.47	0.31	22
Oct-23	24	open channel	downstream	2.25	2	0.47	0.31	22
Oct-22	23	open channel	downstream	1.25	1	0.47	0.31	22
Oct-27	28	smooth ice	upstream	1.25	1	0.47	0.31	11
Oct-28	29	smooth ice	upstream	2.25	2	0.47	0.31	11
Oct-29	30	smooth ice	downstream	1.25	1	0.47	0.31	11
Oct-26	27	smooth ice	upstream	1.25	1	0.47	0.31	22
Oct-25	26	smooth ice	downstream	2.25	2	0.47	0.31	22

Oct-24	25	smooth ice	downstream	1.25	1	0.47	0.31	22
Oct-31	32	rough ice	upstream	1.25	1	0.47	0.31	11
Nov-01	33	rough ice	upstream	2.25	2	0.47	0.31	11
Oct-30	31	rough ice	downstream	1.25	1	0.47	0.31	11
Nov-02	34	rough ice	upstream	1.25	1	0.47	0.31	22
Nov-04	36	rough ice	downstream	2.25	2	0.47	0.31	22
Nov-03	35	rough ice	downstream	1.25	1	0.47	0.31	22
Nov-08	38	open channel	upstream	1.25	1	0.50	0.36	11
Nov-09	39	open channel	upstream	2.25	2	0.50	0.36	11
Nov-07	37	open channel	downstream	1.25	1	0.50	0.36	11
Nov-10	40	open channel	upstream	1.25	1	0.50	0.36	22
Nov-12	42	open channel	downstream	2.25	2	0.50	0.36	22
Nov-11	41	open channel	downstream	1.25	1	0.50	0.36	22
Nov-15	46	smooth ice	upstream	1.25	1	0.50	0.36	11
Nov-16	47	smooth ice	upstream	2.25	2	0.50	0.36	11
Nov-18	48	smooth ice	downstream	1.25	1	0.50	0.36	11
Nov-17	45	smooth ice	upstream	1.25	1	0.50	0.36	22
Nov-14	44	smooth ice	downstream	2.25	2	0.50	0.36	22
Nov-13	43	smooth ice	downstream	1.25	1	0.50	0.36	22
Nov-20	51	rough ice	upstream	1.25	1	0.50	0.36	11
Nov-21	50	rough ice	upstream	2.25	2	0.50	0.36	11
Nov-19	49	rough ice	downstream	1.25	1	0.50	0.36	11
Nov-22	52	rough ice	upstream	1.25	1	0.50	0.36	22
Nov-23	53	rough ice	downstream	2.25	2	0.50	0.36	22
Nov-24	54	rough ice	downstream	1.25	1	0.50	0.36	22

Table 24. Measured experimental data for 54 flume runs. Note: for ADV Q data 'nan' indicates there was an error in the data measurement.

Date run finished	Run #	Cover	Temp	Approach velocity	Water level	ADV Q	Q Discharge (calculated)
			Celsius	cm/s	cm	m³/s	m³/s
Sep-23	1	open channel	11.145	23.2	9.5	0.05	0.04
Sep-26	2	open channel	10.33	23.7	21	0.10	0.10
Sep-22	1	open channel	11.313	24	13	0.06	0.06
Sep-27	4	open channel	10.792	23.2	9.7	0.04	0.05
Sep-28	5	open channel	10.343	22.5	24.4	0.11	0.11
Sep-29	6	open channel	10.647	26.9	13.3	0.06	0.07
Oct-03	10	smooth ice	10.388	23.3	9	0.04	0.04
Oct-04	11	smooth ice	10.267	19.55	21.6	nan	0.08
Oct-05	12	smooth ice	10.435	22.6	13.1	0.06	0.06
Oct-02	9	smooth ice	10.441	23.3	9	0.01	0.04
Oct-01	8	smooth ice	10.361	25.5	25.6	0.13	0.13
Sep-30	7	smooth ice	10.553	21.8	13	0.06	0.06
Oct-07	14	rough ice	10.443	25	9.8	nan	0.05
Oct-08	15	rough ice	10.358	26	20.5	0.09	0.11
Oct-06	13	rough ice	10.507	18.3	13.5	0.05	0.05
Oct-09	16	rough ice	10.412	25	10	nan	0.05
Oct-10	17	rough ice	10.437	21.6	25.5	0.10	0.11
Oct-11	18	rough ice	10.418	18.2	13.4	0.05	0.05
Oct-19	20	open channel	10.22	23.5	9.8	nan	0.05
Oct-20	21	open channel	10.351	27.11	21.4	nan	0.12
Oct-18	19	open channel	10.258	19.4	13	0.05	0.05
Oct-21	22	open channel	10.143	23.5	9.8	nan	0.05
Oct-23	24	open channel	10.341	22.8	24.3	0.11	0.11
Oct-22	23	open channel	10.152	22.6	13.4	0.05	0.06
Oct-27	28	smooth ice	10.121	23.3	9.7	0.03	0.05
Oct-28	29	smooth ice	10.319	23.3	21.5	nan	0.10
Oct-29	30	smooth ice	10.129	20.07	12.9	0.05	0.05
Oct-26	27	smooth ice	10.1	23.3	9.6	0.05	0.04
Oct-25	26	smooth ice	10.391	24.6	25.8	0.13	0.13
Oct-24	25	smooth ice	10.124	22.9	13	0.06	0.06
Oct-31	32	rough ice	9.979	25.08	12.8	nan	0.06
Nov-01	33	rough ice	10.306	28.02	22	nan	0.12
Oct-30	31	rough ice	-	21.6	13	nan	0.06
Nov-02	34	rough ice	10.004	25.08	11.2	nan	0.06

Nov-04	36	rough ice	10.386	21	23.1	0.09	0.10
Nov-03	35	rough ice	10.023	21.6	13.4	0.05	0.06
Nov-08	38	open channel	9.839	23.2	10	nan	0.05
Nov-09	39	open channel	10.161	24.14	21.1	nan	0.10
Nov-07	37	open channel	9.932	20.5	13.2	0.05	0.05
Nov-10	40	open channel	9.723	23.2	9.9	nan	0.05
Nov-12	42	open channel	10.198	22.7	24.6	0.11	0.11
Nov-11	41	open channel	9.699	20.2	13.1	0.05	0.05
Nov-15	46	smooth ice	9.668	22	9.8	0.02	0.04
Nov-16	47	smooth ice	10.093	23.3	21.6	nan	0.10
Nov-18	48	smooth ice	9.669	22.6	13.1	0.05	0.06
Nov-17	45	smooth ice	9.64	22	9.8	nan	0.04
Nov-14	44	smooth ice	10.19	22.5	25.9	0.12	0.12
Nov-13	43	smooth ice	9.773	21.2	13.2	0.06	0.06
Nov-20	51	rough ice	8.89	22.91	13	nan	0.06
Nov-21	50	rough ice	9.76	26	22	nan	0.11
Nov-19	49	rough ice	9.619	22.2	13	0.06	0.06
Nov-22	52	rough ice	8.62	22.91	13	nan	0.06
Nov-23	53	rough ice	9.973	21.5	25.9	0.12	0.11
Nov-24	54	rough ice	9.525	22.5	13	0.06	0.06

Table 25. Measured maximum scour depth and various calculated parameters associated with 54 experimental flume runs.

Date run finished	Run #	Cover	d_{max}/ max scour depth	d_{max}/h	R, hydraulic radius	F_r, Froude number	F_o, densimetric froude number	U_*, shear velocity
			cm		m			m/s
Sep-23	1	open channel	5	0.53	0.09	0.24	3.21	0.13
Sep-26	2	open channel	2.5	0.12	0.17	0.17	3.28	0.18
Sep-22	1	open channel	2	0.15	0.12	0.21	3.32	0.15
Sep-27	4	open channel	5.5	0.57	0.09	0.24	3.21	0.13
Sep-28	5	open channel	1	0.04	0.20	0.15	3.11	0.20
Sep-29	6	open channel	3	0.23	0.12	0.24	3.72	0.15
Oct-03	10	smooth ice	4.5	0.50	0.04	0.25	3.22	0.09
Oct-04	11	smooth ice	4.5	0.21	0.10	0.13	2.70	0.14
Oct-05	12	smooth ice	1.5	0.11	0.06	0.20	3.12	0.11
Oct-02	9	smooth ice	5.5	0.61	0.04	0.25	3.22	0.09
Oct-01	8	smooth ice	2	0.08	0.11	0.16	3.53	0.15
Sep-30	7	smooth ice	1.5	0.12	0.06	0.19	3.01	0.11
Oct-07	14	rough ice	5	0.51	0.05	0.25	3.46	0.10
Oct-08	15	rough ice	4	0.20	0.09	0.18	3.59	0.14
Oct-06	13	rough ice	1	0.07	0.06	0.16	2.53	0.11
Oct-09	16	rough ice	6	0.60	0.05	0.25	3.46	0.10
Oct-10	17	rough ice	2	0.08	0.11	0.14	2.99	0.15
Oct-11	18	rough ice	1.5	0.11	0.06	0.16	2.52	0.11
Oct-19	20	open channel	8	0.82	0.09	0.24	3.61	0.13
Oct-20	21	open channel	6	0.28	0.18	0.19	4.16	0.19
Oct-18	19	open channel	4	0.31	0.12	0.17	2.98	0.15
Oct-21	22	open channel	11	1.12	0.09	0.24	3.61	0.13
Oct-23	24	open channel	4	0.16	0.20	0.15	3.50	0.20
Oct-22	23	open channel	5	0.37	0.12	0.20	3.47	0.15
Oct-27	28	smooth ice	8.5	0.88	0.05	0.24	3.58	0.10
Oct-28	29	smooth ice	9	0.42	0.10	0.16	3.58	0.14
Oct-29	30	smooth ice	5	0.39	0.06	0.18	3.08	0.11
Oct-26	27	smooth ice	12	1.25	0.05	0.24	3.58	0.09
Oct-25	26	smooth ice	4.5	0.17	0.11	0.15	3.78	0.15
Oct-24	25	smooth ice	5	0.38	0.06	0.20	3.52	0.11
Oct-31	32	rough ice	6	0.47	0.06	0.22	3.85	0.11
Nov-01	33	rough ice	7.5	0.34	0.10	0.19	4.30	0.14
Oct-30	31	rough ice	7	0.54	0.06	0.19	3.32	0.11

Nov-02	34	rough ice	9	0.80	0.05	0.24	3.85	0.10
Nov-04	36	rough ice	8	0.35	0.10	0.14	3.23	0.14
Nov-03	35	rough ice	9	0.67	0.06	0.19	3.32	0.11
Nov-08	38	open channel	4.5	0.45	0.09	0.23	3.45	0.13
Nov-09	39	open channel	4.5	0.21	0.17	0.17	3.59	0.18
Nov-07	37	open channel	2	0.15	0.12	0.18	3.05	0.15
Nov-10	40	open channel	6	0.61	0.09	0.24	3.45	0.13
Nov-12	42	open channel	3	0.12	0.20	0.15	3.38	0.20
Nov-11	41	open channel	2	0.15	0.12	0.18	3.01	0.15
Nov-15	46	smooth ice	6	0.61	0.05	0.22	3.28	0.10
Nov-16	47	smooth ice	6	0.28	0.10	0.16	3.47	0.14
Nov-18	48	smooth ice	2.25	0.17	0.06	0.20	3.37	0.11
Nov-17	45	smooth ice	6	0.61	0.05	0.22	3.28	0.10
Nov-14	44	smooth ice	2	0.08	0.11	0.14	3.35	0.15
Nov-13	43	smooth ice	3	0.23	0.06	0.19	3.16	0.11
Nov-20	51	rough ice	6	0.46	0.06	0.20	3.41	0.11
Nov-21	50	rough ice	5	0.23	0.10	0.18	3.87	0.14
Nov-19	49	rough ice	3	0.23	0.06	0.20	3.31	0.11
Nov-22	52	rough ice	7	0.54	0.06	0.20	3.41	0.11
Nov-23	53	rough ice	3	0.12	0.11	0.13	3.20	0.15
Nov-24	54	rough ice	5	0.38	0.06	0.20	3.35	0.11

Table 26. Calculated hydraulic parameters for 54 flume experiments.

Date run finished	Run #	Cover	U*c Critical shear velocity	Re* Shear Reynolds number	T* Dimensionless shear stress,	Manning's n
			m/s			
Sep-23	1	open channel	0.012	5.49	0.029	0.17
Sep-26	2	open channel	0.012	5.13	0.026	0.17
Sep-22	1	open channel	0.012	5.47	0.029	0.17
Sep-27	4	open channel	0.012	5.48	0.029	0.17
Sep-28	5	open channel	0.011	4.80	0.022	0.17
Sep-29	6	open channel	0.014	6.12	0.036	0.17
Oct-03	10	smooth ice	0.014	6.08	0.036	0.17
Oct-04	11	smooth ice	0.010	4.56	0.020	0.17
Oct-05	12	smooth ice	0.013	5.61	0.030	0.17
Oct-02	9	smooth ice	0.014	6.08	0.036	0.17
Oct-01	8	smooth ice	0.013	5.83	0.033	0.17
Sep-30	7	smooth ice	0.012	5.41	0.028	0.17
Oct-07	14	rough ice	0.015	6.45	0.040	0.17
Oct-08	15	rough ice	0.014	6.10	0.036	0.17
Oct-06	13	rough ice	0.010	4.52	0.020	0.17
Oct-09	16	rough ice	0.014	6.43	0.040	0.17
Oct-10	17	rough ice	0.011	4.94	0.024	0.17
Oct-11	18	rough ice	0.010	4.50	0.020	0.17
Oct-19	20	open channel	0.012	4.49	0.037	0.16
Oct-20	21	open channel	0.013	4.75	0.041	0.16
Oct-18	19	open channel	0.010	3.59	0.023	0.16
Oct-21	22	open channel	0.012	4.49	0.037	0.16
Oct-23	24	open channel	0.011	3.95	0.028	0.16
Oct-22	23	open channel	0.012	4.16	0.032	0.16
Oct-27	28	smooth ice	0.014	4.88	0.043	0.16
Oct-28	29	smooth ice	0.012	4.40	0.035	0.16
Oct-29	30	smooth ice	0.011	4.04	0.030	0.16
Oct-26	27	smooth ice	0.014	4.88	0.043	0.16
Oct-25	26	smooth ice	0.013	4.55	0.038	0.16
Oct-24	25	smooth ice	0.013	4.61	0.039	0.16
Oct-31	32	rough ice	0.014	5.06	0.047	0.16
Nov-01	33	rough ice	0.015	5.28	0.051	0.16
Oct-30	31	rough ice	0.012	4.35	0.034	0.16

Nov-02	34	rough ice	0.014	5.15	0.048	0.16
Nov-04	36	rough ice	0.011	3.93	0.028	0.16
Nov-03	35	rough ice	0.012	4.33	0.034	0.16
Nov-08	38	open channel	0.012	4.70	0.033	0.24
Nov-09	39	open channel	0.012	4.51	0.031	0.24
Nov-07	37	open channel	0.011	4.02	0.024	0.24
Nov-10	40	open channel	0.012	4.71	0.034	0.24
Nov-12	42	open channel	0.011	4.17	0.026	0.24
Nov-11	41	open channel	0.010	3.97	0.024	0.24
Nov-15	46	smooth ice	0.013	4.89	0.036	0.24
Nov-16	47	smooth ice	0.012	4.68	0.033	0.24
Nov-18	48	smooth ice	0.013	4.83	0.035	0.24
Nov-17	45	smooth ice	0.013	4.89	0.036	0.24
Nov-14	44	smooth ice	0.012	4.43	0.030	0.24
Nov-13	43	smooth ice	0.012	4.53	0.031	0.24
Nov-20	51	rough ice	0.013	4.90	0.036	0.24
Nov-21	50	rough ice	0.014	5.21	0.041	0.24
Nov-19	49	rough ice	0.012	4.75	0.034	0.24
Nov-22	52	rough ice	0.013	4.90	0.036	0.24
Nov-23	53	rough ice	0.011	4.23	0.027	0.24
Nov-24	54	rough ice	0.013	4.82	0.035	0.24

APPENDIX B – SCOUR HOLE DATA

Table 27. Scour depth values associated with Figure 29, and calculated percentages for open channel flow.

Open run #	$D_{50} = 0.47$ mm	$D_{50} = 0.50$ mm	$D_{50} = 0.58$ mm
	scour depth (cm)		
1	8	4.5	5
2	6	4.5	2.5
3	4	2	2
4	11	6	5.5
5	4	3	1
6	5	2	3
average scour depth	6.33	3.66	3.16
% higher than D_{50}=0.58 mm	50.00	13.64	

Table 28. Scour depth values associated with Figure 30, and calculated percentages for smooth ice cover conditions.

Smooth run #	$D_{50} = 0.47$ mm	$D_{50} = 0.50$ mm	$D_{50} = 0.58$ mm
	scour depth (cm)		
1	8.5	6	4.5
2	9	6	4.5
3	5	2.25	1.5
4	12	6	5.5
5	4.5	2	2
6	5	3	1.5
average scour depth	7.33	4.20	3.25
% higher than D_{50}=0.58 mm	55.68	22.77	

Table 29. Scour depth values associated with Figure 31, and calculated percentages for rough ice cover conditions.

Rough run #	$D_{50} = 0.47$ mm	$D_{50} = 0.50$ mm	$D_{50} = 0.58$ mm
	scour depth (cm)		
1	6	6	5
2	7.5	5	4
3	7	3	1
4	9	7	6
5	8	3	2
6	9	5	1.5
average scour depth	7.75	4.83	3.25
% higher than D_{50}=0.58 mm	58.06	32.75	

APPENDIX C – ARMOUR LAYER DATA

The data in this appendix represents the measured armour layer size for all pier scour holes for all 54 flume experiments.

Table 30. Median size of armour layer in scour hole along with D_{50} of channel bed.

Date run finished	Run #	Cover	D_{50} channel bed	D_{50} armour layer	Geometric standard deviation
			mm	mm	dimensionless
Sep-23	1	open channel	0.58	0.6	3.06
Sep-26	2	open channel	0.58	0.8	2.87
Sep-22	1	open channel	0.58	1.05	2.98
Sep-27	4	open channel	0.58	0.62	3.12
Sep-28	5	open channel	0.58	0.65	2.81
Sep-29	6	open channel	0.58	0.78	3.04
Oct-03	10	smooth ice	0.58	1.25	3.00
Oct-04	11	smooth ice	0.58	0.87	3.06
Oct-05	12	smooth ice	0.58	0.85	2.99
Oct-02	9	smooth ice	0.58	1.81	2.98
Oct-01	8	smooth ice	0.58	0.83	2.98
Sep-30	7	smooth ice	0.58	0.94	3.11
Oct-07	14	rough ice	0.58	1.25	3.22
Oct-08	15	rough ice	0.58	1.8	3.14
Oct-06	13	rough ice	0.58	1.42	2.79
Oct-09	16	rough ice	0.58	1.6	2.67
Oct-10	17	rough ice	0.58	0.85	2.95
Oct-11	18	rough ice	0.58	1.57	2.54
Oct-19	20	open channel	0.47	0.48	2.93
Oct-20	21	open channel	0.47	0.56	2.91
Oct-18	19	open channel	0.47	0.5	1.74
Oct-21	22	open channel	0.47	0.59	3.78
Oct-23	24	open channel	0.47	0.43	2.16
Oct-22	23	open channel	0.47	0.45	2.17
Oct-27	28	smooth ice	0.47	0.4	1.84
Oct-28	29	smooth ice	0.47	0.5	2.46
Oct-29	30	smooth ice	0.47	0.49	1.97
Oct-26	27	smooth ice	0.47	0.55	3.23
Oct-25	26	smooth ice	0.47	0.3	2.91
Oct-24	25	smooth ice	0.47	0.53	2.48

Oct-31	32	rough ice	0.47	0.55	2.83
Nov-01	33	rough ice	0.47	0.45	2.52
Oct-30	31	rough ice	0.47	0.45	3.01
Nov-02	34	rough ice	0.47	0.57	3.53
Nov-04	36	rough ice	0.47	0.49	1.99
Nov-03	35	rough ice	0.47	0.48	1.84
Nov-08	38	open channel	0.50	0.6	3.06
Nov-09	39	open channel	0.50	1.13	3.42
Nov-07	37	open channel	0.50	0.8	3.21
Nov-10	40	open channel	0.50	1.43	3.40
Nov-12	42	open channel	0.50	0.6	3.00
Nov-11	41	open channel	0.50	0.68	3.26
Nov-15	46	smooth ice	0.50	1.4	3.45
Nov-16	47	smooth ice	0.50	1.15	3.21
Nov-18	48	smooth ice	0.50	0.59	3.21
Nov-17	45	smooth ice	0.50	0.68	3.42
Nov-14	44	smooth ice	0.50	0.79	3.18
Nov-13	43	smooth ice	0.50	0.65	3.29
Nov-20	51	rough ice	0.50	0.75	3.32
Nov-21	50	rough ice	0.50	1.18	2.49
Nov-19	49	rough ice	0.50	0.73	3.47
Nov-22	52	rough ice	0.50	0.6	3.16
Nov-23	53	rough ice	0.50	0.59	2.85
Nov-24	54	rough ice	0.50	0.73	3.17

APPENDIX D – REGRESSION ANALYSIS

The data in this appendix presents the various parameter combinations that were used when investigating the best regression model. The graphs below were not included in the main body of the thesis for one of the following reasons:

(a) the regression models produced regression coefficients that did not support previous findings in this study. For example, the regression coefficient for sediment D_{50} would be positive, when in fact findings under section 5.1, indicate that sediment D_{50} actually decreases with increasing scour depth or

(b) the regression model produced supported findings of this study however a stronger correlation was found using various other parameters. For example, it was found that the parameters D_{50}/H and D_{50}/B both typically produced correct regression models, however for the most part, D_{50}/B would produce a stronger correlation.

1.0 Open channel conditions:

$$X = \left(\frac{U}{\sqrt{gH}} \right)^{3.85} \left(\frac{D_{50}}{H} \right)^{-0.44}$$
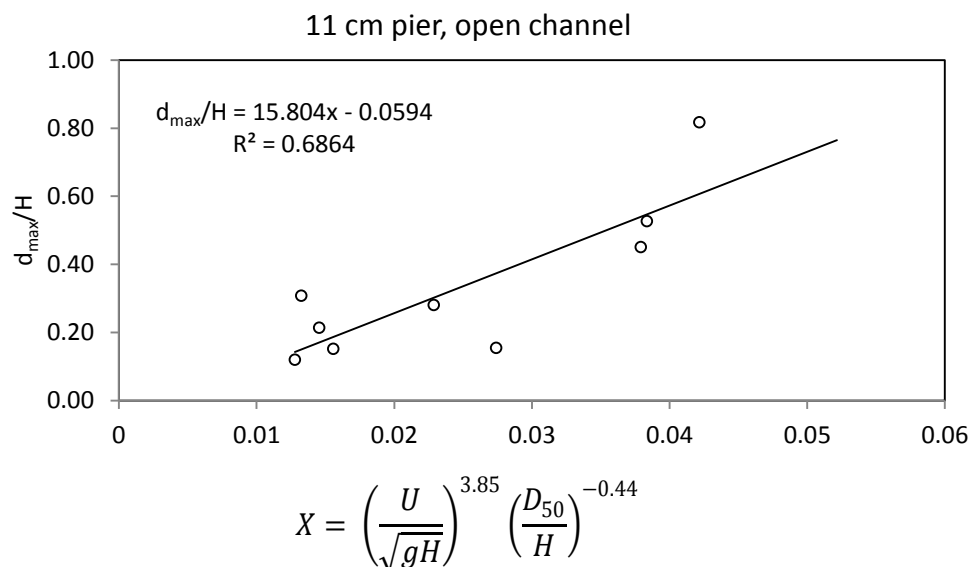
Figure 76. Variation of maximum scour depth for the 11 cm pier under open channel conditions.

22 cm pier, open channel

$d_{max}/H = 4.855x + 0.0162$
$R^2 = 0.5534$

$$X = \left(\frac{U}{\sqrt{gH}}\right)^{5.86} \left(\frac{D_{50}}{H}\right)^{-1.20}$$
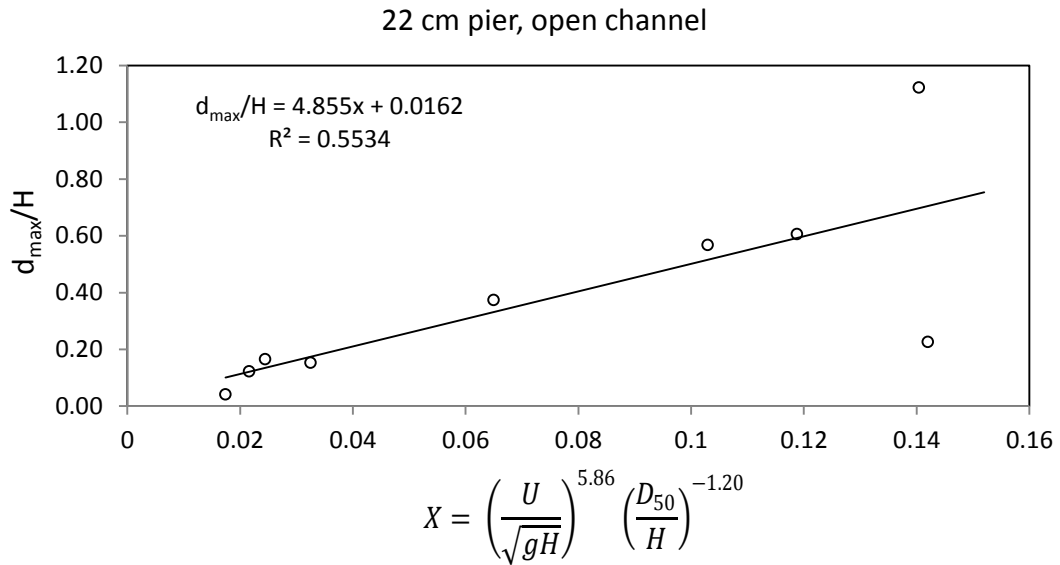
Figure 77. Variation of maximum scour depth for the 22 cm pier under open channel conditions

2.0 Ice covered conditions:

11 cm pier, smooth + rough ice cover

$d_{max}/H = 0.7599 X - 0.0277$
$R^2 = 0.4882$

$$X = \left(\frac{U}{\sqrt{gH}}\right)^{3.57} \left(\frac{D_{50}}{B}\right)^{-0.96} \left(\frac{n_i}{n_b}\right)^{-0.59}$$
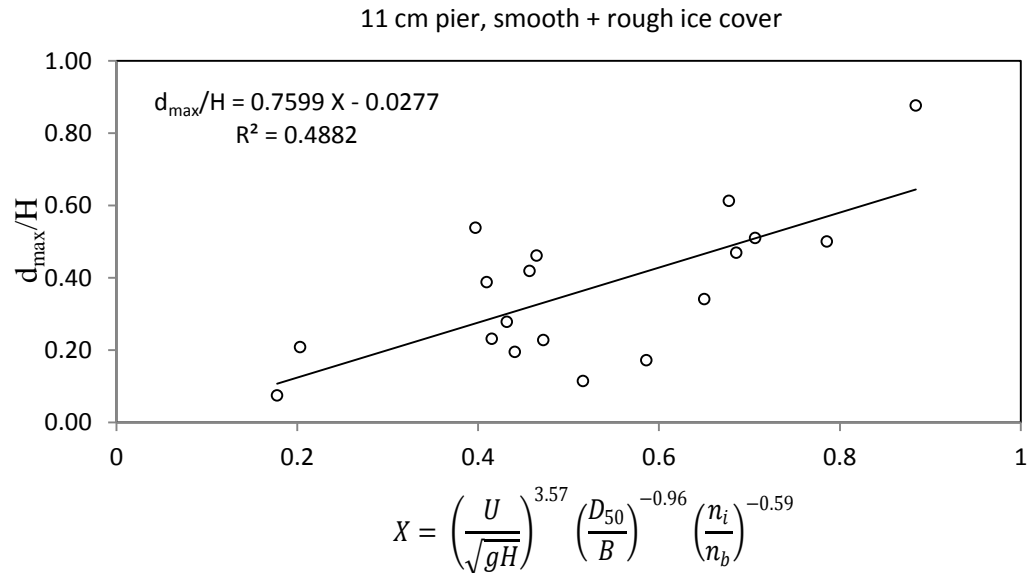
Figure 78. Variation of maximum scour depth for the 11 cm pier under ice covered conditions.

$$X = \left(\frac{U}{\sqrt{gH}}\right)^{5.45} \left(\frac{D_{50}}{H}\right)^{-1.09} \left(\frac{n_i}{n_b}\right)^{1.06}$$
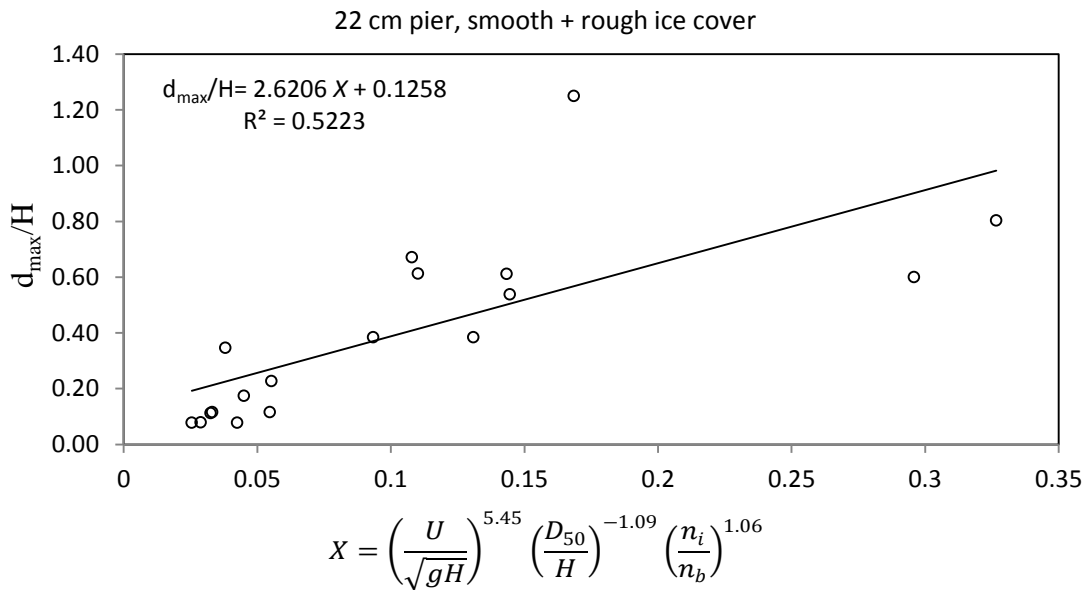
Figure 79. Variation of maximum scour depth for the 22 cm pier under open channel conditions

$$X = \left(\frac{U}{\sqrt{gH}}\right)^{4.04} \left(\frac{D_{50}}{H}\right)^{-0.91} \left(\frac{n_i}{n_b}\right)^{0.17} \left(\frac{b}{H}\right)^{0.23}$$
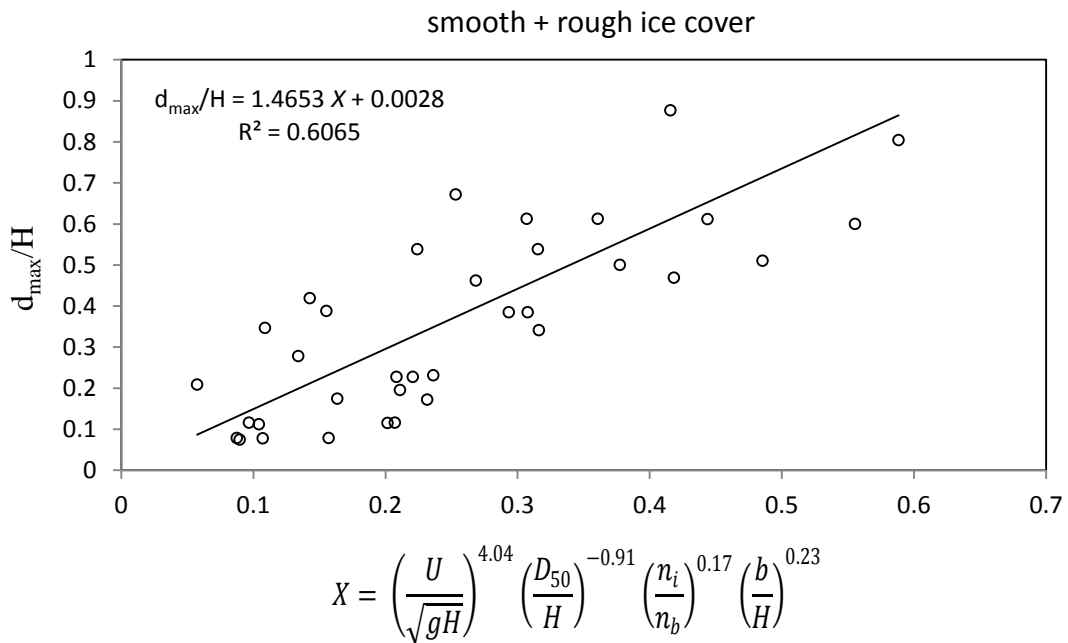
Figure 80. Variation of maximum scour depth under ice covered conditions.

3.0 Armour layer open channel:

open channel

$$d_{max}/H = 4E\text{-}13\ X - 0.01$$
$$R^2 = 0.8493$$

$$X = \left(\frac{U}{\sqrt{gH}}\right)^{4.04} \left(\frac{D_{50}}{B}\right)^{-4.01} \left(\frac{b}{B}\right)^{0.01} \left(\frac{D_{50}Armour}{H}\right)^{-0.15}$$
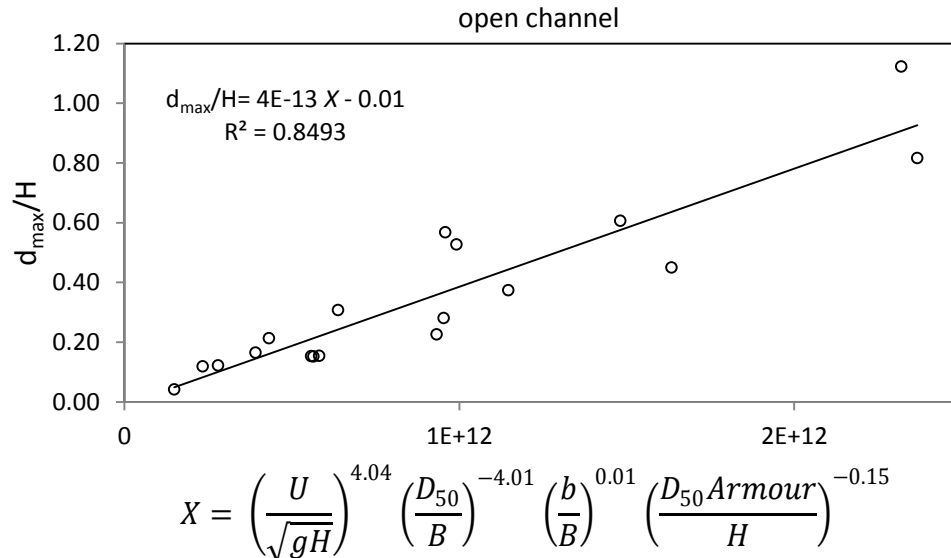
Figure 81. Variation of maximum scour depth under open channel conditions.

3.1 Armour layer ice cover, 11 cm pier:

11 cm pier, smooth + rough ice

$$d_{max}/H = 1.3487\ X - 0.0059$$
$$R^2 = 0.5386$$

$$X = \left(\frac{U}{\sqrt{gH}}\right)^{3.26} \left(\frac{D_{50}}{H}\right)^{-0.42} \left(\frac{n_i}{n_b}\right)^{-0.48} \left(\frac{D_{50}armour}{H}\right)^{-0.35}$$

Figure 82. Variation of maximum scour depth for the 11 cm pier under ice covered conditions. Note the regression coefficient for ice cover roughness not reflect results from this study.

11 cm pier, smooth + rough ice

d_{max}/H = 1E-12 X - 0.0288
R^2 = 0.6999

$$X = \left(\frac{U}{\sqrt{gH}}\right)^{2.01} \left(\frac{D_{50}}{B}\right)^{-3.64} \left(\frac{n_i}{n_b}\right)^{-0.39} \left(\frac{D_{50}\,armour}{H}\right)^{0.03}$$

Figure 83. Variation of maximum scour depth for the 11 cm pier under ice covered conditions. Note the regression coefficient for D_{50} armour does not reflect results from this study.

11 cm pier, smooth + rough ice

d_{max}/H = 1E-12 X - 0.0288
R^2 = 0.6999

$$X = \left(\frac{U}{\sqrt{gH}}\right)^{3.26} \left(\frac{D_{50}}{H}\right)^{-0.77} \left(\frac{n_i}{n_b}\right)^{-0.48} \left(\frac{D_{50}\,armour}{D_{50}\,channel}\right)^{-0.35}$$
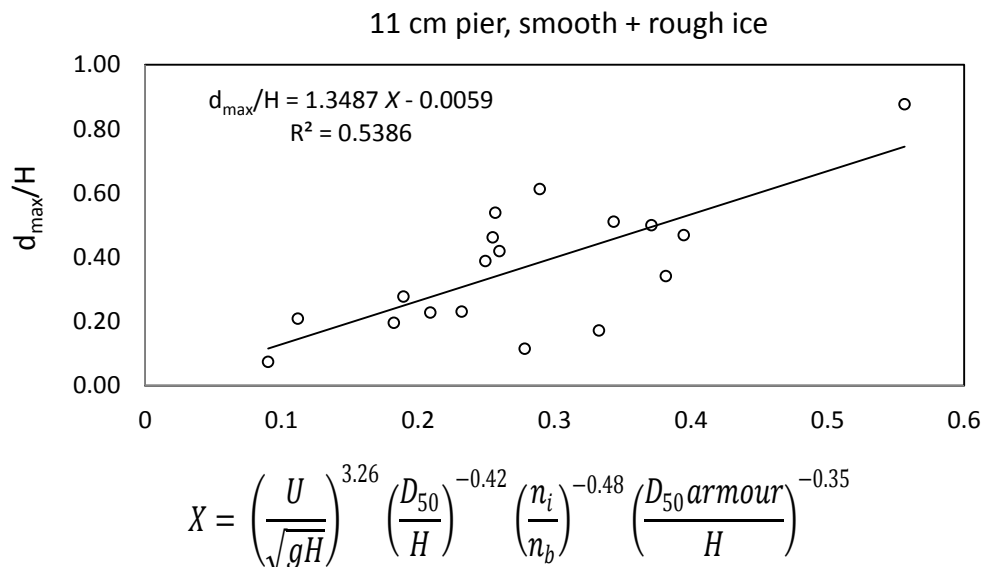
Figure 84. Variation of maximum scour depth for the 11 cm pier under ice covered conditions.

3.2 Armour layer ice cover, 22 cm pier:

22 cm pier, smooth + rough ice

$d_{max}/H = 520.02\ X + 0.0501$

$R^2 = 0.7029$

(y-axis: d_{max}/H; values 0.00, 0.20, 0.40, 0.60, 0.80, 1.00, 1.20, 1.40)

(x-axis: 0, 0.0005, 0.001, 0.0015, 0.002, 0.0025)

$$X = \left(\frac{U}{\sqrt{gH}}\right)^{3.69} \left(\frac{D_{50}}{H}\right)^{1.19} \left(\frac{n_i}{n_b}\right)^{1.04} \left(\frac{D_{50}\,armour}{H}\right)^{-0.93}$$
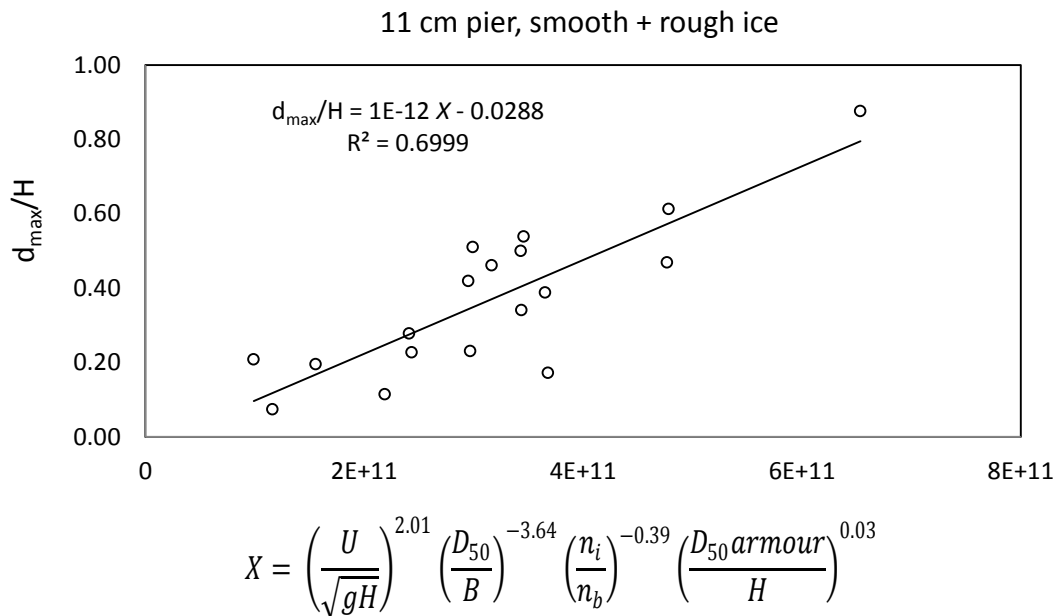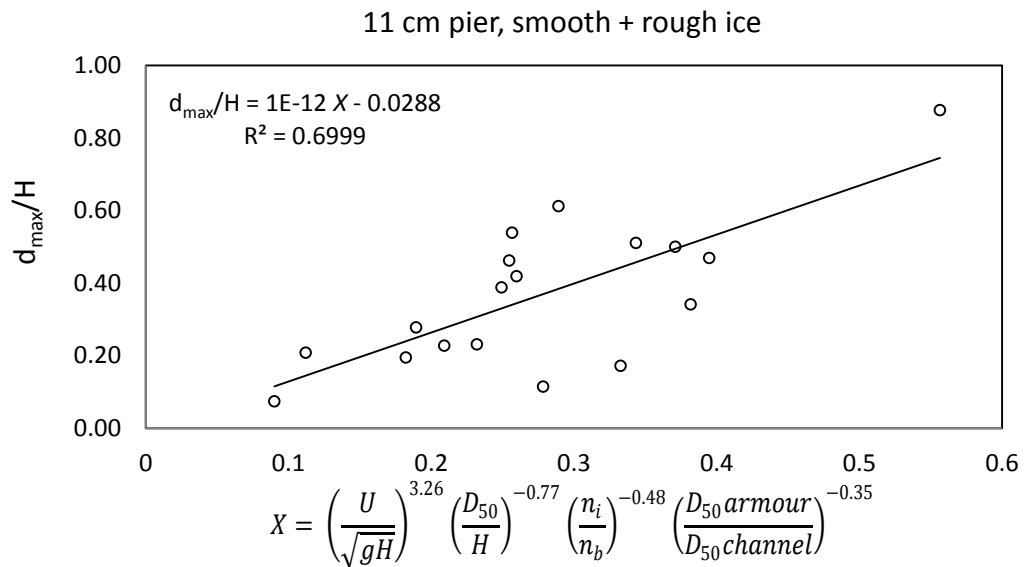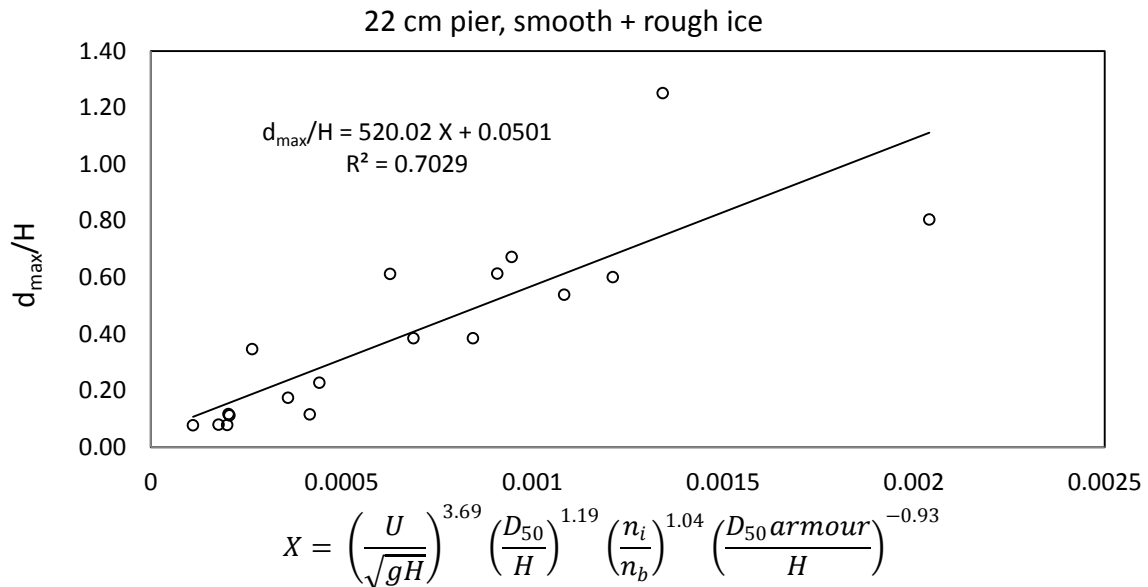
Figure 85. Variation of maximum scour depth for the 22 cm pier under ice covered conditions. Note the D_{50}/H regression coefficient does not reflect results from this study.

22 cm pier, smooth + rough ice

$d_{max}/H = 7E\text{-}17\ X + 0.0537$

$R^2 = 0.7512$

(y-axis: d_{max}/H; values 0.00, 0.20, 0.40, 0.60, 0.80, 1.00, 1.20, 1.40)

(x-axis: 0, 5E+15, 1E+16, 1.5E+16, 2E+16)

$$X = \left(\frac{U}{\sqrt{gH}}\right)^{3.18} \left(\frac{D_{50}}{B}\right)^{-5.04} \left(\frac{n_i}{n_b}\right)^{0.79} \left(\frac{D_{50}\,armour}{H}\right)^{0.16}$$

Figure 86. Variation of maximum scour depth for the 22 cm pier under ice covered conditions. Note the D_{50} armour regression coefficient does not reflect results from this study.

22 cm pier, smooth + rough ice

$d_{max}/H = 7E\text{-}17\ X + 0.0537$
$R^2 = 0.7512$

$$X = \left(\frac{U}{\sqrt{gH}}\right)^{3.69} \left(\frac{D_{50}}{H}\right)^{0.27} \left(\frac{n_i}{n_b}\right)^{1.04} \left(\frac{D_{50}\,armour}{D_{50}\,channel}\right)^{-0.93}$$

Figure 87. Variation of maximum scour depth for the 22 cm pier under ice covered conditions. Note the D_{50}/H regression coefficient does not reflect results from this study.
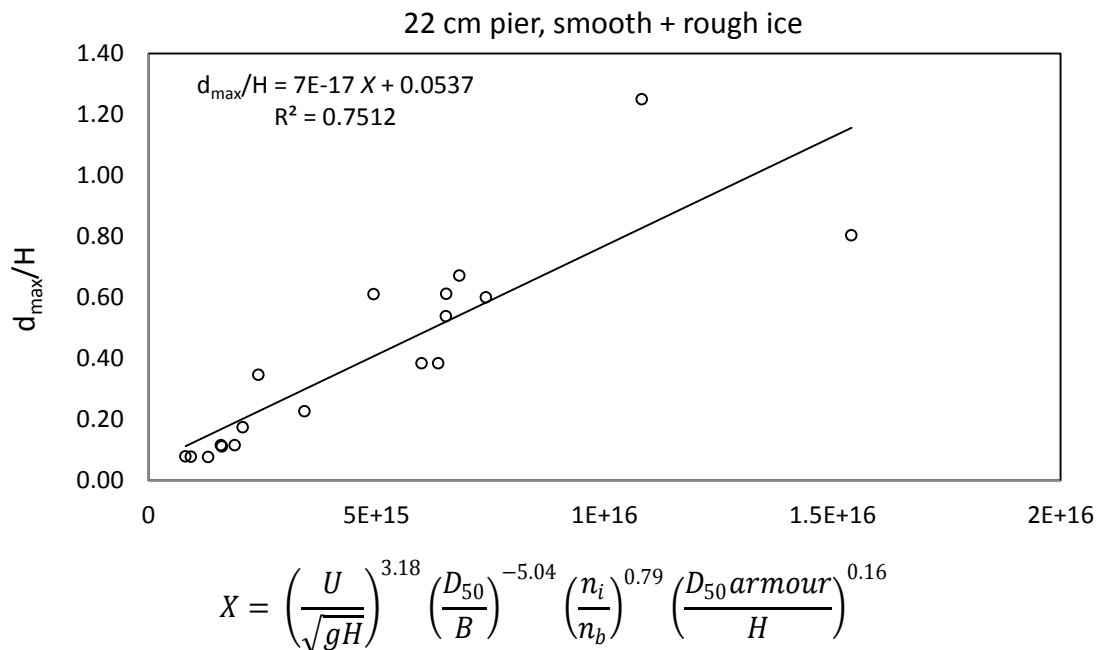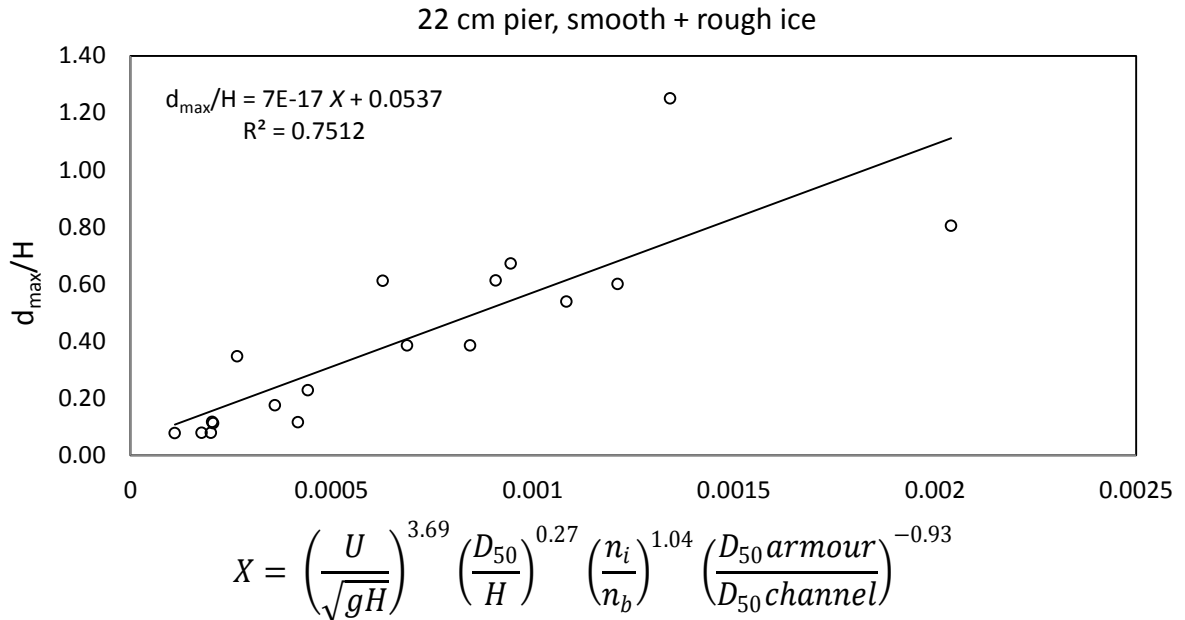
3.3 Armour layer all experiments:

$d_{max}/H = 25.575\ X - 0.003$
$R^2 = 0.6394$

$$X = \left(\frac{U}{\sqrt{gH}}\right)^{3.54} \left(\frac{D_{50}}{H}\right)^{0.21} \left(\frac{n_i}{n_b}\right)^{0.27} \left(\frac{D_{50}\,armour}{H}\right)^{-0.49} \left(\frac{b}{B}\right)^{-0.02}$$
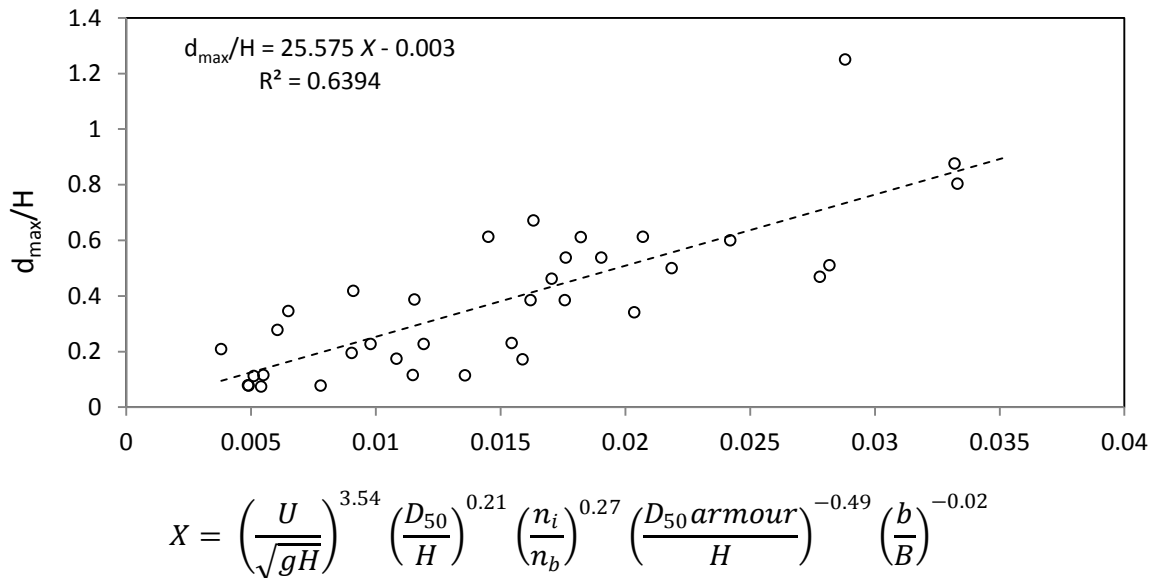
Figure 88. Variation of maximum scour depth under ice covered conditions. Note the D_{50}/H and b/B regression coefficients do not reflect results from this study.

$$X = \left(\frac{U}{\sqrt{gH}}\right)^{2.38} \left(\frac{D_{50}}{B}\right)^{-4.99} \left(\frac{n_i}{n_b}\right)^{0.12} \left(\frac{D_{50}\,armour}{H}\right)^{0.24} \left(\frac{b}{B}\right)^{0.05}$$
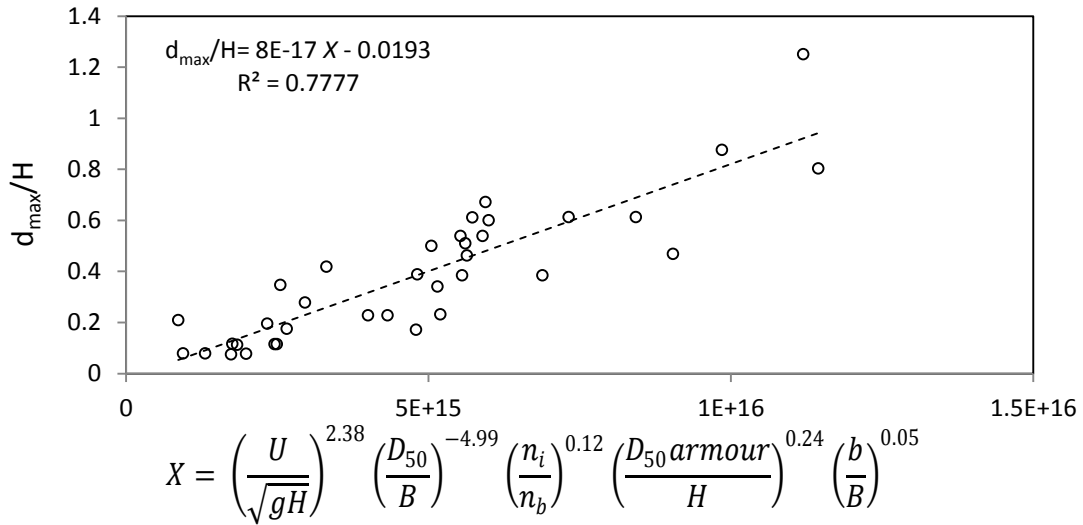
Figure 89. Variation of maximum scour depth under ice covered conditions. Note the D_{50} armour regression coefficient does not reflect results of this study.

$$X = \left(\frac{U}{\sqrt{gH}}\right)^{3.54} \left(\frac{D_{50}}{H}\right)^{-0.29} \left(\frac{n_i}{n_b}\right)^{0.27} \left(\frac{D_{50}\,armour}{D_{50}\,channel}\right)^{-0.49} \left(\frac{b}{B}\right)^{-0.02}$$
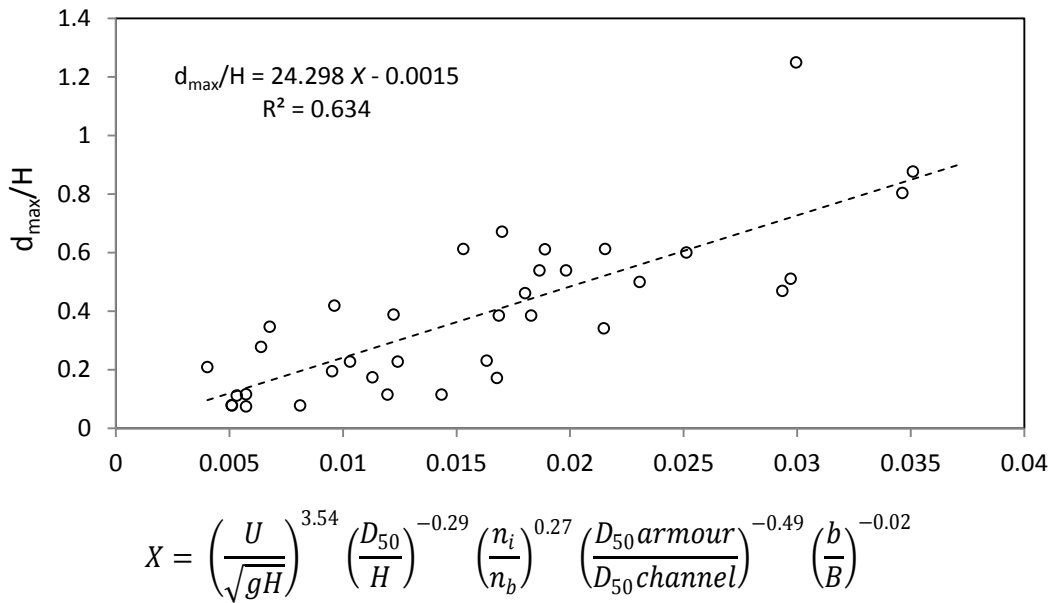
Figure 90. Variation of maximum scour depth under ice covered conditions. Note the b/B regression coefficient does not reflect results from this study.
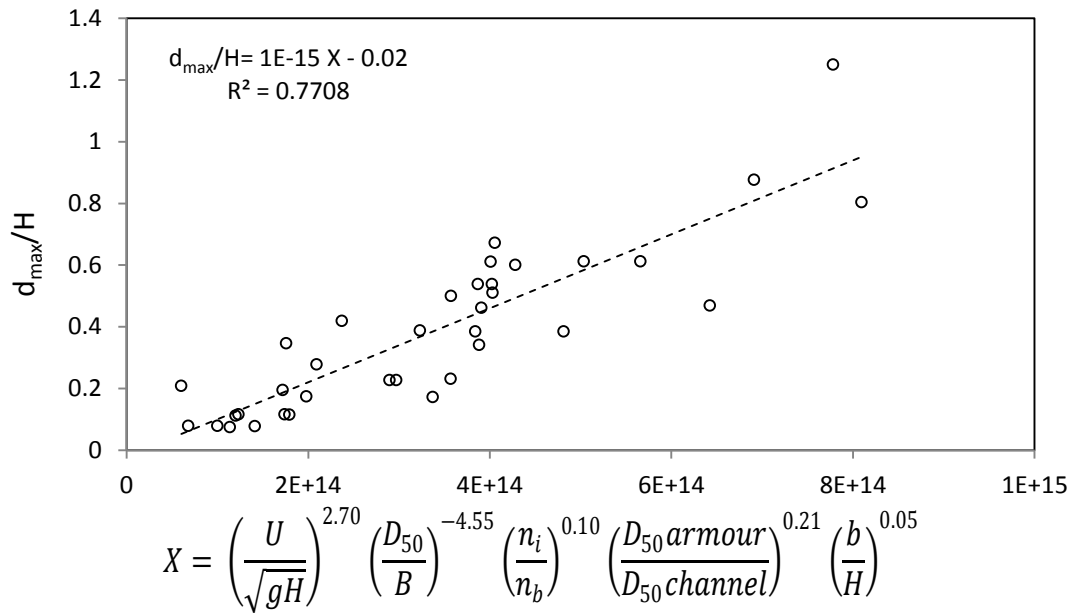
$$X = \left(\frac{U}{\sqrt{gH}}\right)^{2.70} \left(\frac{D_{50}}{B}\right)^{-4.55} \left(\frac{n_i}{n_b}\right)^{0.10} \left(\frac{D_{50}\,armour}{D_{50}\,channel}\right)^{0.21} \left(\frac{b}{H}\right)^{0.05}$$

Figure 91. Variation of maximum scour depth under ice covered conditions. Note the D_{50} armour regression coefficient does not reflect results from this study.